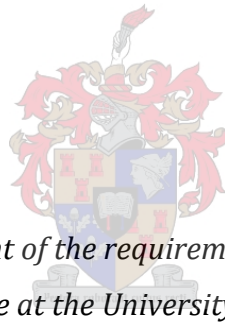# Investigation of heuweltjie structure and soil chemistry in the Buffels River valley and implications for transfer of salts to groundwater

by

Marli Vermooten

Thesis presented in partial fulfilment of the requirements for the degree Master of Science in Earth Science at the University of Stellenbosch

Supervisor: Dr. Jodie Miller[a]

Co-supervisors: Dr. Cathy Clarke[b] and Dr. Michele Francis[b]

[a]Faculty of Science, Department of Earth Science [b]Faculty of AgriSciences, Department of Soil Science

December 2019

Declaration

I declare that Investigation of heuweltjie structure and soil chemistry in the Buffels River valley and implications for transfer of salts to groundwater is my own work, that it has not been submitted for any degree or examination in any other university, and that all the sources I have used or quoted have been indicated and acknowledged by complete references.

By submitting this thesis electronically, I declare that the entirety of the work contained therein is my own, original work, that I am the sole author thereof (save to the extent explicitly otherwise stated), that reproduction and publication thereof by Stellenbosch University will not infringe any third party rights and that I have not previously in its entirety or in part submitted it for obtaining any qualification.

Full name: Marli Vermooten

Date: December 2019

i

Acknowledgements

I would like to thank my main supervisor, Dr. Jodie Miller, for all the effort she put into making this MSc thesis a success. This includes all the advice and direction she has given me, as well as all the funding spent on my project. Without her, this project would not have been successful. I would also like to thank my two co-supervisors, Dr. Cathy Clarke and Dr. Michele Francis for all their advice, especially on experiments done in the lab for my soil samples. I would especially like to extend my thanks to Dr. Michele Francis for all her shared knowledge on heuweltjies and all her help with sampling the heuweltjies in the field. Without her guidance we would have been completely lost. Thank you to Dr. Andrew Watson who spent a lot of time helping me create my heat maps. I would also like to thank Jared van Rooyen for his guidance with the heat maps. Thank you to the Soil Science department for allowing me to do my lab work in your labs and thank you for all your help. It was a pleasure working with you all. Especial thanks to Liana De Witt. For funding, I thank the WRC, Iphakade, and NRF. I would like to thank Integral Laboratories and the CAF of Stellenbosch University for analysing my anions and cations respectively. I would also like to extend my thanks to everyone who came with me on the field trips: Jani van Gend, Ruairi Walker, Dr. Andrew Watson, and Deone Husselman. You all made the field work much more enjoyable. Thank you to Emile Kleyn for all his voluntary help with my lab work, while he was also busy with his MSc. I appreciate all your help so much. I would also like to extend thanks to my sister Anri who came to help me in the lab. Thank you to Ncumisa in soil science who was always there for me when I was having a hard time in the lab, and always lending a hand and listening to the issues I run into with my work. Lastly, I would like to thank my family for their continued support. If it wasn't for all their words of encouragement, I probably would not have made it this far. I am forever grateful towards you all.

Abstract

Globally, soil salinization is a major soil degradation problem. Saline soils damage the land by altering various Earth cycles and are especially a threat to farming. Saline soils can cause salts to leach into the groundwater, causing an increase in groundwater salinity. The Buffels River catchment, situated in the Northern Cape Province of South Africa, is affected by saline groundwater. Various locations along the coastal zone of southern Africa show similar mean annual precipitation profiles as the Buffels River catchment, yet do not suffer from the same salinization levels. Saline waters within this area are also not evenly distributed, suggesting that other factors may play a role in the groundwater salinization. Heuweltjies, circular earth mounds that can be up to 2 m in height and 32 m in width, are abundant in the Buffels River catchment, and have salinity levels an order of a magnitude higher than the surrounding soils, suggesting that heuweltjie salts may be contributing to this groundwater salinization. Detailed analyses were done on two heuweltjies, through excavation, to examine the salt profile of the heuweltjies, as well as other chemical and physical analyses of the sediments. This was done to see if heuweltjies could be contributing to groundwater salinity in this area. In order to gather this information, a range of analytical techniques were employed with the aim of determining whether the heuweltjies are leaching salts into the groundwater system. Amongst the analytical techniques available for this type of profiling, electrical conductivity, pH, mineralogy, particle size analysis, anion and cation profiling, and dissolved silica were analysed. Results showed that heuweltjies have different soil compositions compared to the interheuweltjie sediments. More clay was present on heuweltjie than off heuweltjie. Heuweltjies had elevated salt concentrations compared to the interheuweltjie sediments, and minerals such as gypsum, calcite, and calcium oxalate were only present in the heuweltjie soils. The source of salt is possibly from marine origin. This could be caused by evaporative concentration, transfer of marine blown salts, or termites bringing saline plant materials into the heuweltjies. Calcite was found in the top soils, and gypsum deeper down, indicating that the water is moving downwards. This was concluded since gypsum is a more soluble salt than calcite and moves further down the profile. Preferential flow pathways were observed through granular soils in one heuweltjie, and termite nests and tunnels within the second heuweltjie, aiding in the transfer of salts to the groundwater.

Table of Contents

List of Figures

List of Tables

1 Introduction

Soil salinity is a global soil degradation problem, with saline soils occupying approximately 8 – 10% of the total land surface on Earth (Bui, 2013; Daliakopoulos *et al.*, 2016; Zhang *et al.*, 2017). Salinity can be defined as the concentration of dissolved mineral salts within water or soil, and is one of the most important factors for limiting agricultural crop productivity (Scanlon *et al.*, 2006; Smith & Compton, 2004; Sonmez *et al.*, 2008). Soil salinity leads to degradation of land by altering the hydrological, biochemical, and natural biological cycles of Earth (Daliakopoulos *et al.*, 2016). Environmental factors that can cause soil salinization – also known as primary salinization – include chemical and physical weathering of parent materials, regression and transgression of marine waters, high saline groundwater tables, and transport of wind-blown salts (Daliakopoulos *et al.*, 2016; Huber *et al.*, 2008; Zhang *et al.*, 2017). Human-induced factors – also known as secondary salinization – on the other hand, are mostly as a result of using waters that are rich in salts for irrigation purposes in conjunction with poor drainage circumstances (Daliakopoulos *et al.*, 2016; Huber *et al.*, 2008).

An increase in soil salinity is especially a threat to farming, as it affects crop productivity, seed germination, and water quality, resulting in a decrease in land suitable for agricultural practices (Gorji *et al.*, 2017; Smith & Compton, 2004). An accumulation of salts in the root zones of plants causes a reduction in crop productivity, and consequently impacts food security (Ibrahimi *et al.*, 2014; Seilsepour & Rashidi, 2008). Soil salinity is especially a major limiting factor for land development and crop production in arid and semi-arid coastal areas (Daliakopoulos *et al.*, 2016; Gorji *et al.*, 2017; Scanlon *et al.*, 2006). As saline groundwater can cause an increase in soil salinity, likewise an increase in soil salinity can cause groundwater resources to become more saline through leaching of the salts to the water table (Benito *et al.*, 2010; Naicker & Demlie, 2014).

The Northern Cape Province of South Africa, in particular the Buffels River catchment (Figure 1.1), is affected by saline groundwater. As there are no safe surface water supplies in this region, the people rely heavily on groundwater (Abiye & Leshomo, 2013). Having high salt concentrations in groundwater is a dilemma, especially when this water is used for agriculture, as it increases the salinity of the soils. In a country that experiences

frequent droughts, this can be a great threat to food production (Daliakopoulos *et al.*, 2016). Traditionally, salinity has been attributed to evaporation and evapotranspiration, which exceeds the mean annual precipitation (MAP) in this region (Barica, 1972; Smith & Compton, 2004). However, many places within the coastal zone of southern Africa, including Namibia, show similar MAP profiles and associated high evaporation rates, yet do not suffer from the same levels of salinization. The saline groundwater is also not uniformly distributed, and as a result, these features suggest that there are other factors at play in the development of saline groundwater.
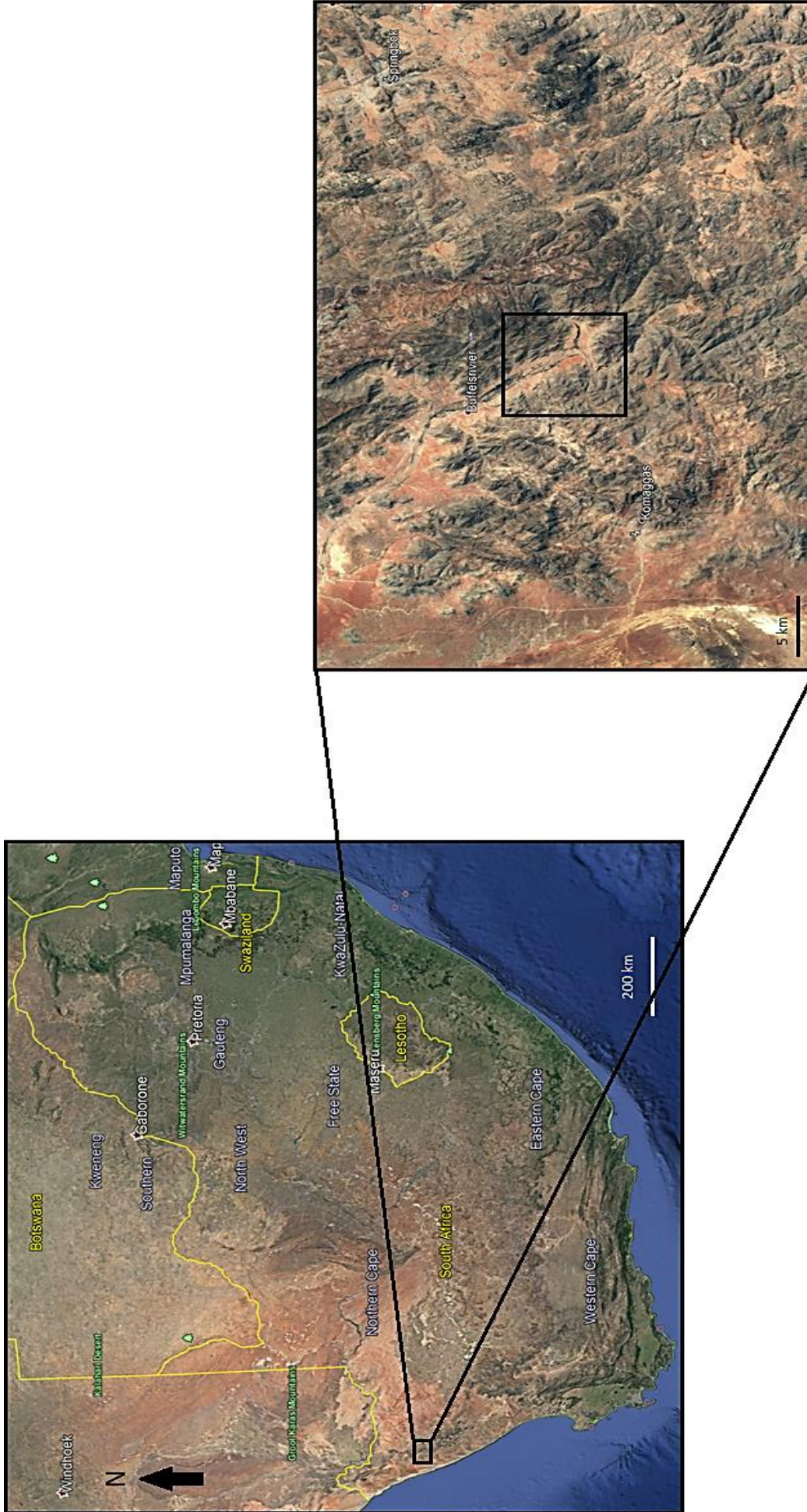
Figure 1.1: Google Earth Pro™ picture depicting the study location with respect to where it is in South Africa. The area shown in the box close to the town of Buffelsrivier was the specific focus site

Recently, it has been discovered that heuweltjies – at least in the area around the Buffels River, west of Springbok (Figure 1.1) – have salinity levels an order of a magnitude higher than the surrounding interheuweltjie material (van Gend, 2018). Heuweltjies are thought to be paleo-termite mounds that form distinct "spots" across a large area of the coastal and Northern Cape regions of South Africa (McAuliffe *et al.,* 2019a; McAuliffe *et al.,* 2019b). However, it is important to note that the termite mound is not the same landform as the heuweltjie. The termite mound forms first, and then the heuweltjies form as a result of subsequent processes that favour its development around the termite mound (Mcauliffe *et al.*, 2018). Satellite images show heuweltjies to be abundant in the Buffels River catchment (Figure 1.2).
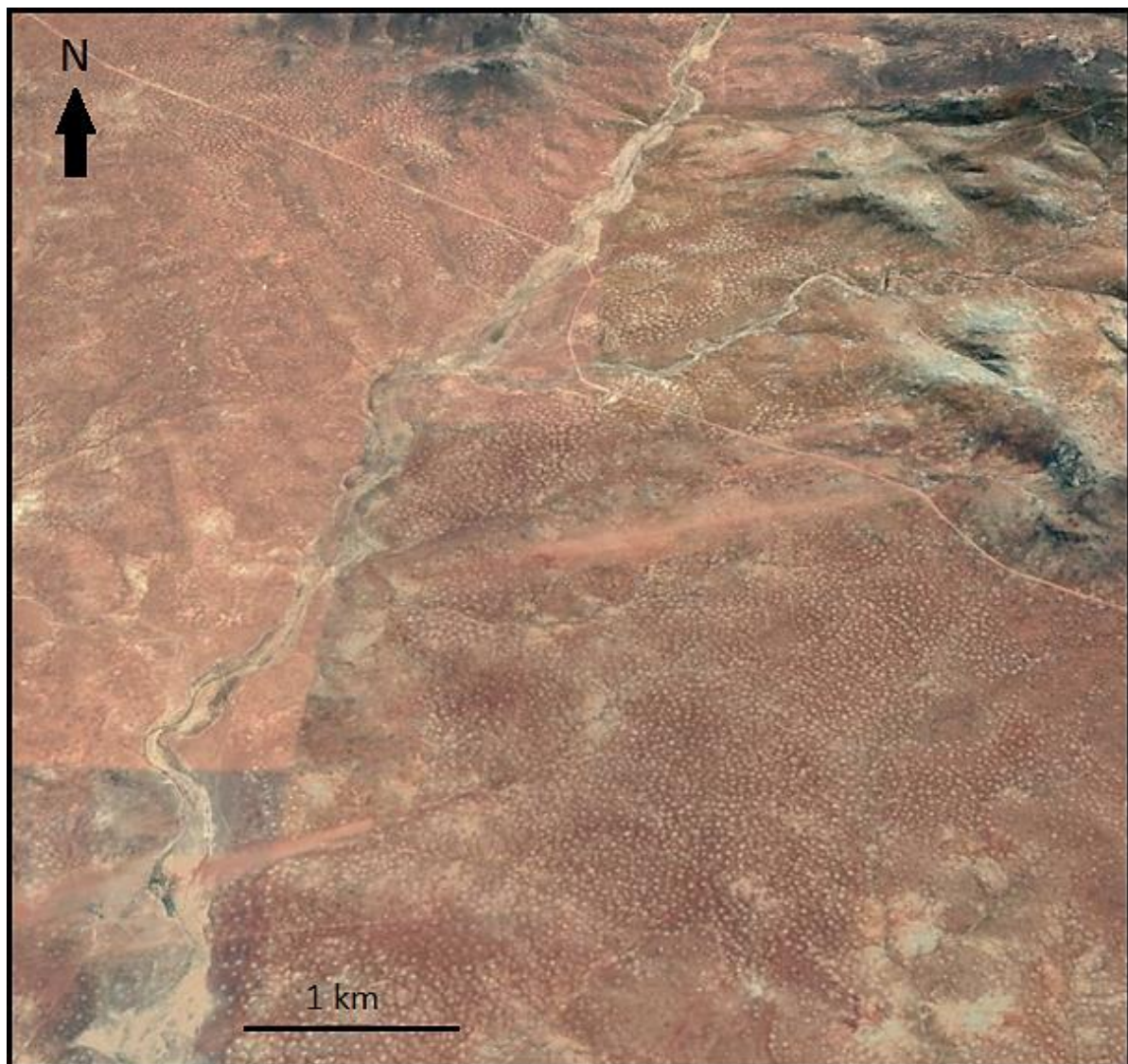
Figure 1.2: Google Earth Pro™ image showing the abundance of heuweltjies (lighter coloured spots) close to Kommagas (see Figure 1.1), Northern Cape, within the Buffels River catchment area.

Heuweltjies typically show up due to distinct differences in vegetation cover on the domal surface in comparison to the interheuweltjie material, with vegetation either being more or less dense on the heuweltjies than the surrounding sediments (Schmiedel *et al.*, 2015). Heuweltjies have different soil compositions due to paleo as well as recent termite activity (Luther-Mosebach *et al.,* 2012; McAuliffe *et al.*, 2014). Their surfaces are made of fine, unconsolidated, and uncemented materials (McAuliffe *et al.*, 2019b) and the centres usually have higher silt and clay content, lower stone content, and better water availability than the surrounding sediments (Kunz *et al.*, 2012; Schmiedel *et al.*, 2015). Three prominent heuweltjie features are outlined by McAuliffe *et al.* (2019b): (1) heuweltjie soils are enriched with plant nutrients; (2) they have enhanced calcium carbonate concentrations as compared to off-mound sediments; and (3) they are highly regularly spaced. Similarly, Francis & Poch (2019), McAuliffe *et al.* (2019b), and Midgley *et al.* (2002) also found increased calcium carbonate concentrations within heuweltjies.

In comparison, understanding of the salt content of heuweltjies is relatively poor. Only a handful of studies have briefly mentioned that heuweltjies were found to be saline, but no further details were mentioned (Francis *et al.*, 2007; Kunz *et al.*, 2012). McAuliffe *et al.* (2014) mentioned in their study on heuweltjies near Soebatsfontein (~80 km south west of Springbok) and Graafwater (~330 km south of Springbok) that the salt content of the heuweltjies were extremely elevated (>5000 ppm) at a depth of about half a meter. In some of the mounds they analysed, the salt concentrations at one metre depth were two to three times more than it was at the half a metre depth. McAuliffe *et al.* (2019b) mentioned in their research close to Vanrynsdorp in the Western Cape (261 km south of Springbok) that the reason for no vegetation cover on eroding domes in this area is due to the deeper exposed heuweltjie soils having much higher salt content than that of the non-eroded, vegetated heuweltjie surfaces. They found an eroded heuweltjie with a total soluble salt concentration of 14000 ppm. McAuliffe *et al.* (2019a) also found higher total soluble salt content within a heuweltjie at Inverdoorn, Western Cape (562 km south of Springbok), compared to the inter-heuweltjie material. In a study done by van Gend (2018) in the Buffels River catchment area, heuweltjie sediments were found to have much higher salt content than the inter-heuweltjie sediments, with elevated electrical conductivity (EC) values in the centre of the heuweltjies. None of the above-mentioned studies examined the nature of the salts in detail – only total dissolved salts (TDS) or EC measurements were made.

The unsaturated zone (UZ) in soil is the only link between the surface of the land and groundwater, and is therefore crucial for groundwater recharge (Huang *et al.*, 2017a; Huang, *et al.*, 2017b; Huang *et al.*, 2016). The UZ is a storage facility for water and contaminants, consequently causing a delay in the release of its influx into the groundwater table, or saturated zone (Huang *et al.*, 2017a; Huang *et al.*, 2017b; Huang *et al.*, 2016). Heuweltjies introduce heterogeneity to the unsaturated zone.

What is not known about heuweltjies is if they do contribute to the groundwater salinity in this area – whether the salts are leaching through to the groundwater. It is also uncertain as to what types of salts are found within the heuweltjies, and where they are hosted. Therefore, in this study, the salt profiles for two excavated heuweltjies were examined in detail with the goal of better understanding the salt distribution throughout the heuweltjies, as well as its link to groundwater salinity. The role that the specific heuweltjie soils plays in this salt transfer were also analysed. In order to gather this information, a range of analytical techniques were employed. Amongst the analytical techniques available for this type of profiling, pH, electrical conductivity, mineralogy, particle size analysis, anion and cation profiling, and dissolved silica were analysed.

1.1 Problem Statement

Since some heuweltjies are considered paleo-structures (Midgley *et al.*, 2002; Potts *et al.*, 2009), this raises the possibility that the salts in the groundwater are not just as a result of evaporation and arid environments, but also due to leaching of salts from the heuweltjies, in which case the salts are themselves a paleo-feature. As heuweltjies are not uniformly distributed along the west coast and the Northern Cape (Cramer *et al.,* 2017; Picker, *et al.*, 2007), their density and distribution could be key to understanding the distribution of saline groundwater in these same areas.

The key to resolving the nature of the heuweltjie salts is to fully understand the sediment making up the heuweltjies, which salts dominate the heuweltjies, as well as where and how the salt is hosted within the heuweltjies. Once it is known if the salts do leach down the heuweltjie soil profile, it can be determined whether this is a cause of the groundwater salinity. If it is, something may be done about it, helping the communities in this area to purify their groundwater sources and increase local farming, developing more work opportunities in a work-scarce area.

1.2 Aims & Objectives

The goal of this project was to excavate two heuweltjies in the Northern Cape Province, near Buffels River, to determine their chemical and physical properties. The intention was to reveal the type of salts located within the heuweltjies and analyse if these salts could be a source for groundwater salt, or vice versa. Three key objectives were defined:

Objective 1: To analyse the composition and structure of two heuweltjies.

- What type of soil is present within the heuweltjies, and does this differ from the interheuweltjie soils?
- What is the mineralogy of the heuweltjie soils?
- Is there a significant difference in particle size and mineralogy between the two heuweltjies?

Objective 2: To fully characterise the salt profile within the heuweltjies.

- What types of salts are hosted within the heuweltjie soils?
- Where are these salts hosted within the heuweltjie, including mineral hosts and salt coatings?
- Is there a difference in the salt content and where the salts are hosted within the two heuweltjies relative to their location?

Objective 3: To determine if the salts are transferred into the groundwater system, and if so, to establish the mechanism by which it occurs.

- Do the salts extend and increase in concentration down the heuweltjie profile? What is the source of these salts?
- Are the soil solutions unsaturated, saturated, or supersaturated with respect to a particular salt and so are they stable or unstable with respect to movement within the heuweltjies?
- If the salts are not transferred to the groundwater, does the saline groundwater in turn have an effect on increasing heuweltjie salinity?

1.3 Background

In this section, background information about heuweltjies, along with the geology, climate, soil, and vegetation of Namaqualand will be discussed.

1.3.1 Heuweltjies

Heuweltjies (see Figure 1.3) are circular earth mounds that can be up to 2 m in height and 32 m in width, and have a large distribution throughout the Western and Northern Cape provinces of South Africa, occupying approximately 14-25% of the surface of the land (Cramer *et al.*, 2017; Cramer *et al.*, 2012; Cramer & Midgley, 2015; Francis *et al.*, 2012a; Francis & Poch, 2019; Kunz *et al.*, 2012; McAuliffe *et al.*, 2019b; McAuliffe *et al.*, 2014; Schmiedel *et al.*, 2015).
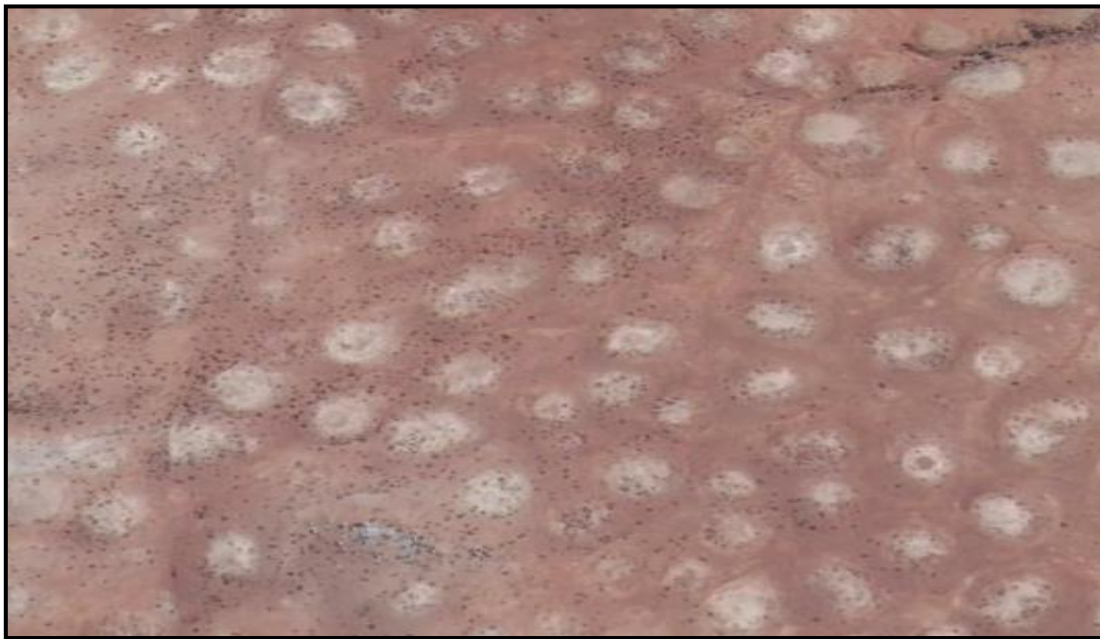
Figure 1.3 Google Earth Pro™ image of a section of the heuweltjieveld next to Buffels River.

In South Africa, heuweltjies are most commonly found throughout the arid to semi-arid, sparsely vegetated Namaqualand, Succulent Karoo, and Fynbos biomes (Francis *et al.*, 2012a; Francis & Poch, 2019; Kunz *et al.*, 2012; McAuliffe *et al.*, 2014; Picker *et al.*, 2007). They occur in mountain valleys, land flats and lowlands, and are mostly absent from mountainous areas (Picker *et al.*, 2007). The most cited argument for the origin of heuweltjies states that they are termite mounds, formed by the southern harvester termite species, *Microhodotermes viator* (Francis *et al.*, 2012a; Francis & Poch, 2019; Kunz *et al.*, 2012; McAuliffe *et al.*, 2019b; McAuliffe *et al.*, 2014; Picker *et al.*, 2007;

Schmiedel *et al.*, 2015), but the agent of formation continues to be debated. Cramer *et al.* (2017) speculated that the heuweltjie mounds are much larger than more recent *M. viator* nests, and so it is unlikely that these termites created the heuweltjies. An alternate theory depicts that heuweltjies formed as a result of erosion of "regularly spaced shrub clumps" (Cramer *et al.*, 2017, 2012). These vegetative clusters are then thought to produce feedbacks that result in creation of what Cramer & Midgley (2015) refer to as 'islands of fertility.' These islands are thought to form as a result of shrubs and trees trapping sediment, increasing nutrient availability and soil moisture (Cramer & Midgley, 2015).

McAuliffe *et al.* (2014) exhibited soil stratigraphic and developmental evidence that heuweltjies form through aeolian deposition. However, they suggested that its "developmental pathway" involves not only physical, but also biological processes. Termite colonies are usually regularly spaced as a result of territorial interactions (McAuliffe *et al.*, 2014; Mcauliffe *et al.*, 2018). Fertile islands are then created by these termites, where the soils are enriched in plant nutrients, further encouraging the formation of denser patches of vegetation (McAuliffe *et al.*, 2014). These patches of vegetation then catch and preserve aeolian sediments, which in turn creates the mounds (McAuliffe *et al.*, 2014; Mcauliffe *et al.*, 2018).

Heuweltjies have attracted scientific attention for a long time as a result of their remarkable influence on vegetation variety within these biomes, with different vegetation growing on the heuweltjie than on the interheuweltjie (Francis & Poch, 2019; Kunz *et al.*, 2012; Schmiedel *et al.*, 2015). This has to do with the heuweltjies having very different soil properties compared to the surrounding soils (McAuliffe *et al.*, 2019a; McAuliffe *et al.*, 2019b), contributing considerably to the local biodiversity (Luther-Mosebach *et al.,* 2012; McAuliffe *et al.*, 2014). The chemical and physical properties of the heuweltjies enable it to have higher nutrient and water contents as a result of higher organic carbon content (Francis *et al.*, 2012a; Kunz *et al.*, 2012). Heuweltjie centres usually have an increased calcium carbonate concentration, soil pH, total nitrogen and total organic carbon content compared to the outside fringes of the heuweltjie and interheuweltjie soils (McAuliffe *et al.*, 2019a; Schmiedel *et al.*, 2016). Heuweltjies tend to have higher clay content, and are prone to be more alkaline and enriched with silica than the surrounding soils (Francis *et al.*, 2007).

McAuliffe *et al.* (2014) concluded that both young and old heuweltjies occur together in certain areas. Younger mounds consist of fine to very fine sandy loam sediments, have little calcium carbonate accumulation – and hence no cemented calcite horizons – and also show minimal pedogenic alteration (McAuliffe *et al.*, 2014). Older heuweltjies have a petrocalcic layer, usually about 50 cm to 1 m down into the heuweltjie, with petroduric horizons at the edges (Francis *et al.*, 2007; Francis & Poch, 2019; McAuliffe *et al.*, 2019a; Midgley *et al.*, 2002). These petrocalcic horizons are indurated calcium carbonate cemented, are either platy or massive, and are very hard (WRB, 2014). These layers are noticeable due to strong effervescence with 1 M hydrochloric acid, and usually have a thickness greater than 10 cm (WRB, 2014). Heuweltjies are mostly situated on non-calcareous sandy soils, and so calcite accumulation cannot be coming from the parent materials; therefore, it must be derived from non-lithogenic origins, such as termites bringing plant material into the heuweltjies (Francis & Poch, 2019). The organic matter of the plant material can then be decomposed, also forming calcite (Francis & Poch, 2019). The excrement of *M. viator* termites occupying heuweltjies includes calcium oxalate (Francis *et al.*, 2012a; Francis & Poch, 2019; McAuliffe *et al.*, 2019a). Calcium oxalate is a low solubility mineral that is commonly found within plants (Uren, 2018). When the *M. viator* termites ingest the plant material, it is transported to the heuweltjie soils via their excrement, suggesting that the oxalate-carbonate pathway operates within heuweltjies (Francis *et al.*, 2012a; Francis & Poch, 2019; McAuliffe *et al.*, 2019a). Oxalotrophic fungi and bacteria then decompose the calcium oxalate and alkalise the soil pH, causing calcite to precipitate (Francis *et al.*, 2012a; Francis & Poch, 2019; McAuliffe *et al.*, 2019a). The overall reaction that occurs during the decomposition of oxalate via oxidation and forming calcite is as follows (Uren, 2018):

$$2CaC_2O_4 + 2O_2 + 4H^+ \rightarrow 2CaCO_3 + 2H_2O + 2CO_2 \qquad (1.1)$$

Through use of ^{14}C dating on the calcite layer embedded in older heuweltjies, an age of 20000 – 35000 years was formulated (Midgley *et al.*, 2002; Potts *et al.*, 2009). As a result, the calcite layer could help trace back to the approximate age of when the heuweltjies formed. The calcite is a secondary process, however, and does not give the exact age of when the heuweltjie formed.

1.3.2 Geology of Namaqualand

Namaqualand is subdivided into the following three geological provinces (Tankard, *et al.*, 2009): (1) a Phanerozoic cratonic cover, (2) the basement rocks of the Namaqua Province, and (3) the volcano-sedimentary Gariep Complex rocks (Abiye & Leshomo, 2013). Most of the crystalline basement rocks are found in the Namaqua Province, with the margins of the Province being concealed underneath younger rocks of the Nama, Gariep, and Karoo sequences (Abiye & Leshomo, 2013). The rocks in the Central Zone are known to cover most of Bushmanland and Namaqualand (Abiye & Leshomo, 2013).

The area of this study is located in the larger Bushmanland Sub-Province (BSP) of Namaqualand, situated in the Namaqua Sector of the Namaqua-Natal belt (Macey *et al.*, 2018). It surrounds the southern and western margin of the Kaapvaal Craton (Bial *et al.*, 2015), as can be seen in Figure 1.4 .The Namaqua-Natal province forms a belt of continuous high-grade rocks, modelled due to arc-continent and/or continent-continent collision, and has indentation-escape tectonics alongside the southern, south-western, eastern, and south-eastern side of Proto-Kahalari, known to be between the ages of 1.2 and 1.0 Ga (Jacobs *et al.*, 2008). Within South Africa, the Namaqua-Natal Province is divided into two sectors exposed as outcrops, known as the "Natal Sector" in Kwazulu-Natal, and the "Namaqua Sector" situated in the Northern Cape Province (Jacobs *et al.*, 2008). Evidence suggests that the Namaqua and Natal sectors are part of a 1400 km x 1400 km wide exposed orogenic belt that extends underneath central South Africa's Phanerozoic Karoo Supergroup (Jacobs *et al.*, 2008). The Natal sector consists of a juvenile crust of ~1.2 Ga years, produced in island arcs, "accreted to the Archaean Kaapval Crator at ~1.1 Ga" (Macey *et al.*, 2017). The Namaqua Sector consists of supracrustal rocks and polymetamorphosed and polydeformed granitic gneisses, formed as a result of two techno-magmatic cycles in the Mesoproterozoic and Paleoproterozoic eras (~1350 – 950 Ma and ~2050 – 1800 Ma respectively; Macey *et al.*, 2018; Macey *et al.*, 2017). In the western part of the Namaqua sector, it consists of a SW-vergent thrust sheet in a NW-trending stack, and is distinguished based on its tectonic, metamorphic, and lithostratigraphic histories (Macey *et al.*, 2017; Macey *et al.*, 2018). The Namaqua sector consists of the Bushmanland and Richtersveld subprovinces (Figure 1.4), as well as the Kakamas, Kaaien, and Areachap terranes, all bound by Mesoproterozoic shear zones (Jacobs *et al.*, 2008).
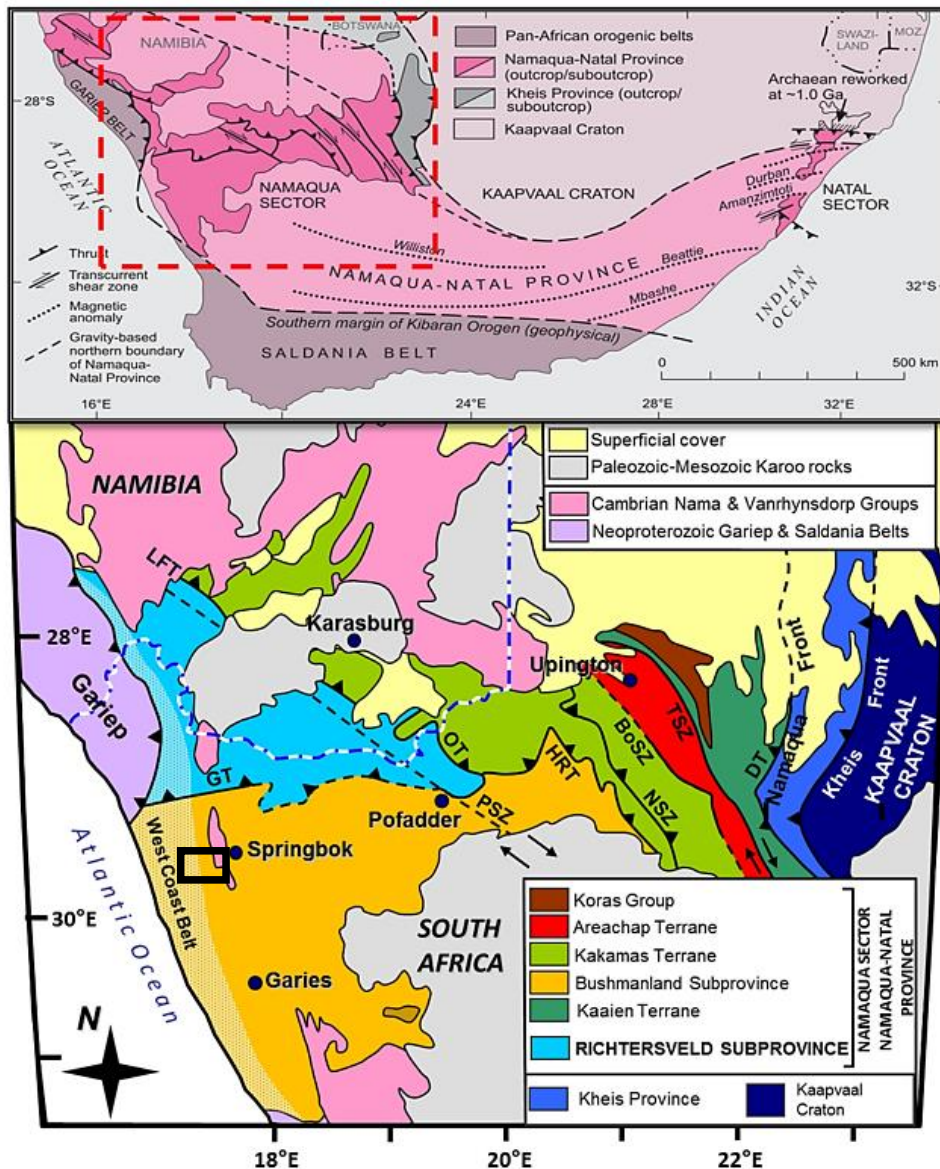
Figure 1.4: Location of the Namaqua sector within the Namaqua-Natal Province (top), as well as the sub-provinces and terranes of the Namaqua sector (bottom; by Macey et al., 2017). The location focused on for this study is within the Bushmanland subprovince, just west of Springbok (shown in the black box in bottom map). Black box in bottom map is an addition not shown in the original figure.

The BSP of the Namaqua sector, located at the bottom of the regional tectonic pile, forms its most structurally and southerly lowermost domain (Macey *et al.*, 2018). The BSP is an approximately 1000 m thick succession (Bailie *et al.*, 2007). It consists mostly of granites and granulite to amphibolite-facies gneisses (Abiye & Leshomo, 2013; Macey *et al.*, 2017), with its north-western part dominated by migmatites and granite gneisses (Macey *et al.*, 2018). The rest of the BSP consists of pre- and post-tectonic Mesoproterozoic granites intermixed with slim screens and sporadic belts of high grade paragneisses (Macey *et al.*, 2018). The BSP developed around the world class Pb-Zn-Cu-Ag deposits located in the

Aggeneys District (Bailie *et al.*, 2007; Macey *et al.*, 2018), where it consists mostly of aluminous schists, with lesser amounts of shale, ferruginous quartzite, amphibolite and calc-silicate assemblages, and iron formations (Bailie *et al.*, 2007).

The two suites located in the BSP in the area of research includes the Spektakel suite and the Little Namaqualand suite (see Figure 1.5). The Spektakel suite consists of the Rietberg granite, Kweekfontein granite, and Concordia granite gneiss, while the Little Namaqualand suite consists of the Nababeep and Modderfontein granite gneisses (Clifford *et al.*, 1995; Clifford *et al.*, 2004; Raith, 1995). The Spektakel suite is the "largest tectonic domain" in the Namaqua Sector, consisting mostly of undistorted charnockites and granites (Macey *et al.*, 2018). The Little Namaqualand suite consists of megacrystic gneisses and "quartz-feldspar-biotite augen gneisses" (Raith, 1995). Both the Nababeep and Modderfontein granite gneisses in the Little Namaqualand suite are affected by granulite-facies of approximately 1.2 Ga (Colliston *et al.*, 2012; Raith, 1995), while the Spektakel Suite is approximately 1100 Ma (Colliston *et al.*, 2012).
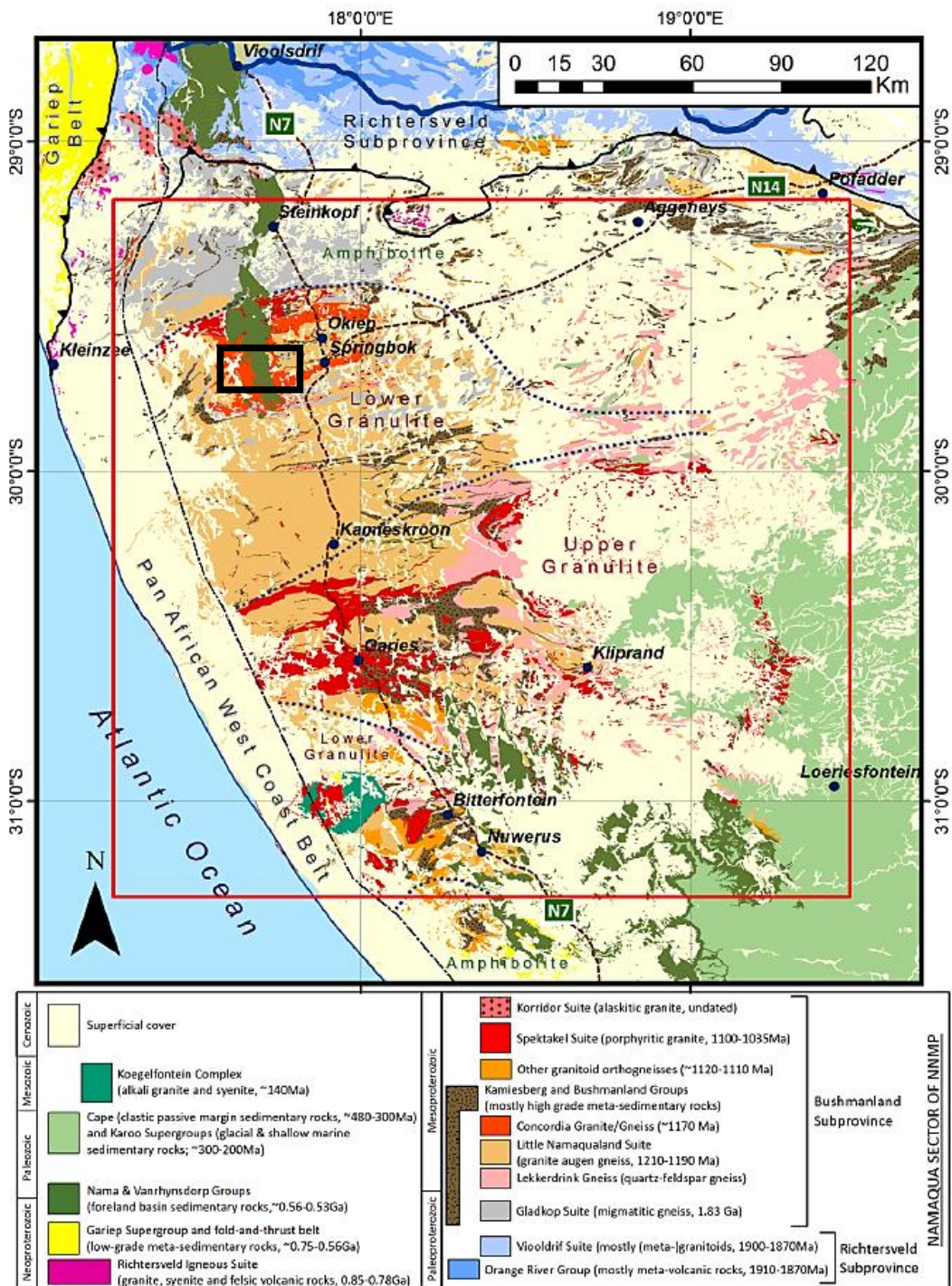
Figure 1.5: The Bushmanland Sub-Province (from Macey et al., 2018). Study site is depicted in area surrounded by the black box (note that the black box is an addition not depicted in the original figure).

1.3.3   Climate of Namaqualand

Namaqualand is situated in the driest south-western part of South Africa (Abiye & Leshomo, 2013). It is classified as being a semi-arid, winter rainfall region (Cowling *et al.*, 1999; Davis *et al.*, 2016). Along the coast, temperatures range from 21℃ in the warmest month, to 8℃ in the coldest. More inland, mean temperatures range from 38℃ in the warmest month, to 4℃ in the coldest (Singer, Kirsten & Buhmann, 1995). Frost occurs occasionally on upland peaks during the winter, and temperatures as high as 40℃ have been recorded when an inflow of turbulent, hot air, referred to as 'berg winds,' flow towards the coast from southern Africa's high altitude plateaus during the winter months (Cowling *et al.*, 1999). Namaqualand is prone to droughts, and has had numerous droughts in the past (Kelso & Vogel, 2007). The coastal plain of Namaqualand experiences evaporation rates of around 2000 mm per year (Francis, 2019). Mean annual precipitation in the north-west area is 50 mm (see Figure 1.6a), while it can be up to 400 mm in the Kamiesberg (Cowling *et al.*, 1999; Davis *et al.*, 2016; MacKellar *et al.*, 2007). Most of the area, however, receives less than 150 mm per year (Cowling *et al.*, 1999), which has a direct impact on the recharge of groundwater (Abiye & Leshomo, 2013). This low rainfall region is a unique feature, underpinning many of the unusual biological processes and patterns of this region (Cowling *et al.*, 1999). Due to the geography of the area being so different, as it ranges from having areas of high mountains to land flats, the climate is not uniform throughout (MacKellar *et al.*, 2007). The climate is primarily determined by the circumpolar westerly airstream and the southern subtropical high pressure system (Davis *et al.*, 2016). Periods of low rainfall and climate stress in Namaqualand is as a result of the combination of these pressure systems that dominate the sea surface and the region on land (Kelso & Vogel, 2007). Less moisture is advected over the western coast as a result of the Benguela current, therefore resulting in the development of desert climates along the interior and western coast (Davis *et al.*, 2016; Kelso & Vogel, 2007). Fog generated by the Benguela current forms a significant moisture source in the region (Davis *et al.*, 2016; Kelso & Vogel, 2007). This, along with dewfalls, have at times exceeded the rainfall throughout the wet season (Davis *et al.*, 2016).
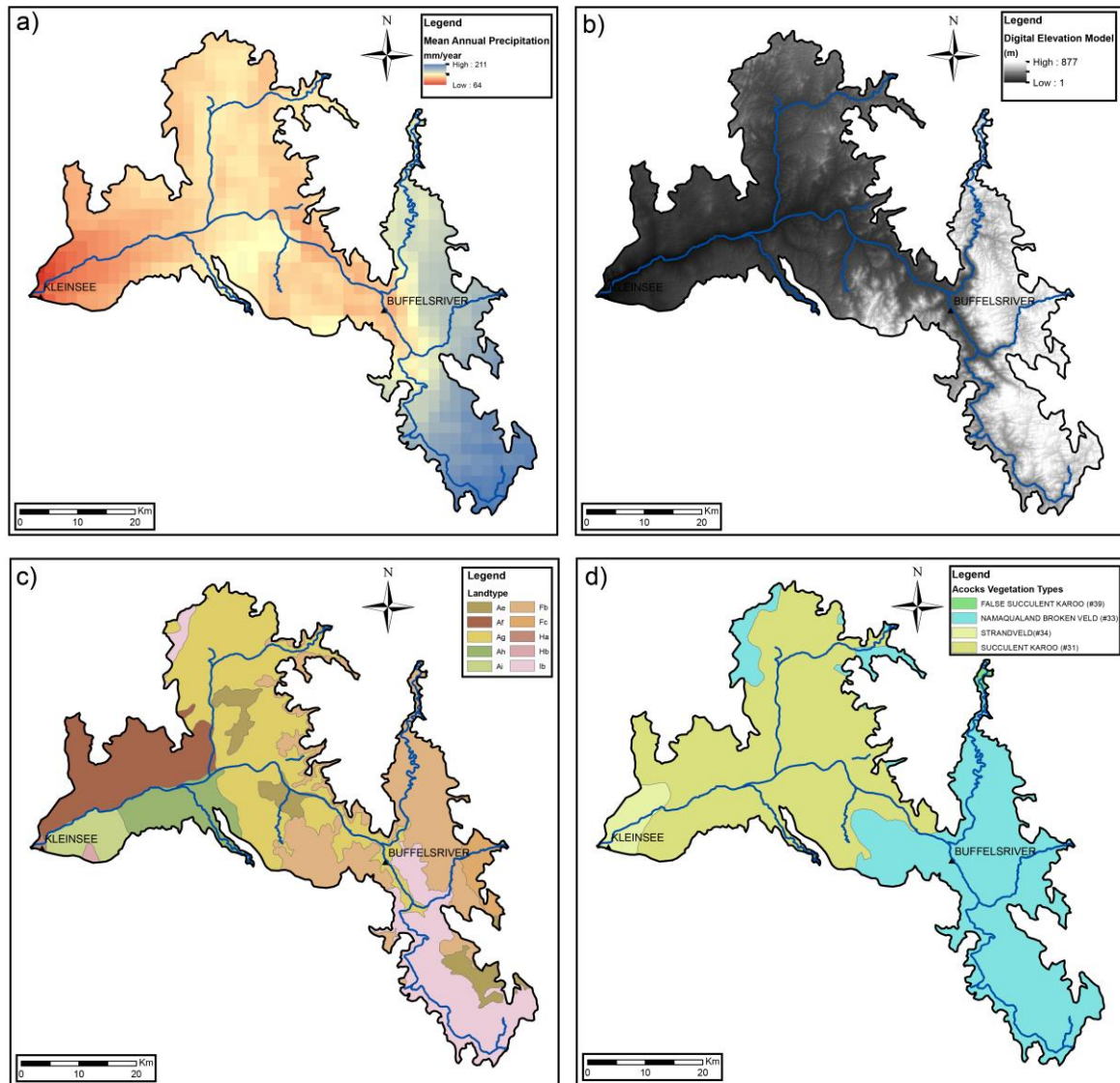
Figure 1.6: a) Mean annual precipitation map of the Buffels River catchment; b) Digital elevation of the Buffels River catchment; c) Land type of the Buffels River catchment; d) Vegetation types present in the Buffels River catchment (by Miller & Watson, 2018)*.*

Namaqualand is an area specifically vulnerable to climate change (Davis *et al.*, 2016). In their study, Davis *et al.* (2016) noted, through analysing weather station data, that there has been an increase in the occurrence of warm extremes, but a decrease in the occurrence of cold extremes. They also observed that warm spell duration significantly increased in certain areas, such as Springbok. Their research has shown that the average maximum and minimum temperatures in Namaqualand have been increasing at a rate of 0.11°C and 0.14°C respectively per decade between the years of 1901 and 2009, noting that the minimum temperatures have been increasing at a faster rate than the maximum

16

temperatures. Davis *et al.* (2016) also observed that the rate of warming has amplified over the last two decades. They did not, however, find clear evidence of a significant increase or decrease in rainfall over the area of Namaqualand in the past 30 years. An increase in temperature will cause more evaporative transport, causing the area to become even drier, even if there is no change in precipitation. This will certainly put pressure on the livestock in this area through heat stress, and it may also place pressure on other agricultural sectors, as it could cause an increase in certain pathogens and pests (Davis *et al.*, 2016).

1.3.4 Soil of Namaqualand

Namaqualand has soils typical to that of an arid environment (Francis *et al.*, 2007). The distribution of the main soil types in the area of interest consists mostly of deep yellow and red sandy soils, where the red sands furthest inland are the oldest (Francis *et al.*, 2007). The soils along the coast are mostly regic, grey calcerous sands (Cowling *et al.*, 1999). The materials underlying these soils are either rocks such as shale, granite, gneiss, and migmatites, or unconsolidated sands, normally strongly calcified and weathered (Singer *et al.*, 1995).

Many of the evaporate minerals, such as halite, gypsum, sepiolite, palygorskite, and calcite are also contained within these soils (Francis, 2019; Francis *et al.*, 2007; Francis & Poch, 2019). The sepiolite-bearing soils normally occur within the more calcareous soils, and are found in the coastal plains, starting from the Kleinzee-Hondeklip Bay area (Francis, 2019; Singer *et al.*, 1995). The palygorskite-bearing soils are abundant in calcareous, unconsolidated sands; these soils occur inland, following the Orange River eastwards (Francis, 2019).

The soils of Namaqualand have been shown to modify water infiltrability, often exhibiting crust formation at the pedoderm – a thin soil layer at the interface of the atmosphere which expresses certain properties much stronger than the remainder of the surface soil horizon (Fey *et al.*, 2006; Francis *et al.*, 2007).

A zone of closed hills and mountains with higher relief (1000 m amsl) is situated in this area of Namaqualand, where the plain of low relief has shallow soils that overlie a silica-cemented layer (Francis *et al.*, 2007). Arid environments are known to have cemented soil horizons due to intense evaporation (Francis *et al.*, 2007; Singer *et al.*, 1995). Along

with the alkaline conditions present, localised precipitation of calcium, silica, and magnesium solutes occurs, either in combination with carbonates, sulphates, and sepiolite, or alone (Francis *et al.*, 2007). This precipitation usually causes the formation of calcite or silica-cemented layers.

1.3.4.1 Calcium carbonate enriched horizons

Carbonate-cemented horizons can range from hardpan horizons to calcified nodules (Francis *et al.*, 2007). These horizons normally have high amounts of clay present, and are more common than the silica-cemented horizons (Francis *et al.*, 2007).

Calcium carbonate enriched horizons can be classified as being either petrocalcic or calcic horizons. Calcic horizons, on the other hand, are soft carbonate horizons that have an accumulation of non-cemented secondary carbonates and is usually present as calcium carbonate impregnation of the matrix, as fine (<1 mm) calcite particles, or various coatings, veins, nodules, etc. (Soil Survey Staff, 2015; WRB, 2014). Calcic accumulation usually occurs within parent material and subsurface horizons. If calcic horizons become indurated, petrocalcic horizons are formed, and usually occur as platy or massive structures (WRB, 2014). Petrocalcic horizons refer to the accumulation of continuously indurated or cemented secondary carbonates, or hard carbonate horizons (Soil Survey Staff, 2015; WRB, 2014). These horizons are either platy or non-platy (nodular or massive) calcium carbonate layers and is usually present as either petrified lamellar calcrete or just lamellar calcrete (Soil Survey Staff, 2015; WRB, 2014). Petrified lamellar calcrete normally consists of one or more very hard layers that are more cemented than lamellar calcrete and are pink to grey in colour (WRB, 2014). Lamellar calcrete, on the other hand, has layers varying in thickness, ranging from a few millimetres to centimetres, and are usually pink or white in colour (WRB, 2014).

1.3.4.2 Gypsum enriched horizons

In arid and semi-arid regions of the world, calcic and petrocalcic horizons are usually associated with gypsic and petrogypsic horizons if the groundwater is enriched in sulphate, or the soils contain sulphates (Soil Survey Staff, 2015; WRB, 2014). Gypsum could occur as either gypsic or petrogypsic horizons. Gypsic horizons have an accumulation of non-cemented, secondary gypsum, and could either be present as a surface or subsurface horizon (Soil Survey Staff, 2015; WRB, 2014). These horizons

normally occur as coatings, coarse crystals, nests, powdery accumulations, etc. (WRB, 2014). Petrogypsic horizons form when gypsic horizons become indurated, forming massive or platy structures (WRB, 2014)). These are root-restrictive subsoil horizons, as the accumulation of gypsum present within these horizons plug and cement the pores that were present in the soil with its lenticular gypsum crystals (Soil Survey Staff, 2015; WRB, 2014)

1.3.4.3   Silica cemented layers

There are two morphologically distinct silica-cemented horizons that occur in southern Africa. These are 'dorbank', as classified according to the South African system (Soil Classification Working Group, 1991; WRB, 2014) and 'silcretes.' Dorbank is equivalent to a 'petroduric' classification according to the WRB (2014), and to the 'duripan' of Soil Taxonomy (Soil Survey Staff, 2015). These dorbank layers can be defined as a layer that has an accumulation of secondary silica, which can either be indurated or continuously cemented (Clarke *et al.*, 2016; WRB, 2014)). It is usually reddish brown in colour, and air-dried fragments do not slake in water (WRB, 2014). Calcium carbonate is sometimes present as a secondary cementing agent (Clarke *et al.*, 2016; WRB, 2014). These horizons have a thickness greater than 1 cm and cannot be penetrated by roots in the cemented or indurated parts (WRB, 2014). It usually has a very firm consistency when moist and is very hard when dry (WRB, 2014).

Silcrete refers to a material indurated with silica (Milnes & Twidale, 1983). Silcrete is usually pale in colour, suggesting silica cementation and accumulation in sandy materials under hydromorphic conditions (Ellis & Lambrechts, 1994). It is very hard, has a massive structure, and is usually 1 – 2 m thick (Ellis & Lambrechts, 1994). Ellis & Lambrechts (1994) found that, in areas which contain both silcrete and dorbank, the silcrete normally occurs as cappings on old landscapes, while dorbank normally occurs on lower lying surfaces where erosion has occurred – hence, dorbank normally forms underneath the soil surface. Silcretes in South Africa are generally considered to be older, and commonly occur as cappings on deep kaolinitc weathering profiles in the coastal regions (Summerfield, 1983) with the silcretes typified by higher TiO_2 than dorbank as well as containing more SiO_2 and more crystalline forms of silica than the dorbank (Francis, 2012b; Summerfield, 1983).

19

The accumulation of Si in soil horizons occurs as a result of "silicification" (Sommer, Kaczorek, Kuzyakov & Breuer, 2006). This high concentration of Si could come from groundwater, weathering of dust, transport from higher elevation areas, or from the upper soil horizons (Sommer *et al.*, 2006). The areas mostly affected by an increase in Si are usually areas experiencing drought (Sommer *et al.*, 2006), or semi-arid and arid regions, such as in the Northern Cape. It is assumed that most of the Si that forms the silica-cemented duripans is as a result of leaching of primary Si from the upper horizons, with the Si becoming hardened in the lower layers during dry seasons (Kendrick *et al.*, 2006). The dorbank layers are mostly present in the interheuweltjie soils, not so much within the heuweltjies themselves (Francis & Poch, 2019).

1.3.5 Vegetation of Namaqualand

Namaqualand's vegetation is dominated by the Succulent Karoo and Nama-Karoo biomes (see Fig. 1.6d; Kunz *et al.*, 2012). The Succulent Karoo biome, along with the Fynbos Biome, have been categorised as belonging to the Greater Cape Floristic Kingdom (Luther-Mosebach *et al.*, 2012). The Succulent Karoo Biome has been recognised for its uniqueness, and is considered as the only fully arid ecoregion amongst 25 biodiversity hotspots globally, hosting approximately 5000 vascular species of plants, 40% of which are endemics (Cowling *et al.*, 1999; Luther-Mosebach *et al.*, 2012). Succulents are very dominant in Namaqualand's flora (Cowling *et al.*, 1999), and hold 40% of this plant species, specifically in the Succulent Karoo Biome (Luther-Mosebach *et al.*, 2012). The area also houses approximately 480 geophyte species (Cowling *et al.*, 1999). The Lowland Succulent Karoo is the most widespread and characteristic vegetation area in Namaqualand, mostly hosting dwarf leafy succulent members (Cowling *et al.*, 1999). Locally-endemic dwarf succulent shrub species in Namaqualand are mostly clustered together in rocky, broken habitats, and found less on weathered quartz veins and quartzites or loamy and sandy flats (Cowling *et al.*, 1999).

1.4 Soil chemistry

In this section, various soil chemistry methods of analysis, such as EC and ion profiling, will be presented. Information of calcite and gypsum accumulation in heuweltjies will also be discussed.

1.4.1 Electrical Conductivity

Electrical conductivity (EC) can be defined as a measurement of how easily an electrical current passes through water (Bui, 2013). Physicochemical soil properties that influence soil EC include soil texture, water content, bulk density, soil salinity, saturation percentage, subsoil characteristics, cation exchange capacity, organic matter content, and temperature (Corwin & Lesch, 2005; Grisso *et al.*, 2009; Ma *et al.*, 2011). In saline soils, most of the variation in EC is as a result of salts present within the soil (Sudduth *et al.*, 2017). Soil salinity is defined as soils with an EC greater than 4 dS m^{-1} measured at 25 °C (Bui, 2013). It can suggest the presence of sulphates, chlorides, nitrates, and bicarbonates of calcium, potassium, sodium, and magnesium (Bui, 2013; He *et al.*, 2012). Saline soils generally have a certain horizon chemistry (Bui, 2013), and so analysing the EC of the soil horizons could be beneficial in determining whether or not the salts are moving down the soil horizons.

1.4.2 Ion profiling

1.4.2.1 *Chloride*

Solute profiles of the UZ can provide vital information on how groundwater is being recharged by using tracers, such as chloride (Cl$^-$) (Huang *et al.*, 2016; Johnston, 1987). As salts are not always evenly distributed throughout the soil profile, it is beneficial to have a Cl$^-$ profile of the heuweltjies to determine if the salts are contributing to groundwater salinity (Daliakopoulos *et al.*, 2016; Huber *et al.*, 2008). Analysing the Cl$^-$ profile will give insight into how the groundwater is recharged, but also in the amount of salts leaching down to the groundwater (Daliakopoulos *et al.*, 2016; Huber *et al.*, 2008). If the chloride concentration is shown to increase down the soil profile, this may indicate that the salts are transferred to the groundwater via leaching or other pathways.

1.4.2.2   Sulphate

Sulphur (S) is found in organic and inorganic forms within soils (Tabatabai, 1987). It originates from various anthropogenic and natural sources as either particulate, gaseous, or solution forms (Edwards *et al.*, 1992). Atmospheric S inputs are either from direct dry deposition, or wet deposition (Edwards *et al.*, 1992). Although there are many forms of S in the biosphere, sulphate (SO_4^{2-}) has received a lot of attention due to its mobility, precipitation reactions, availability to microorganisms and plants, and specifically due to its reactivity with positively charged soil surfaces (Tabatabai, 1987). Sulphate usually occurs as water-soluble salts, insoluble forms, or adsorbed by soil colloids (Tabatabai, 1987). SO_4^{2-} transport within soil profiles depend on its concentration within the soil solution, movement, pattern of water movement within the soils, and its reaction with the solid phase components (Tabatabai, 1987). When monovalent cations, such as potassium (K^+) and sodium (Na^+), are in abundance, leaching loss of SO_4^{2-} is great (Tabatabai, 1987).

The ability of soils to adsorb SO_4^{2-} depends on its pH, clay content, the associated cation, and the nature of the clay minerals, as well as the amount of Fe and Al oxides present (Martinez *et al.*, 1998; Tabatabai, 1987). Sulphate adsorption is usually more dominant within subsoil horizons as there is normally more clay, along with Al and Fe oxides (Tabatabai, 1987). Sulphates also favour adsorption within soils that have a lower pH (Tabatabai, 1987). If waters within soils have relatively high concentrations of SO_4^{2-} and calcium (Ca^{2+}), gypsum precipitates (Papadopoulos, 1984).

1.4.2.3   Dissolved silica

Silicon, the second-most ample element in earth's crust (28.8%), is one of the basic components of almost all soils, as it is found in most parent materials (Eby, 2004:214; Sommer *et al.,* 2006). Silica (Si) occurs mostly in the form of crystalline silicates including feldspar, quartz, plagioclase, clay minerals, orthoclase, and amorphous silica (Clarke, 2003; Saccone *et al.*, 2006; Georgiadis *et al.*, 2013). It plays a crucial role in biogeochemical processes, as it regulates atmospheric carbon dioxide, buffers against soil acidification, and is a nutrient for terrestrial and marine biota (Derry *et al.*, 2005; Georgiadis *et al.*, 2014).

The flux of Si in soils is mainly through water, with silicic acid ($H_4SiO_4^0$) being its main component in soil solutions in the form of monomeric silicic acid at lower pH (Sommer *et al.*, 2006). The most important factors affecting Si concentrations in soil solution are weathering, parent material, temperature, stage of soil development, dissolution of silicate minerals, pore water residence time, temperature, biochemical activity, and depth (Derry *et al.*, 2005; Georgiadis *et al.*, 2013; Sommer *et al.,* 2006). The concentration of Si in soil solution normally varies from 0.4 and 2000 µmol L^{-1} (Georgiadis *et al.*, 2013; Sommer *et al.*, 2006). Soluble silica concentrations in silica-water systems are pH independent below a pH of 9 – however, there is usually an increase in soluble silica at a pH greater than 9, where silicic acid starts deprotonating (Georgiadis *et al.*, 2013; Jones & Handreck, 1963; McKeague & Cline, 1963; Milnes & Twidale, 1983). As the flux of Si in soils is mainly through water, this may aid in determining if the water is moving into the heuweltjies through the groundwater system, or if the waters within the heuweltjie are moving into the groundwater. As heuweltjies have an increased silica content with respect to other soils (Francis *et al.*, 2007), this indicates that there is more movement of water within the heuweltjies. Determining movement of silica could determine the movement of other ions within the heuweltjies as well, as water movement is expected to be higher where silica concentrations are higher. The flux of dissolved Si in soils could also aid in determining whether silicate grain dissolution occurs as a result of pressure that is generated by crystallization of calcite (Singer *et al.*, 1995). If this is the case, then calcite should be present and mostly saturated within the heuweltjie structure.

1.4.3   Gypsum and calcite accumulation within heuweltjies.

Having soils containing both calcium carbonate and gypsum is very beneficial in determining the movement of water within the soil. If gypsum precipitates at a greater depth than calcium carbonate within the soil profile, then the dominant water movement is downwards (Casby-Horton *et al.*, 2015). If the opposite is true, then the water movement is upwards through capillary action (Casby-Horton *et al.*, 2015). Determining which is above which within the heuweltjies will help in determining the source of salts within the heuweltjies by showing the direction of water movement.

1.4.3.1 Gypsum

Gypsum is the most abundant sulphate mineral found in soils, and is most abundant in arid and semi-arid regions of the world (Casby-Horton *et al.*, 2015). Gypsum-rich soils are commonly found in lower landscape regions, such as valleys, where shallow groundwater or runoff contains Ca^{2+} and SO_4^{2-} ions (Casby-Horton *et al.*, 2015). The presence of gypsum imparts specific properties to soils that affect its development and soil morphology (Casby-Horton *et al.*, 2015). These include water and nutrient availability to plants, water-holding capacity, soil texture, and root growth. Under normal conditions, gypsum is somewhat water soluble (Casby-Horton *et al.*, 2015; Papadopoulos, 1984). Papadopoulos (1984) found that the precipitation of gypsum is harmful to soil and plants, as there is an increased concentration of salts in soil solution, especially of halite. This occurs due to an increase in the solutions ionic strength and its ion pair formation (Papadopoulos, 1984). Therefore, if high concentrations of gypsum are present within the heuweltjie, then high concentrations of halite are also expected.

1.4.3.2 Calcite

Inorganic carbonates within soils predominantly take place in the forms of dolomite and calcite, with calcite being most abundant in soils (Loeppert & Suarez, 1996). Carbonates are mostly present in neutral to alkaline soils and occur as nodules in some acidic soils (Loeppert & Suarez, 1996). Calcic horizons are secondary horizons that form as a result of calcium carbonate ($CaCO_3$) (WRB, 2014). It is mostly present within subsoil horizons, in surface horizons, or parent materials (WRB, 2014). It exists in coarse-clay and fine-silt particle size fractions (Loeppert & Suarez, 1996). Calcite in arid soils has long been viewed as an inorganic process, resulting when dissolved $CaCO_3$ crystalizes when the soil dries (Fauriel & Laloui, 2012; Monger *et al.*, 1991). However, more recent studies have shown that microorganisms play a significant role in calcite precipitation in both paleosols and modern soils (Fauriel & Laloui, 2012; Francis & Poch, 2019; Monger *et al.*, 1991). Research has shown that calcite is present within heuweltjies due to an increased Ca^{2+} content within the soils compared to its surroundings (Francis *et al.*, 2012a; Francis & Poch, 2019). As the presence of calcite also increases the amount of salts within the soils (as it increases the EC of the soils), its occurrence within the heuweltjies could aid in the increased salinity compared to the interheuweltjie soils.

2 Methods and Materials

An outline of the methods followed for sample analyses can be seen in Figure 2.1. The project consisted of the selection of specific sampling sites, sampling procedures, and the analytical methods that followed sampling. In order to choose two heuweltjies for excavation, many heuweltjies had to be sampled and analysed to determine their salinity. Once the heuweltjies were chosen, they were excavated and sampled by collecting small samples (named the pH & EC samples in Figure 2.1) and larger detailed samples. The soils were brought back to the lab and analysed for pH, EC, soil texture, clay mineralogy, and various anions and cations. Once all data was obtained, it was processed and shown in a presentable manner.
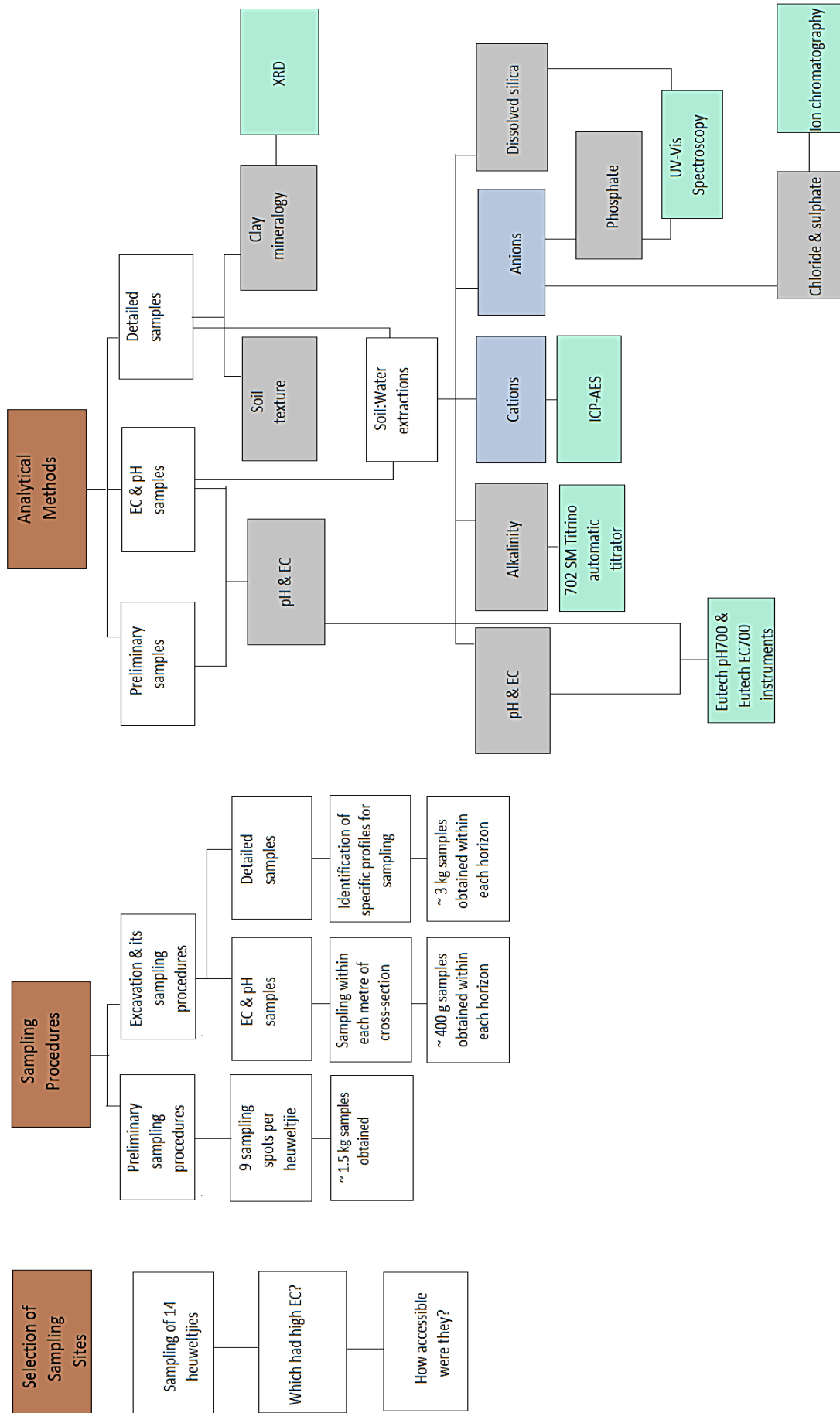
Figure 2.1: Simplified outline of methods followed.

26

2.1 Study site

The study site is situated in the Buffels River valley in the Northern Cape Province, approximately 43 km west of Springbok, near town of Buffelsrivier. Buffelsrivier is a small town, with roughly 3000 people living there (van Gend, 2018). Just outside of Buffelsrivier, there are many heuweltjies (see Figure 2.2). These heuweltjies have saline cores, and are thought to contribute to the saline groundwater in this area (van Gend, 2018). Since the Buffels River is dry on the surface, the only source of water for the people in this area is through use of groundwater resources. As a result, these resources have become depleted, with some of their boreholes running dry. The main employment opportunity for the people of Buffelsrivier is at the surrounding mines in the area. However, due to mining activities scaling down over the past few years, there has been a significant increase in unemployment for the people of Buffelsrivier (van Gend, 2018).
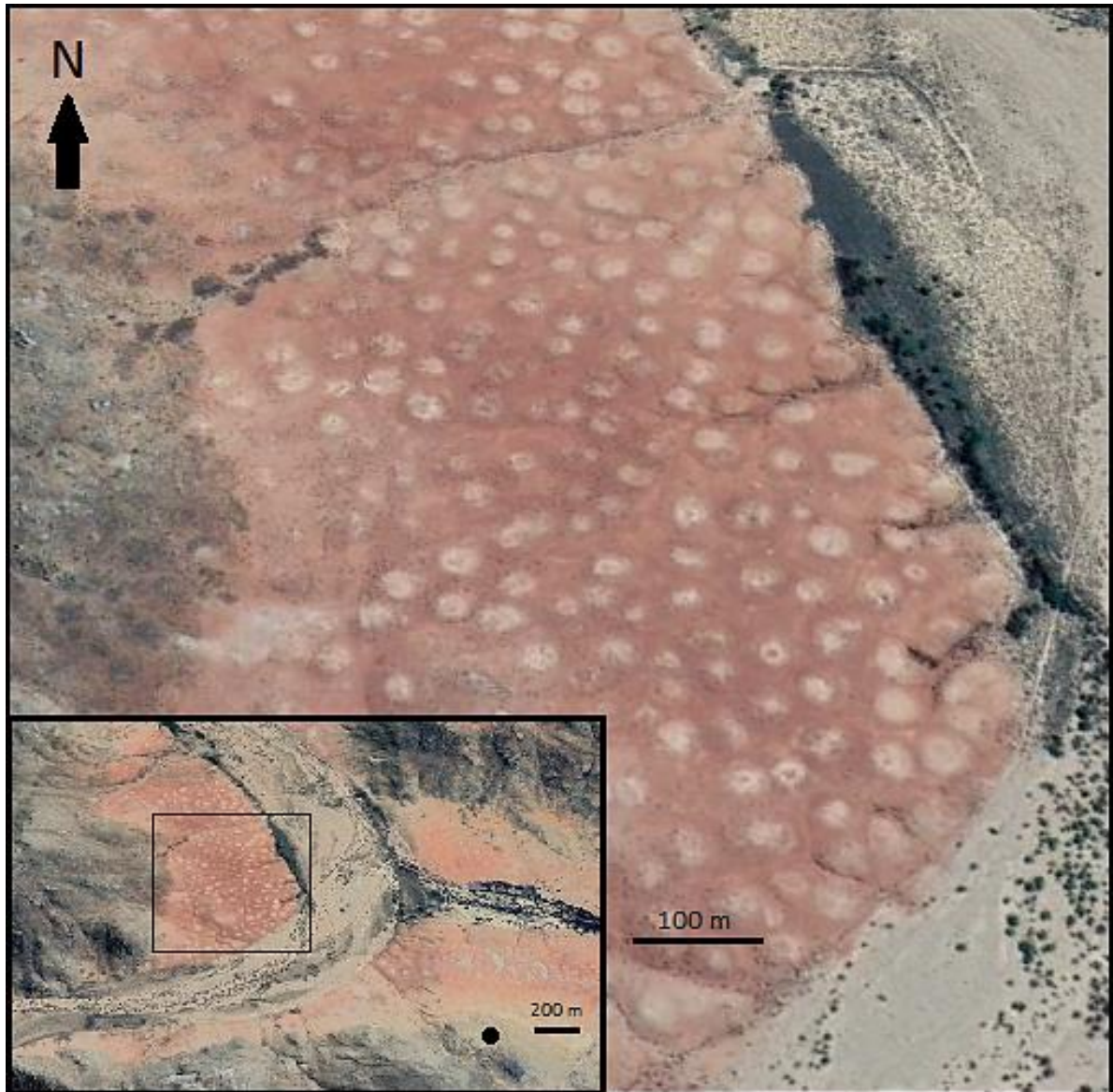
Figure 2.2:Google Earth Pro™ image of the heuweltjieveld situated just past the town of Buffelsrivier (black dot shows from where the picture in Figure 2.3 was taken from, aimed at the zoomed in heuweltjieveld in this image).

Figure 2.3: The Buffels River valley (Photo credit to Ruairi Walker).

2.2   Selection of sampling sites

In order to determine which heuweltjies would be suitable for excavation, two preliminary field studies were conducted. This preliminary data is part of a linked study on heuweltjies, and so is not reported within this study. However, the data collected from the linked study was used to determine which heuweltjies would be suitable for excavation. A total of 14 heuweltjies were sampled to determine which heuweltjies were most saline. The heuweltjies were located close to Buffelsrivier, Kommagas and on the way to Soebatsfontein. These areas were chosen for preliminary analysis as a result of previous studies that have found heuweltjies in the area to be saline. Once EC and pH values were obtained for the preliminary samples, a decision was made on which two heuweltjies would be excavated. Not only were EC values taken into consideration for the decision, but also the accessibility of the heuweltjies for the excavator, as it had to be transported to the site, adding to the cost of hiring the instrument. After all this information was taken into consideration, the two heuweltjies chosen for excavation were situated just past the town of Buffelsrivier. Those chosen for excavation from the linked study were heuweltjie 1 (BR01) and 4 (BR04), as highlighted red in Figure 2.4. These heuweltjies will from hereon be called H1 and H4 respectively.
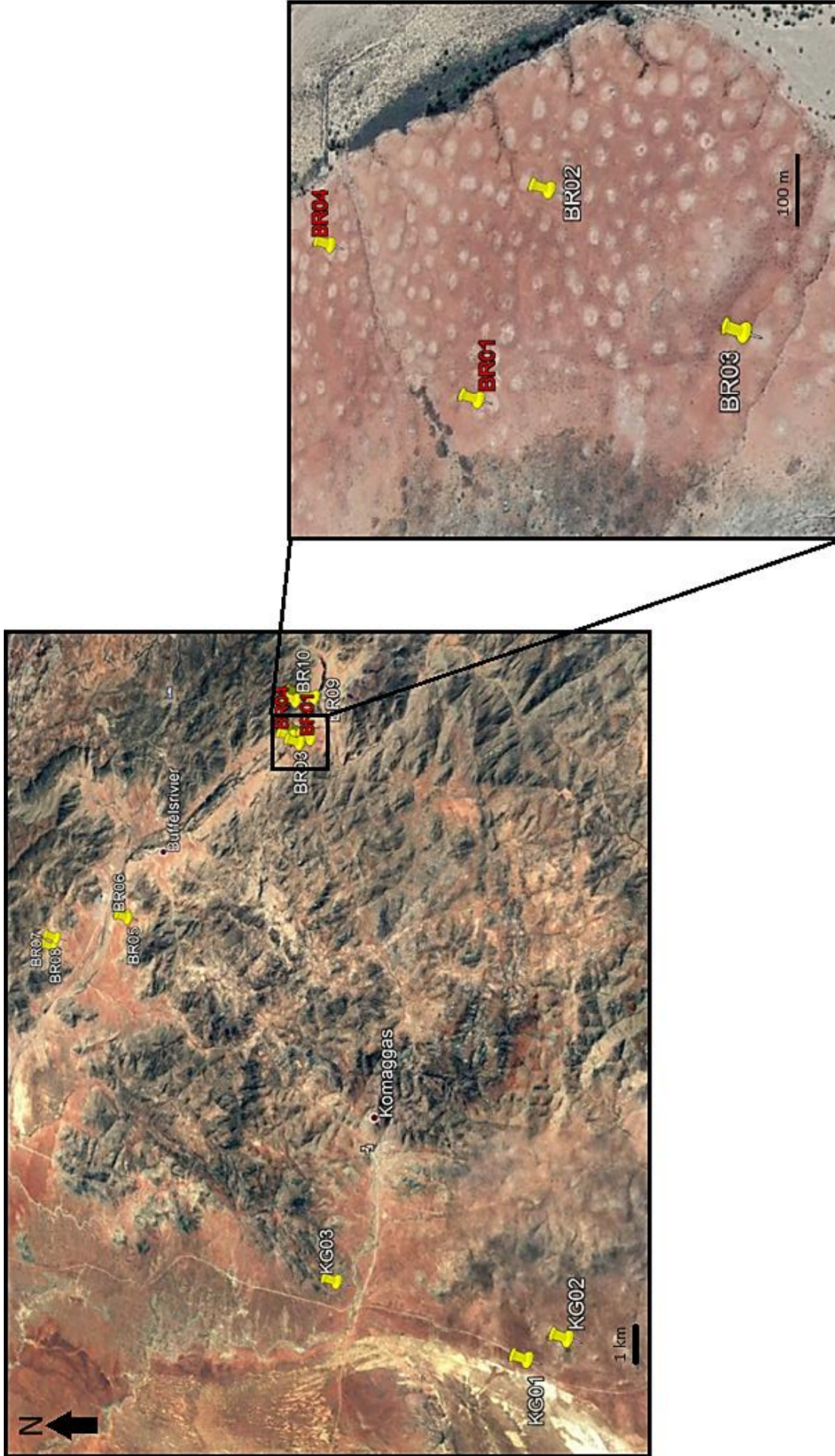
Figure 2.4: Google Earth Pro™ image showing locations of 14 heuweltjies sampled and specifying location of selected heuweltjies for excavation. BR1= H1; BR4 = H4 (Note: KG refers to the heuweltjies sampled close to Kommagas and on the way to Soebatsfontein, while BR refers to those sampled close to Buffelsrivier).

2.3 Sampling procedure

In the following section, the procedures followed for sampling of the heuweltjies, as well as how the samples were labelled, will be discussed.

2.3.1 Sampling of excavated heuweltjies

On the 11th of September 2018, the chosen heuweltjies were excavated with a 220 PC Komatsu excavator. This was done by digging a trench through the heuweltjies up to approximately 2 – 3 m deep, depending on how deep the excavator could go, as the dorbank layer hindered it from going deeper in certain areas. The two heuweltjies excavated were done so in an east to west direction, and a trench was also cut through from the middle of the heuweltjie to the south end (see Figure 2.5).
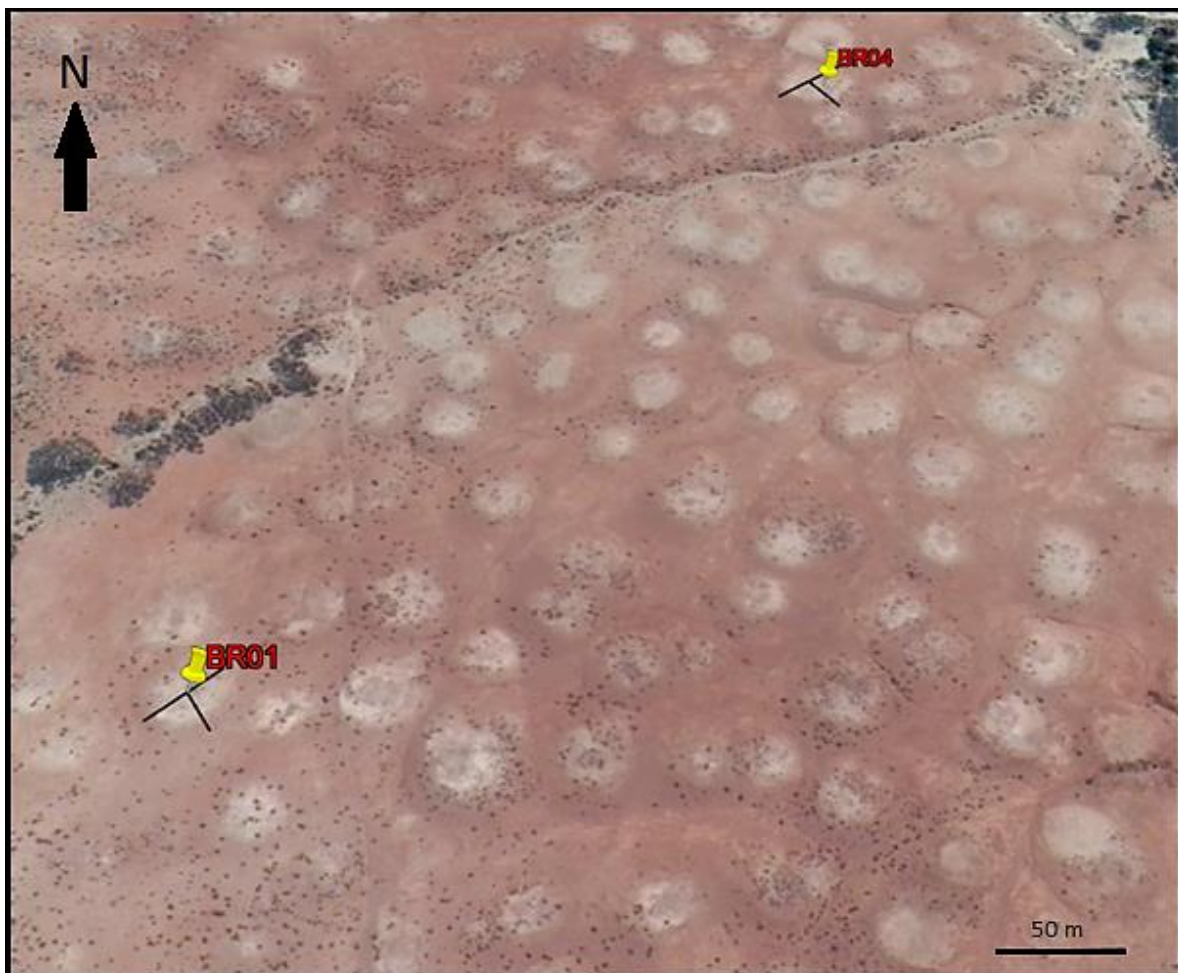
Figure 2.5: Google Earth Pro™ picture showing how heuweltjies were excavated. BR01= H1; BR04= H4.

31

A part of the interheuweltjie on the sides was also excavated for comparison and to note any differences between the heuweltjie and interheuweltjie areas. The interheuweltjie areas could not be excavated as deep as the heuweltjie itself, however, as a result of the hard dorbank layer. From the 12th to the 16th of September, detailed sampling and analysis of the heuweltjie faces took place. Samples were taken for EC within each meter of the heuweltjie and interheuweltjie cross section (1 – 58 m) in a west to east direction on the north wall. Samples were collected within each soil horizon, and subsequently 1 to 6 soil samples were obtained, depending on how deep the heuweltjie was excavated at the cross section. Approximately 100 to 400 g of soil was collected for each soil sample, depending on accessibility, as some of the horizons had hard carbonate or silica cemented soils which were more difficult to sample. These samples were placed in individual labelled plastic bags and then placed in larger bags to ensure no contamination or sample spillage. For H1, 203 samples were obtained, while for H4, 179 samples.

Figure 2.6: A) Excavation of H1; B) Perspective from inside of H1.

Detailed sampling was executed within each heuweltjie in selected profiles by taking bulk samples of up to 3 kg of sediment within depth ranges of the profile and placing the bags into second labelled bags to ensure no contamination took place. Pictures were taken of each detailed profile (as seen in Figure 2.7) and soil texture, soil type, and soil colour were

determined in the field for each horizon of the profile (all detailed soil profile descriptions can be seen in section 3.1). Colour classification was completed in the field by use of a Munsell colour chart. Detailed samples were also taken in the interheuweltjie area for comparison to the heuweltjie samples. Bioturbation and preferential flow pathways were sampled and analysed where visible in the heuweltjies to see if the salt content within the termite burrows was higher than outside the burrows. Dorbank was collected at the edges of the interheuweltjie area of H4 by use of a pickaxe.
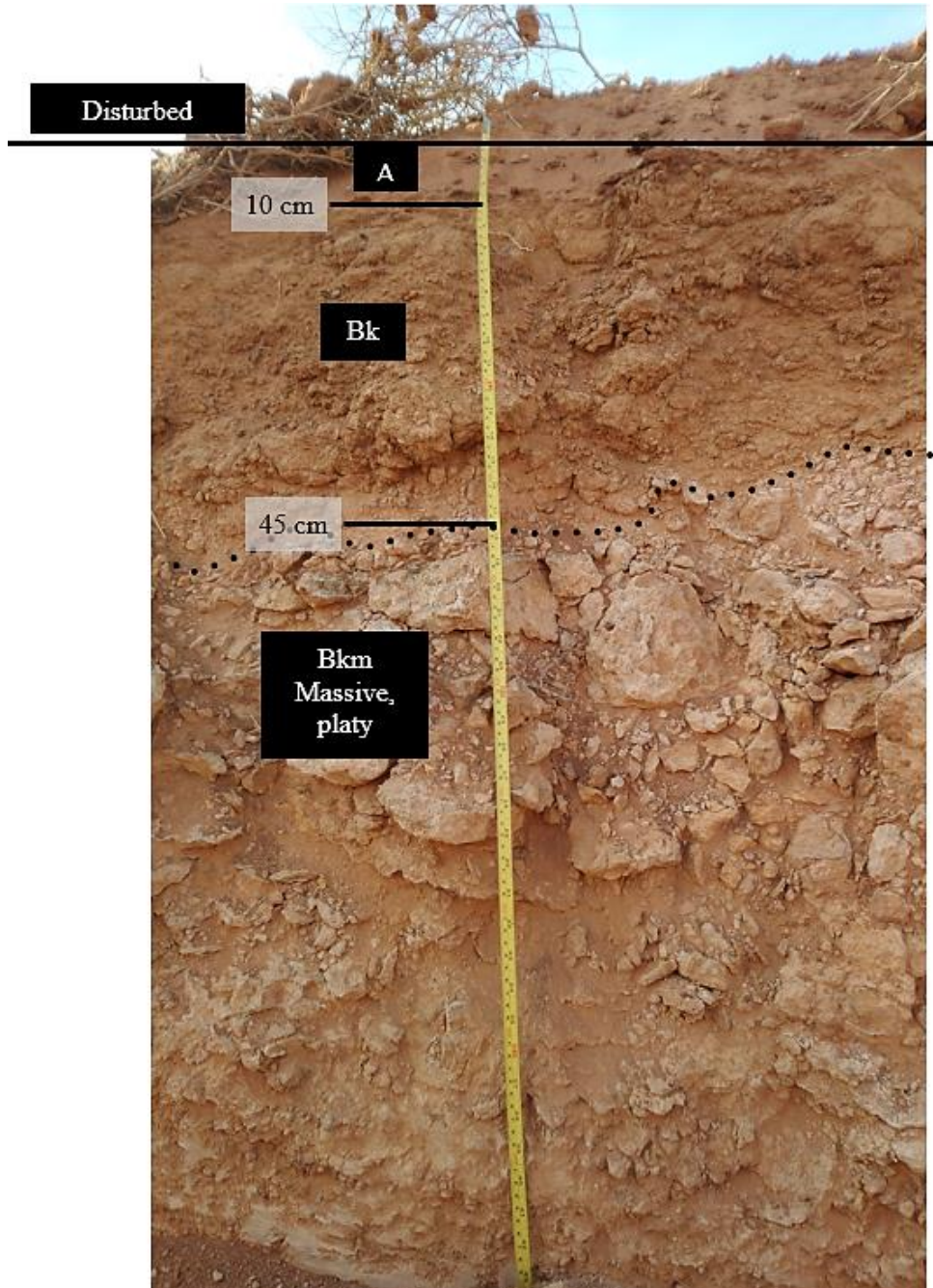
Figure 2.7: Detailed profile outline for H1-12. Bk: carbonate accumulation; Bkm: carbonate cementation.

33

2.3.2 Sample labelling

The samples obtained were labelled in a specific manner. All sample numbers go by the following outline:

$$HX\text{-}Y\text{-}Z \qquad (2.1)$$

where HX refers to which specific heuweltjie the sample is taken from and can be either H1 or H4; Y is the cross section distance from the west end of the heuweltjie, in metres, at which the sample was taken (1 – 58 m), and Z refers to the depth, in cm, down the specific sediment profile at that point. For example, if a sample was taken for H1 at a cross section distance of 4 m and a depth of 30 cm, the sample is called H1-4-30. If only HX-Y is mentioned, with no Z, this refers to the entire soil profile at that distance from the west end.

2.4 Analysis techniques

All samples obtained in the field were returned to Stellenbosch University, where they were processed. The analyses done on the samples were pH, EC, particle size, clay mineralogy, anions, cations, and dissolved silica.

2.4.1 Soil pH and EC

Samples were air-dried and carefully crushed with a mortar and pestle to ensure that no hard calcrete and dorbank fragments remained. Samples were sieved using a 2 mm sieve. pH and EC measurements were performed for all samples specifically collected for such analyses from excavation.

Methods of analysing EC include saturated paste extract (EC_e) and electrical conductivity in soil solution (EC_w) at various soil: water ratios. These ratios include 1:1, 1:2, 1:2.5, 1:5, and 1:10 (Aboukila & Norton, 2017; He *et al.*, 2012; Sonmez *et al.*, 2008). EC_w measurements are advantageous as they require less labour and are more rapid (Sonmez *et al.*, 2008). However, EC_w is only useful when the objective is to analyse the relative changes (Aboukila & Norton, 2017). If absolute solute content is required, EC_e is better to use (Aboukila & Norton, 2017). Conversely, highly significant ($p<0.001$) relationships have been found between EC_e and $EC_{1:1}$ (Zhang *et al.*, 2005). Additionally, when pH is measured in the lab, it is analysed in a 1:2.5 soil: water ratio (Sonmez *et al.*, 2008).

34

As relative changes were the goal for EC measurements, EC_w was measured in a 1:5 soil: deionised water ratio. pH measurements were also done in a 1:5 soil: deionised water ratio. EC_w and pH were determined by adding 50 mL of water to 10 g air-dried soil samples (1:5 soil: deionised water), shaken on the shaker for 30 minutes, left to stand for 30 minutes, and then analysed by means of a Eutech CON700 probe and a Eutech pH700 probe for EC_w and pH respectively (Sonmez *et al.*, 2008).

2.4.2   Soil texture

For soil texture analysis, 33 detailed samples were chosen. The indurated samples were all crushed with a mortar and pestle and sieved, and the procedure outlined in Soil Classification Working Group (1991) was followed. Carbonates were removed using a 1 M sodium acetate (NaOAc) solution corrected to a pH of 5. Aliquots of NaOAc were added, the samples shaken and allowed to stand, centrifuged, and again added until no more fizzing occurred in the samples. Silica was removed by adding 0.1 M sodium hydroxide (NaOH) solution. Organic matter (OM) was also removed from the samples using hydrogen peroxide (H_2O_2). The soil samples were placed in 250 mL Erlenmeyer flasks and placed in a hot bath, where the H_2O_2 was added to the samples. As the samples did not contain a lot of iron, it was not removed, especially since the clay in these samples would also be used for mineralogy via x-ray diffraction (XRD). If iron were removed, these samples would not have been suitable for such analyses (Soil Classification Working Group, 1991).

Once all organic matter had been removed, the samples were dried and then placed in a blender with Calgon solution (sodium hexametaphosphate) to disperse the soil particles. The dispersed suspension was placed into 1000 mL measuring cylinders after being passed through a 0.053 mm sieve. The sand fractions were placed into a petri dish and dried in the oven. Once the temperature of the soil solution in the measuring cylinder had stabilized, the temperature was measured, the samples shaken, and silt and clay were measured by sedimentation rate according to the temperature of the solution. Sand fractions were sieved using 0.5 mm, 0.25 mm, 0.106 mm, and 0.053 mm sieves. From all the data obtained, the equations outlined below were used to determine texture types (Soil Classification Working Group, 1991):

Sand fractions:

$$\text{Sieved fractions (\%)} = \frac{D \; x \; 100}{E} \qquad (2.2)$$

Silt and clay fractions:

$$\text{Percent fine silt and clay (F)} = \frac{(A-C) \; x \; 1000 \; x \; 100}{E \; x \; 25} \qquad (2.3)$$

$$\text{Percent clay (G)} = \frac{(B-C) \; x \; 1000 \; x \; 100}{E \; x \; 25} \qquad (2.4)$$

$$\text{Percent fine silt = F} - \text{G} \qquad (2.5)$$

$$\text{Percent coarse silt = 100} - \text{sum of sand fractions} - \text{F} \qquad (2.6)$$

where A is the mass (g) of the pipetted clay and fine silt, B is the mass (g) of pipetted clay, C is the mass correction for the dispersing agent (0.011g), D is the mass (g) of the sand fraction obtained on the sieve, and E is the mass of the pre-treated oven dried total sample (Soil Classification Working Group, 1991).

2.4.3 Clay mineralogy

Once soil texture analysis was completed, the same soil solutions in the measuring cylinders were used to obtain clay for mineralogy. This was done by collecting the top 200 mL from the measuring cylinders in a separate glass beaker approximately 8 hours after it was shaken. The measuring cylinders were refilled with 200 mL of deionised water and shaken again. A second aliquot of 200 mL of the clay containing solution (top 200 mL) was collected from the measuring cylinder after another 8 hours. This procedure was performed roughly 7-8 times per sample to ensure that enough clay was obtained to use for mineralogy. The samples were suction filtered, where the clay was caught on ceramic discs while the water passed through. Each sample was split in two, and one was washed with 1 M magnesium chloride ($MgCl_2$) solution and the other with 2 M potassium chloride (KCl) solution. The samples were washed with deionised water and dried in the oven to remove excess water and placed in small brown bags to be sent to iThemba LABS for analyses. XRD analysis was done with a step-size of 0.05 degrees and a step-time of 40 seconds using a Bruker D8 Advance Powder Diffractometer with a graphite monochromator, 40 mA and 40kV, as outlined by Francis *et al.* (2012a).

Once the data was obtained and graphs plotted for each soil horizon, maximum peak values were converted to nm and identified according to which mineral was present at that specific wavelength. Peaks were identified by assigning specific nm to each mineral. If minerals were not present in the lower ° 2theta range, then they were not expected to occur at higher ranges. Initial gypsum peaks were identified at 0.75 nm, while calcium oxalate was identified at 0.60 nm. Initial illite and kaolinite peaks were identified at 1.00 nm and 0.70 nm respectively, while quartz and calcite's initial peaks were identified at 0.43 nm and 0.30 nm respectively. Hydroxyapatite's initial peak was identified at 0.334 nm, albite at 0.40 nm, and microcline at 0.35 nm.

2.4.4 Anions, cations, and dissolved silica

The aim for the analysis of anions, cations, and dissolved silica was to determine whether rainwater has filtered through the heuweltjies to the groundwater, taking with it dissolved salts. Therefore, analysis of 1:1 soil-water extracts were performed, to indicate what the composition of the water would be once it comes into contact with the soil horizons. All these analyses were done on water soluble solutions.

All detailed samples were selected for anion and cation analyses, along with smaller samples spread throughout both heuweltjies which were initially obtained for EC and pH measurements. Samples were selected throughout both heuweltjies to ensure that at least every second or third metre within the heuweltjie would have data for the anion and cation analyses, amounting to 187 samples. Depending on sample size, 100 g or 150 g of soil was taken from each sample, and 100 mL or 150 mL of deionised water was added respectively, as the procedure was done in a 1:1 ratio. The samples were shaken in plastic bottles, as glass could cause the possibility of the silica analyses to be influenced. The samples were shaken for an hour, as outlined by Rhoades (1996), and extracted through suction filtration with Buchner funnels, collecting the water in plastic containers. The samples were further filtered with 0.45 μm cellulose acetate filters. As many samples did not have enough solution for all analyses that were to be performed on them, all filtered samples were diluted further in a 1:1 soil water: deionised water ratio by volume. Once all data was obtained, values were multiplied by two to correct for the dilution factor.

Samples were transferred to conical polypropylene tubes for later analysis of anions and cations, as well as other 50 mL plastic bottles for alkalinity, pH, EC, phosphate, and

dissolved silica analyses. Samples were kept in the fridge at all times, except when analysed. For Cl^- and SO_4^{2-}, samples were analysed via ion chromatography at Integral Laboratories, while cations were analysed via ICP-AES at Stellenbosch University's Central Analytical Facility (CAF). Cation samples were acidified before analysis.

2.4.4.1 Alkalinity, pH, and EC

All samples were analysed for alkalinity using a 702 SM Titrino automatic titrator. 10 mL of sample was titrated with a standard 0.01M HCl solution. The equation used to determine alkalinity was as follows:

$$Alkalinity\ (mg \cdot L^{-1}) = \frac{N_{acid} \times V_{acid}(mL)}{V_{sample}(mL)} \times equivalent\ weight\ of\ CaCO_3 \times 1000 \quad (2.7)$$

Where N_{acid} is the normality of the acid, V_{acid} is the volume of the acid in mL and V_{sample} is the volume of the sample. pH and EC of each sample was also taken along with alkalinity measurements. Alkalinity and EC values were multiplied by 2 to correct for the dilution factor, introducing a small amount of error to the alkalinity values.

2.4.4.2 Phosphate analysis

Water soluble phosphates were analysed using the procedure outlined by Murphy & Riley (1962). A stock phosphate solution was prepared from potassium dihydrogen phosphate, and standards of 0.2, 0.3, 0.5, 0.7, and 1 mg·L⁻¹ were prepared to create a calibration curve for obtaining the unknown concentrations. A mixed reagent was prepared by adding 5 N sulphuric acid, ammonium molybdate, ascorbic acid, and potassium antimonyl tartrate solutions together. 8 mL of the mixed reagent was added to 40 mL of the extracted water sample and filled up to 50 mL with distilled water. The samples were measured with the Jenway 7315 Spectrophotometer within 10 minutes of adding the mixed reagent. The mixed reagent was added to the standards and unknowns to produce the blue colour for analysis. All unknown absorbance values were obtained at a wavelength of 882 nm, as outlined by Murphy & Riley (1962). A graph of absorbance vs. concentration was created for the standards, and the equation for the line of best fit (forced through zero) was used to calculate the unknown concentrations of the samples (lowest limit of detection was an absorbance of 0.007). As 40 mL of sample was added to a 50 mL (±0.5 mL) solution, corrections had to be made to obtain actual phosphate concentrations. As a result, it was multiplied by 1.25 (4:5 ratio).

2.4.4.3   Dissolved silica analysis

Dissolved silica was analysed using two different methods. The measurements were performed on the water extractions which were also used for ion analyses, and as stated in section 1.4.2.3, dissolved silica is usually in the form of monomeric silicic acid (Georgiadis *et al.*, 2013). All solutions were prepared using plastic ware. Standards were created using the method outlined by Yang *et al.* (2015) for soluble silica. A silica stock solution was prepared using sodium metasilicate. From this, 5 standards were made, consisting of 0.2, 0.6, 1.0, 1.4, and 1.8 mg·L^{-1} silica. This was done by initially adding 10 mL of deionised water and 10 mL of hydrochloric acid (HCl) to the solutions, placing it in a water bath at 25°C, and once the reaction was complete, adding 20 mL of 0.5 M boric acid. After adjusting the pH to 1.4, 10 mL of absolute ethyl alcohol and 15 mL of 5% m/v ammonium molybdate were added. Once 20 minutes had passed, 10 mL of oxalic-tartaric acid (0.5 M-0.5 M) and 5 mL of 2% m/v ascorbic acid were added. The colour began changing, and the standards analysed at 812 nm, using the Jenway 7315 Spectrophotometer. A solution without the stock Si solution was also made and analysed. The standard absorbance values were subtracted from this value, and so the standard curve (with lowest detection limit of an absorbance of 0.165 for the solution without stock Si) was created, forcing the line through zero.

For analysing the unknowns, the method outlined by Jones & Dreher (1996) was followed. The solutions prepared to add to the unknowns were 0.5 M sulphuric acid (H_2SO_4), ammonium molybdate, 20% m/v tartaric acid, and a reducing solution consisting of sodium bisulphite, sodium sulphite, and 1-amino-2-naphthol-4-sulfonic acid. 10 mL of both H_2SO_4 and ammonium molybdate were added to 1 mL of unknown, and after approximately two minutes, 5 mL of both tartaric acid and the reducing solution were added. The colour changed, and the samples were analysed within 30 minutes. Scans were done at 812 and 820 nm, and the highest peaks were found at 812 nm. As a result, all absorbance values at 812 nm were used. Unknown concentrations were obtained using the standard curve created.

2.5   Data processing

In the following section, the data processing procedures for analysing ion activities, saturation indices, and heat maps are explained.

2.5.1   Ion activity and saturation index data analysis

Square brackets [ ] denote ion activities. In the law of mass action, activity refers to a measure of the effective concentration of a species, as opposed to the actual concentration (Appelo & Postma, 2005:123; Eby, 2004:30). It is a measure of how a species would behave in a real solution, while concentration is a measure of how a species would behave in an ideal solution (Atkins & De Paula, 2010:192; Eby, 2004:30). The activity of a species depends on the ionic strength of its medium (Skoog *et al.*, 2004:271). Ion activity is related to concentration through the activity coefficient:

$$\gamma_i = \frac{a_i}{m_i} \qquad (2.8)$$

where γ_i is the activity coefficient, a_i is activity, and m_i is concentration (Eby, 2004:31; (Skoog *et al.*, 2004:271). The activity coefficient measures the effectiveness at which a species influences the equilibrium in which it participates (Skoog *et al.*, 2004:272).

Saturation index (SI) is the log(IAP/K_{eq}) for a dissolution reaction, where IAP is the ion activity product, and K_{sp} is the equilibrium constant (Appelo & Postma, 2005:130; Eby, 2004:49). When SI=0 (IAP = K_{eq}), the mineral and solution are in equilibrium (Appelo & Postma, 2005:130). When the SI < 0, the solution is undersaturated; when SI > 0, it is supersaturated (Appelo & Postma, 2005:130).

All major anion and cation data obtained from section 2.4.4 were analysed using the computer program PHREEQC (Interactive Version 3.4.0) for speciation (activity) and saturation index (SI) data. PHREEQC is a computer program designed to execute a wide range of geochemical calculations for aqueous species (Parkhurst & Appelo, 2013). It determines the degrees of saturation for species in solution with respect to gas and mineral phases and calculates the partitioning of elements amongst aqueous species (Eby, 2004:47). PHREEQC was developed for calculating hydrogeochemistry of the 'real world,' and is used for modelling data (Appelo & Postma, 2005:135). It helps to gain a better understanding of how concentrations are being affected by various transport and

chemical processes (Appelo & Postma, 2005:135). PHREEQC is based on the equilibrium chemistry of aqueous solution interactions with gases, minerals, solid solutions, sorption surfaces, and exchangers (Parkhurst & Appelo, 2013).

According to the PHREEQC calculation for seawater by Nordstrom *et al.* (1979), seawater has an ionic strength of 0.67. Speciation calculations showed that the ionic strength ranged from 0.002 to 0.620, and hence all fell below that of the concentration for seawater. The 1:1 extractions correspond to the sodium chloride dominance criteria of PHREEQC. This therefore suggest that the additional Specific Ion Interaction (*sit.dat*) activity coefficient model was satisfactory for performing speciation calculations within the soils analysed. Solubility equations with their equilibrium constants for the major salts are displayed below (Table 2.1).

Table 2.1: Solubility equations and equilibrium constants for specific minerals analysed.

Mineral	Solubility equation	Equilibrium constant (K_{sp})
Calcite	$CaCO_3 = Ca^{2+} + CO_3^{2-}$	-8.45
Gypsum	$CaSO_4 \cdot 2H_2O = Ca^{2+} + SO_4^{2-} + 2H_2O$	-4.61
Halite	$NaCl = Na^+ + Cl^-$	1.58
Hydroxyapatite	$Ca_5OH(PO_4)_3 = 5Ca^{2+} + OH^- + 3PO_4^{3-}$	14.78
Quartz	$SiO_2 + 2H_2O = H_4SiO_4$	-3.79
Amorphous silica	$SiO_2 + 2H_2O = H_4SiO_4$	-2.74

Chloride, of the eight principal solutes dominating the chemistry of natural water, is mostly conserved over the widest concentration range (Eugster & Jones, 1979). This has to do with anion exchange being minor, and because Cl^- remains in solution until saturation of halite (Eugster & Jones, 1979). Saturation indices are numerical, and hence can be plotted against independent salinity variables (log activities; Francis, 2008). Therefore, SI's could be plotted against $\log[Cl^-]$.

Correlation coefficients were determined for each graph plotted to determine the correlation between the two variables. Pearson correlation coefficients were determined using Excel 2016, and p values were calculated using the regression analysis tool at a 5% confidence level.

41

2.5.2 Heat maps

Major ion data obtained in section 2.4.4, pH, EC, and SI values obtained in section 2.5.1 were plotted as heat maps. The objective for making heat maps was to visualize how the various ions and SI data are spread throughout the heuweltjie structures, to see if there is a trend in concentrations increasing downwards, and where the salts are undersaturated and saturated. A DSM 2 m box in ArcGIS was obtained from which to find the elevation data for the two heuweltjies excavated. Sampling points were plotted going down into both heuweltjies as cross sections. Once this was done, heat maps were created using Surfer®. All values were interpolated using Kriging, and linear variograms were created to determine which direction (i.e. diagonally, horizontally or vertically) had the best correlation.

SI plots were all made using the same scale of +4 to -10, in order to distinguish which salts were more saturated or undersaturated throughout the heuweltjie profiles. The scales for each separate ion analysed are not directly comparable with each other, although each separate ion is comparable within itself for both heuweltjies (for example, potassium has the same scale for both H1 and H4).

2.5.2.1 *Variograms*

Variograms are used to validate how good the spatial autocorrelation is within ArcGIS and Surfer®. The variograms for heat maps can display various prediction errors. Where there are no points within the heuweltjie structure, high prediction error would be present. However, towards the edges of the heuweltjie structures, there would not be any prediction error as that data would only be trailing from one direction. Interpolation of the concentrations and SI values throughout the heuweltjie could be poor due to the heuweltjies having so many different changes within soil horizons, and this cannot be accounted for specifically with the Kriging of the data.

All variograms created were fitted as linear correlations. The best fit was chosen for each separate heat map created, and variogram parameters for each can be seen in Table 2.2 and Table 2.3. R^2 values displayed are poor due to the non-continuity of the nature of the heuweltjie soils. An ideal fit linear model, as was depicted for H1's pH and EC variograms, are shown below (Figure 2.8).

42
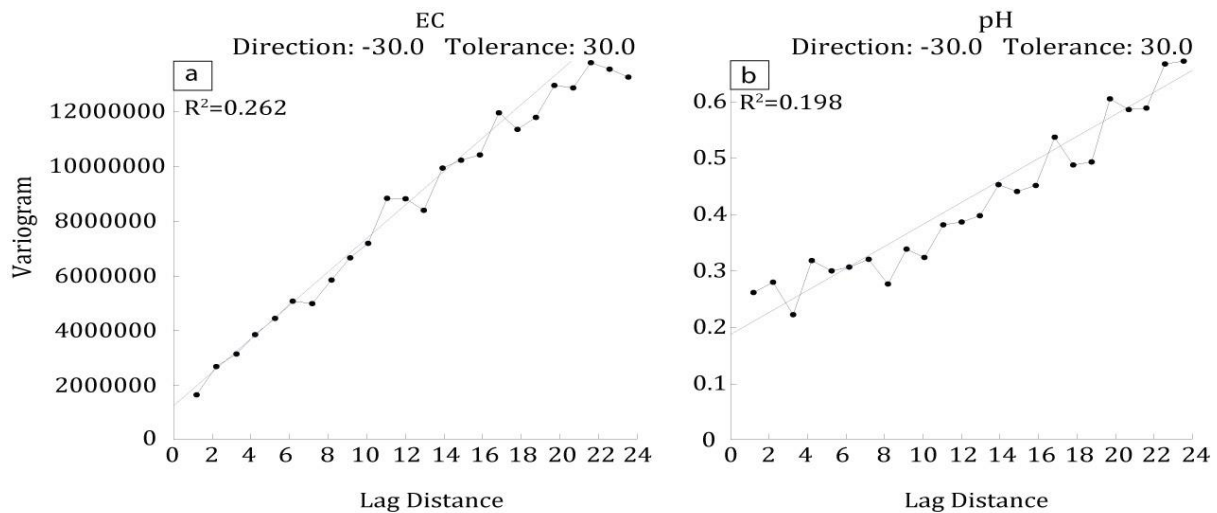
Figure 2.8: H1 variograms for EC (a) and pH (b).

2.5.2.1.1   Heuweltjie 1

EC had good correlation in all directions within H1, with its best correlation being diagonally. All data was mainly skewed to the left, with a normal distribution otherwise. pH had the best correlation diagonally, with some vertical and horizontal correlation as well. Values were normally distributed. Sodium had weak vertical correlation; however, in all other directions (diagonally and horizontally) correlation was fairly good, with horizontal being best. Data was mainly skewed to the left, with some spread throughout. Chloride's best correlation was found horizontally. Data was mainly skewed to the left. Sulphate had good horizontal and diagonal correlation. Data was slightly skewed to the left. Dissolved silica had the best correlation diagonally. Data was skewed to the left. Calcium had good diagonal correlation, with its best correlation being horizontally. Data was skewed to the left. Magnesium's correlation was best horizontally, with poor correlation otherwise. Data was skewed to the left. Potassium's correlation was best horizontally. Data was skewed to the left. Bicarbonate also had its best correlation horizontally. Data was skewed to the left. Amorphous silica had its best correlation diagonally. Data was evenly distributed. Hydroxyapatite had its best correlation diagonally. Data was skewed to the right, with some even distribution throughout. Gypsum had no vertical correlation; however, horizontal correlation was present. Data was skewed to the right. Calcite's correlation was best diagonally. Data was skewed to the right. Halite had no horizontal correlation; however, diagonal correlation was present. Data was mostly skewed to the right.

Table 2.2: Variogram data of H1 for all ion and SI data plotted as heat maps.

H1	Model Fit	Direction of best fit	Tolerance	R^2	Distribution (Skewness)
EC	Linear	-30.0	30.0	0.262	Left
pH	Linear	-30.0	30.0	0.198	Normal
Sodium	Linear	0.0	30.0	0.208	Left
Chloride	Linear	-90.0	30.0	0.160	Left
Sulphate	Linear	-90.0	30.0	0.386	Left
Dissolved Si	Linear	-30.0	30.0	0.220	Left
Calcium	Linear	0.0	30.0	0.197	Left
Magnesium	Linear	0.0	30.0	0.193	Left
Potassium	Linear	0.0	30.0	0.121	Left
Bicarbonate	Linear	0.0	30.0	0.087	Left
Amorphous Si	Linear	-60.0	30.0	0.251	Even distribution
Hydroxyapatite	Linear	-30.0	30.0	0.066	Right
Gypsum	Linear	-90.0	30.0	0.250	Right
Calcite	Linear	-60.0	30.0	0.138	Right
Halite	Linear	0.0	30.0	0.335	Right

2.5.2.1.2   Heuweltjie 4

EC had good diagonal and horizontal correlation for H4, with the best being diagonal. Data was slightly skewed to the left. pH also had horizontal and diagonal correlation, with diagonal being best. Data was evenly distributed. Sodium had its best correlation horizontally. Data was skewed to the left. Chloride did not have very good correlation in most directions; however, diagonal correlation was present. Data was skewed to the left. Sulphate had low correlation in most directions, with horizontal correlation being the best. Data was skewed to both the left and right. Dissolved silica had its best correlation diagonally. Data was mostly skewed to the left. Calcium and magnesium both had some diagonal and horizontal correlation, with horizontal being best. Data was mostly skewed to the left with some even distribution throughout for both calcium and magnesium. Potassium had its best correlation horizontally, with poor correlation in all other directions. Data was skewed to the left. Bicarbonate had poor correlation in most directions, with the best being diagonally. Data was skewed to the left. Amorphous silica had its best correlation diagonally, with no correlation in any other direction. Data was evenly skewed in all directions. Hydroxyapatite had the best correlation diagonally. Data was skewed slightly to the right. Gypsum had its best correlation diagonally, with

correlation being poor in all other directions. Data was skewed to the right. Calcite had its best correlation diagonally. Data was slightly skewed to the right. Halite had the best correlation horizontally. Data was skewed to the right.

Table 2.3: Variogram data of H4 for all ion and SI data plotted as heat maps.

H4	Model Fit	Direction of best fit	Tolerance	R^2	Distribution (Skewness)
EC	Linear	30.0	30.0	0.054	Left
pH	Linear	-30.0	30.0	0.025	Even distribution
Sodium	Linear	0.0	30.0	0.041	Left
Chloride	Linear	-150.0	30.0	0.056	Left
Sulphate	Linear	0.0	30.0	0.044	Left & right
Dissolved Si	Linear	-30.0	30.0	0.038	Left
Calcium	Linear	0.0	30.0	0.019	Left
Magnesium	Linear	0.0	30.0	0.065	Left
Potassium	Linear	0.0	30.0	0.094	Left
Bicarbonate	Linear	60.0	30.0	0.007	Left
Amorphous Si	Linear	-90.0	30.0	0.046	Evenly skewed
Hydroxyapatite	Linear	-60.0	30.0	0.071	Right
Gypsum	Linear	-30.0	30.0	0.050	Right
Calcite	Linear	-90.0	30.0	0.140	Right
Halite	Linear	0.0	30.0	0.133	Right

3 Results

In this section, all data obtained from the sampling procedures and data processing, as discussed in sections 2.4 and 2.5, is presented.

3.1 Heuweltjie profiles

Detailed heuweltjie profiles were drawn for each entire heuweltjie while in the field and are illustrated in Figure 3.1 and Figure 3.11. The depth shown on the two heuweltjie profile descriptions shows the initial top depth of the heuweltjies at 0 cm. It is important to know that this depth is only 0 cm for the highest point. When the top of the heuweltjie is at a lower elevation elsewhere, the depth would still be zero, although it is not indicated as such with the y-axis. For example, at a cross section distance of 40 m for H1, it appears as if its top depth is between 70 and 80 cm (Figure 3.1). However, this is also the 0 cm depth for that specific profile. It is also important to note that the A horizon is not shown in either heuweltjie profile description, as it is less than 10 cm deep. All horizons were classified according to the FAO (2006) Guidelines for Soil Description.

The detailed soil profile pictures are also displayed below. Tables outlining detailed soil profile descriptions can be seen in Appendix A.

3.1.1 Heuweltjie 1 profile descriptions

For H1 (Figure 3.1), the top soils were mostly Bw soils at the edges and had an accumulation of carbonates otherwise (Bk). Bw soils refer to the development of colour or structure in a soil.
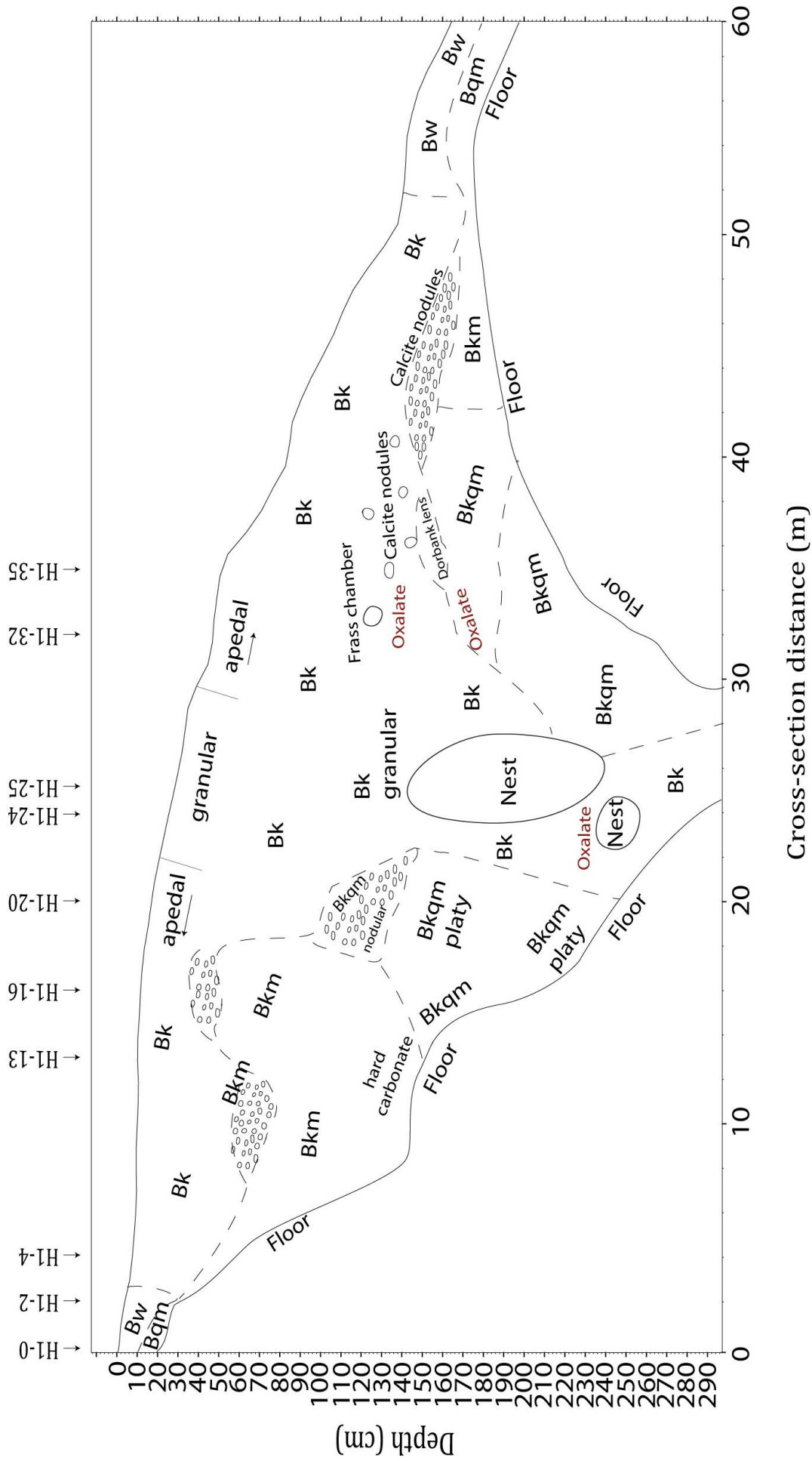
Figure 3.1 Soil profile descriptions for H1. Plot was made at a x3 exaggeration. Model profiles are indicated above the heuweltjie outline. Bk= carbonate accumulation; Bw= development of colour and structure; Bkm= carbonate cementation; Bqm = silica cementation; Bkqm= carbonate and silica cementation.

At H1-0 and H1-2, where the first detailed soil profiles were taken, the soils deeper than 22 cm for H1-0 and 30 cm for H1-2 were silica cemented (Bqm), indicating the formation of the dorbank layer below the interheuweltjie soils (see Figure 3.2). For both H1-0 and H1-2 (Figure 3.2a and b), the Orthic A horizon had a thick 2 mm surface crust, was dry, loose, and had an apedal structure, with some fine roots present as well. The development of colour and structure (Bw) horizon for this profile was a slightly hard coarse sandy loam (5% clay) and was apedal to weakly platy. Fine calcite-filled root channels were present, where the soil structure became more platy to coarsely blocky. Other than for the fine calcite filled root channels present, both the Orthic A and the development of colour and structure (Bw) horizons were not calcareous. A wavy transition was observed to the very hard, massive to platy silica cemented (Bqm) dorbank layer.
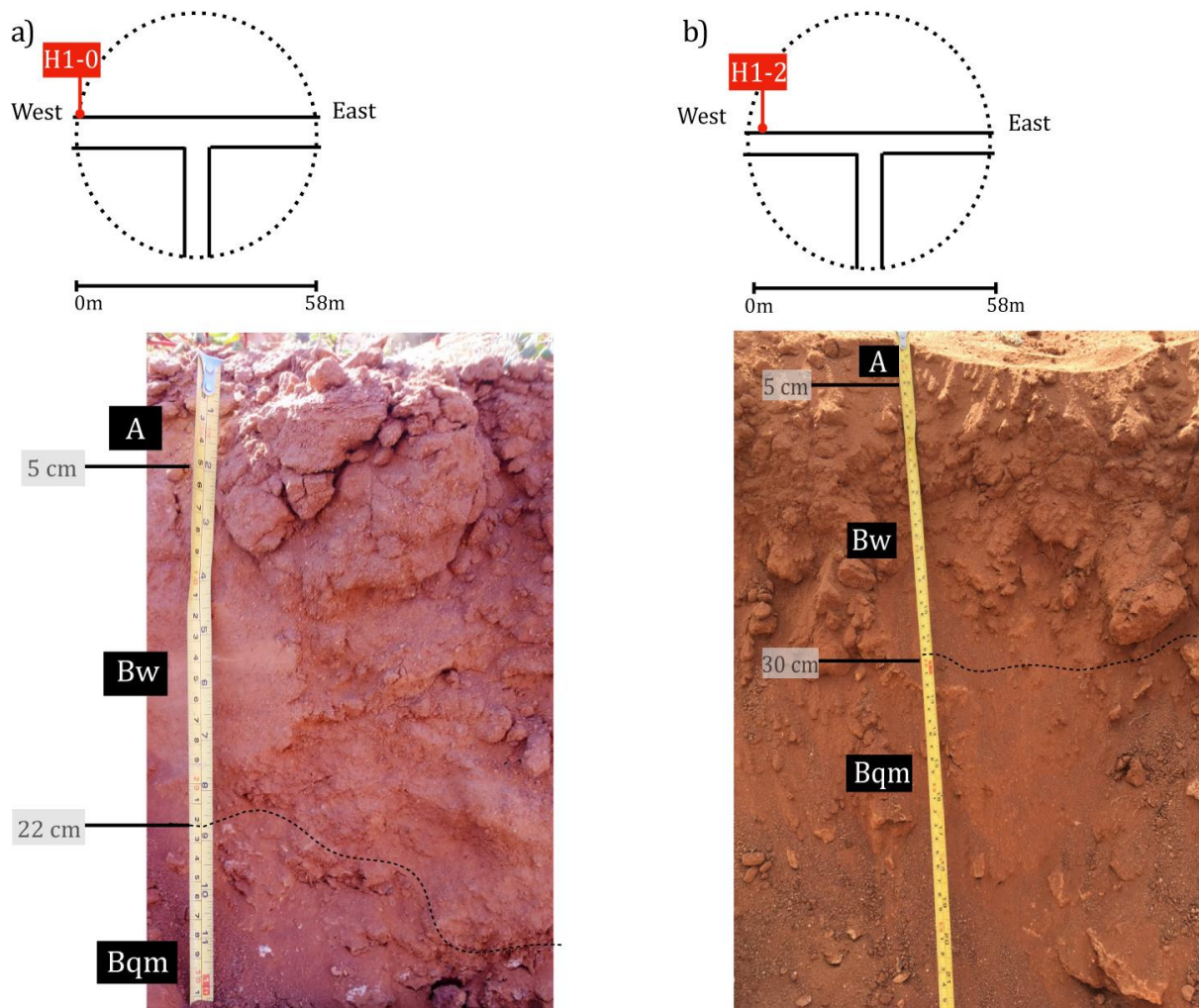
Figure 3.2: Detailed soil profile pictures for H1-0 (a) and H1-2 (b). Bw = development of colour and structure; Bqm = silica cementation.

48

A gradual transition from a development of colour and structure horizon (Bw) to a carbonate accumulated horizon (Bk) took place at a cross section distance of 4 m (H1-4) within the top soils, also moving from silica cementation (Bqm) to carbonate cementation (Bkm) as the soil moves from interheuweltjie to heuweltjie soils (see Figure 3.3). This was the first noted calcareous detailed profile. Its Orthic A horizon was a loose, apedal, coarse sandy loam (3-5% clay), and had a few fine roots present. The carbonate accumulated (Bk) horizon was also a coarse sandy loam (10% clay), but had a more friable, platy structure. The carbonate cemented (Bkm) horizon was a firm to very firm hard carbonate.
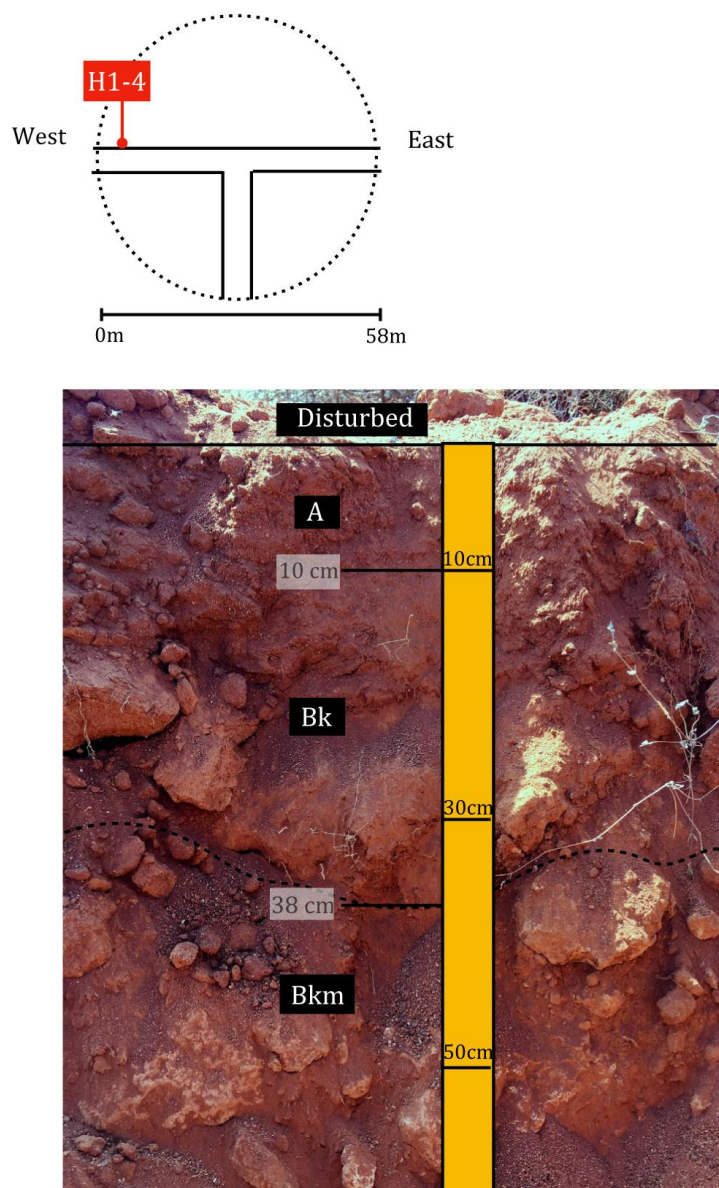
Figure 3.3: Detailed soil profile picture of H1-4. Bk = an accumulation of carbonates; Bkm = carbonate cementation.

49

Soils from a cross section of 0 – 22 m were mostly apedal (single grained or massive structures). The apedal soils in this section were single grained within the top soils, becoming more massive by having carbonate cementation (Bkm) deeper down, with some carbonate and silica cementation (Bkqm) from H1-13 onwards as well. Carbonate cemented (Bkm) nodules were present in this section (specifically at H1-13), separating the carbonate accumulated (Bk) from the carbonate cemented (Bkm) soils.

For H1-13, the Orthic A horizon had a loose apedal structure (Figure 3.4). The carbonate accumulated (Bk) horizon was a loose, dry and apedal sandy silt loam (7% clay), having a weak coarse platy structure, and had a gradual transition to the carbonate cemented (Bkm) horizon through many calcite nodules. The carbonate cemented (Bkm) horizon was strongly calcareous and had a 5 cm thick laminar capping as well as a coarse to massive platy structure. It was highly indurated at the top of the horizon, becoming less indurated towards the lower part of the horizon. The carbonate and silica cemented (Bkqm) horizon had a slightly calcareous, highly cemented, firm structure. Some well-rounded cobbles were present, along with many angular fragments. Its interstitial material was classified as being a coarse loamy sand (10% clay).
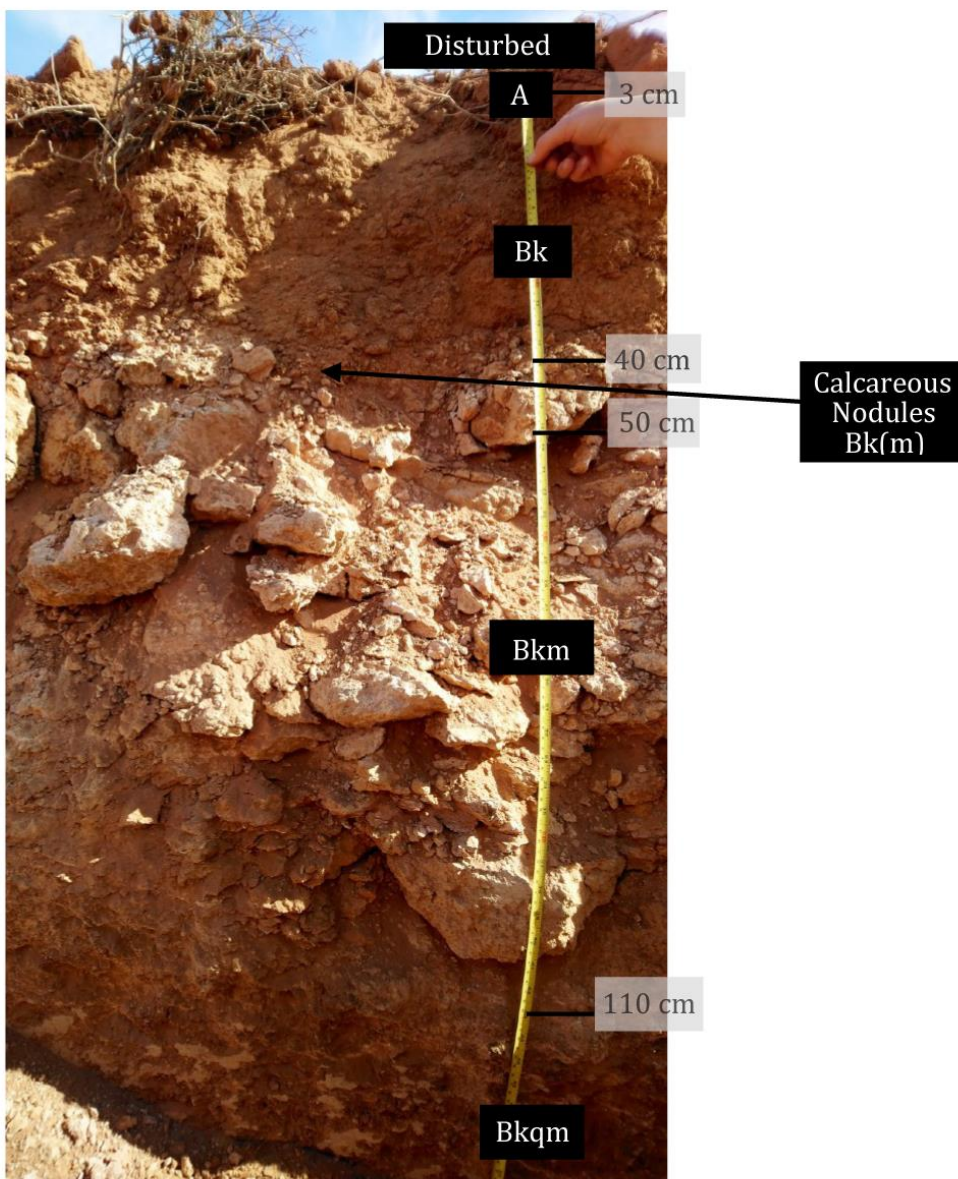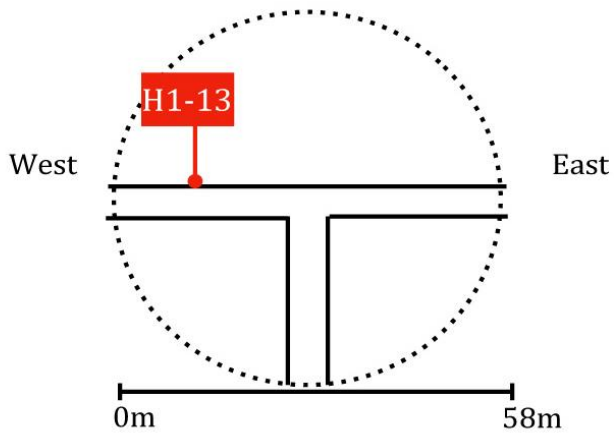
Figure 3.4: Detailed soil profile picture for H1-13. Bk = carbonate accumulation; Bkm = carbonate cementation; Bkqm = carbonate and silica cementation.

H1-16 (Figure 3.5) had active termites at the base of the profile. Its Orthic A horizon was a fine, silty loam (12% clay), with a loose apedal consistency. A few impregnated calcite nodules were present, along with some fine roots. Many 1 mm – 1 cm pores were also present within the horizon. The first carbonate accumulated (Bk1) horizon was a fine silty loam (17% clay) with a loose consistency and a large, platy structure. Many fine roots with 1 mm pores were present, along with some impregnated calcite nodules. The second carbonate cemented (Bk2) horizon was a neocarbonate B transitioning to a soft carbonate. It was a medium sandy loam, with moderately impregnated calcite nodules, with the amount of calcite nodules increasing down the horizon. Many small pores (1 mm diameter) and macropores (1 cm diameter) were present, along with a few fine roots. The carbonate cemented (Bkm) horizon was a hard carbonate with laminar calcrete. Higher up within this horizon, it was more platy, while grading down to a nodular structure deeper down in the horizon. The carbonate and silica cemented (Bkqm) horizon was a slightly hard coarse loamy sand (10% clay). It was strongly indurated with calcite and had a massive to weak coarse platy structure. Silica impregnated calcite nodules were also present, cutting across the calcite veins.
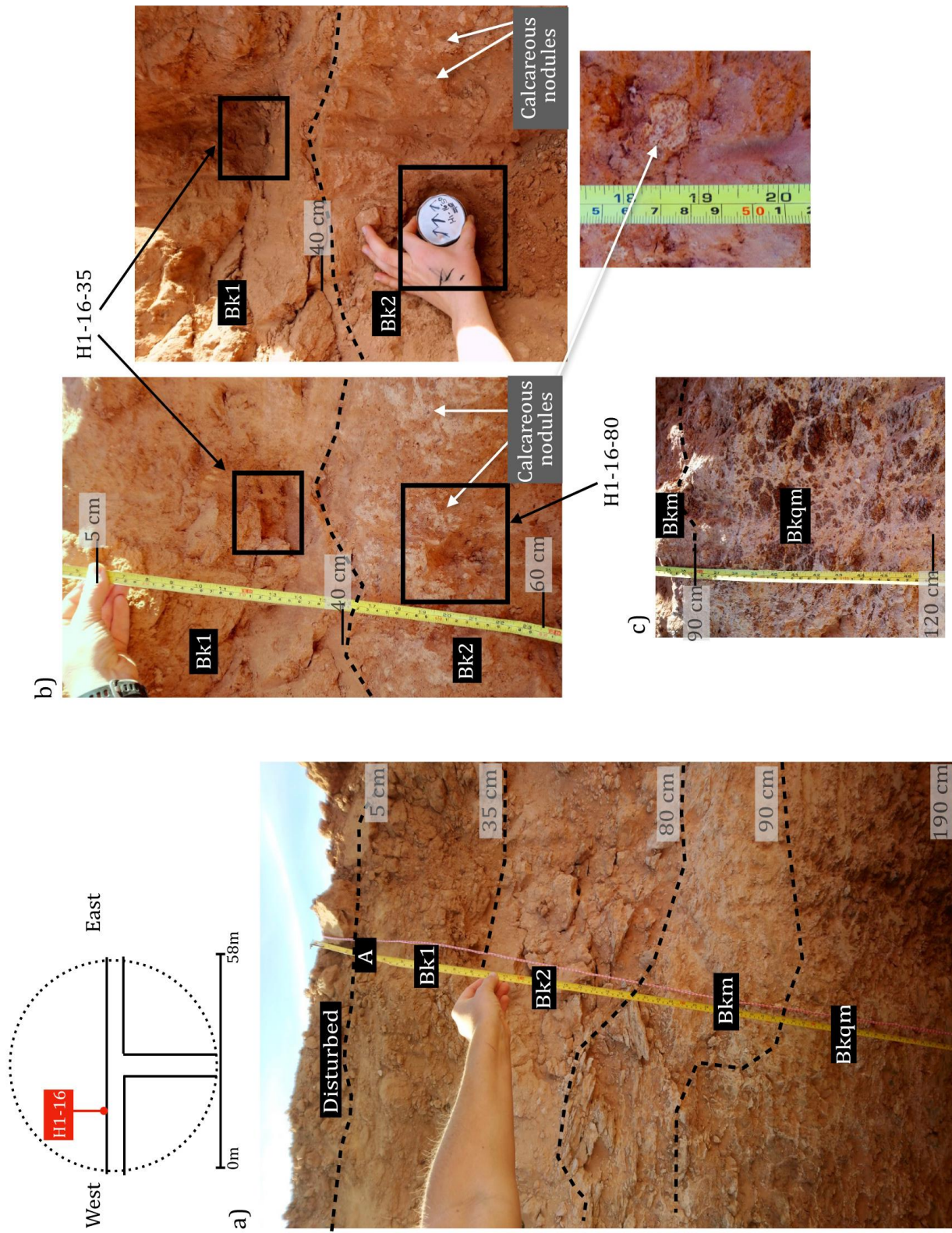
Figure 3.5: Detailed soil profile pictures for H1-16. a) Shows the entire heuweltjie profile; b) is composed of three pictures and shows in detail some of the nodules present from 40 to 60 cm; c) shows the carbonate and silica cementation present from 90 to 120 cm. Bk = carbonate accumulation; Bkm = carbonate cementation; Bkqm = carbonate and silica cementation.

At H1-20, active termites were found at the base. The Orthic A horizon had a dry, gradual transition to the carbonate accumulated (Bk) horizon. This Bk horizon had an apedal to granular structure, and had a gradual, wavy transition to the carbonate and silica cemented (Bkqm) horizon, which contained calcrete nodules within this transition area (see Figure 3.6).
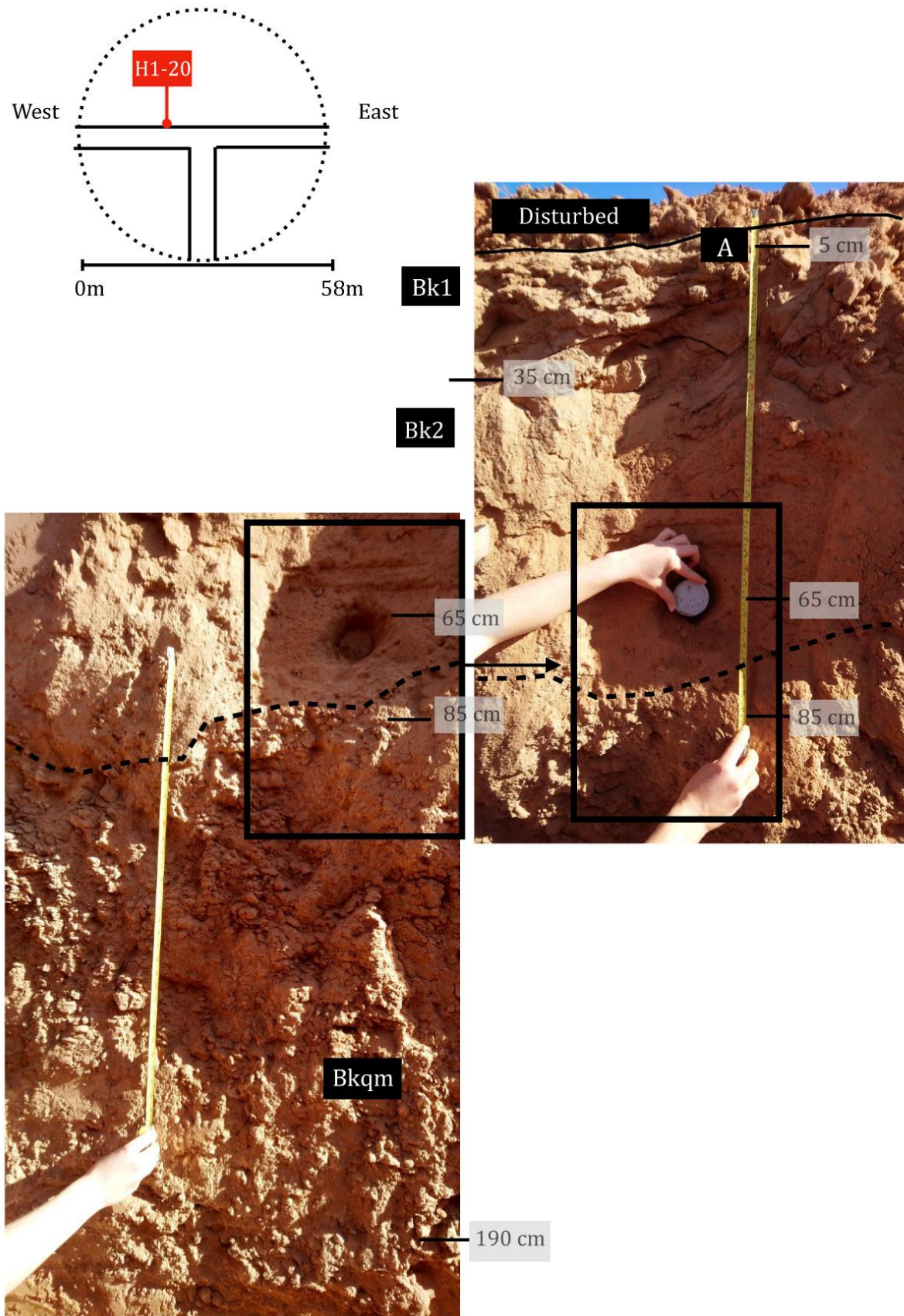
Figure 3.6: Detailed soil profile pictures of H1-20. Bk = carbonate accumulation; Bkqm = carbonate and silica cementation.

From a cross section distance of 22 – 28 m, a granular texture was observed (Figure 3.1). This can be accounted for by termite bioturbation, as other studies have found termite activity to produce soil horizons or profiles of granular structure (Jouquet *et al.*, 2016; Jungerius *et al.*, 1999). Within this section, two termite nests were also found, one at 24 m and one at 25 m.

At H1-24 (see Figure 3.7), active termites were present at the base. The Orthic A horizon was a fine silty loam (10% clay) with a slightly sticky, loose consistency and apedal structure, with a few fine roots present as well. The first carbonate accumulated (Bk1) horizon had a dry, granular structure with a loose to slightly firm fine sandy loam (12% clay) texture. Small micro tunnels filled with white precipitate were also present, along with an elongated chamber filled with micro excrement pellets (1 mm diameter). The second carbonate accumulated (Bk2) horizon was a coarse sandy loam (17% clay) and contained many micro tunnels with a 1 mm diameter, along with weakly impregnated calcite nodules. Strongly impregnated manganese (Mn) oxide concretions were also present. The third carbonate accumulated (Bk3) horizon was friable to hard, and had a slightly angular, blocky structure. It consisted of a coarse to very coarse loamy sand. Micro excrement pellets were also present, although they were more cemented than in the overlying horizon. Dark indurated nodules were present, possibly with some silica and Mn oxides present as well. The nest was present within the next soil horizon. It was silicified, with the possibility of having calcite finely layered with silica. The final carbonate accumulated (Bk4) horizon had the same structure as Bk3, except with darker concretions and no calcite nodules present, although some Mn oxide precipitate was present.
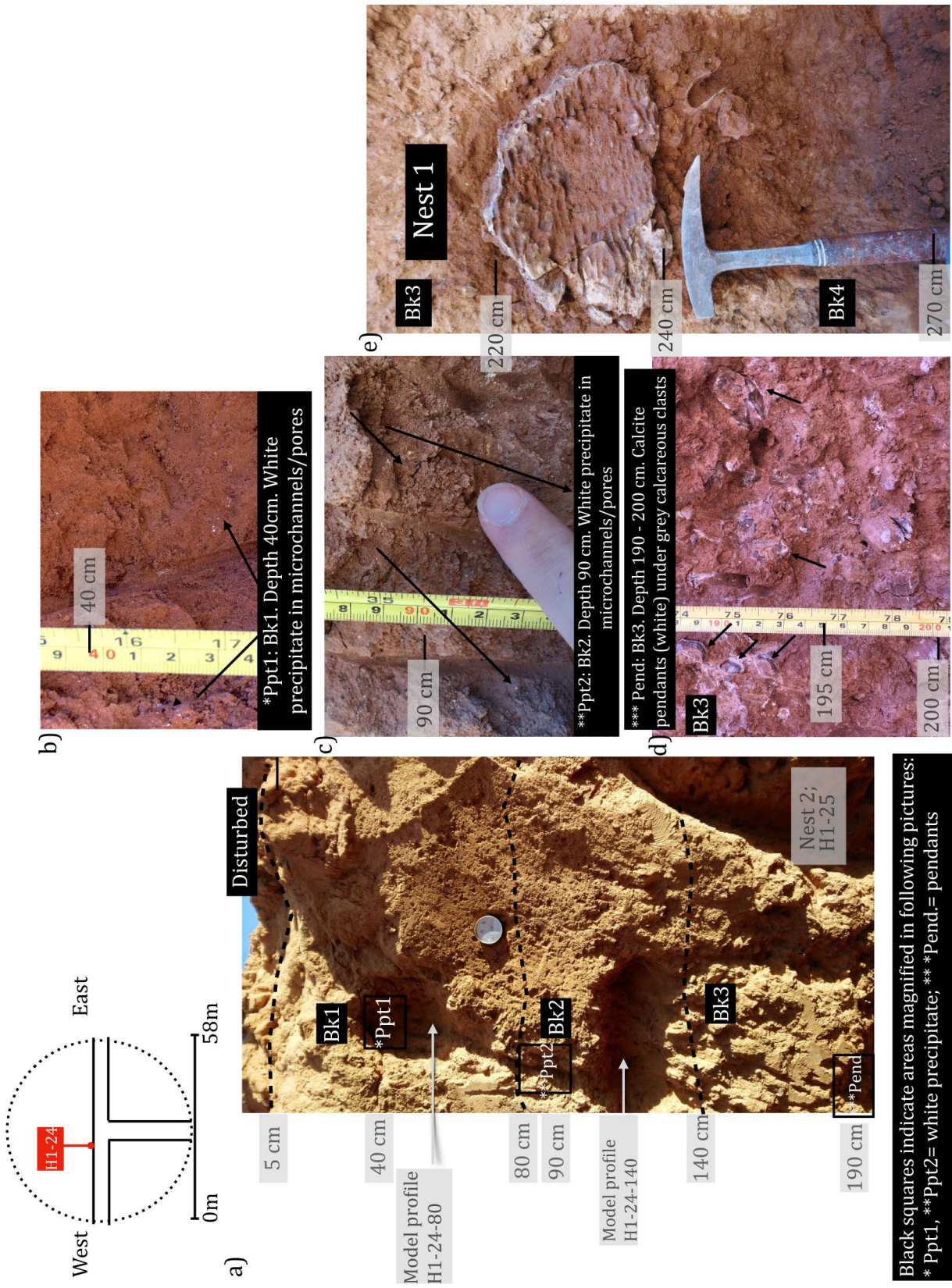
Figure 3.7: Detailed soil profile pictures of H1-24. a) Consist of the entire profile, and b), c) and d) show the magnified Ppt and Pend areas within the initial picture; e) shows the silicified nest. Bk = carbonate accumulation.

H1-25's Orthic A horizon was a fine silty loam (10% clay) with a loose consistency, and some fine roots (Figure 3.8). Both the Bk1 and Bk2 horizons were the same as that of H1-24. The large nest was set in the third carbonate accumulated (Bk3) horizon. It was oval shaped and tapered down towards a highly bioturbated and indurated layer. The nest had a hard coating of 3 – 5 cm thick that was presumably made of silica. The soil found within the nest was moist, and could be rolled into a donut shape with a diameter of 10 cm. This soil was classified as being a clayey loam (30%). Many fine precipitates were also present within the nest structure, along with many tunnels and mottles. The last carbonate accumulated (Bk4) horizon situated below the nest was friable to hard, and had an angular blocky structure, and was classified as a coarse loamy sand. Some Mn oxide precipitate was also present.
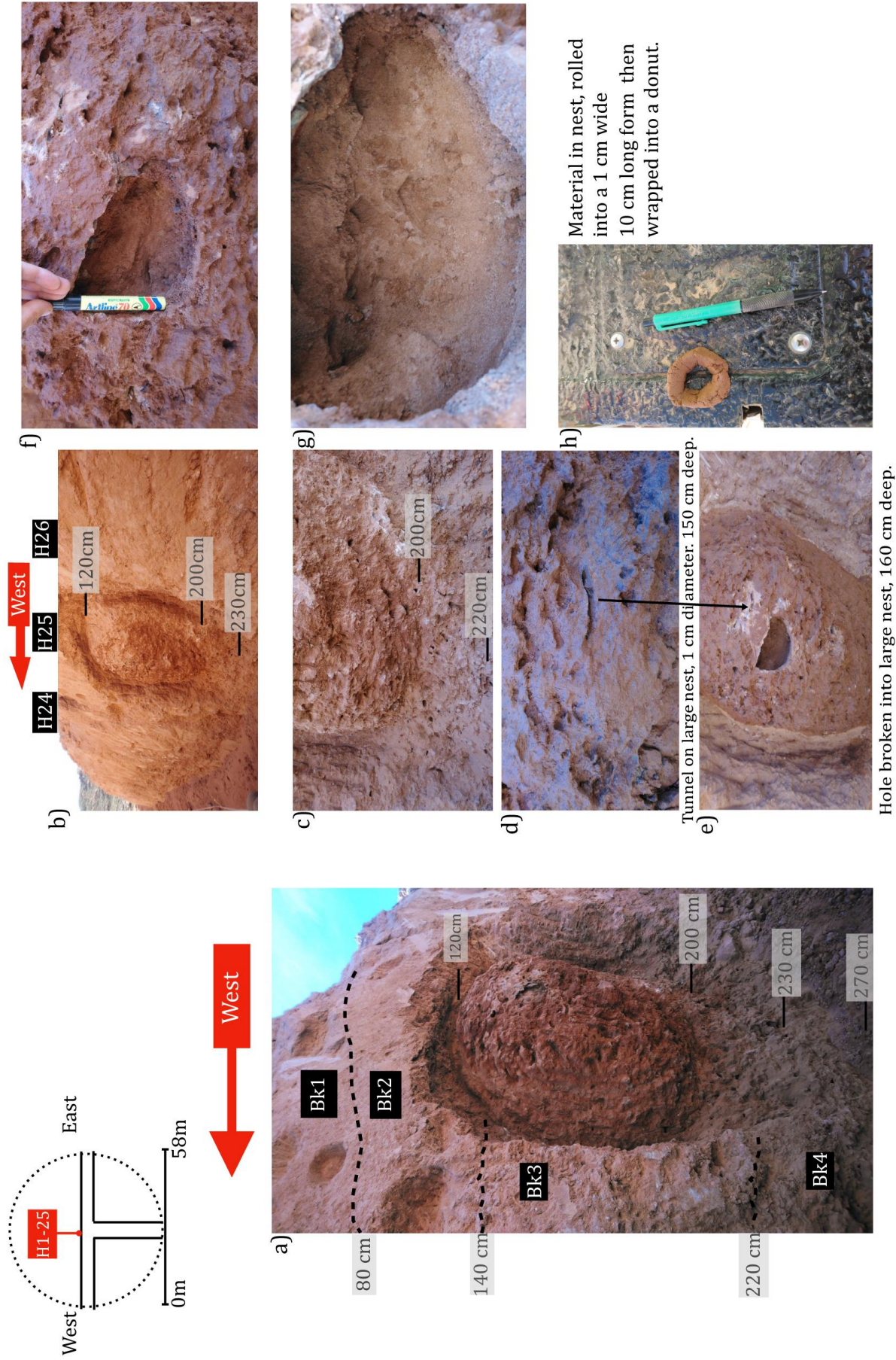
Figure 3.8: Detailed soil profile description of H1-25. Bk refers to carbonate accumulation. a) Picture showing entire detailed profile; b) shows detailed profile from a different angle; c) shows the bottom of the nest; d) shows one of the large tunnels on the nest; e) depicts the hole broken into the nest; f) gives the scale of the hole in the nest; g) shows the mottles and white precipitate within the nest; h) shows how the nest material could be rolled into a donut shape. Bk = carbonate accumulation

59

For H1-32 (*Figure 3.9*), the Orthic A horizon was a loose, apedal fine silty loam. The carbonate accumulated (Bk) horizon had a slightly firm to loose structure throughout the horizon, and was classified as a fine sandy to silty loam (12% clay). Root hairs with a 1 mm diameter filled with white precipitate were also present, along with 1 cm diameter tunnels. Active termites were present within this horizon and were found repairing a 2 cm chamber wall with moist micro aggregates (1-2 mm diameter) that were freshly prepared. A chamber filled with termite frass was also present within this horizon, along with an organic matter filled chamber deeper down the horizon. The silica accumulated (Bq) horizon contained Si impregnated nodules, along with a powdery matrix. The silica cemented (Bqm) horizon had a hard, platy structure, being more indurated at the top of the horizon than the bottom. Its structure became more platy as depth increased. Hard silica nodules were also present throughout, again set in a white matrix. The lowest horizon for this profile, a carbonate and silica cemented (Bkqm) horizon, had a very hard, platy structure with many micropores. Mn oxide coatings were present on the plates, micropores, and channels.
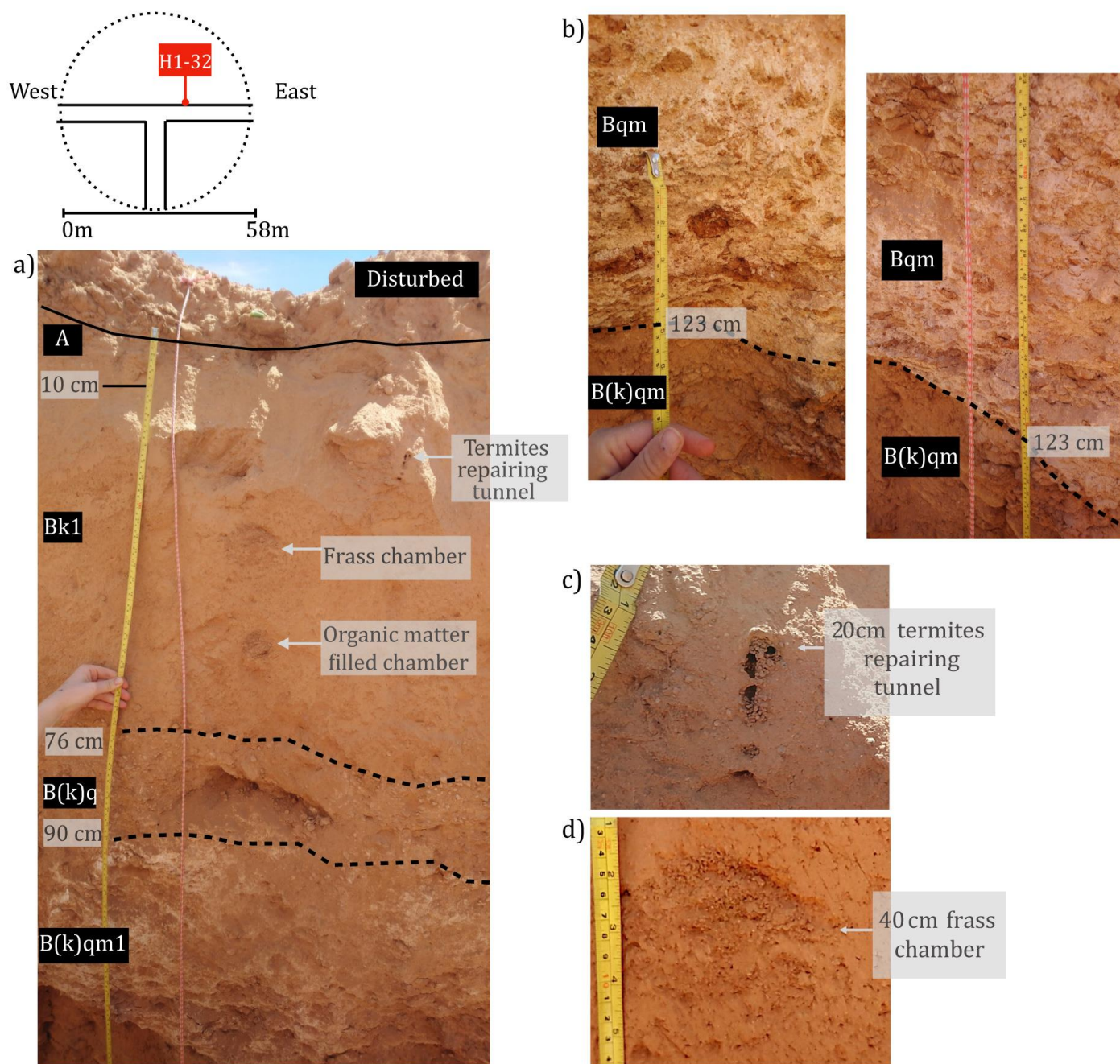
Figure 3.9: Detailed soil profile description of H1-32. a) shows the entire detailed profile; b) consists of two pictures and shows the visible colour change from the Bqm to B(k)qm horizons at 123 cm; c) is a close-up of the termites repairing their tunnels; d) is a close-up of the frass chamber. Bk = carbonate accumulation; Bkq = carbonate and silica accumulation; Bkqm = carbonate and silica cementation.

H1-35's Orthic A horizon was classified as being a fine silty loam (F*igure 3.10*). The carbonate accumulated (Bk) horizon had an apedal, loose to friable structure and was classified as a sandy clay loam (17% clay). Many channels and fine root hairs were present and filled or coated with white precipitate. Many weakly impregnated calcite nodules were present. Occasional fine channels and micro excrement were also present within this horizon. The silica accumulated (Bq) horizon had very hard nodules, assumed to be silica indurated. Few fine roots were present, along with many fine white precipitates. The bottom horizon, a carbonate and silica cemented horizon (Bkqm) was silica indurated, and had a coarse platy structure, with Mn oxide lenses throughout.
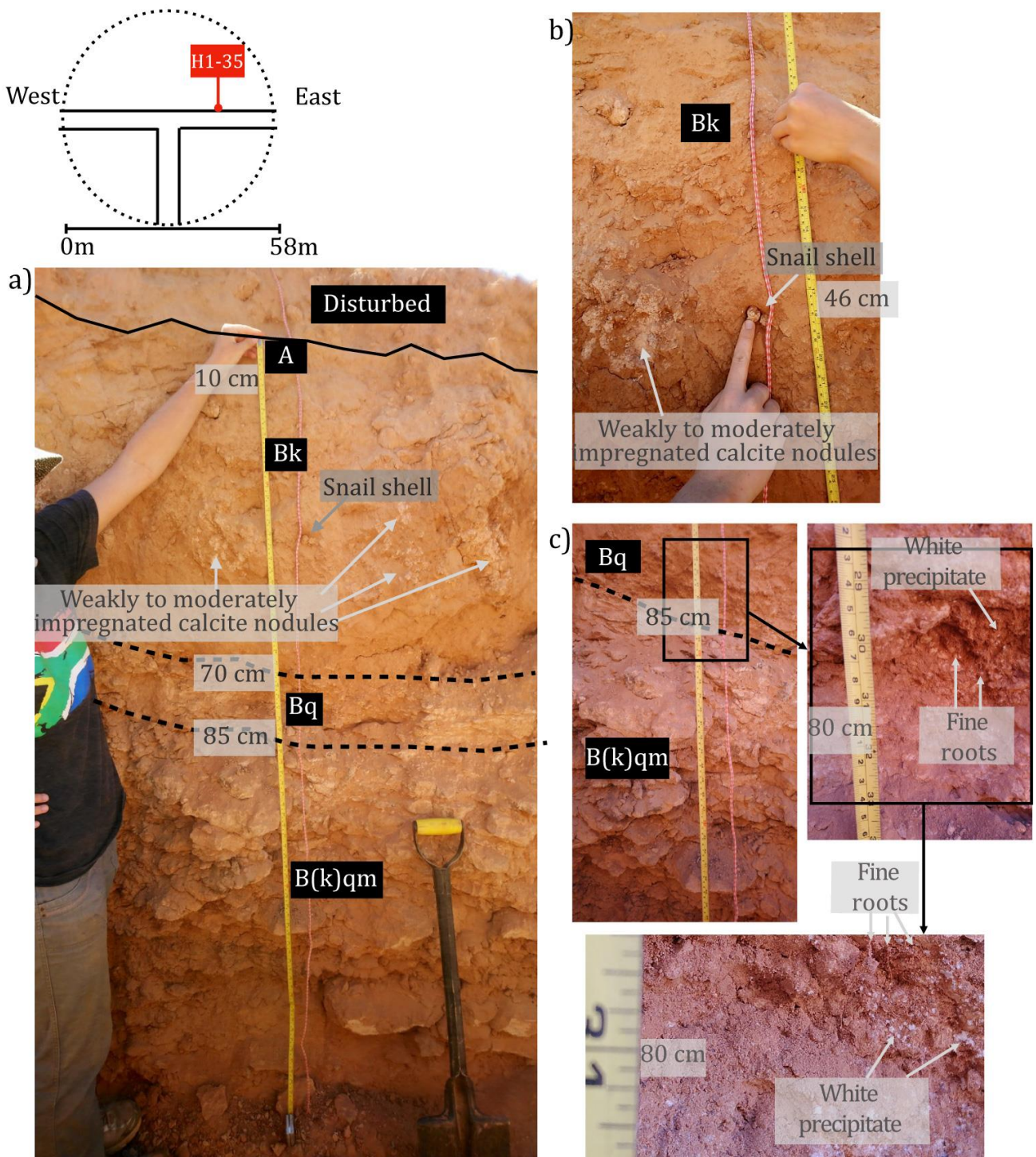
Figure 3.10: Detailed soil profile description of H1-35. a) shows the entire detailed profile; b) is a close-up of the impregnated calcite nodules close to 46 cm; c) consists of three pictures showing where the white precipitate and fine roots are present within the Bq horizon. Bk = carbonate accumulation; Bq = silica accumulation; Bkqm = carbonate and silica cementation.

For the rest of the heuweltjie structure (where no detailed profiles were analysed) an accumulation of calcite nodules was present close to the frass chamber and separating the carbonate accumulated (Bk) and carbonate and silica cemented (Bkqm) horizons from each other. From a cross section distance of approximately 40 – 46 m, many calcite nodules were present between the two horizons. Coming to the end of the heuweltjie structure, towards the interheuweltjie soils, a gradual transition takes place from the top soils being carbonate accumulated (Bk) to a development of colour and structure (Bw), with a silica cemented (Bqm) horizon below these soils, again indicating the formation or presence of dorbank in the shallow interheuweltjie soils.

3.1.2 Heuweltjie 4 profile descriptions

For H4, carbonate accumulation (Bk) was present throughout the topsoil horizons, with calcite nodules present at cross sections of approximately 19, 22, 38, 40 and 42 m. Going down the soil horizons, soils mostly have an accumulation of silica and gypsum cementation (Bqym) from a cross section distance of approximately 12 – 25 m. From 25 – 38 m, the second horizon also had an accumulation of carbonates (Bk) present. Silica indurated nodules are present throughout the heuweltjie structure (and will also be pointed out when discussing the detailed soil profiles). Four nests, of which one was a collapsed nest, were present throughout the heuweltjie structure, with one of the nests having visible tunnels (cross section distance of 42 m) with gypsum present as a lining, situated in a silica cemented (Bqm) layer. H4 had a shallow dorbank horizon within the middle of the heuweltjie structure (cross section distance of 24 – 28 m), and so could not be excavated deeper, as depicted in Figure 3.11.
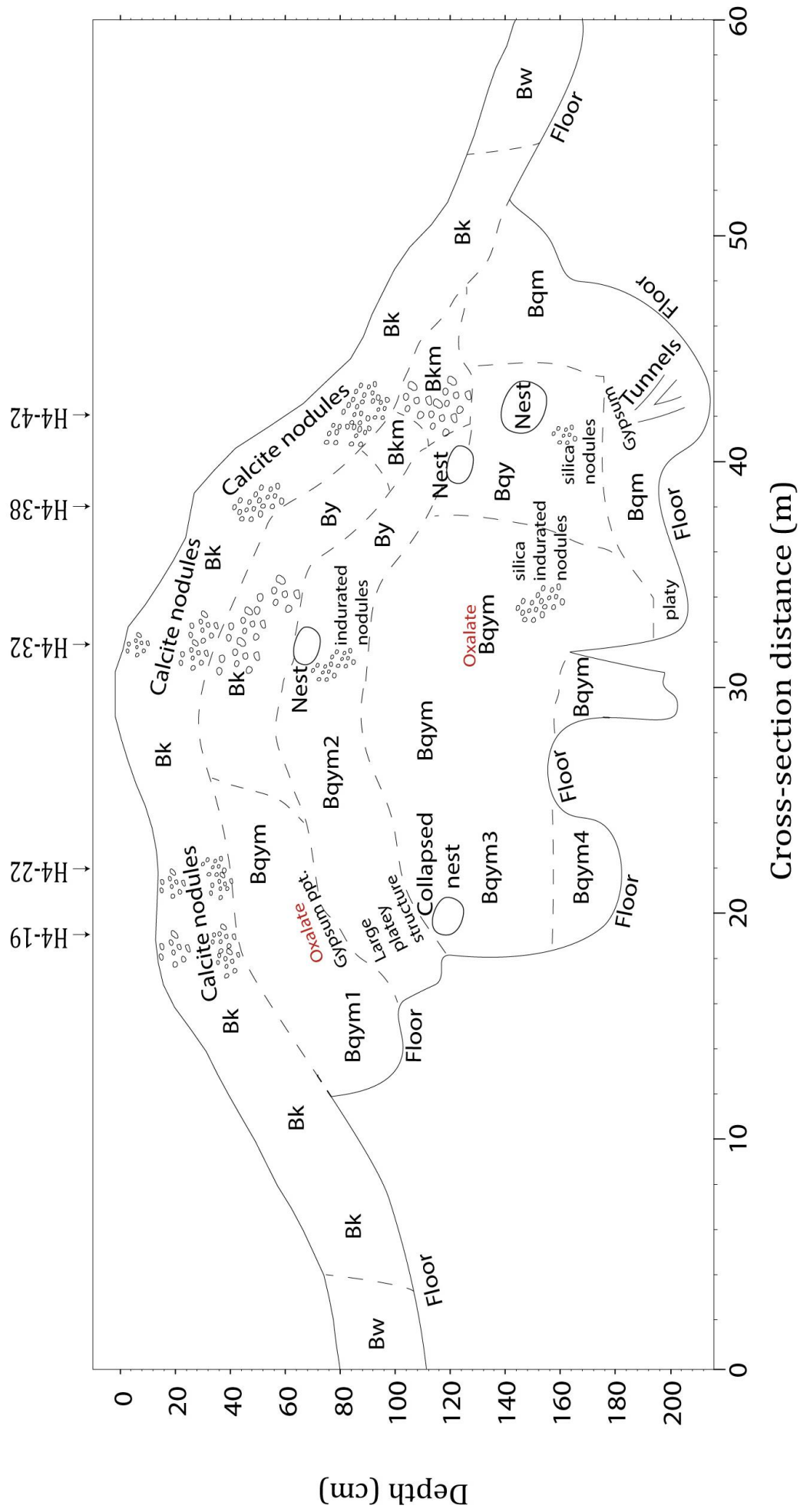
Figure 3.11: Soil profile descriptions for H4. Plot was made at a x3 exaggeration. Model profiles are indicated above the heuweltjie out line. Bw = development of colour and structure Bk= carbonate accumulation; By= gypsum accumulation; Bqm= silica cementation; Bqym= silica and gypsum

65

The first detailed profile analysed for this heuweltjie was at H4-19 (see Figure 3.12). The Orthic A horizon was a fine, sandy loam (15% clay), had a loose consistency and an apedal structure. A few weakly to moderately impregnated calcite nodules were also present within this horizon, with few fine roots also present. The carbonate accumulatied (Bk) horizon was also a fine sandy loam (17% clay), and had an apedal structure with a loose consistency. It contained many more weakly to moderately impregnated medium to coarse calcite nodules than the Orthic A horizon, also with few fine roots present. The first silica and gypsum cemented (Bqym1) horizon had a fine silty clay texture (18% clay). It had a hard consistency, large platy structure, and was highly indurated, with white precipitate coatings, which was thought to be gypsum precipitate. The second silica and gypsum cemented (Bqym2) horizon had a large, platy structure of hard consistency, with white gypsum precipitate on the ped surfaces. Few fine roots and white precipitate root clasts were also present. A collapsed nest was present within this horizon. Its soil was classified as being a medium sandy loam (12%), with a granular structure. Its consistency was friable, and many elongated, filled and indurated burrows were present. The third silica and gypsum cemented (Bqym3) horizon consisted of very hard and firm, silica indurated, unconsolidated material, with abundant Mn oxide present.
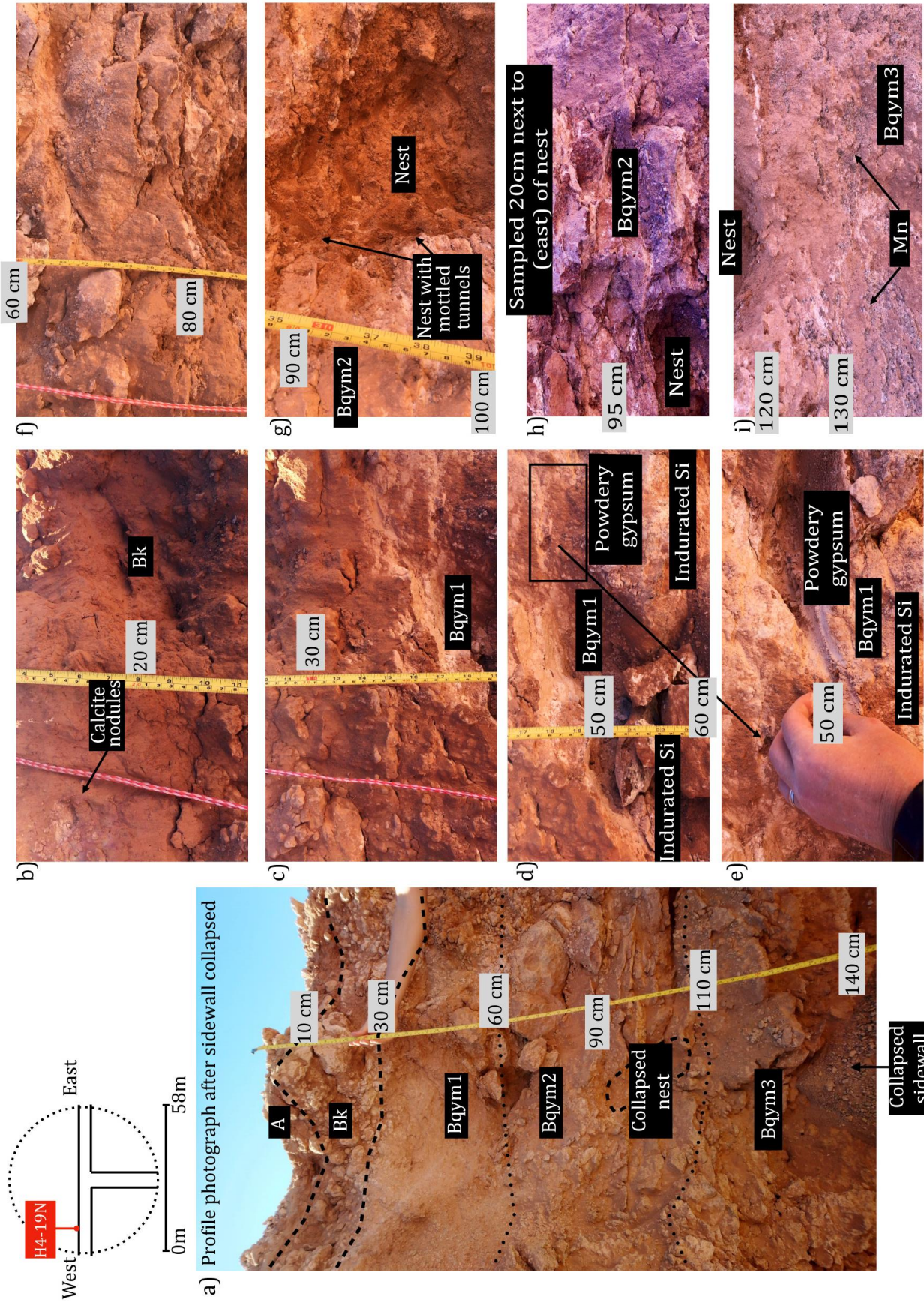
Figure 3.12: Detailed soil profile description of H4-19. a) Shows the entire detailed profile; b) shows the calcite nodules close to 20 cm; c) depicts the transition from Bk to Bqym1; d) and e) show the powdery gypsum, present at around 50 cm, f) shows the soil right above the collapsed nest; g) is of the collapsed nest; h) is a zoomed in picture showing the Bqym horizon next to the nest; i) shows the manganese present within the bottom horizon. Bk = carbonate accumulation; Bqym = carbonate and silica cementation.

Soil profile H4-22's (Figure 3.13) Orthic A horizon was a fine sandy loam (15%) with an apedal structure with loose consistency. A few calcite nodules of medium size were present. Few white micro channels and fine roots were also present. The carbonate accumulation (Bk) horizon also had a fine sandy loam texture (17%), an apedal structure with a loose consistency. Many more calcite nodules were present within this horizon, along with few fine white filament-type precipitates. The first silica and gypsum cemented (Bqym1) horizon had a large, platy structure with a hard consistency that was highly indurated with silica. A gypsum precipitate coating was present on the indurated material. The second silica cemented (Bqym2) horizon within this profile had a similar structure to Bqym1. However, the gypsum coating was less prominent, with a white and pinkish-white powdery interstitial material present instead. The last two silica and gypsum cemented (Bqym3 and Bqym4) horizons were both unconsolidated to platy dorbank soils. Reddish brown, angular, hard silica cemented nodules (also known as durinodes) were present. Lenses that formed a matrix area for the white powdery interstitial precipitate were also present. The lowest horizon, the silica cemented horizon (Bqm), was similar to the Bqym3 and 4 horizons, but did not have the gypsum coatings present. A platy structure was present with an increase in induration towards the base of the heuweltjie.
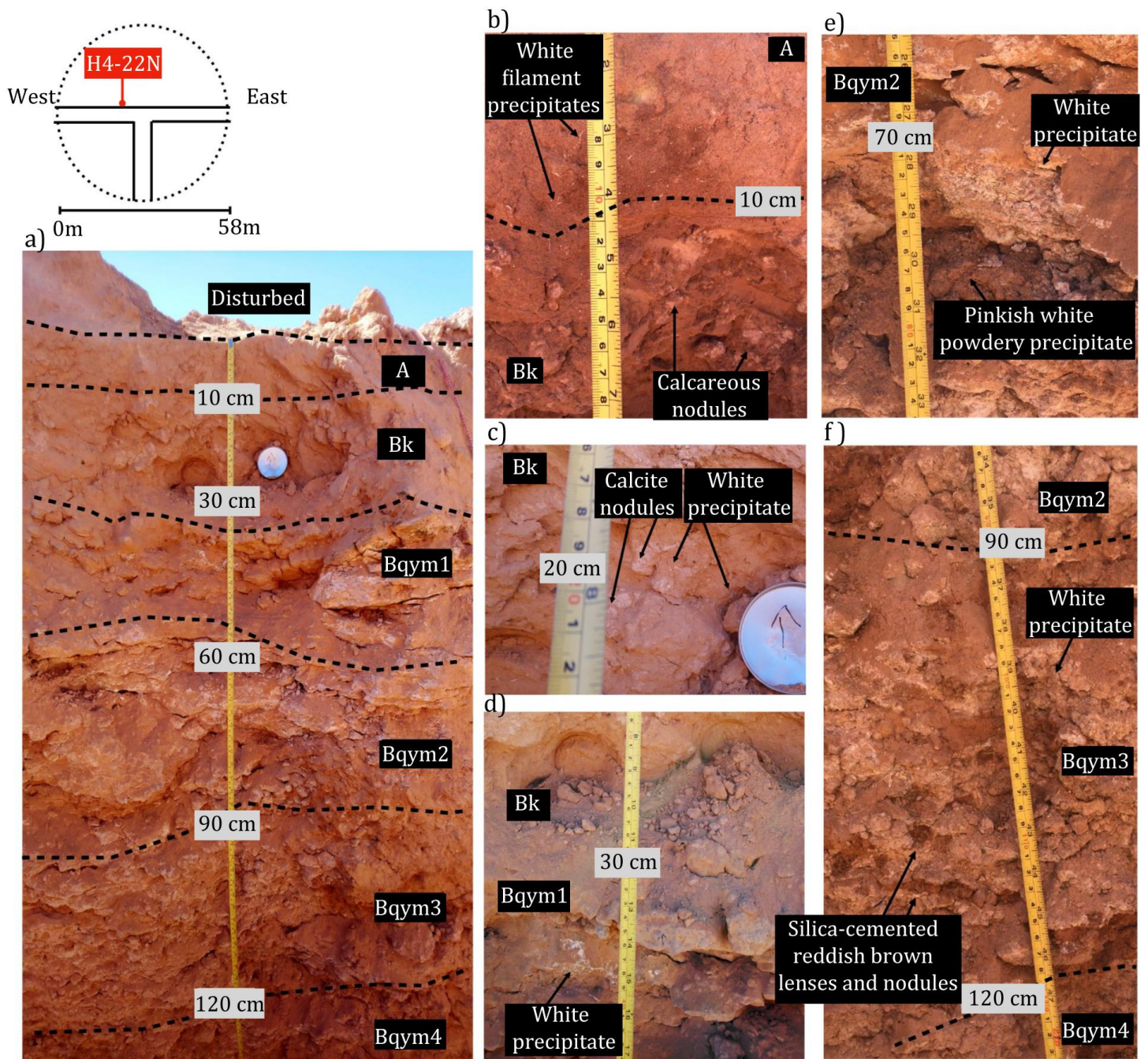
Figure 3.13: Detailed soil profile description of H4-22. a) Shows the entire detailed profile; b) is a close-up picture showing the white filament precipitates located above 10 cm depth; c) shows the calcite nodules and white precipitate located around 20 cm depth; d)and e) show white precipitates around 35 cm and below 70 cm respectively; f) also shows white precipitate below 90 cm depth, as well as silica cemented nodules and lenses. Bk = carbonate accumulation; Bqym = carbonate and silica cementation.

The next detailed soil profile, H4-32 (Figure 3.14), had a fine sandy loam texture (15%) with an apedal structure and loose consistency. Few medium calcite nodules were present, along with few white filament type-precipitates and fine roots. The first carbonate accumulation (Bk1) horizon was a fine, sandy loam (17%) with a loose consistency and an apedal structure. Unlike the Orthic A horizon, Bk1 had many medium to large, weakly to moderately impregnated calcite nodules, along with few white filament-type precipitates. The second carbonate accumulation (Bk2) horizon had a medium sandy loam texture with a granular structure and loose consistency. Very many moderate to strongly impregnated calcite nodules were present, along with few fine roots and few white filament-type precipitates. Within the next horizon, the nest was present. It had a medium sandy loam texture, with a slightly firm granular structure. Very many indurated nodules were present below the nest, along with few fine roots and white filament-type precipitates. The silica and gypsum cemented (Bqym) horizon had a fine, silty loam texture, with a loose, apedal, coarse and platy structure. Many indurated silica nodules were present, along with disseminated Mn oxide. Many lenses of a fine pinkish white powdery gypsum were present. The deepest horizon, the silica cemented (Bqm) horizon, was a platy, indurated silica cemented colluvium/alluvium.
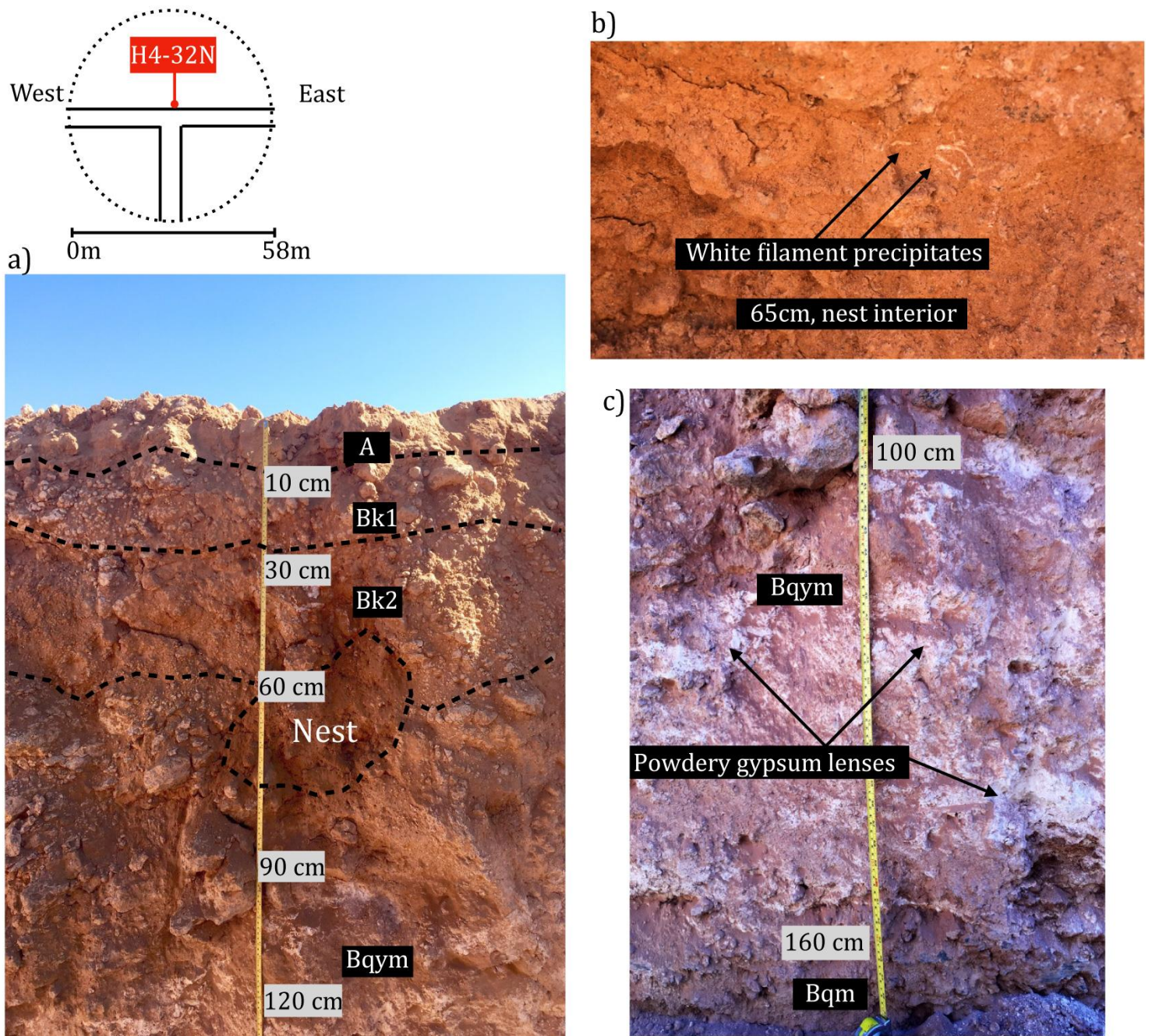
Figure 3.14: Detailed soil profile description of H4-32. a) shows the entire detailed profile; b) shows the white precipitates present within the nest; c) points out the powdery gypsum lenses in the Bqym horizon. Bk = carbonate accumulation; Bqm = silica cementation; Bqym = carbonate and silica cementation.

The Orthic A horizon for profile H4-38 (Figure 3.15) was the same as that of H4-32. The carbonate accumulated (Bk) horizon was a fine, sandy loam (17% clay) with a loose consistency and apedal structure. Many medium to large calcite nodules were present, especially at a depth of 25-40 cm. A few white filament-type precipitates and fine roots were also present. The first gypsum accumulated (By1) horizon had a fine silty loam (18%) texture, with an apedal, loose consistency. Gypsum was present within this horizon. The second gypsum accumulated (By2) horizon had the same texture and consistency as By1. The silica and gypsum accumulated (Bqy) horizon was a coarse, loamy sand with a moderately loose apedal structure. A few indurated infilled termite burrows were present, along with very many white filament-type precipitates. The silica cemented (Bqm) horizon was a silica indurated alluvium/colluvium with a coarse, platy structure. Many angular, along with few well-rounded cobbles were present. Few white lens-like precipitates were present around the more red silica indurated material.
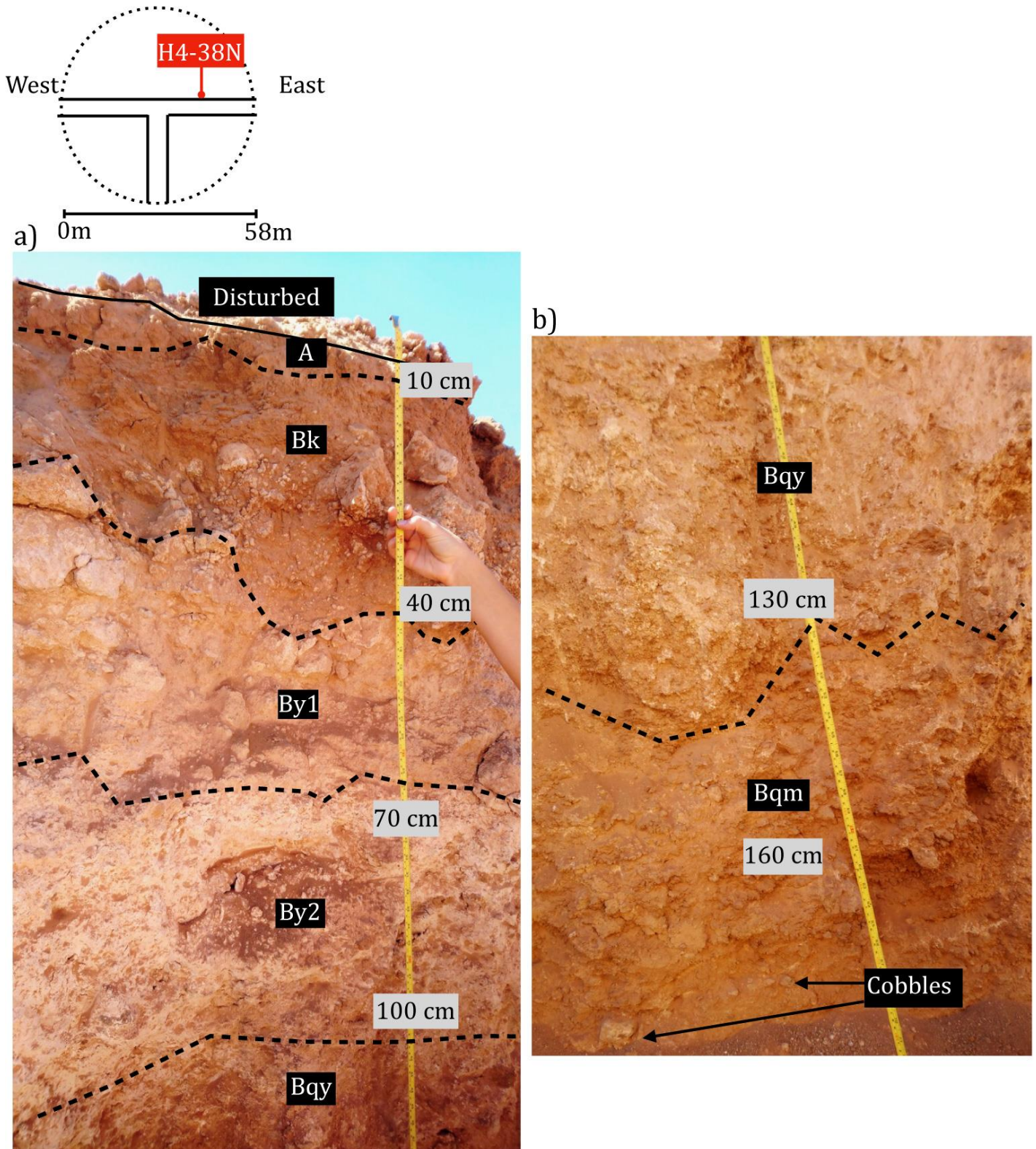
Figure 3.15: Detailed soil profile description of H4-38. Both a) and b) together make up the entire detailed profile depth, with a) going down to approximately 120 cm, and b) down to the bottom. Bk = carbonate accumulation; By = gypsum accumulation; Bqy = silica and gypsum accumulation; Bqm = silica cementation

The last H4 profile on the north wall was H4-42 (Figure 3.16). Its Orthic A horizon was the same as H4-32 and H4-38. The first carbonate accumulated (Bk1) horizon was a fine, sandy loam (17%), with a granular structure and loose consistency. Many medium to large calcite nodules were present, along with few fine roots and white filament-type precipitates. The voids present within this horizon were filled with amorphous black organic matter. The next carbonate-enriched to carbonate-cemented (Bk2 to Bkm) horizon had a weak platy structure with a slightly hard consistency. Many weakly impregnated calcite nodules were present, along with many white filament precipitates. The next horizon was the nest, where termite activity was present and active. The texture was classified as a fine sandy loam, with a loose, granular consistency. Many dark reddish indurated tunnels lined with clay and organic matter were present. Amorphous organic matter was present on the inner side of the clay lining. A few medium silica nodules were also present. The next layer consisted of the lower part of the nest and its tunnels. At 135 to 160 cm, a large tunnel was present, with gypsum present right above the tunnel. The tunnel was lined with clay, representing an impremeable barrier. The tunnel was more moist than the surrounding soils. The tunnels were actively repaired by the termites over the three days of sampling within the field. The deepest horizon, the silica cemented (Bqm) horizon, was weakly indurated with silica, along with some transported material, such as round and angular cobbles.
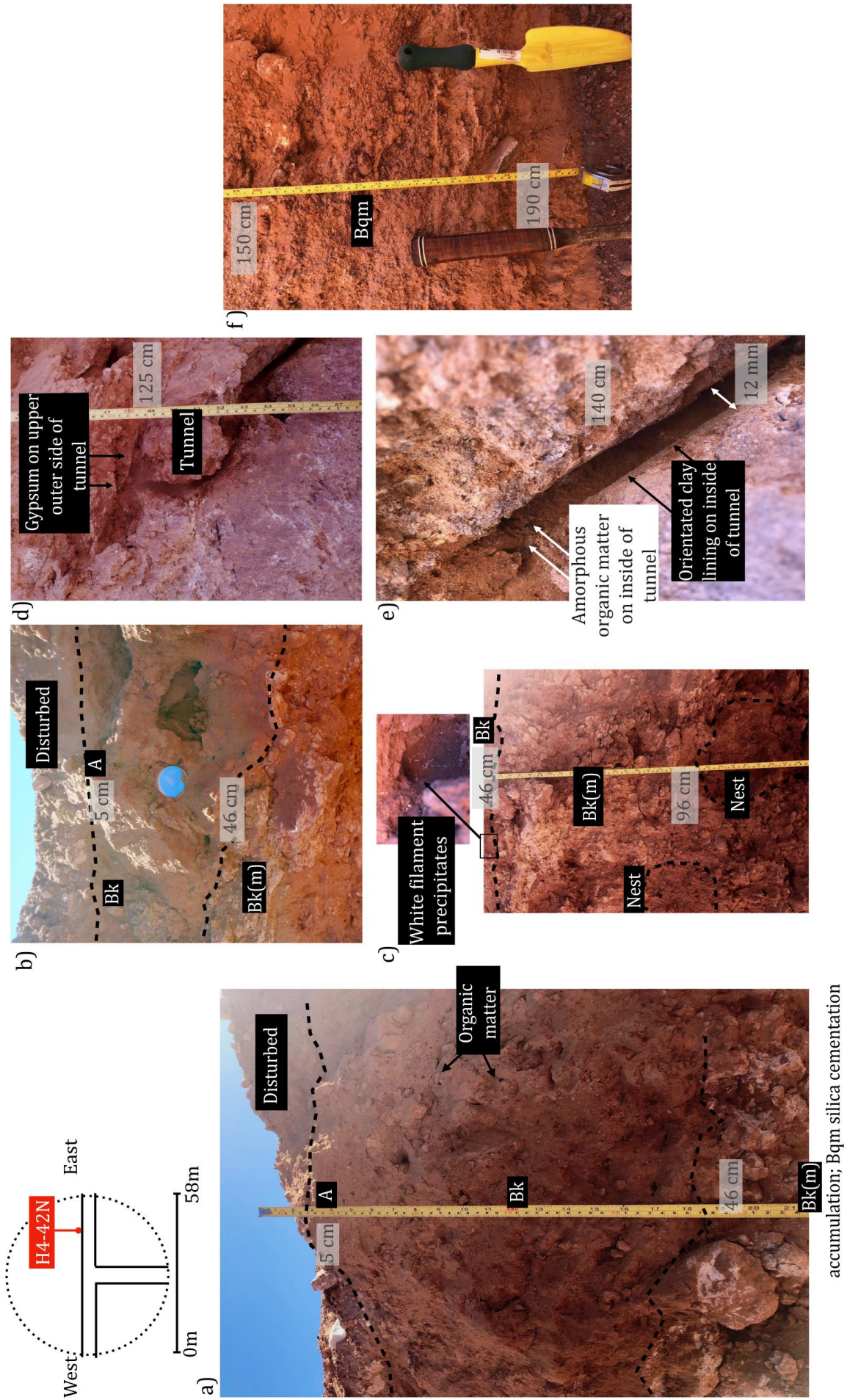
Figure 3.16: Detailed soil profile description of H4-42. a) Shows top part of detailed profile; b) shows close-up of top three soil horizons; c) indicates where the two nests within this profile are located; d) shows the structure of the tunnels; e) is a close-up picture of one of the tunnels at 140 cm depth; f) shows the soil horizons below the tunnels. Bk = carbonate cementation; Bkm = carbonate accumulation; Bqm = silica cementation.

accumulation; Bqm silica cementation

One detailed soil horizon was analysed on the south wall (see Figure 3.17), straight across from H4-42N (H4-42S). Its Orthic A horizon was a fine sandy loam (15%) with a loose consistency and apedal structure with few fine roots present. The carbonate accumulated (Bk) horizon was a fine sandy loam (17% clay), also with a granular structure, loose consistency, and some fine white roots. The next horizon, a silica cemented (Bqm1) horizon, had a very firm, coarse to platy, silica indurated structure. Below the Bqm1 horizon, another nest was present (this may have been part of the H1-42N nest before the excavator cut a deep trench in it). It was oval shaped, with a thick chert/ silica coating/impregnation on its outer edge, with active termites inside of the nest, along the inner silica-lined edge. Many tunnels (12 mm diameter) were present, with some being partially filled with frass micro aggregates. The lowest horizon, another silica cemented (Bqm2) horizon, consisted of indurated silica and transported materials.
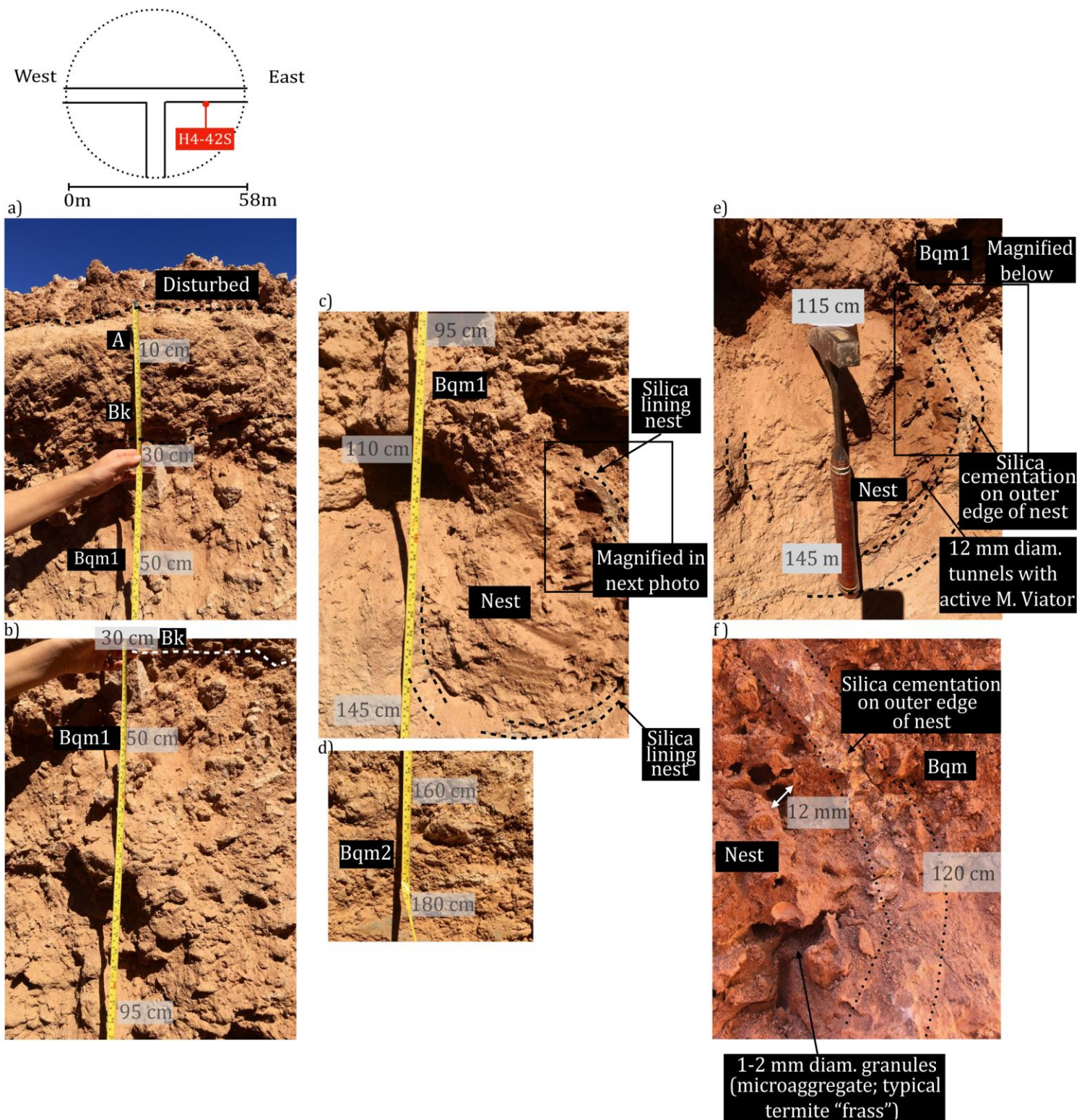
Figure 3.17: Detailed soil profile description of H4-42S. a) to d) shows the entire detailed profile from top to bottom; e) is a magnified picture of a portion of the nest shown in c); f) is a magnified area of e), showing the silica cementation on the outer edge of the nest, as well as the termite frass within the nest. Bk = carbonate accumulation; Bqm = silica cementation.

77

3.2 Soil EC and pH

When plotting pH against EC, a trend can be seen for most of the samples (Figure 3.18), although there are outliers as well. EC appears to increase from a pH of 6 to around 7.5, with its highest peak being at 13749 µS cm⁻¹. Most EC values fall below 8000 µS cm⁻¹ above a pH of 8.5, and thereafter EC values decrease to zero. H1 had a variation in EC of 49 µS cm⁻¹ to 13794 µS cm⁻¹, while H4 had a variation of 47 µS cm⁻¹ to 12457 µS cm⁻¹. For pH, H1 varied from 6.09 to 9.79, while H4 varied from 6.06 to 9.87. There were no major differences in EC and pH with respect to both heuweltjies.
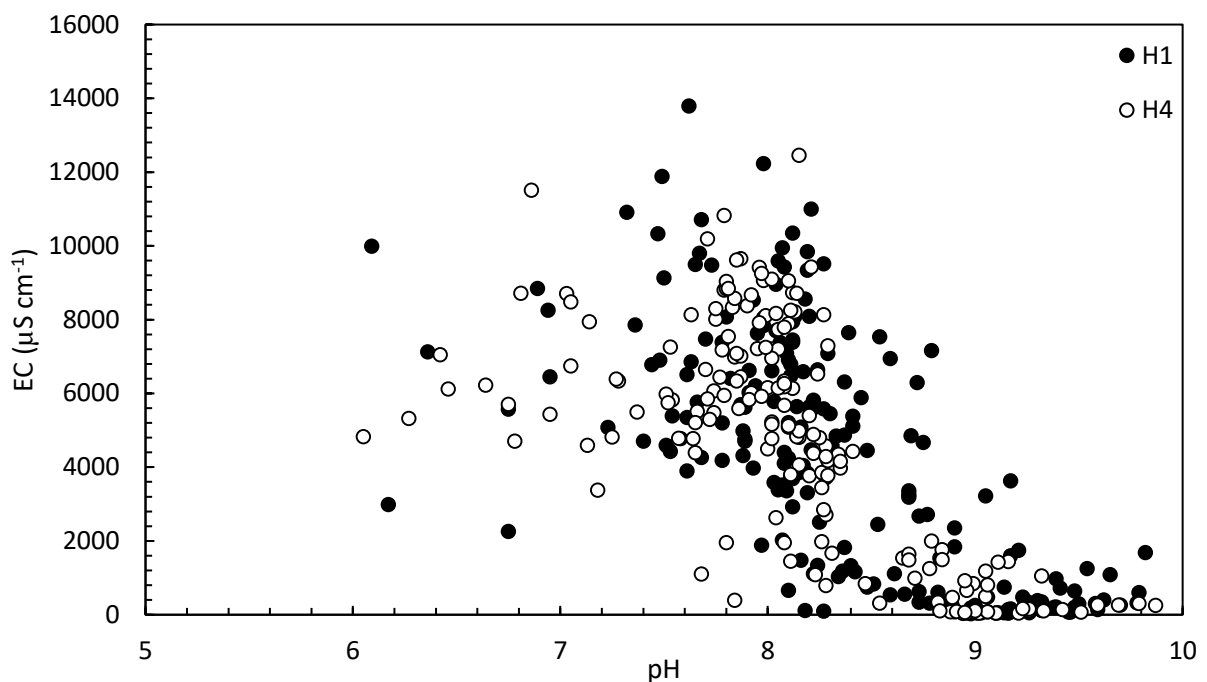
Figure 3.18: pH vs EC for H1 and H4 for 1:5 soil: deionised water samples.

3.3 Particle size

The following section shows the results obtained for particle size analysis of H1 and H4.

3.3.1 Heuweltjie 1

Most of the soils analysed in H1 were sandy loams (see Figure 3.19 and Table 3.1). At H1-4, in the interheuweltjie area, 4 m from the west end of the heuweltjie trench, the sediment analysed was coarser than the heuweltjie soils and was classified as being sand to loamy sand. Most of the heuweltjie soils were less coarse than the interheuweltjie soils. The sediment sampled at greater depths were classified as sand, which would be expected as it gets closer to the dorbank layer. The large nest close to the centre of the heuweltjie was classified as being a loam.
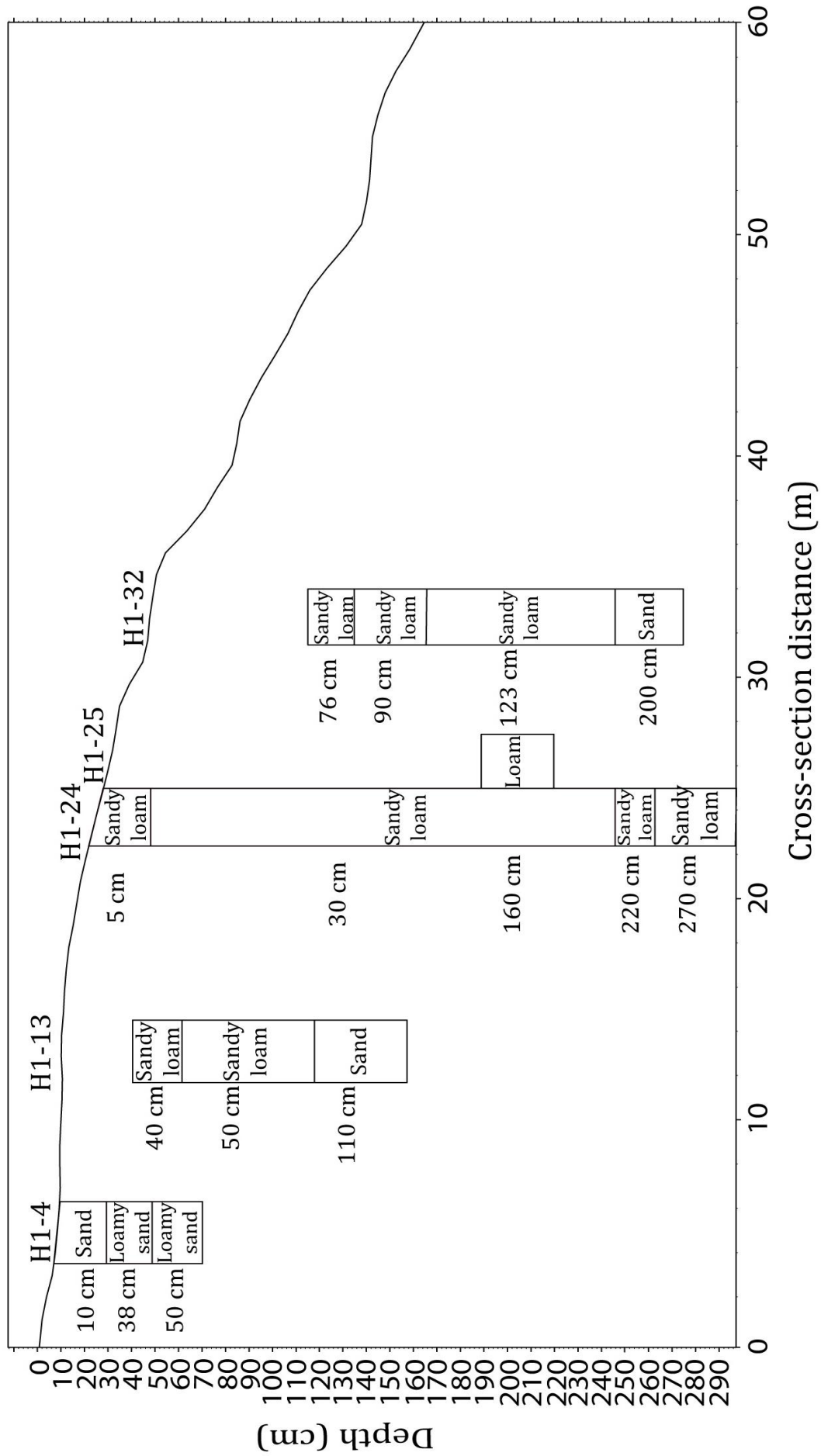
Figure 3.19: Cross-sectional depiction of soil texture within H1. Heuweltjie outline is plotted with a x3 exaggeration.

Table 3.1: Particle size data for H1.

Sample ID	% sand	% silt	% clay	Soil Classification
H1-4-10	93.06	4.04	2.91	Sand
H1-4-38	85.55	8.53	5.92	Loamy sand
H1-4-50	78.62	21.28	0.10	Loamy sand
H1-13-40	53.92	34.20	11.87	Sandy loam
H1-13-50	61.62	29.90	8.49	Sandy loam
H1-13-110	93.98	5.07	0.95	Sand
H1-24-5	52.65	35.63	11.72	Sandy loam
H1-24-30	53.62	33.65	12.72	Sandy loam
H1-24-220	63.62	27.86	8.52	Sandy loam
H1-24-270	62.55	34.41	3.04	Sandy loam
H1A-25-160	51.13	33.56	15.31	Loam
H1-32-76	63.25	32.72	4.03	Sandy loam
H1-32-90	75.06	17.51	7.43	Sandy loam
H1-32-123	65.13	30.73	4.14	Sandy loam
H1-32-200	94.84	2.24	2.92	Sand

3.3.2 Heuweltjie 4

Although a similar trend was noted for H4, it did, however, have more loamy sand classifications than H1 (see Figure 3.20 and Table 3.2). No interheuweltjie detailed samples were obtained in the field, and the smaller samples obtained did not contain enough soil for particle size and other analyses combined. Therefore, it could not be determined whether the heuweltjie and interheuweltjie soils would have had different textures, although it is assumed that the interheuweltjie would again have a coarser texture than the heuweltjie itself. For H4-19-80, 19 m from the west end of the heuweltjie trench, a distinction was made between the coarse and fine samples from this depth, with the coarse being more sandy – a loamy sand – than the fine sample, which was classified as a loam. The lower depths within the heuweltjie were mostly loamy sands, again indicating that the heuweltjie sediments become coarser the closer it gets to dorbank. For H1-19-110, the sample taken from a termite nest, did not classify as a loam. The same would be assumed for H4-42S-100's nest (see Table 3.2).
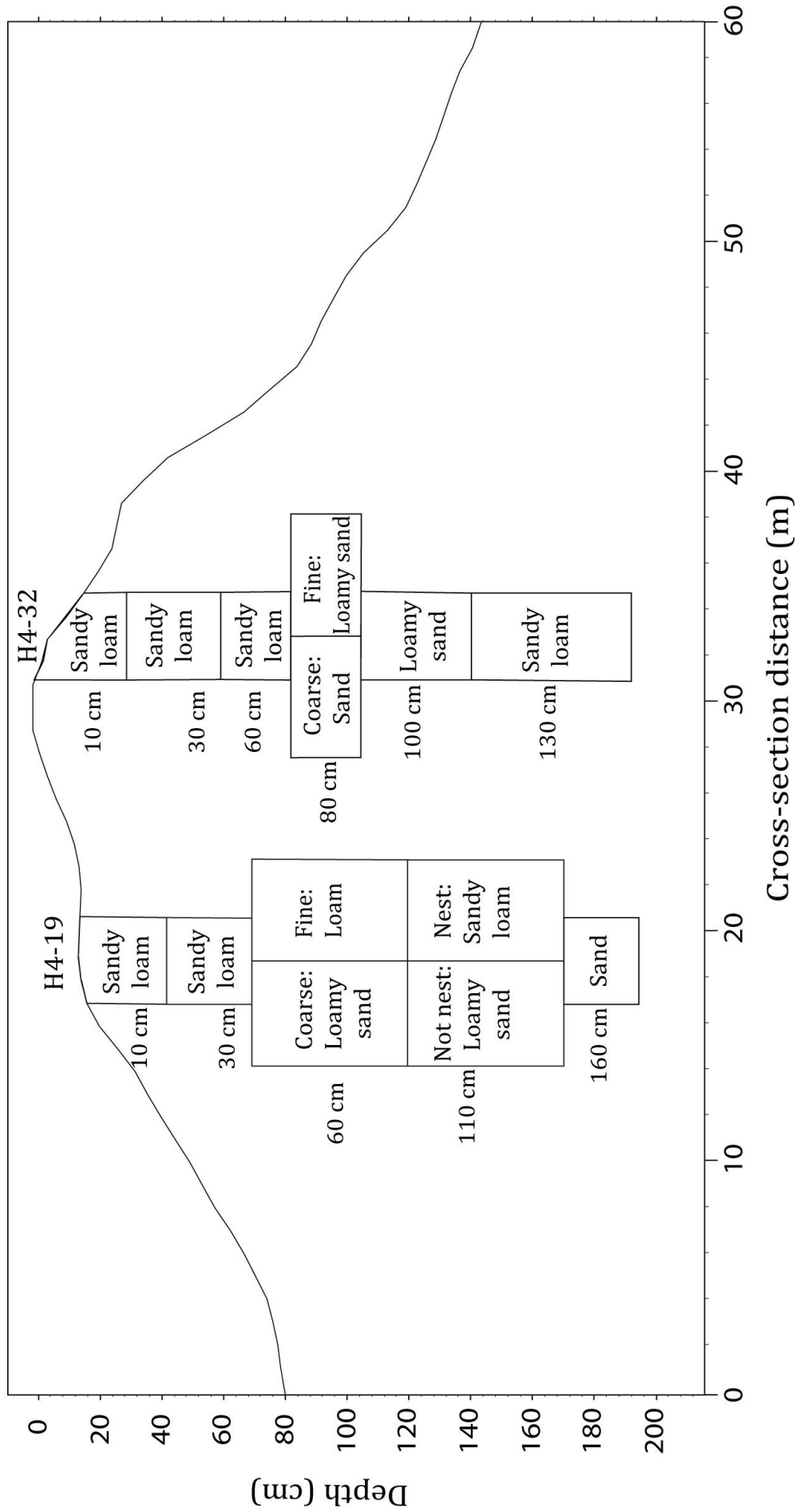
Figure 3.20: Cross-sectional depiction of soil texture within H4. Heuweltjie outline is plotted with a x3 exaggeration.

Table 3.2: Particle size data for H4.

Sample ID	% sand	% silt	% clay	Soil Classification
H4-19-10	67.39	29.55	3.07	Sandy loam
H4-19-30	68.37	31.52	0.11	Sandy loam
H4-19-60 (coarse)	79.79	18.06	2.15	Loamy sand
H4-19-60 (fine)	48.85	42.14	9.01	Loam
H4-19-110 (not nest)	85.79	11.01	3.20	Loamy sand
H4-19-110 (nest)	73.74	21.96	4.31	Sandy loam
H4-19-160 (dorbank)	92.06	7.82	0.11	Sand
H4-32-10	70.48	23.26	6.26	Sandy loam
H4-32-30	64.72	29.15	6.14	Sandy loam
H4-32-60	70.02	20.72	9.27	Sandy loam
H4-32-80 (fine)	79.74	16.22	4.04	Loamy sand
H4-32-80 (coarse)	88.19	9.84	1.97	Sand
H4-32-100	80.08	14.91	5.01	Loamy sand
H4-32-130	60.63	30.87	8.50	Sandy loam
H4-42-30 S	64.17	29.08	6.75	Sandy loam
H4-42-50 S	84.63	13.22	2.16	Loamy sand
H4-42-110 S (Nest)	62.97	28.38	8.65	Sandy loam
H4-42-150 S	88.90	8.96	2.14	Sand

When comparing particle size for both heuweltjies, no profound differences were noted, as the most abundant particle size class for both was sandy loam. One difference that could be noted would be that the nests in H4 did not contain as much clay as that of H1.

3.4 Mineralogy

Clay mineralogy was performed on 33 detailed soil samples. The following section displays the magnesium treated clay separates. Four untreated soil samples, obtained from the bulk samples that did not undergo any treatment, were also analysed for mineralogy. No major differences were noted between H1 and H4, other than that H4 contained more gypsum than H1. H4 had peaks for hydroxyapatite, while H1 did not. Both heuweltjies also had calcium oxalate peaks, with H1 showing very strong evidence for the presence of calcium oxalate at H1-24.

3.4.1 Heuweltjie 1

3.4.1.1 *Interheuweltjie soil*

No changes in mineralogy were observed down the interheuweltjie horizons within the H1-4 profile (Figure 3.21). Initial quartz and illite peaks were identified at 1.00 nm and 0.70 nm respectively. Quartz had its initial peak at 0.43 nm, with a large second peak at 0.33 nm.
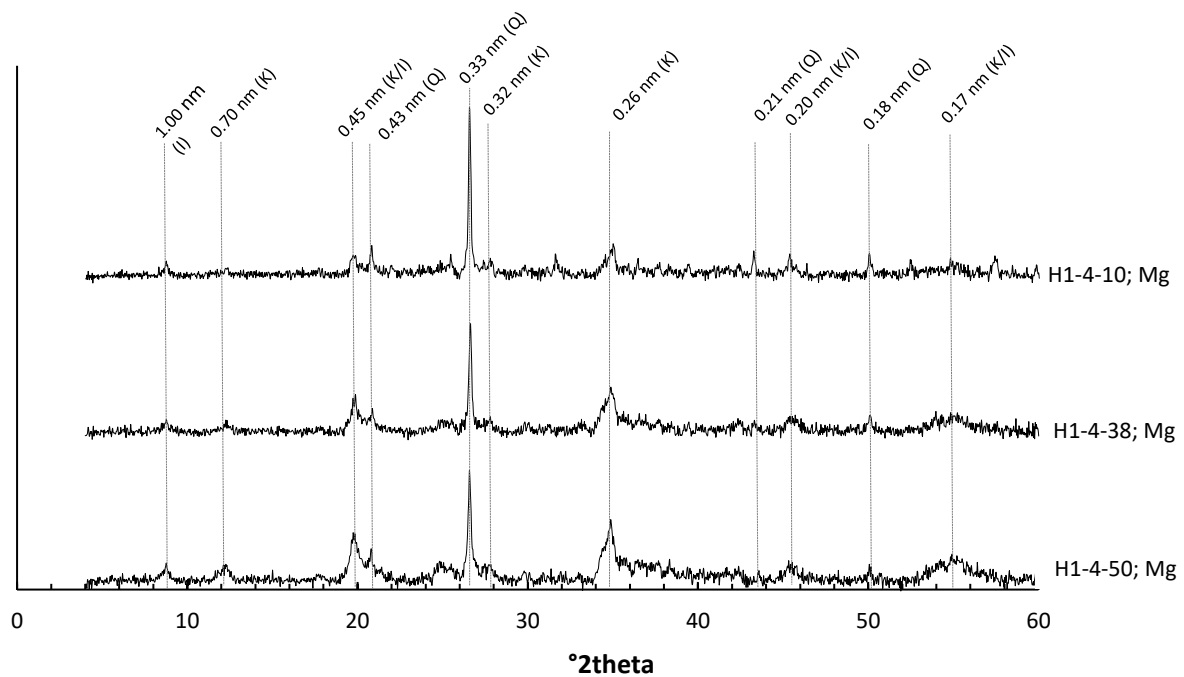
Figure 3.21: XRD peaks for H1-4 Mg treated clay separates of interheuweltjie soil (I= illite, K= kaolinite, Q= quartz).

3.4.1.2 *Heuweltjie soil*

There were no changes in mineralogy of the clay size fraction down the profile 13 m from the west end of the heuweltjie trench, H1-13 (Figure 3.22). Small peaks were identified for illite (I) and kaolinite (K) at 1.00 nm and 0.70 nm respectively. Calcite (C) was present throughout the profile, with its initial peak at 0.39 nm, and a strong peak at 0.30 nm. Quartz (Q) showed an initial small peak at 0.43 nm, with a strong peak at 0.33 nm.
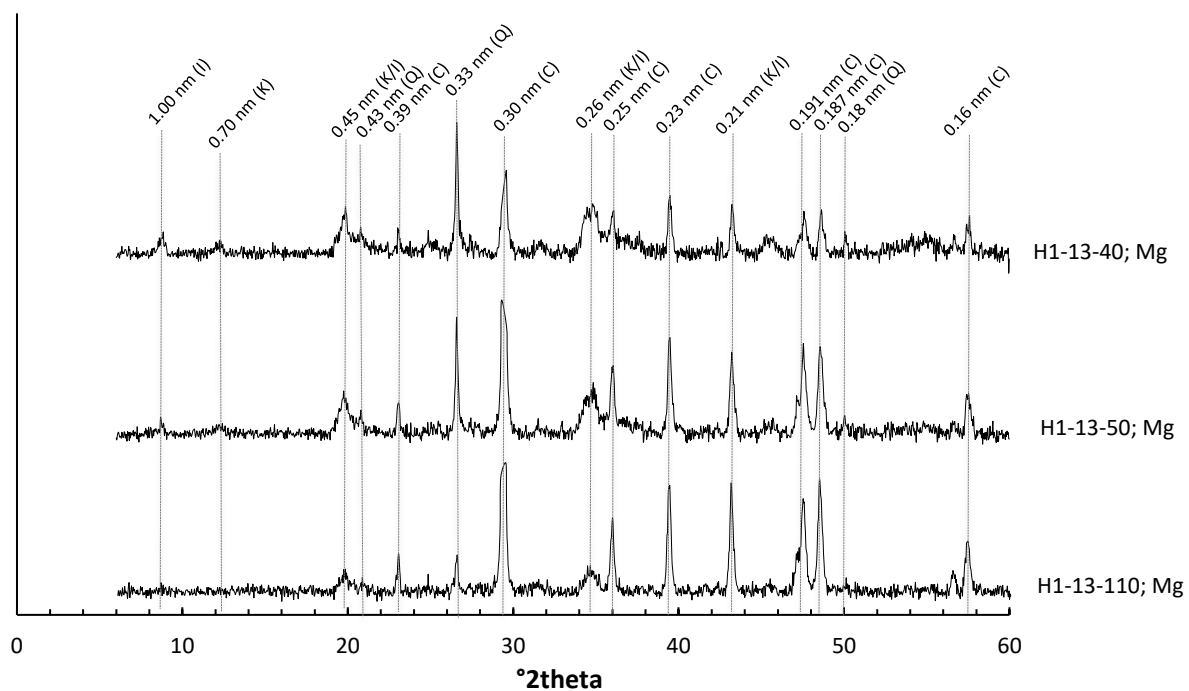
Figure 3.22: XRD peaks for H1-13 Mg treated clay separates (I= illite, K= kaolinite, Q= quartz, C= calcite).

In Figure 3.23, the entire H1-24 profile was analysed for clay mineralogy, along with the large nest at H1-25, which is also present within this figure. A similar trend was seen for the profiles in the centre of the heuweltjie associated with the large and small nests, H1-24 and H1-25 respectively, as there were no major changes in the minerals of the clay fraction throughout the profile (Figure 3.23). Small peaks were identified at 1.00 nm and 0.70 nm for illite and kaolinite respectively. A small peak for quartz was identified at 0.43 nm, with a stronger peak showing at 0.33 nm. Calcite showed a strong peak at 0.30 nm at the depths of 5 and 30 cm for H1-24, as well as in the nest, H1-25-160. Below the nest area of H1-24 (220 and 270 cm depths), no calcite was present.
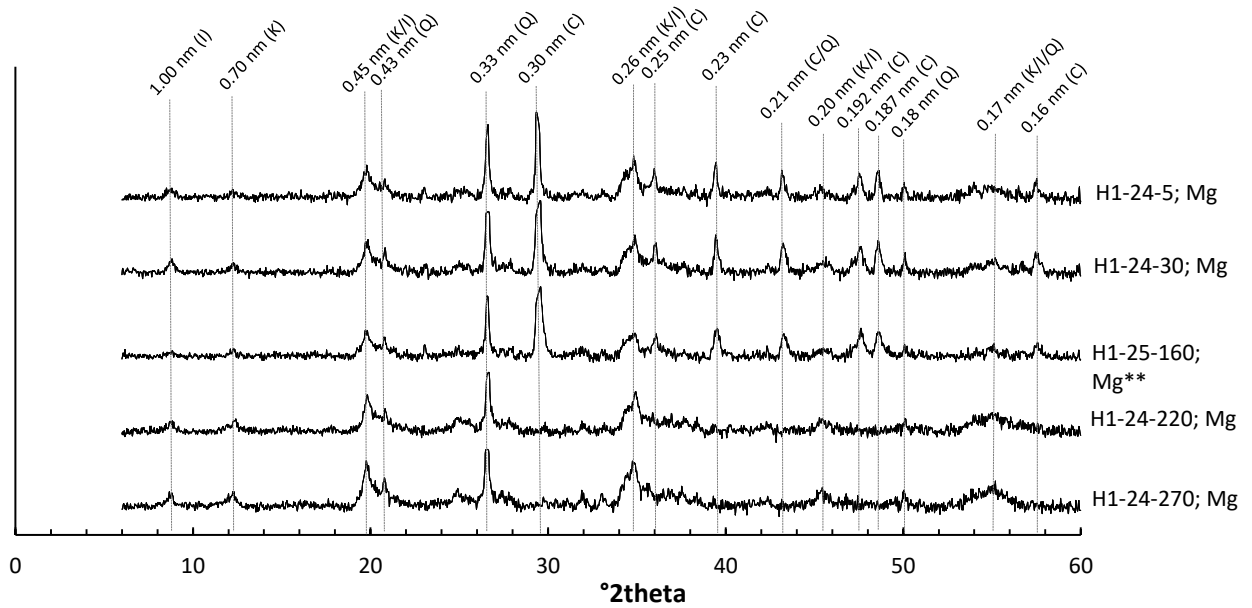
*Figure 3.23: XRD Peaks for H1-24 & 25 Mg treated clay separates. ** Refers to the large nest sample situated at a cross section of 25 m (I= illite, K= kaolinite, Q= quartz, C= calcite).*

There were major changes in the soil mineralogy going down the H1-32 soil profile (Figure 3.24) further towards the eastern edge of the heuweltjie. However, a similar trend was seen for the 76 cm and 200 cm depths. At a depth of 90 cm, the peaks identified were gypsum (G) and calcium oxalate (O). The initial strong peak identified at this depth for gypsum occurred at 0.75 nm, and the initial small peak for calcium oxalate at 0.60 nm. At 123 cm, calcium oxalate was the only mineral identified, with its initial strong peak observed at 0.60 nm. At the top and bottom depths (76 and 200 cm), small peaks were identified for illite and kaolinite at 1.00 nm and 0.70 nm respectively. Peaks for quartz were also identified, with a small peak at 0.43 nm and a strong peak at 0.33 nm.

86
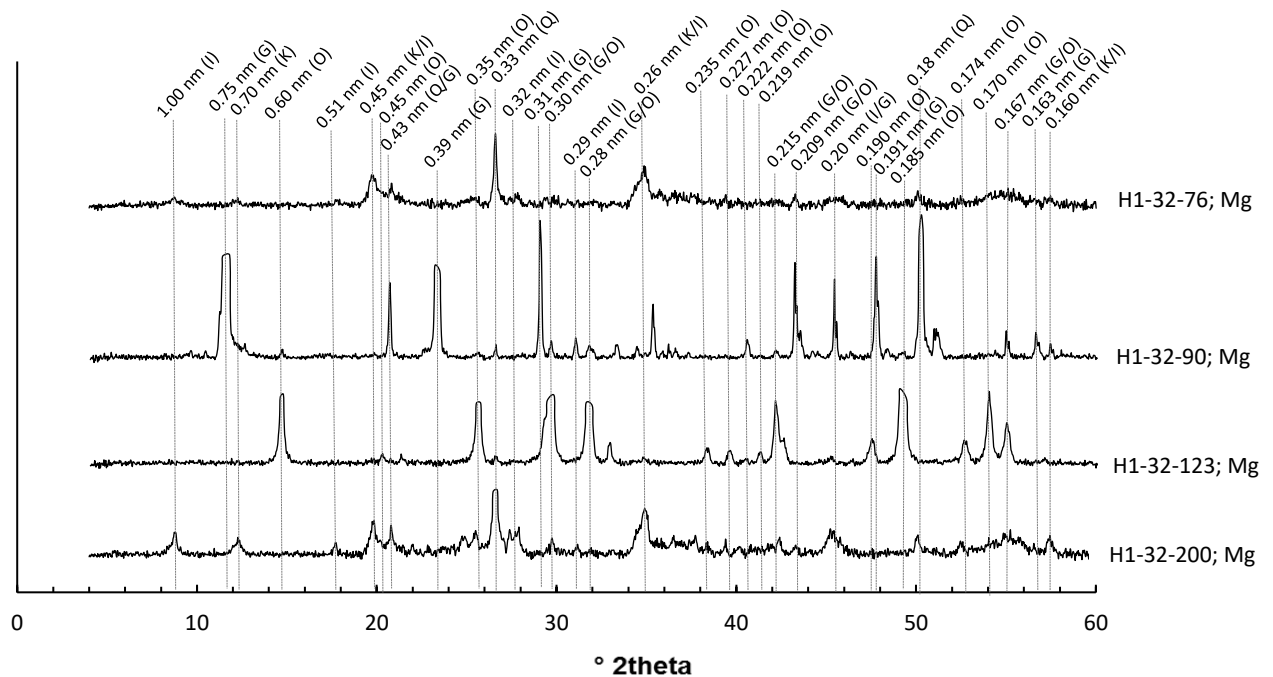
Figure 3.24: XRD Peaks for H1-32 Mg treated clay separates (I= illite, K= kaolinite, Q= quartz, G= gypsum; O= calcium oxalate).

3.4.2   Heuweltjie 4

A similar trend can be seen throughout the soil profile H4-19, the detailed soil profile closest to the west end (Figure 3.25), for all depths other than at 60 cm. Small peaks were identified for illite and kaolinite at 1.00 nm and 0.70 nm respectively, for all depths other than 60 cm. Strong quartz peaks at 0.33 nm were also identified for these depths, as well as strong calcite peaks at 0.30 nm. At the 60 cm depth, for the coarse fraction, most of the peaks identified were for hydroxyapatite (H), with the initial small peak at 0.334 nm, and a stronger and broader peak at 0.28 nm. The fine fraction at the 60 cm depth consisted of gypsum, with its initial strong peak at 0.75 nm. Calcium oxalate was also present in this horizon, with its initial peak at 0.60 nm.

87
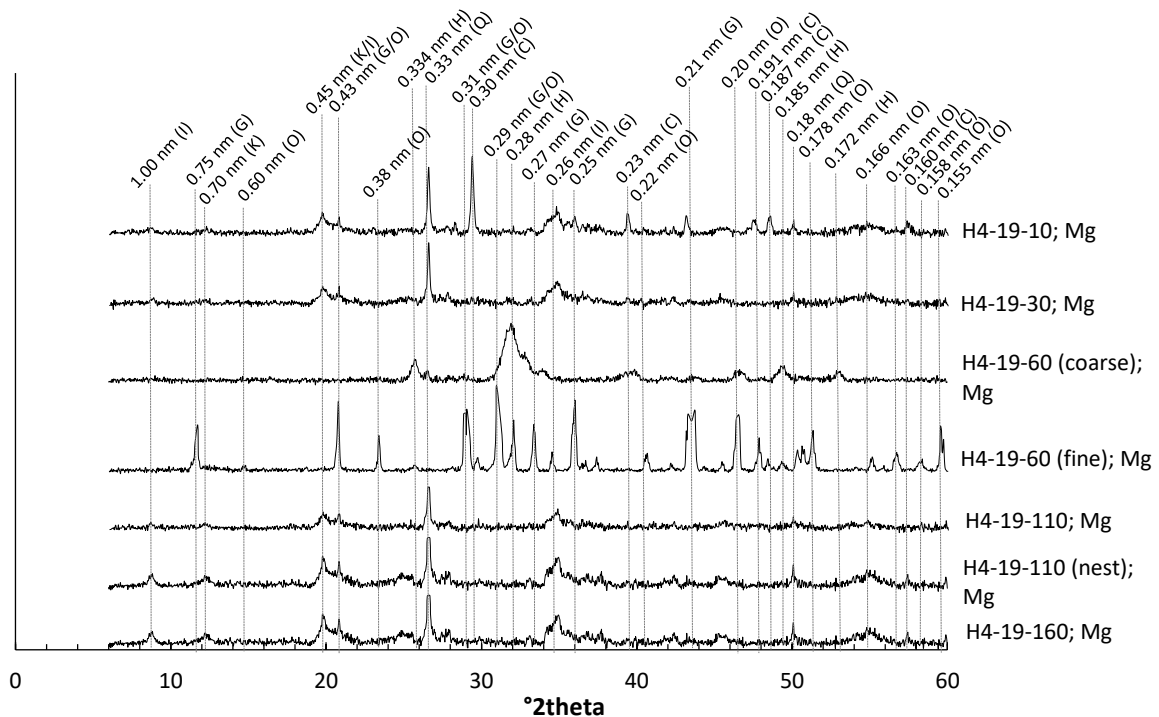
Figure 3.25: XRD Peaks for H4-19 Mg treated clay separates (I= illite, K= kaolinite, Q= quartz, G= gypsum, H= hydroxyapatite, C = calcite, O= calcium oxalate).

All depths of H4-32 (the detailed profile closer to the eastern edge of the heuweltjie) other than 130 cm, showed a similar initial trend (Figure 3.26). Small peaks were identified for illite and kaolinite at 1.00 nm and 0.70 nm respectively. A small peak was identified for quartz at 0.43 nm, and a large peak at 0.33 nm. The first three depths (i.e. 10, 30 and 60 cm) also showed the presence of calcite, while the other three did not. For the top three depths, a small peak at 0.38 nm, and a large peak at 0.303 nm were identified for calcite. At the depth of 130 cm, the initial peak at 0.60 nm was identified as calcium oxalate. All other peaks identified in this horizon were also for calcium oxalate.

88
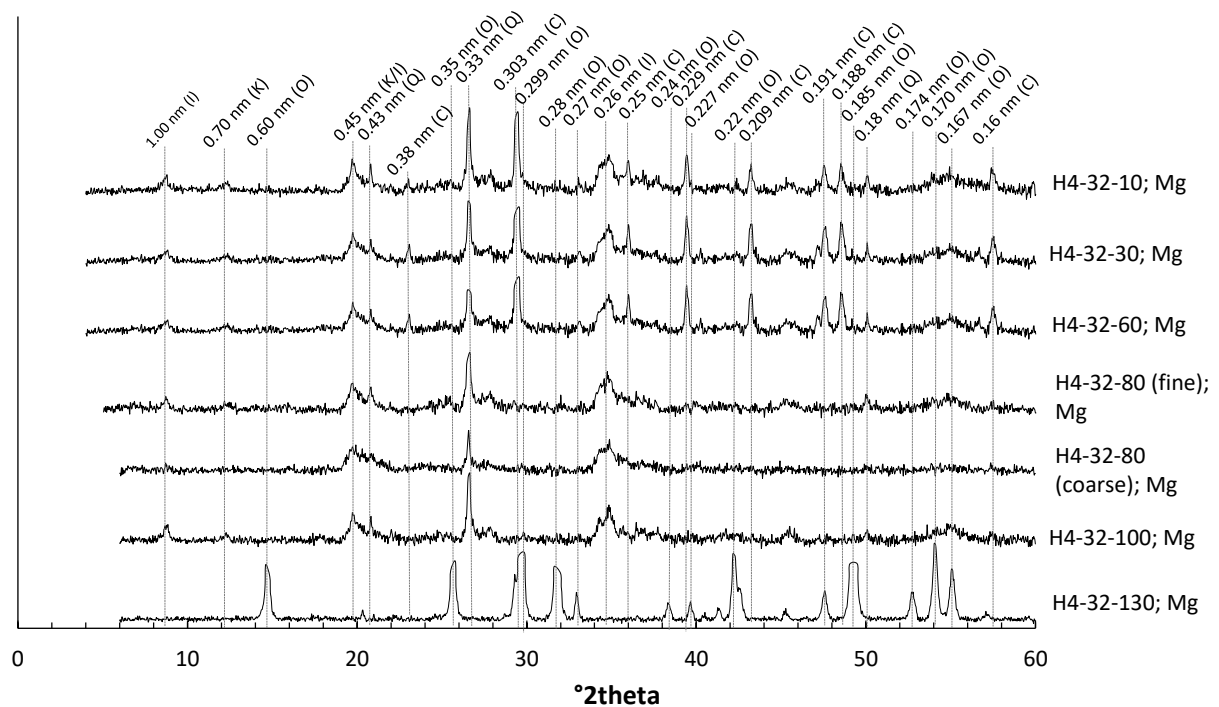
Figure 3.26: XRD Peaks for H4-32 Mg treated clay separates (I= illite, K= kaolinite, Q= quartz, C= calcite; O= calcium oxalate).

H4-42S (42 m from the west end of the trench, situated on the south wall) consisted mostly of illite, kaolinite, quartz and calcite (Figure 3.27). The top three horizons (30, 50, and 110 cm) showed consistency in their peaks, while at a depth of 150 cm, the main peaks identified were for calcite, with an initial calcite peak at 0.38 nm, and a strong peak at 0.30 nm. For the other depths, small peaks were identified for illite and kaolinite at 1.00 nm and 0.70 nm respectively. A small peak was identified for quartz at 0.43 nm, with a larger peak at 0.33 nm, identified at all depths. The top depths (i.e. 10, 30 and 60 cm) also contained calcite, although not as much as at 150 cm.

89
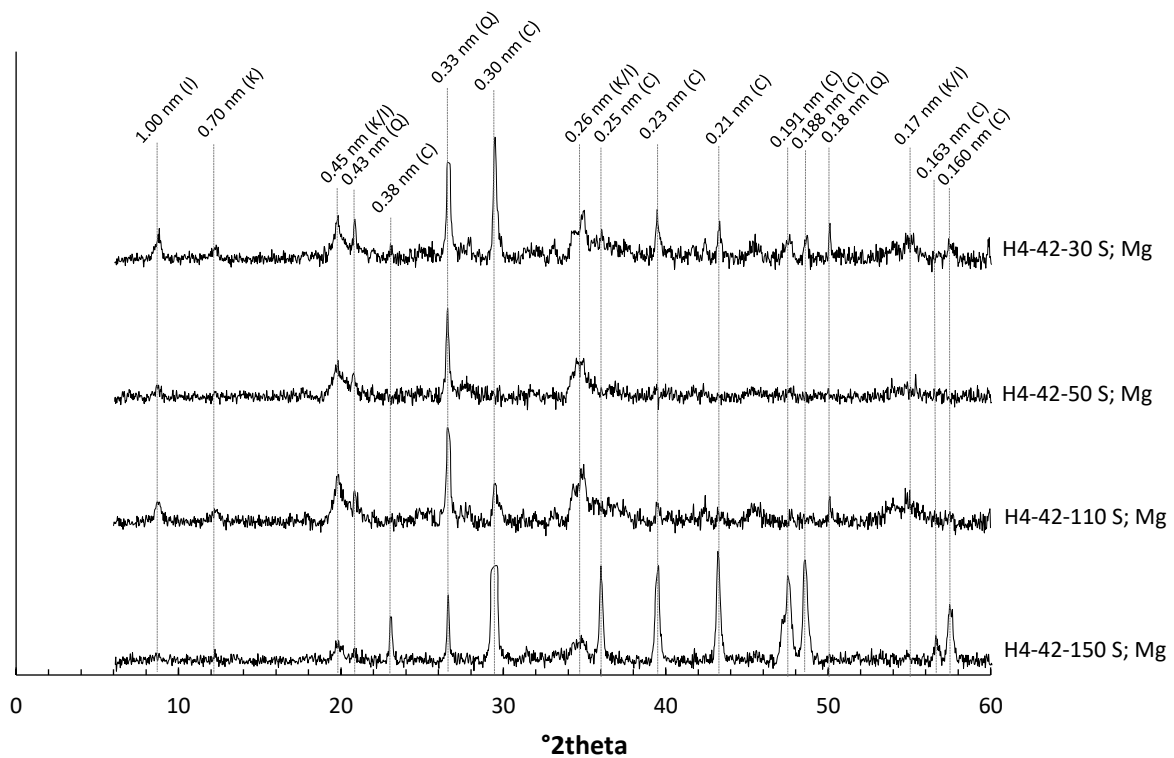
Figure 3.27: XRD Peaks for H4-42S Mg treated clay separates (I= illite, K= kaolinite, Q= quartz, C= calcite).

3.4.3 Termite frass and faecal pellet mineralogy

For H1, no significant change was noted between the faecal pellets and the sample at 30 cm depth within H1-24 (Figure 3.28), the profile with the smaller nest situated close to the centre of the heuweltjie (refer to Figure 3.1 and Figure 3.7). Small peaks were identified for illite at 1.00 nm and 0.45 nm. Quartz showed a strong peak at 0.43 nm. Albite (A) was also present in these samples, with its initial peak identified at 0.40 nm. Microcline (M) was identified through small peaks at 0.35 nm and 0.291 nm. The samples also contained calcite, with a strong peak identified at 0.31 nm. The faecal pellets contained a suggestive calcium oxalate peak at 0.60 nm.
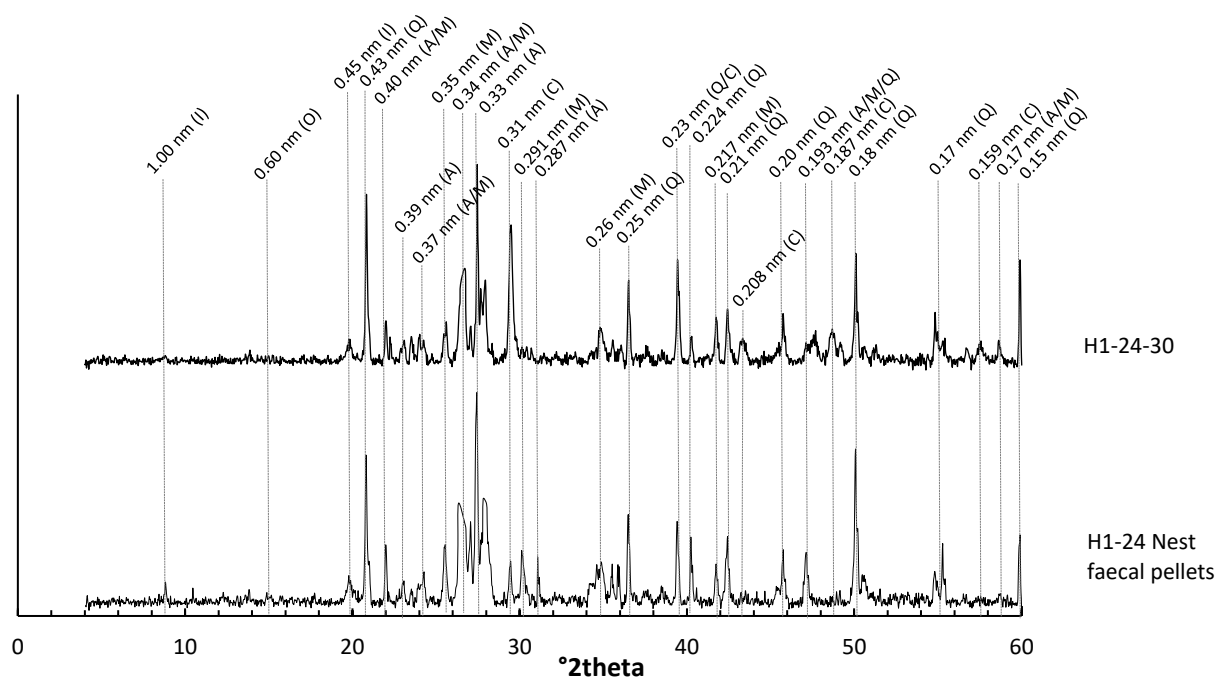
Figure 3.28: XRD Peaks for H1-24 with no treatment (I= illite, Q= quartz, M= microcline, A=albite, C = calcite, O= calcium oxalate).

For H4, a slight difference was noted between the frass and the 140 cm depth for H4-42 (Figure 3.29), situated closer to the eastern end of the heuweltjie trench (see Figure 3.11 and Figure 3.16). This profile had active termites and was situated 2 m north of the H4-42S profile, which was located on the opposite side of the trench wall. The frass sample contained gypsum, while the other did not. The initial strong gypsum peak for the frass sample occurred at 0.77 nm, with another at around 0.43 nm, where the strong quartz peak is in the 140 cm depth sample. Albite was present within both samples, with an initial peak at 0.40 nm, and a strong peak shown at 0.32 nm, along with other peaks throughout. Quartz showed a strong peak for both samples at 0.33 nm as well.

91
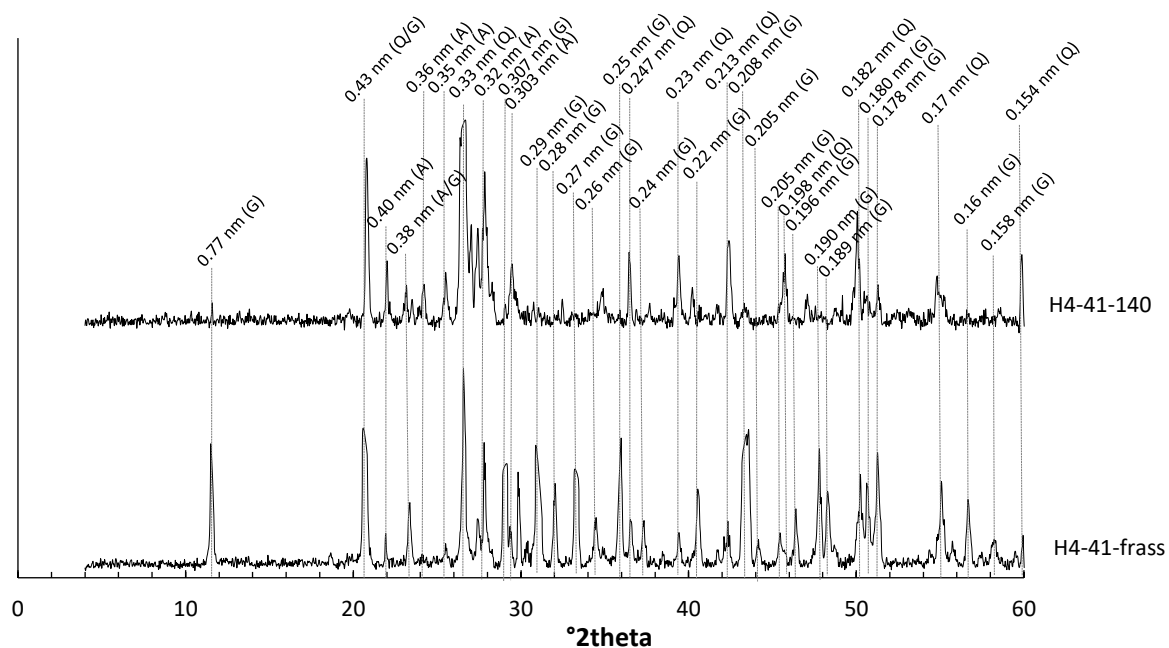
Figure 3.29: XRD Peaks for H4-42 with no treatment (Q= quartz, G= gypsum, A = albite).

3.4.4 Spatial variation in mineralogy

Illite, kaolinite, and quartz were mostly present throughout all horizons and all heuweltjie profiles. Only illite, kaolinite and quartz were present within the interheuweltjie soils.

Calcite

Calcite was not present in all heuweltjie profiles analysed. From the XRD data for H1-13 (Figure 3.22), calcite was present within all horizons of the profile. The calcite was present in carbonate accumulated (Bk) horizons, where some calcite nodules were also present in the top horizons. The top two horizons of H1-24 (at 5 and 30 cm; Figure 3.23) contained calcite. These horizons were carbonate accumulated (Bk). The untreated H1-24 samples (at 30 cm and the termite frass close to the nest; Figure 3.28) also contained calcite. These samples were also obtained from the carbonate accumulated horizons (Bk). H1-25 (the large nest sample at 160 cm) contained calcite as well.

For H4, calcite was present in the top horizons of H4-19 (Figure 3.25), again where the soils have an accumulation of carbonates, along with many calcite nodules. For H4-32 (Figure 3.26), calcite was present in the top three soil horizons (10, 30 and 60 cm), again all present within the carbonate accumulated horizons containing many calcite nodules.

92

Within H4-42S (Figure 3.27), calcite was present throughout the carbonate accumulated horizons, along with the nest located at around 110 cm depth, and the soil below the nest.

Gypsum

In H1, gypsum was present in H1-32 (Figure 3.24) at a depth of 90 cm, close to the frass chamber (see Figure 3.1). In H4, it was present within the fine soil obtained in H4-19 (Figure 3.25) at a depth of 60 cm. This is located where the gypsum precipitate was noted within the heuweltjie profile (see Figure 3.11). At H4-42 (the untreated sample and termite frass; Figure 3.29), gypsum was present within both the frass sample and the sample at 140 cm depth (Figure 3.28). The frass sample was obtained from the nest, and the sample situated at 140 cm was located by the tunnels, where gypsum was observed.

Microcline

Microcline was only present within H1. For the H1-24 untreated sample (Figure 3.28), it was present within both the nest faecal pellets, and within the 30 cm horizon, which is a carbonate accumulated horizon (Bk). At H1-32 (Figure 3.24), microcline was present within the bottom soil horizon, Bkqm (carbonate and silica cementation).

Albite

Albite was present within the untreated samples for both heuweltjies. In H1-24 (Figure 3.28), it was present within the faecal pellets (close to the nest within this profile) and at 30 cm. For H4-42 (Figure 3.29), albite was also present within the frass and at a depth of 140 cm. The frass was present within the nest, while the other was present by the termite tunnels.

Hydroxyapatite

Hydroxyapatite was only present within one soil horizon, H4-19-60 (coarse; Figure 3.25). The location of this sample was within the Bqym (silica and gypsum cementation) horizon.

Calcium oxalate

Calcium oxalate was present in both heuweltjies. Within H1, calcium oxalate was present at H1-32 (Figure 3.26) at 90 cm and 123 cm depths. At 90 cm, the calcium oxalate was present within the carbonate accumulated (Bk) horizon, just below the termite frass chamber. The calcium oxalate present at 123 cm depth was situated within the bottom

Bkqm (carbonate and silica cementation) horizon (see calcium oxalate locations in Figure 3.1). A suggestive calcium oxalate peak was also found for the untreated sample, H1-24 faecal pellets, situated in the Bk horizon close to the termite nest (Figure 3.28). For H4, calcium oxalate was present in the fine fraction of H4-19-60 (Figure 3.25). This is situated within the Bqym horizon (silica and gypsum cementation), close to where the gypsum precipitate was found, above the collapsed nest (see Figure 3.11). It was also present at H4-32-130 (Figure 3.26), again within the Bqym horizon.

3.5 Ionic activities and saturation indices of major ions

The water extraction data was divided into two separate categories for H1 and H4 and used for calculating ion activity and saturation indices for specific minerals. These minerals were chosen based on data obtained from the clay mineralogy results, along with others that were presented in research articles on heuweltjies (such as sepiolite). Ion activity (Figure 3.30), saturation indices plotted against Cl^- (Figure 3.31), and saturation indices plotted against pH (Figure 3.32) were analysed, and results are shown below.

3.5.1 Ion activities

The variation in activity of all ions with Cl^- is consistent with the seawater dilution line, as there is a significant ($p=0.000$) positive correlation between Na^+ and Cl^- (Figure 3.30a). K^+ remains constant as evaporation increases (Figure 3.30b), as shown by its non-significant ($p>0.05$) correlation, with activity values ranging from around -2 to -4 once Cl^- increases past -1. The ions Mg^{2+}, Ca^{2+}, and SO_4^{2-} increase as evaporation rates increase (Figure 3.30c, d and e), although at slopes less than that of the conservative solutes Na^+ and Cl^-. Mg^{2+} and Ca^{2+} have significant ($p=0.000$) positive correlations to $\log[Cl^-]$, although not as high a correlation as Na^+. SO_4^{2-} does not have as high a positive correlation with $\log[Cl^-]$, yet the correlation is still significant ($p=0.000$). SO_4^{2-} decreases slightly at higher evaporation rates. Bicarbonate (HCO_3^-) decreases slightly as evaporation increases (Figure 3.30f), and therefore has a significant ($p=0.000$) negative correlation with $\log[Cl^-]$. $H_4SiO_4^0$ remains constant throughout as evaporation increases (Figure 3.30g), although its activity is higher in H4 than H1. As its remained constant, $H_4SiO_4^0$ had a weak correlation ($p=0.000$) with $\log[Cl^-]$. pH values decrease slightly as evaporation increases

(Figure 3.30h), and is therefore slightly negatively correlated with Cl^-, with its correlation being significant (p=0.000). Hydrogen phosphate (HPO_4^{2-}) decreases as evaporation increases (Figure 3.30i). Dihydrogen phosphate ($H_2PO_4^-$) decreases slightly as evaporation increases (Figure 3.30j), but not at the same rate as HPO_4^{2-}. Both HPO_4^{2-} and $H_2PO_4^-$ are therefore negatively correlated (p=0.000) with $\log[Cl^-]$.
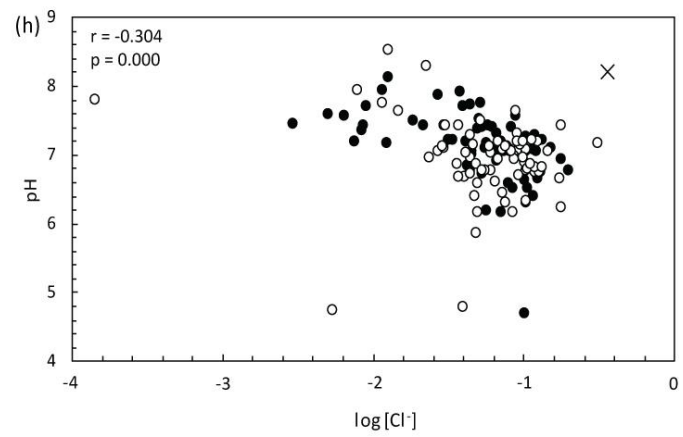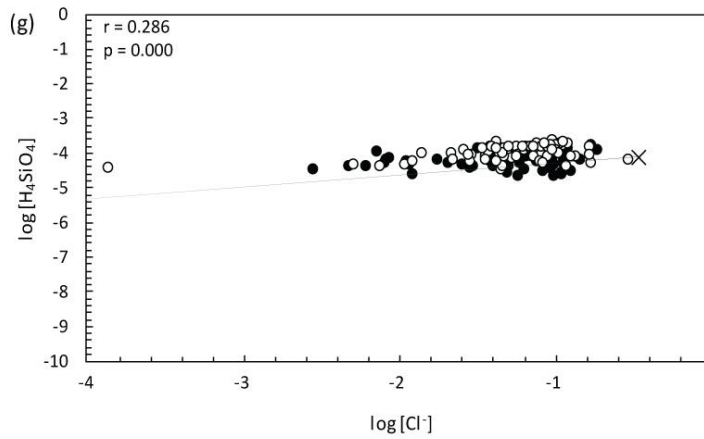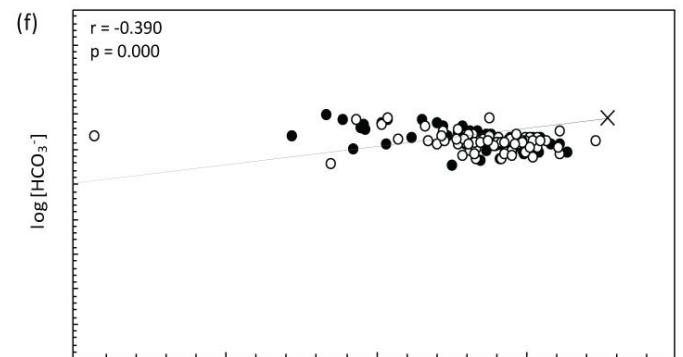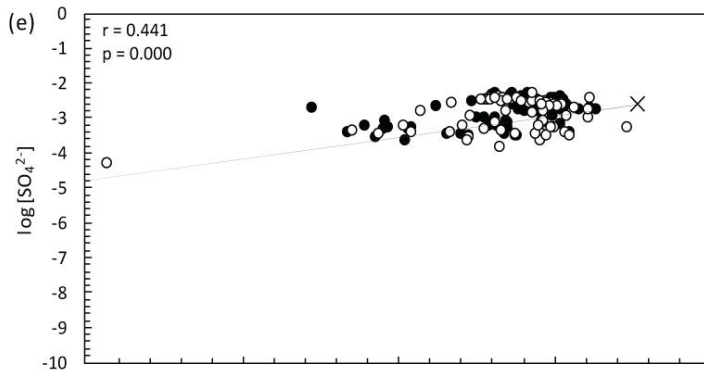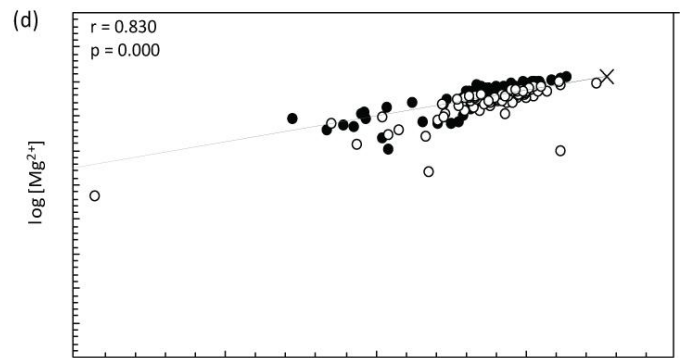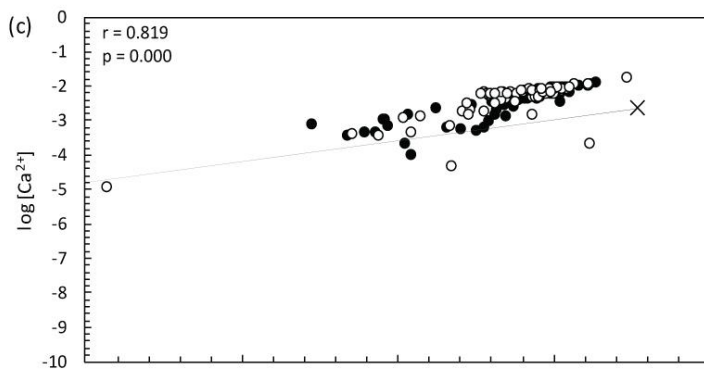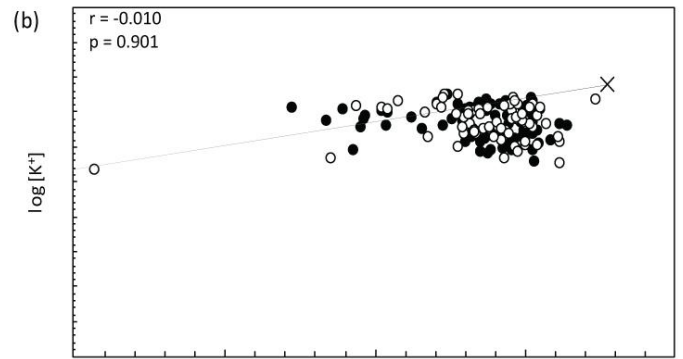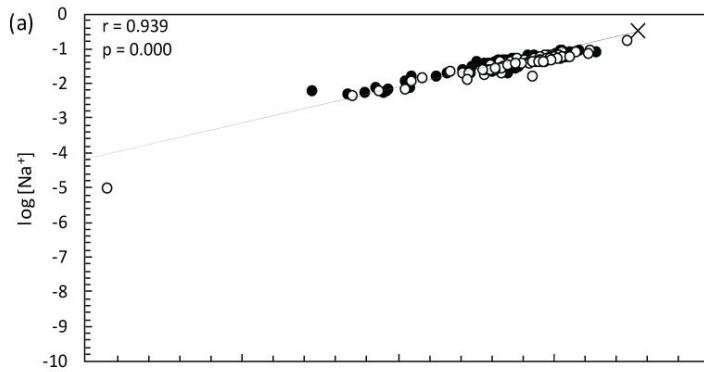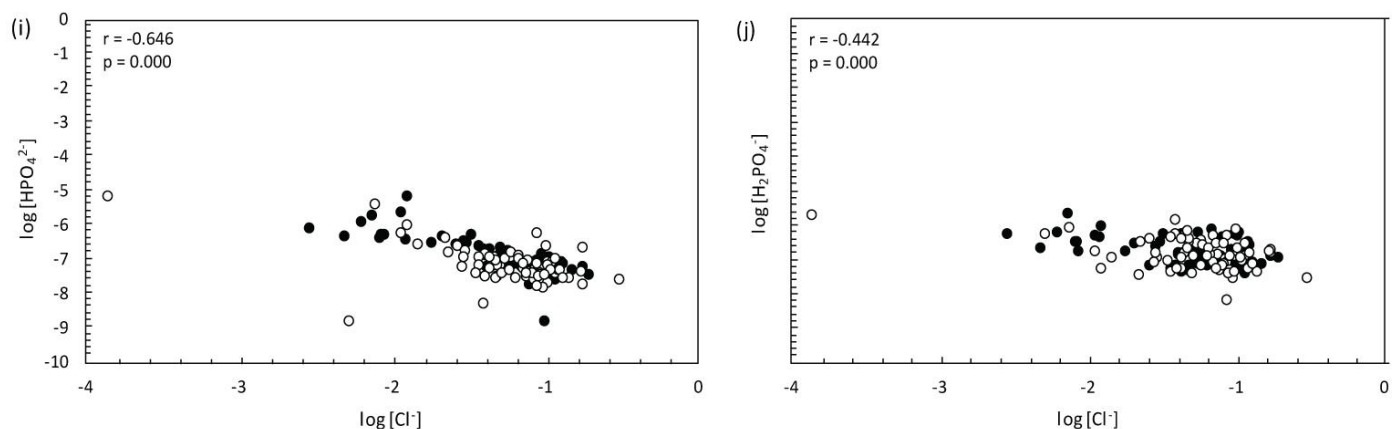
Figure 3.30: Variation of ionic activity with Cl⁻ in 1:1 soil: deionised water extracts. Solid circles represent samples from H1; open circles represent samples from H4; × represents the seawater composition.

3.5.2 Saturation indices

3.5.2.1 Saturation indices with respect to evaporation

Halite remained undersaturated (Figure 3.31a), and had a significant (p=0.000) positive correlation with log[Cl⁻]. Consequently, all Cl⁻ was assumed to have remained in solution, causing it to be suitable for use as a proxy for evaporative concentration. Calcite SI falls mostly within the 0 to -2 range (Figure 3.31b), indicating that it is close to saturation, with a few samples being saturated. Calcite had poor correlation (p<0.05) with log[Cl⁻], and so does not become more saturated as evaporation increases. Gypsum is also mostly undersaturated within the heuweltjies (Figure 3.31c), and has a good and significant (p=0.000) positive correlation with log[Cl⁻], indicating that an increase in evaporation causes it to become more saturated, as seen by the few falling on the zero line at higher evaporation rates. Hydroxyapatite is mostly saturated to supersaturated (Figure 3.31d), with a few outliers being undersaturated. It has a very poor and non-significant (p>0.05) correlation with log[Cl⁻], and so is not affected by evaporation rates. Quartz SI falls between +2 and -2, with most being close to saturation or undersaturated (Figure 3.31e). Amorphous silica, on the other hand, mostly has a SI of close to -2, with all samples being undersaturated (Figure 3.31f). Sepiolite is also undersaturated for all samples (Figure 3.31g). Quartz, amorphous Si and sepiolite all have poor correlation (p<0.05) with log[Cl⁻], and so are not affected by increasing evaporation rates.

97
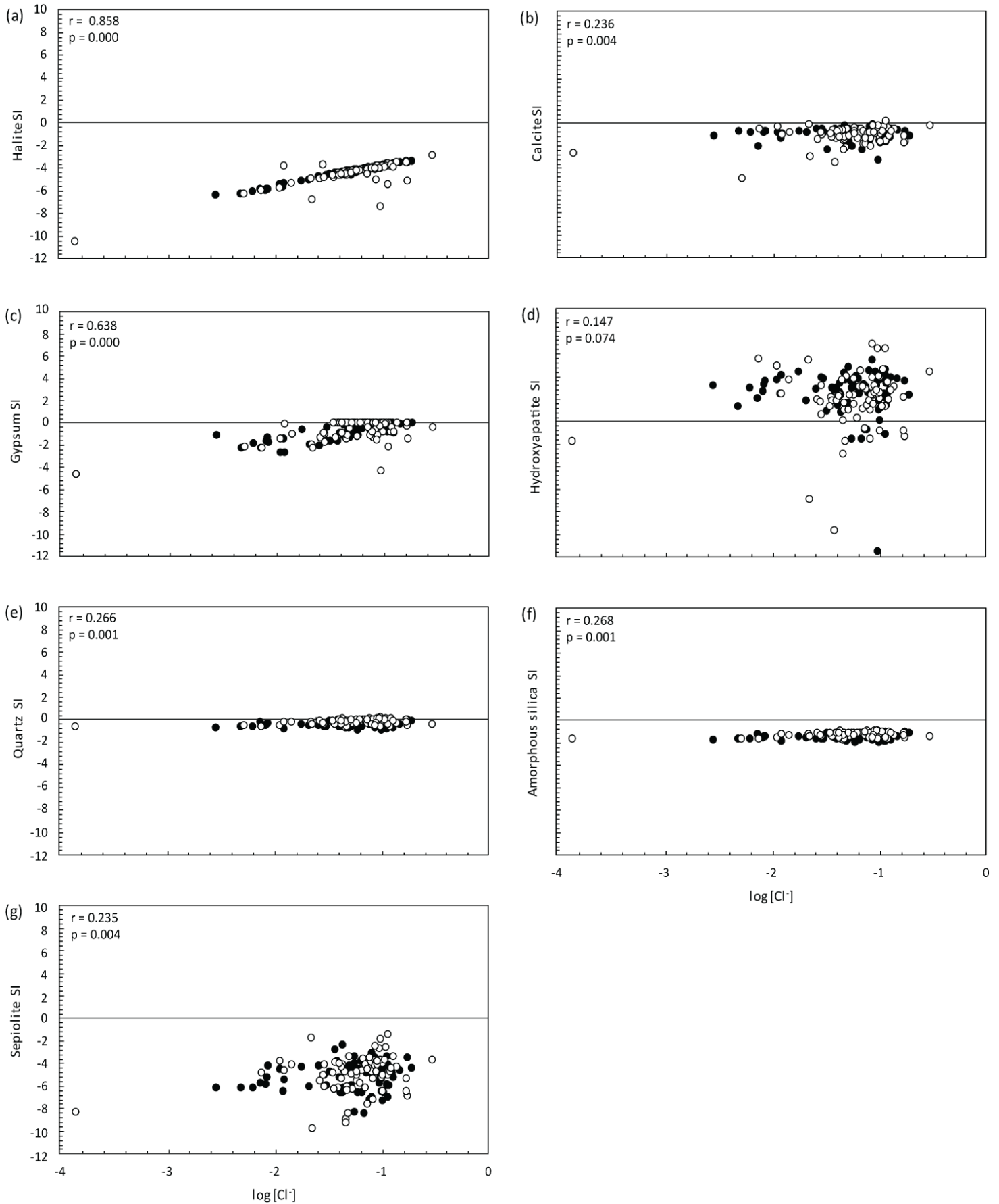
Figure 3.31: Variation of saturation indices with Cl- in 1:1 soil: deionised water extractions. Symbols same as in Figure 3.30.

98

3.5.2.2   Saturation indices with respect to pH

The SI of halite is not pH dependent, and has poor ($p<0.05$) negative correlation with pH (Figure 3.32a). Calcite has a significant ($p=0.000$) positive correlation with pH (Figure 3.32b). It increases in saturation as pH increases, levelling off at a pH of around 7. Gypsum's SI is slightly pH dependent and has a significant ($p=0.000$) positive correlation (Figure 3.32c). Hydroxyapatite's SI is greatly affected by pH (Figure 3.32d), as seen by its significant ($p=0.000$) positive correlation with pH. A major increase of saturation can be seen, with a few undersaturated samples at a pH close to 5, and most samples being oversaturated above a pH of 6. Quartz and amorphous silica (Figure 3.32e and f) are not pH dependent, and have poor correlation ($p=0.000$) with pH. Sepiolite's SI increases along with pH (Figure 3.32g), and has a significant positive ($p=0.000$) correlation with pH; however, it does not reach saturation.
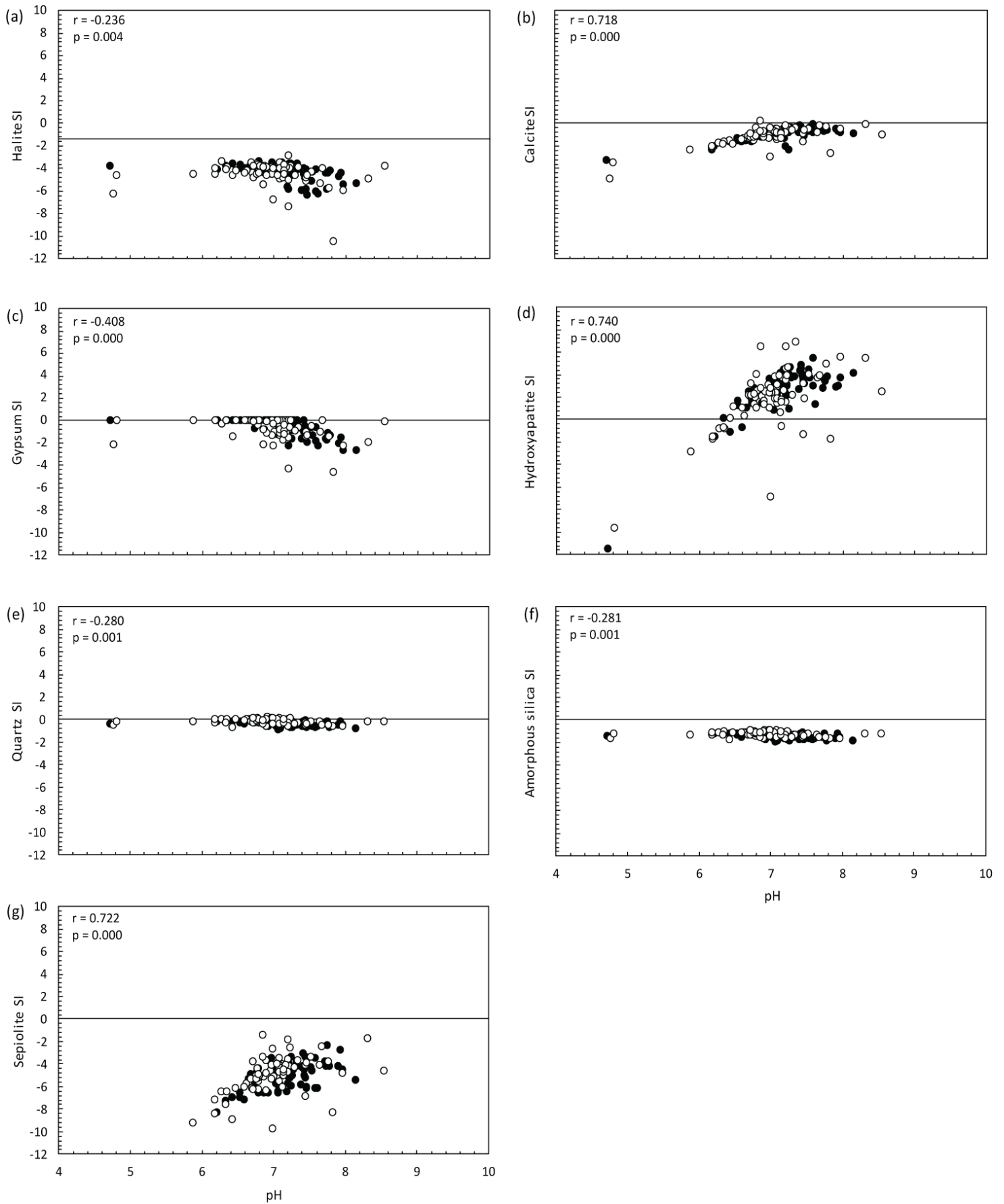
Figure 3.32: Variation of mineral SI with pH in 1:1 soil: deionised water extracts. Symbols same as in Figure 3.30.

3.6 Spatial variation in salts

Fifteen heat maps were created per heuweltjie for major ions, EC, pH, and saturation indices. Heat maps are discussed according to the trend throughout the heuweltjie profile. Each heat map will also be linked to the heuweltjie texture classifications (Figure 3.33a and Figure 3.34a).

3.6.1 Heuweltjie 1

3.6.1.1 Distribution of salts

EC for H1 (Figure 3.33b) has its highest values in the centre of the heuweltjie, with the interheuweltjie soils having much lower EC values. The high EC values extend down to about 2.5 m within the heuweltjie. pH has its highest values at the edges of the heuweltjie (Figure 3.33c), with pH decreasing deeper down into the heuweltjie structure. Na^+ and Cl^- follow a similar trend to each other (Figure 3.33d and e), with their values being higher in the middle of the heuweltjie with respect to its edges. A high concentration strip of Na^+ and Cl^- seems to move from the top to the bottom of the heuweltjie structure. SO_4^{2-} concentrations are higher deeper down within the heuweltjie structure (Figure 3.33f), closer to the deepest sampling points at the cross section distance of 15 m. Dissolved silica is also higher deeper down within the heuweltjie structure (Figure 3.33g) and has higher concentrations closer to the interheuweltjie (cross section distance of ~ 0-10 m). Ca^{2+} concentrations are not as high as Na^+ (Figure 3.33h) but does seem to follow the same trend as Na^+ and Cl^-, with higher concentrations at a cross section distance between 25 -35 m. Concentrations are not as high going down into the heuweltjie, however. Mg^{2+} concentrations are also highest within the middle of the heuweltjie cross section (Figure 3.33i), with high concentrations at around 35 m within the cross section. K^+ concentrations (Figure 3.33j) are highest going down within the heuweltjie at a cross section distance of around 25 m. Concentrations are very low everywhere else. HCO_3^- concentrations (Figure 3.33k) are highest at the edges and at the top of the heuweltjie structure.

Amorphous silica is close to saturation (Figure 3.33l), although still undersaturated, at the deepest sampling points from a cross section distance of 0-40 m within the heuweltjie structure. It follows a very similar trend to that of dissolved silica concentrations. Closer

to the surface, amorphous silica is more undersaturated. Hydroxyapatite is saturated throughout the heuweltjie structure (Figure 3.33m). Gypsum is undersaturated close to the interheuweltjie (Figure 3.33n). Deeper into the heuweltjie structure, the gypsum becomes saturated. This follows a similar trend as the movement of SO_4^{2-} throughout the heuweltjie. Calcite, on the other hand, is close to saturation mostly within the top soil horizons of the heuweltjie (Figure 3.33o). Halite is undersaturated throughout the heuweltjie structure (Figure 3.33p). It is closest to saturation within the middle cross section of the heuweltjie, while it is more undersaturated close to the interheuweltjie. It is important to note the trend of calcite being closest to saturation at the top, with gypsum being closer to saturation closer to the bottom of the heuweltjie soil horizons, along with halite. For all saturation indices, hydroxyapatite was most saturated, while halite was most undersaturated.

3.6.1.2   Salt distribution with respect to heuweltjie profile descriptions

For H1, EC seems to be high where the soils are granular in texture, starting at the top of the heuweltjie, and moving downwards to the two large nests (Figure 3.33a and b). The soils in this region of the heuweltjie range from an accumulation of carbonates (Bk) to carbonate and silica cementation (Bkqm). EC values also seem to be higher where active termites were found (cross-section distance of about 32 to 35 m). pH values (Figure 3.33c) lower into the heuweltjie are associated with carbonate accumulated (Bk) soils moving towards carbonate and silica cemented (Bkqm) soils. The lowest pH values are found close to the termite frass chamber. Na^+ and Cl^- (Figure 3.33d and e) follow a similar trend, with Na^+ having quite high concentration close to the silica and carbonate cemented (Bkqm) area. Na^+ and Cl^- concentrations are high where the nests are located, although concentrations seem to be higher next to the nests rather than within the nests. Concentrations are also high where the termite frass and the calcite nodules close to it were found. SO_4^{2-} (Figure 3.33f) was mostly located within the carbonate and silica cemented (Bkqm) soils, as well as where the nests are located. Some high concentrations were found at the termite frass area. Dissolved silica (Figure 3.33g) seems to move throughout the carbonate cemented (Bkm) and carbonate and silica cemented (Bkqm) soil horizons, with high concentrations close the termite frass area as well. High concentration was also found at the dorbank lens within the heuweltjie situated close to the termite frass chamber (cross section of 32 m). Highest Ca^{2+} concentrations (Figure

3.33h) are mostly located where an accumulation of calcite nodules within the carbonate accumulated (Bk) horizon are present, also the area of the termite frass. Ca^{2+} concentrations are not as high as expected at the nests. Highest Mg^{2+} concentrations (Figure 3.33i) are located by the termite frass area, where there is an accumulation of calcite nodules. K^+ concentrations (Figure 3.33j) are highest where the soils are apedal, and moves from carbonate accumulation (Bk), to carbonate cementation (Bkm), and then carbonate and silica cemented (Bkqm) soils going down the heuweltjie profile. HCO_3^- concentrations (Figure 3.33k) are highest where the carbonate cemented (Bkm) nodules are present at the edges of the heuweltjie cross sections.

Amorphous silica (Figure 3.33l) is closest to saturation within the carbonate and silica cemented (Bkqm) horizons of the heuweltjie structure, while it is more undersaturated within the carbonate accumulated (Bk) layers. Hydroxyapatite (Figure 3.33m) SI values are similar throughout the heuweltjie profile layers, being closest to undersaturation at the platy carbonate and silica cemented (Bkqm) horizon. Gypsum (Figure 3.33n) is saturated through the carbonate accumulated (Bk) and carbonate and silica cemented (Bkqm) horizons going down the profile, being undersaturated in the carbonate cemented (Bkm) horizons at the interheuweltjie. Calcite is closest to saturation within the carbonate accumulated (Bk) horizons and where calcite nodules are present, also extending to the carbonate and silica cemented (Bkqm) horizons at the bottom of the heuweltjie. Calcite (Figure 3.33o) is more undersaturated at the platy carbonate and silica cemented (Bkqm) horizon next to the two nests, as well as the carbonate accumulated (Bk) and the development of colour and structure (Bw) layers in the interheuweltjie. Halite (Figure 3.33p) is closest to saturation throughout all different soil horizons of the heuweltjie.
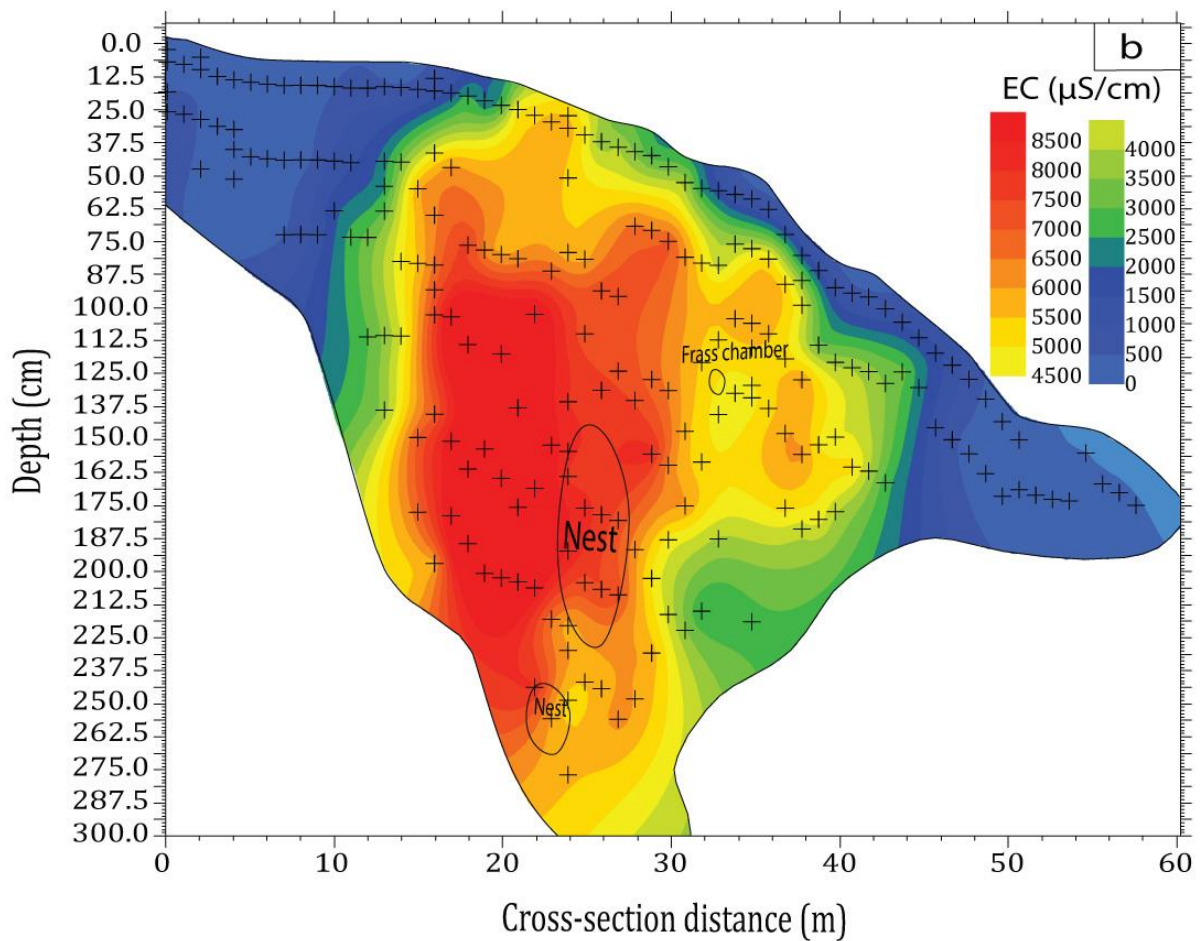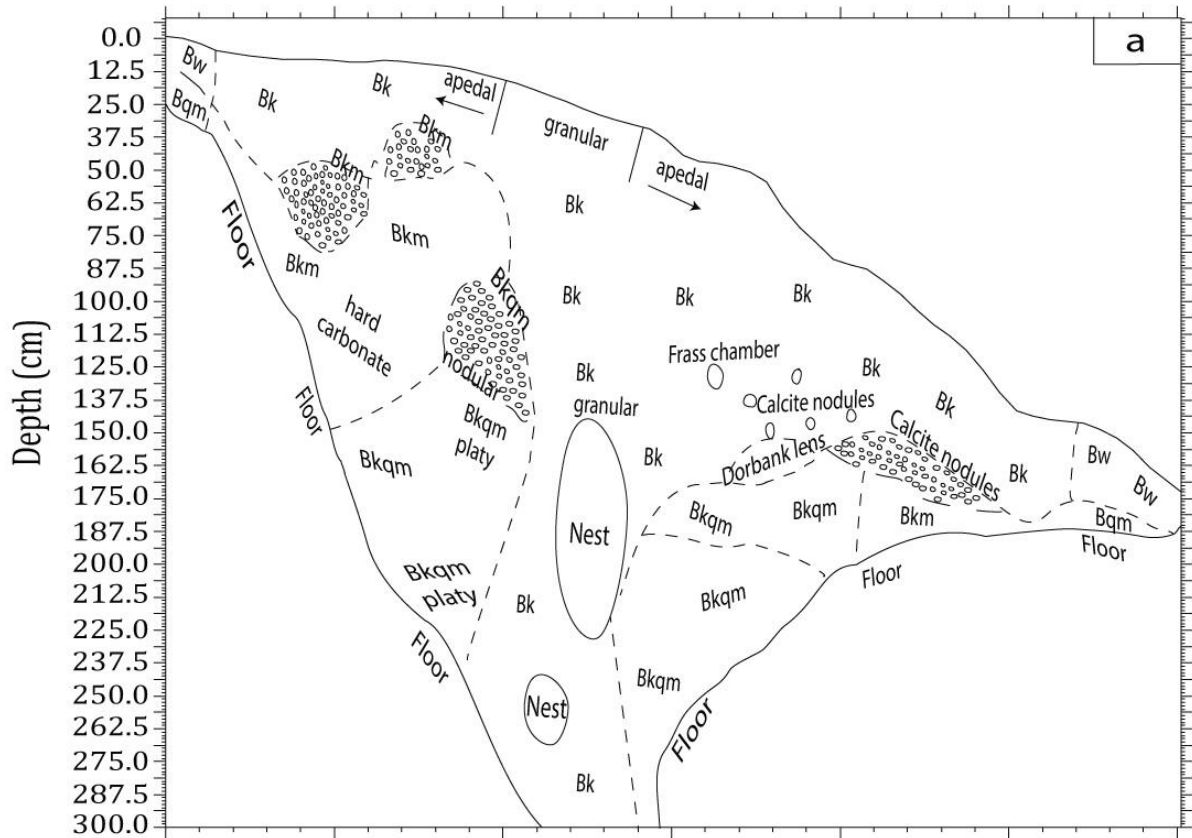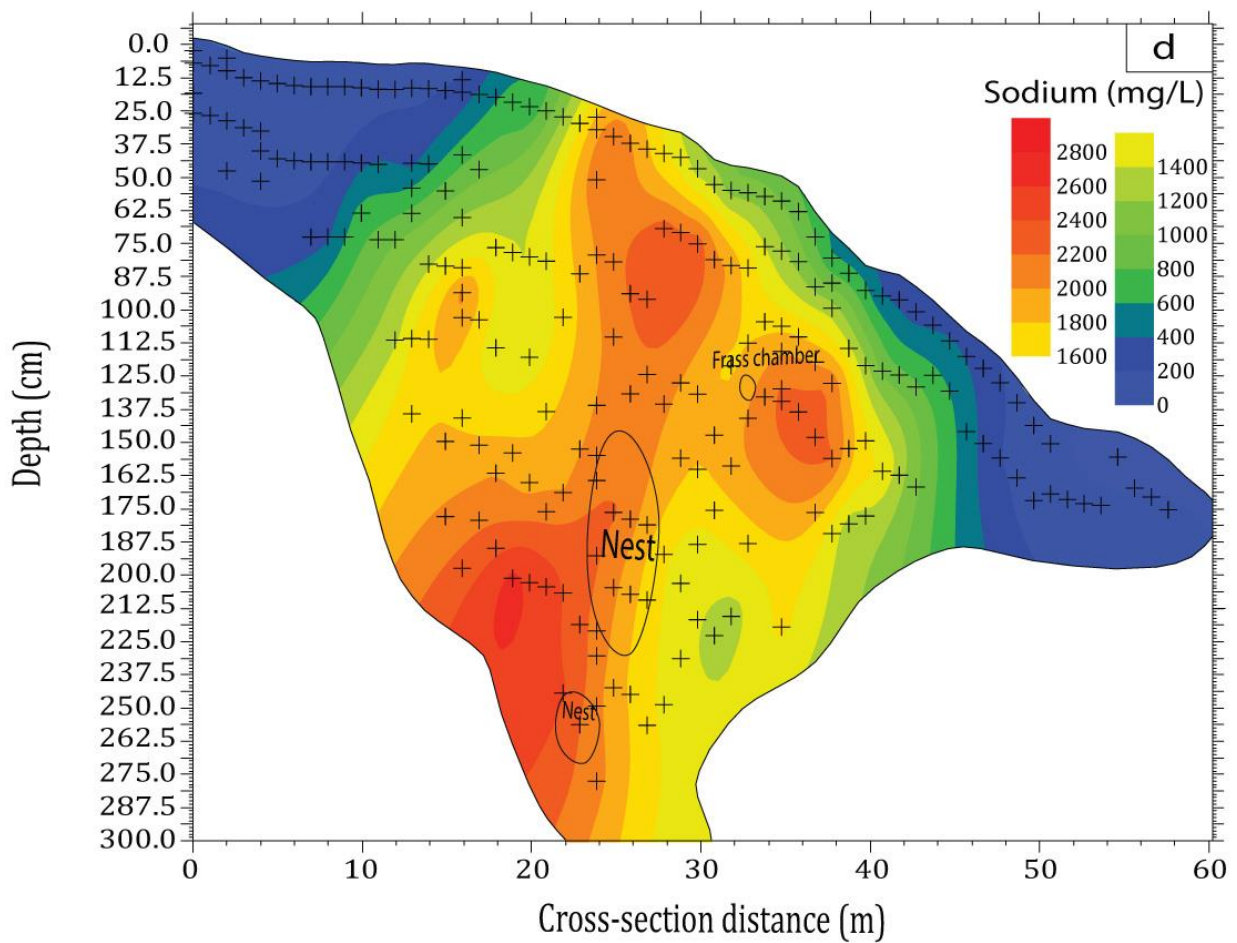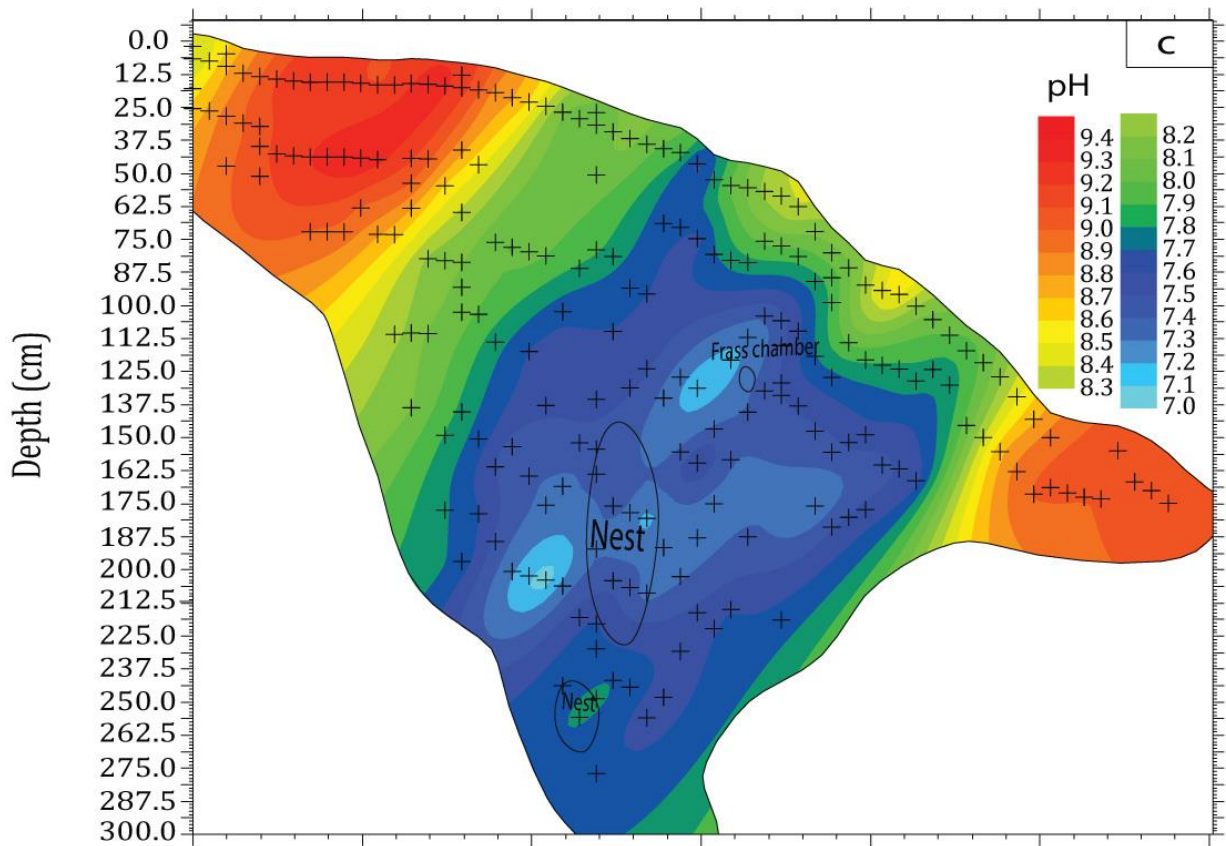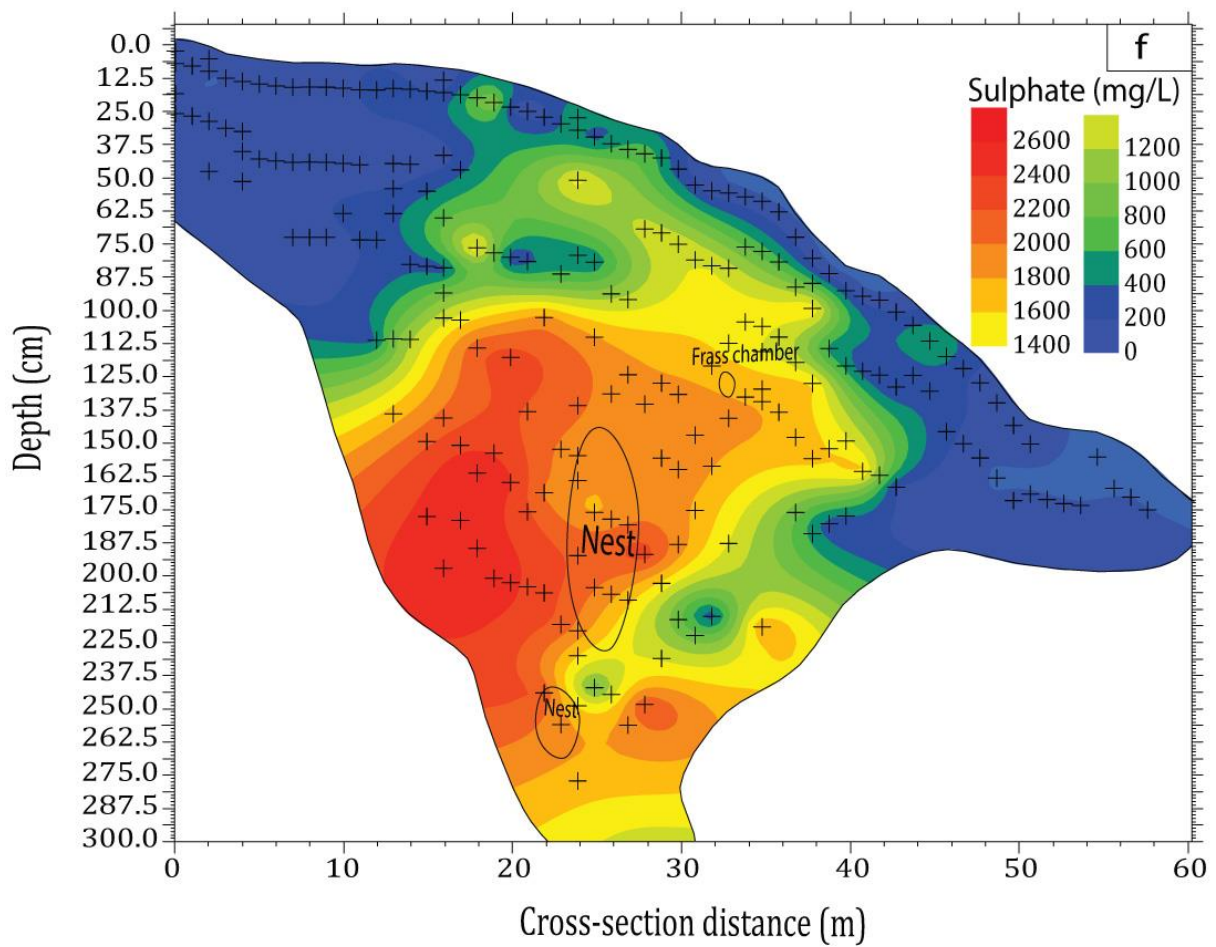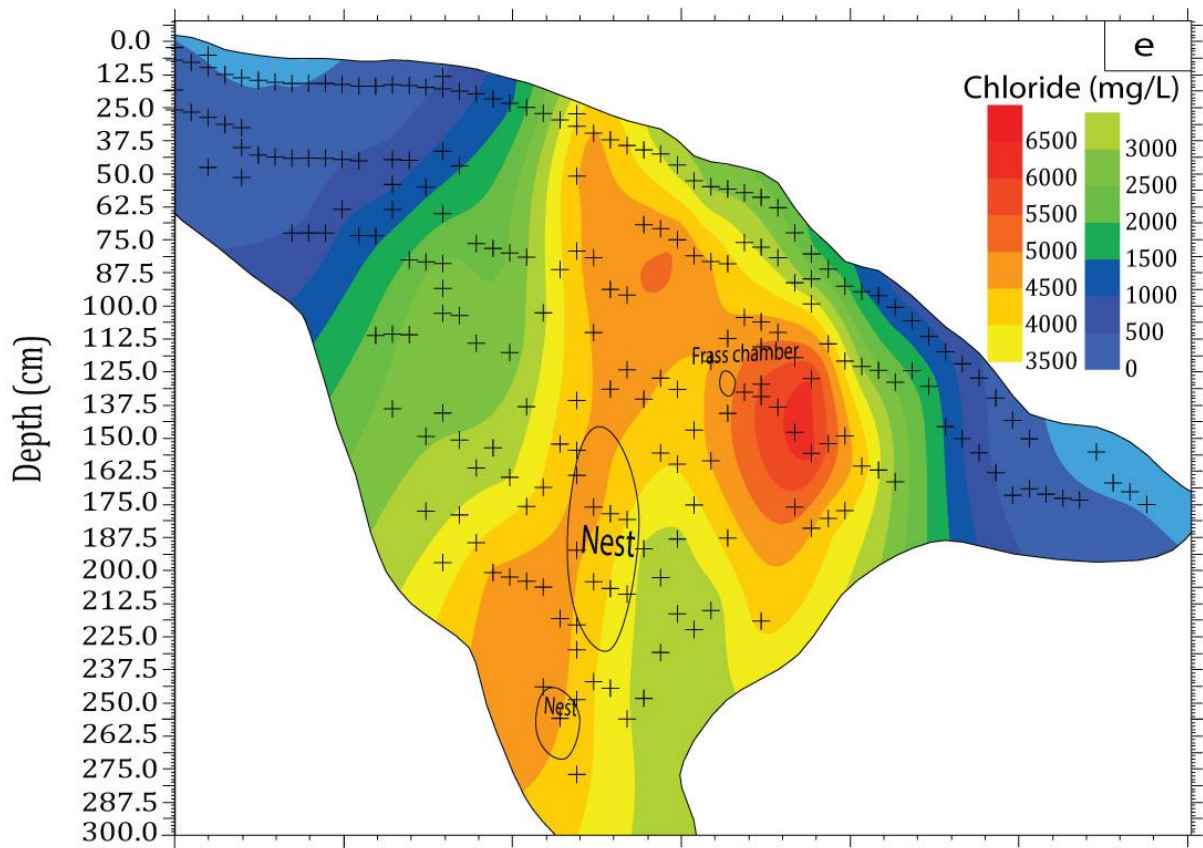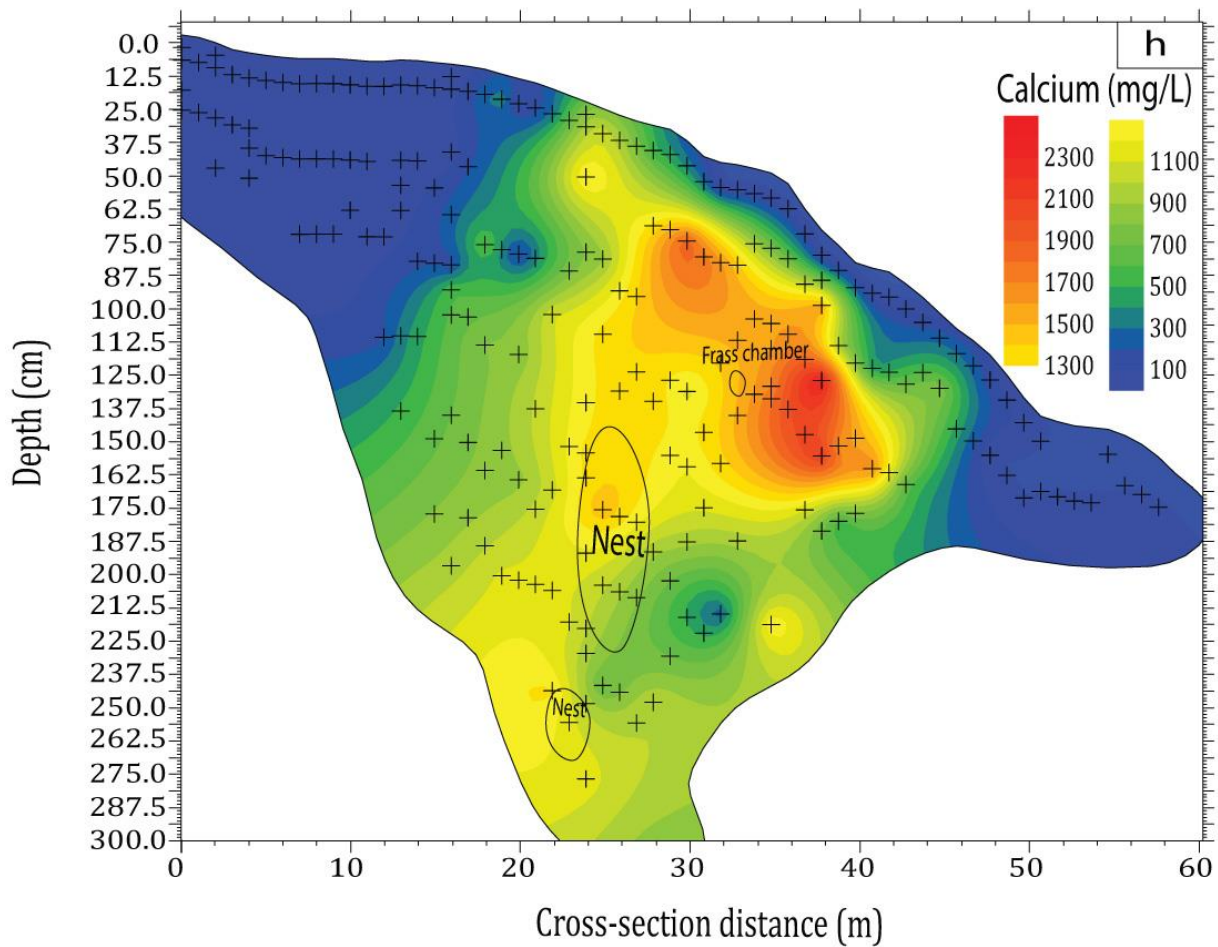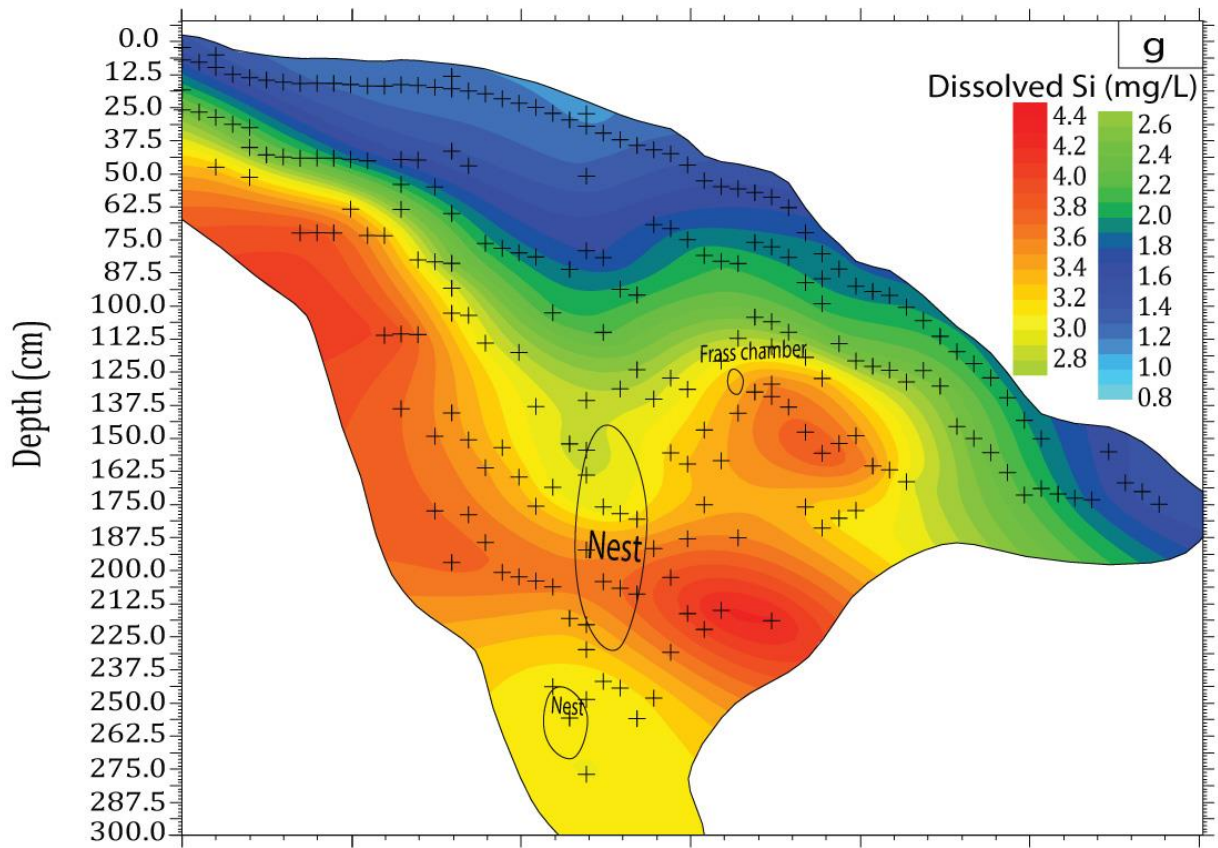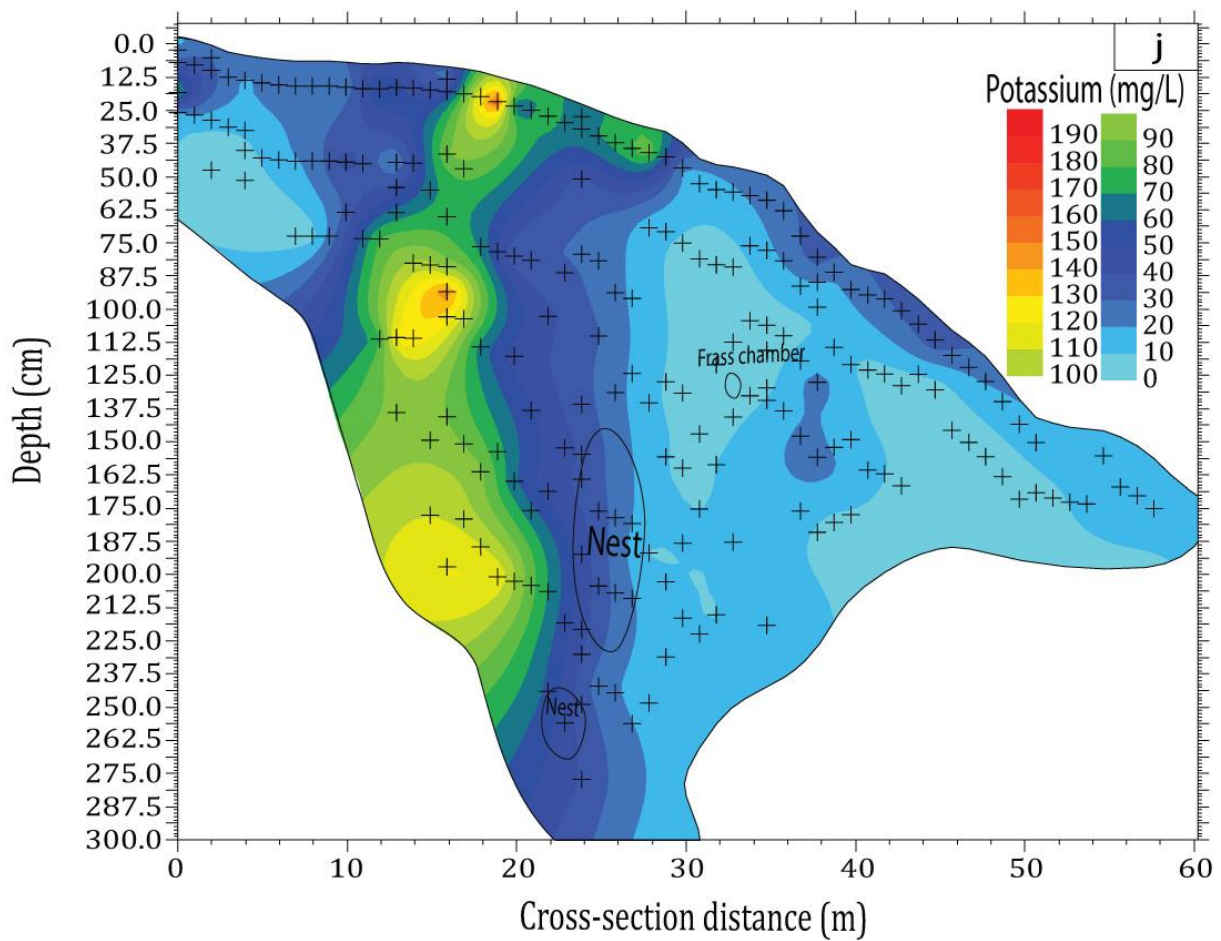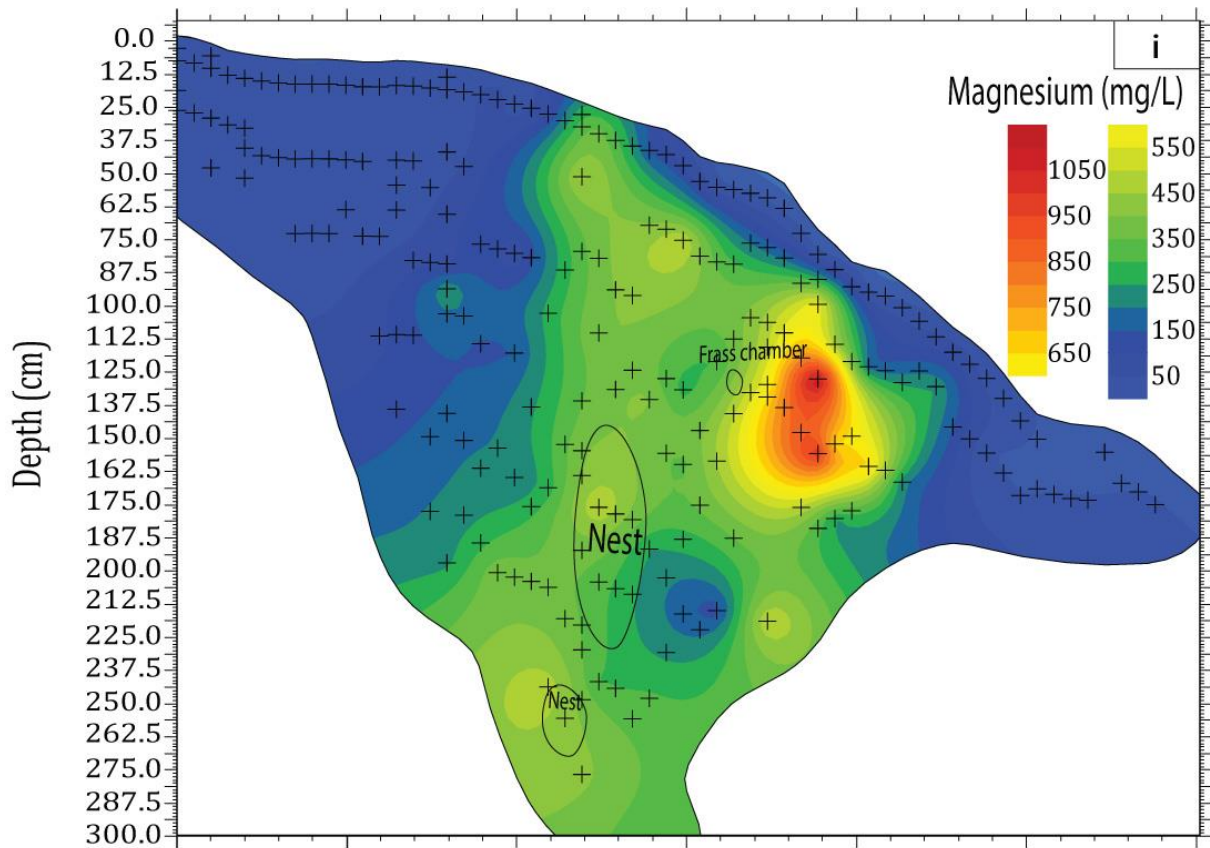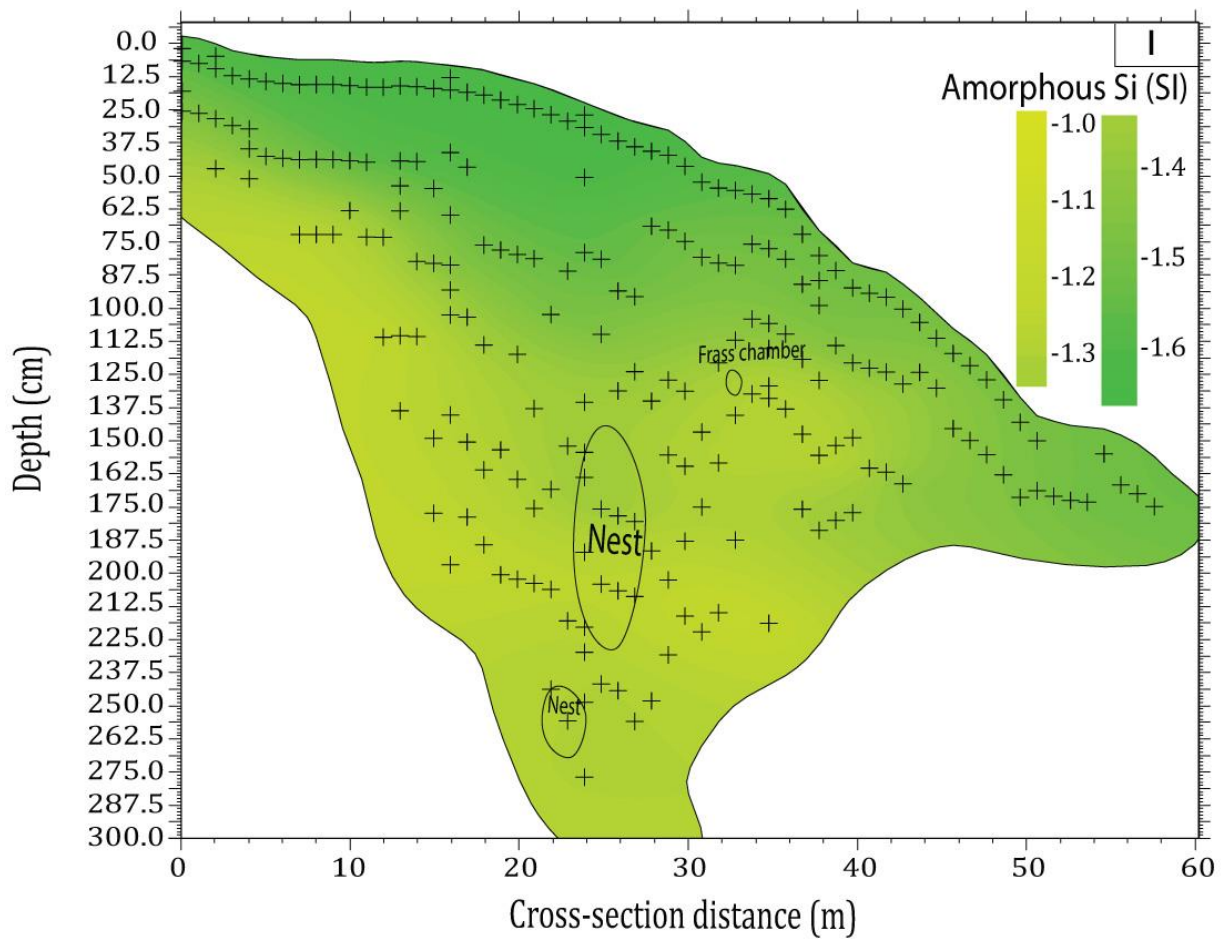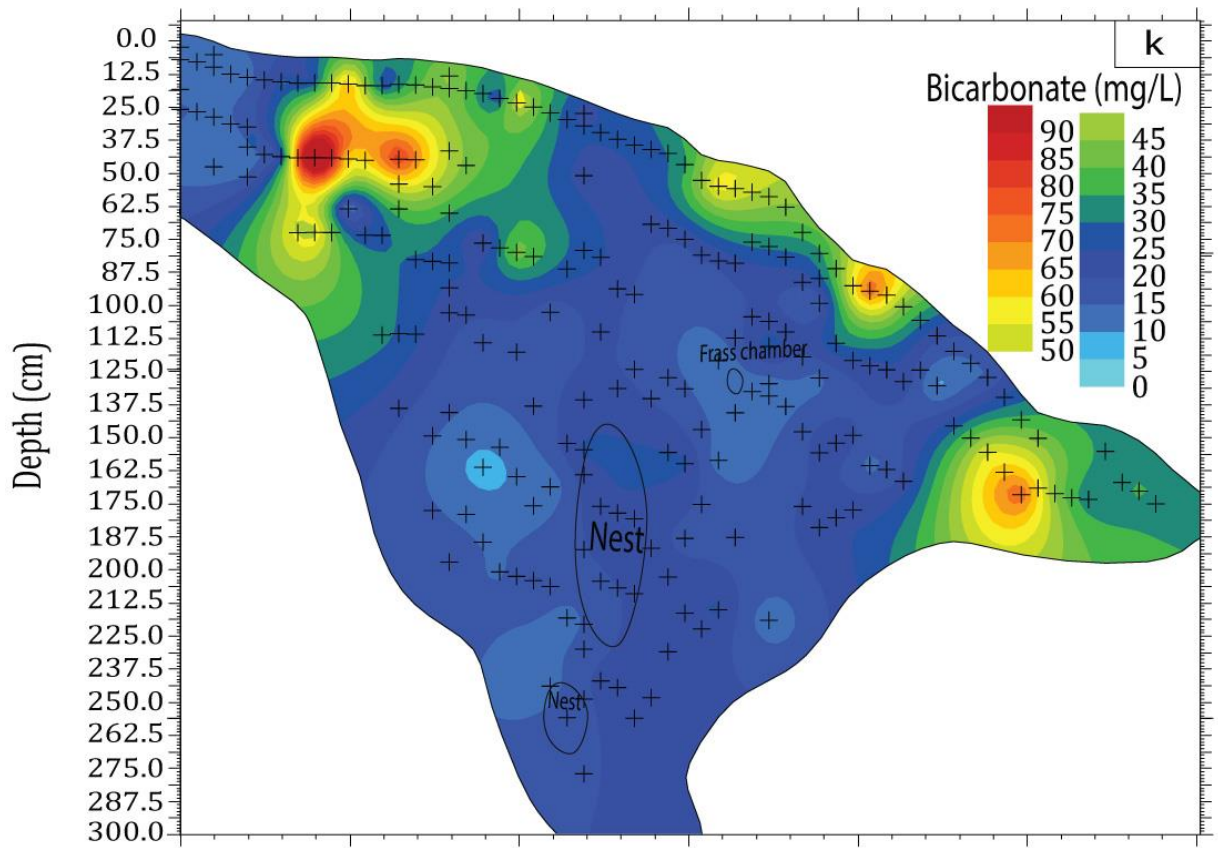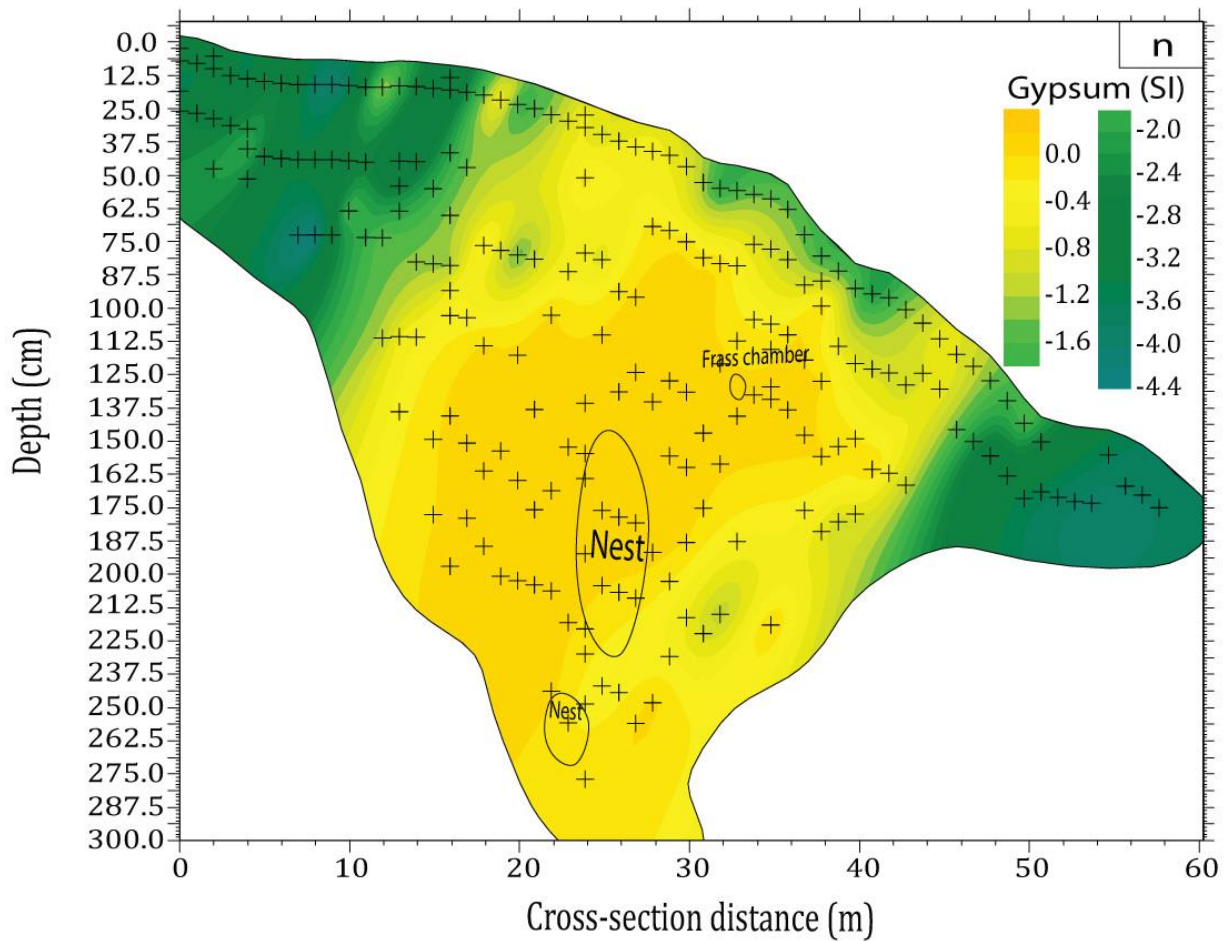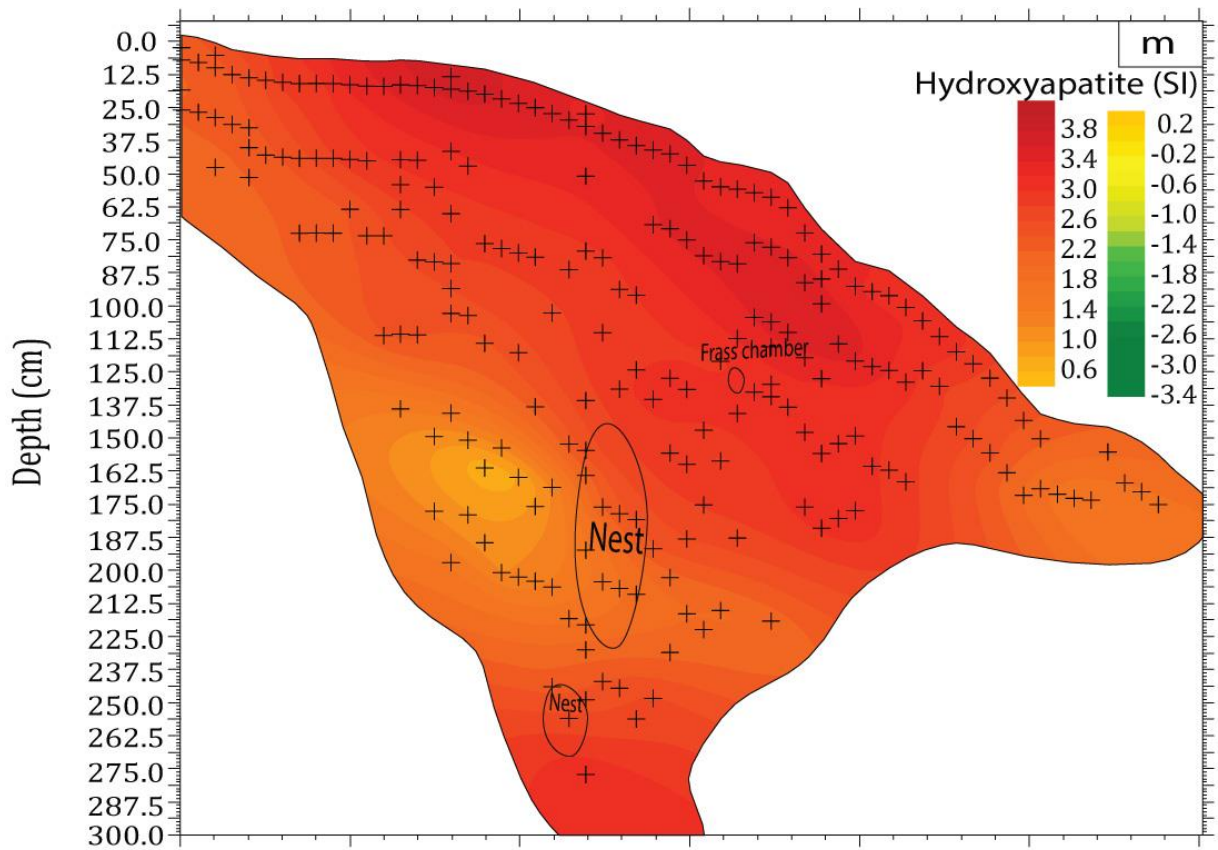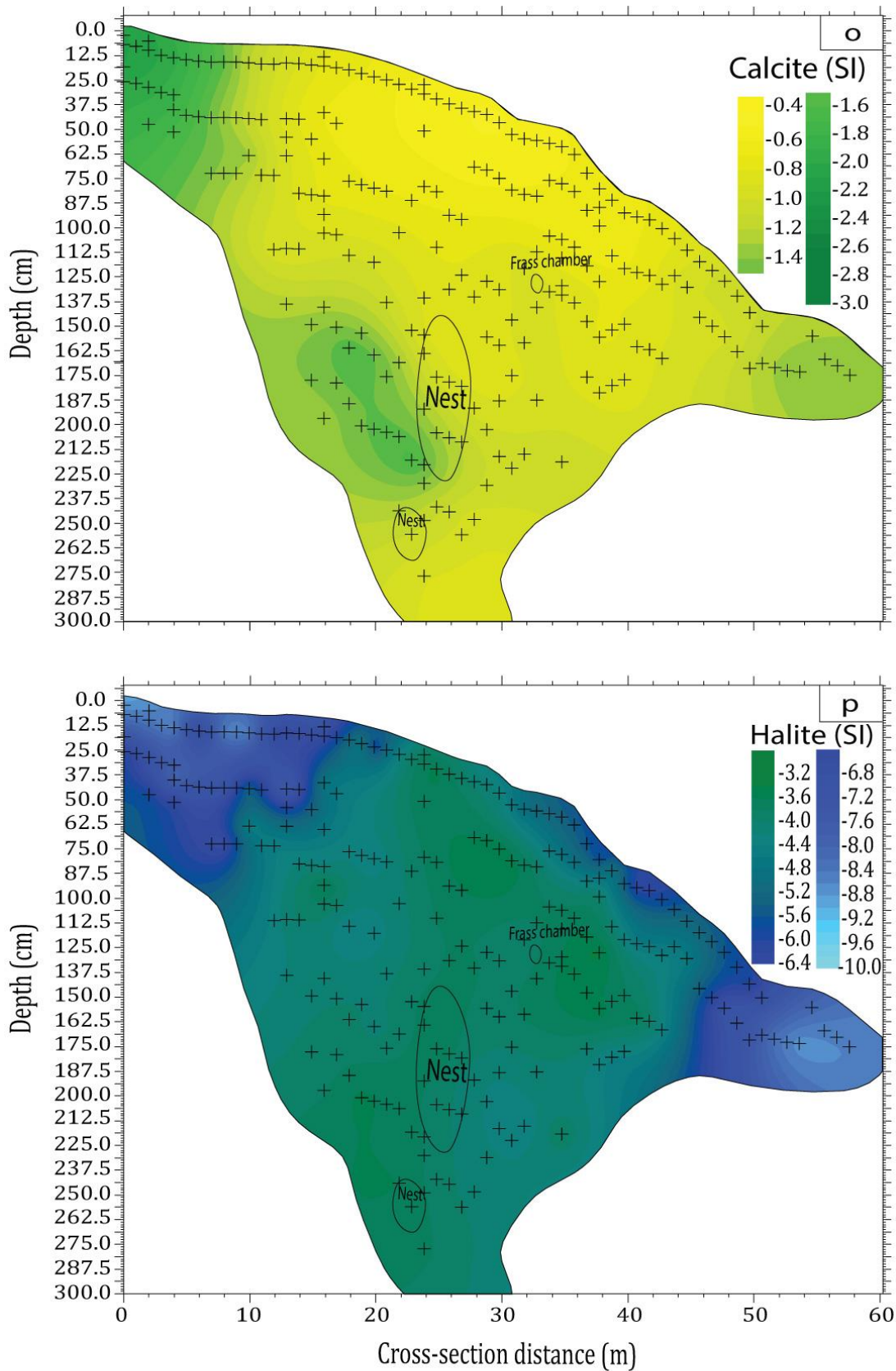
Figure 3.33: + denotes all sampling points within heuweltjie structure. a denotes H1's different soil profile descriptions at a x5 exaggeration (Bk= carbonate accumulation; Bw= development of colour and structure; Bkm= carbonate cementation; Bqm = silica cementation; Bkqm= carbonate and silica cementation). All other graphs are heat maps of concentration and SI down the heuweltjie profile at a x5 exaggeration.

111

3.6.2 Heuweltjie 4

3.6.2.1 Distribution of salts

EC for H4 (Figure 3.34b), like in H1, was higher within the centre of the heuweltjie structure compared to the interheuweltjie areas. However, H4's EC overall was lower than that of H1. pH (Figure 3.34c) was highest within the top soils and interheuweltjie areas, with a decreasing trend going down into the heuweltjie structure. pH values for H4 were lower than that of H1. Na^+ and Cl^- followed a very similar trend to each other (Figure 3.34d and e), with the highest concentrations being at a cross-section distance of around 25 m within the top soils. Concentrations were lower for Na^+ and Cl^- in H4 than in H1. SO_4^{2-} concentrations are highest in the deepest soil horizons in the middle of the heuweltjie (Figure 3.34f) and had lower concentrations than that of H1. Dissolved silica is highest at the deepest sampling spots within the heuweltjie (Figure 3.34g), decreasing upwards and outwards, with its lowest concentrations being within the interheuweltjie. H4 had higher dissolved silica concentrations than H1. Ca^{2+} and Mg^{2+} concentrations were higher within the heuweltjie structure than the interheuweltjie (Figure 3.34h and i), with some high concentration areas closer to the soil surface, and some closer to the bottom. Ca^{2+} and Mg^{2+} concentrations were both higher in H1 than H4. K^+ concentrations were highest within the top soils at a cross section distance of 30 m (Figure 3.34j). High concentrations of K^+ also extend from the surface to the lowest sampling points at a cross section distance of 42 m. H4 had higher K^+ concentrations than that of H1. HCO_3^- concentrations were highest within the top soil interheuweltjie samples (Figure 3.34k), with some high concentrations within the top soils of the heuweltjie itself. H1 had the highest HCO_3^- concentrations.

Amorphous silica is closer to saturation, although still undersaturated, going down the heuweltjie structure (Figure 3.34l), and follows a very similar trend to that of H1 (Figure 3.33l). Hydroxyapatite is mostly saturated throughout the heuweltjie structure (Figure 3.34m). However, at a cross sectional distance of between 30 and 40 m, it becomes undersaturated. The interheuweltjie soils are also undersaturated in hydroxyapatite. H1 is more saturated in hydroxyapatite than H4. Gypsum (Figure 3.34n) is saturated deeper down into the heuweltjie structure from a cross-section distance of around 20 to 40 m. The top soils and interheuweltjie soils are mostly undersaturated. It follows a similar trend to that of H1. Calcite is mostly undersaturated within the heuweltjie structure

(Figure 3.34o). It is closest to saturation within the top soils of the heuweltjie at cross sectional distances of around 20 m and then also at 45 m. H4 follows a similar trend as H1 for calcite. Halite (Figure 3.34p) is undersaturated throughout the heuweltjie structure, being closest to saturation, although still undersaturated, within the centre of the heuweltjie cross section. H4 follows a similar trend as H1. The SI of calcite and gypsum for H4 follow a similar trend to that of H1, with calcite being closest to saturation in the top soils, and gypsum being closer to saturation in the deeper soil horizons. From all saturation indices, hydroxyapatite was most saturated, while halite was most undersaturated, following the same trend as H1.

3.6.2.2   *Salt distribution with respect to heuweltjie profile descriptions*

For H4, EC (Figure 3.34b) is highest mostly within the gypsum accumulated (By), silica cemented (Bqm), and gypsum and silica cemented (Bqym) soils. EC is also high by the nests (cross section distance of 40 – 42 m), as well as within the tunnels. EC is high in the top horizons where calcite nodules are present (cross section distance of 22 m). pH is highest at the edges of the heuweltjie within the carbonate accumulated (Bk) soil. pH (Figure 3.34c) is lower close to the collapsed nest (cross section distance of ~20 m). pH values are lowest within the lower silica and gypsum cemented (Bqym) horizons, as well as where the nests and silica nodules are present. Na^+ and Cl^- (Figure 3.34d and e) both follow a similar trend, with highest values being in the top soils where calcite nodules are present (at cross section distance of 20-22 m). This then extends down towards the collapsed nest area, going through the various silica and gypsum cemented (Bqym) horizons. SO_4^{2-} concentrations (Figure 3.34f) are highest within the lower silica and gypsum cemented (Bqym) soils within the heuweltjie structure. Dissolved silica (Figure 3.34g) concentration is highest within the lower silica and gypsum cemented (Bqym) layers as well, becoming less close to the top carbonate accumulated (Bk) horizons. It is also high where all nests are located. Ca^{2+} and Mg^{2+} concentrations (Figure 3.34h and i) are highest where the calcite nodules are present throughout the heuweltjie structure, as well as at the termite tunnels (cross section distance of ~42 m). Lower concentrations are present throughout the heuweltjie structure within all the different soil horizons. K^+ concentrations (Figure 3.34j) are highest within the carbonate accumulated (Bk) soils, with high concentrations moving from the top to the bottom of the heuweltjie profile through the tunnels and nest. HCO_3^- concentrations (Figure 3.34k) are highest in the top

carbonate accumulated (Bk) soils. However, it is not present everywhere within these soils.

Amorphous silica (Figure 3.34l) is closest to saturation, although still undersaturated, throughout all the silica and gypsum cemented (Bqym) horizons, being most undersaturated within the top carbonate accumulated (Bk) horizons. Hydroxyapatite (Figure 3.34m) is saturated within most soil profiles throughout the heuweltjie structure. However, it is undersaturated where the silica indurated nodules (cross section distance of 34 m) are present. Gypsum (Figure 3.34n) is mostly saturated throughout all silica and gypsum cemented (Bqym) soils and where the silica indurated nodules are present, being more undersaturated within the carbonate (Bk) and gypsum (By) accumulated horizons. Calcite (Figure 3.34o) is closest to saturation within the carbonate accumulated (Bk) heuweltjie soils, as well as all the nests present within the heuweltjie. It is more undersaturated where the silica indurated nodules are present. Halite (Figure 3.34p) is closest to saturation within the silica and gypsum cemented (Bqym) soils. It is also quite high where the nest and its tunnels are present.
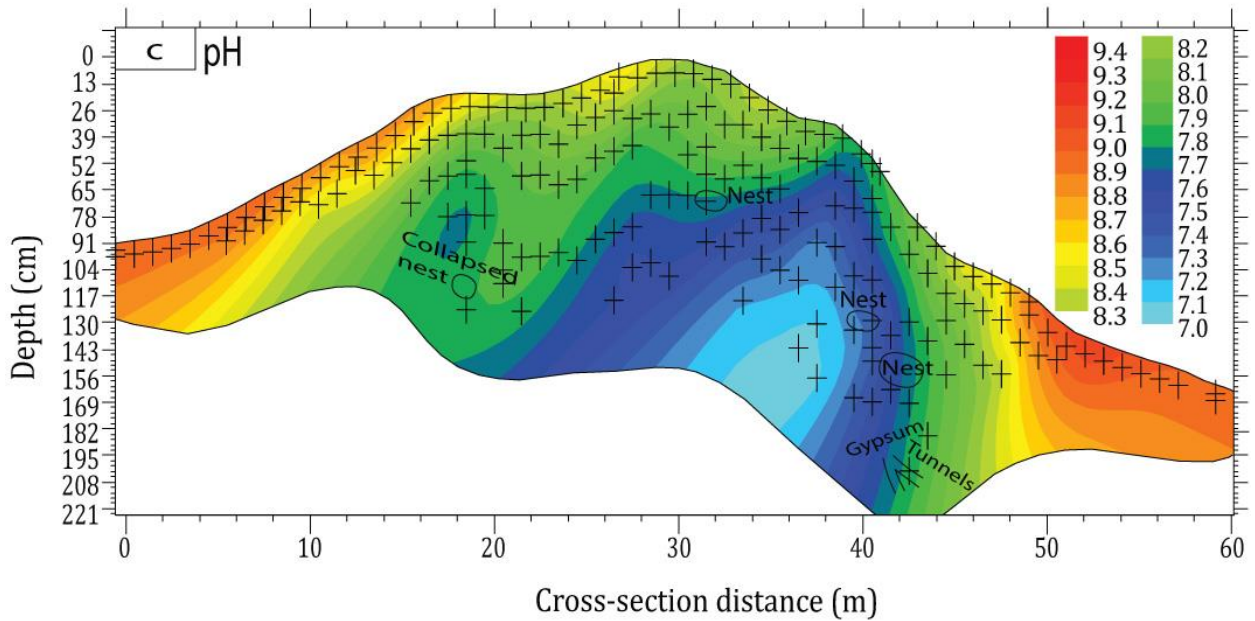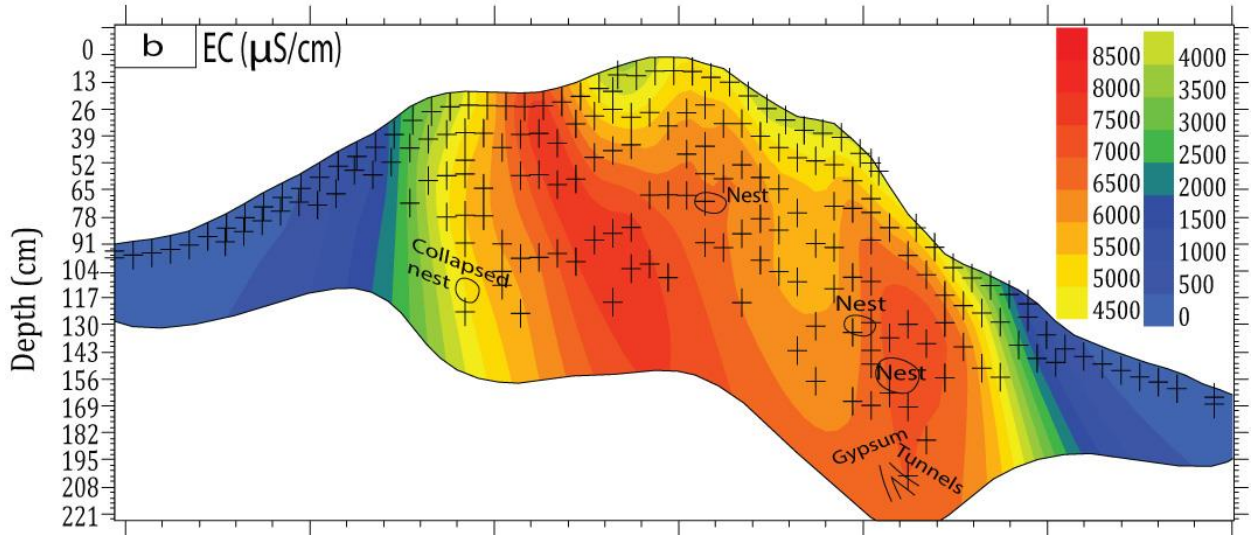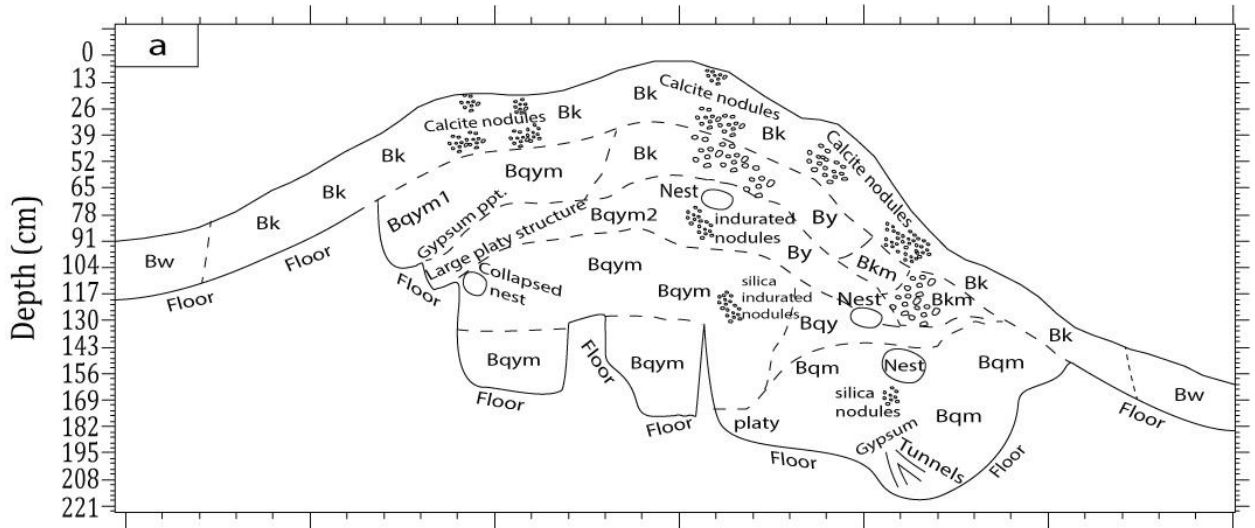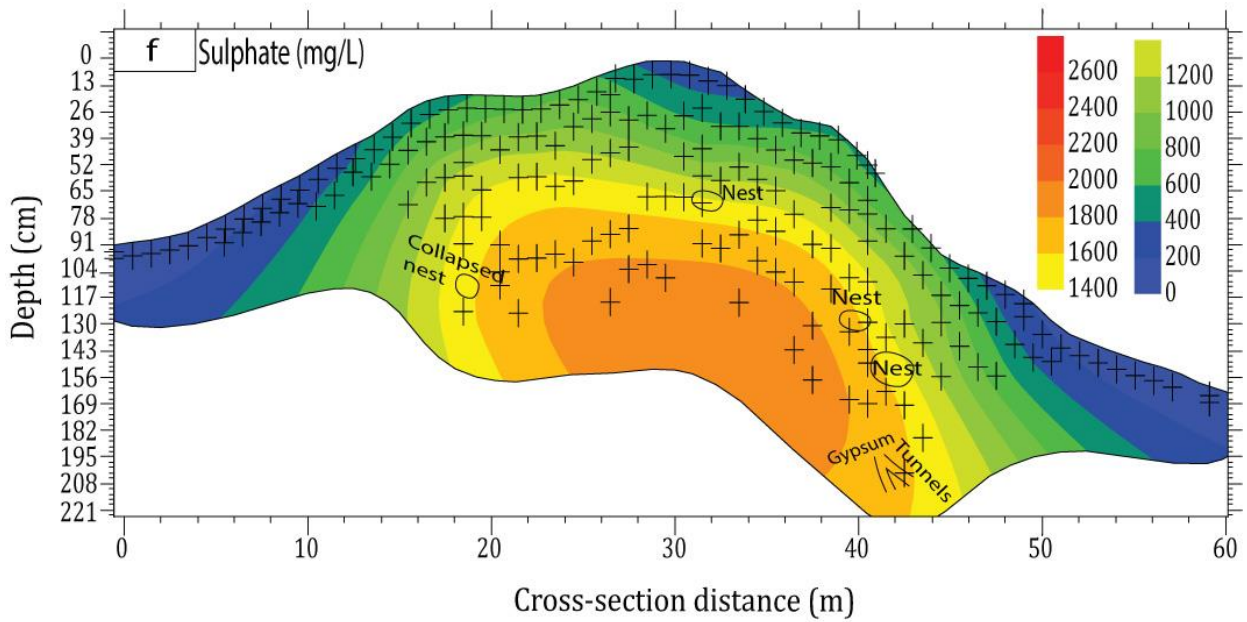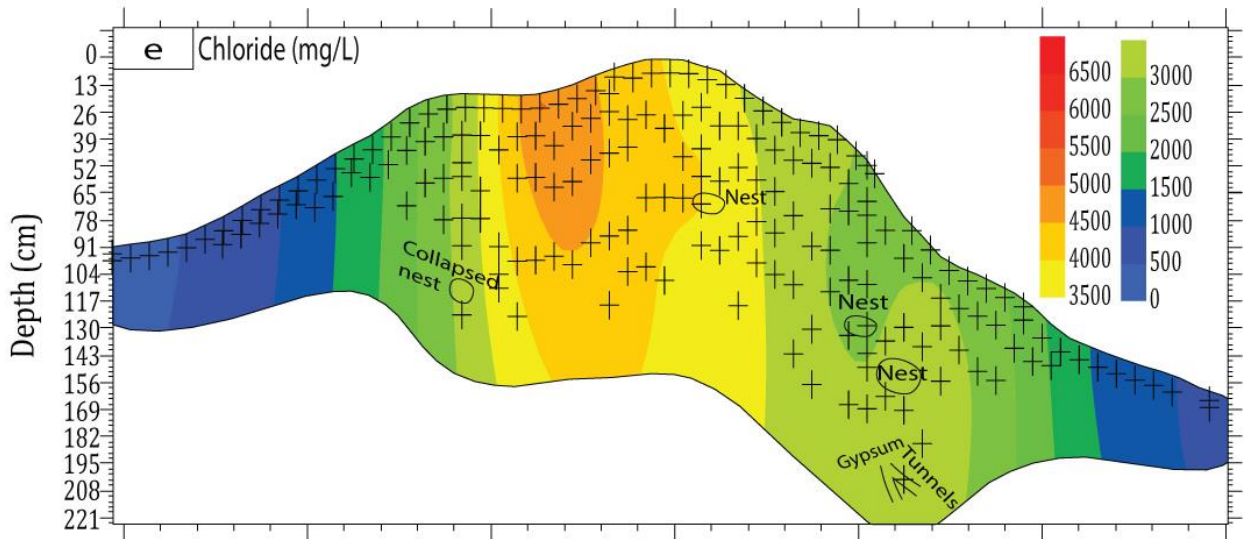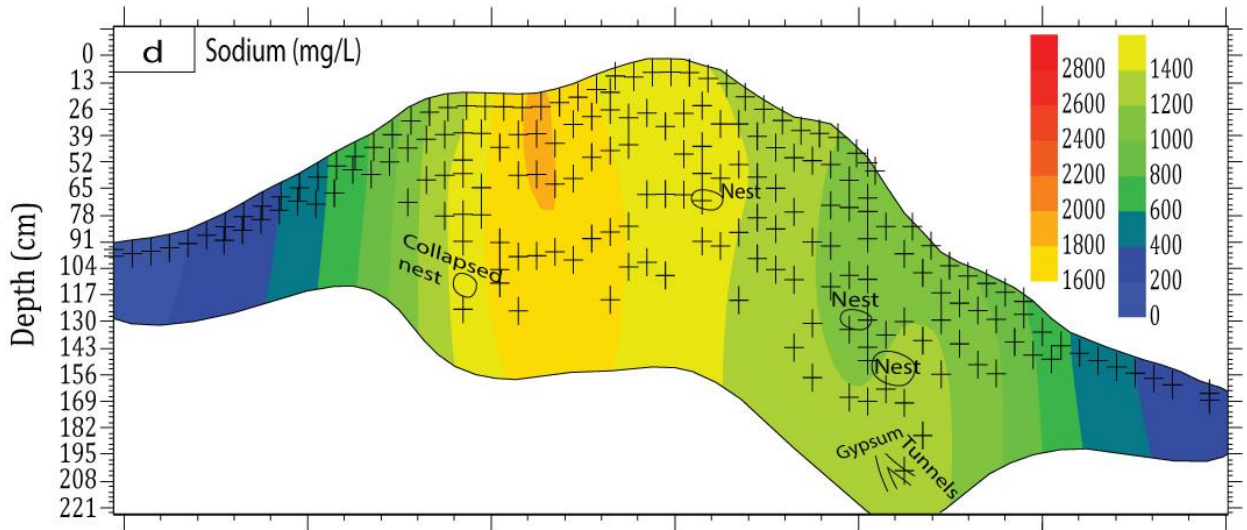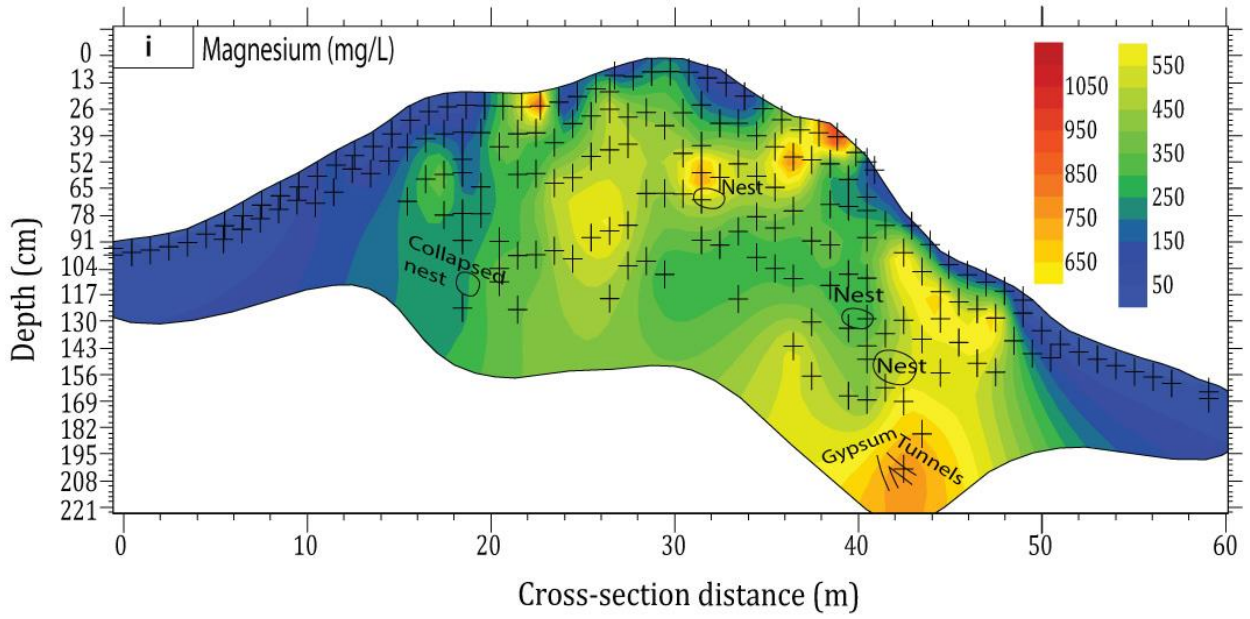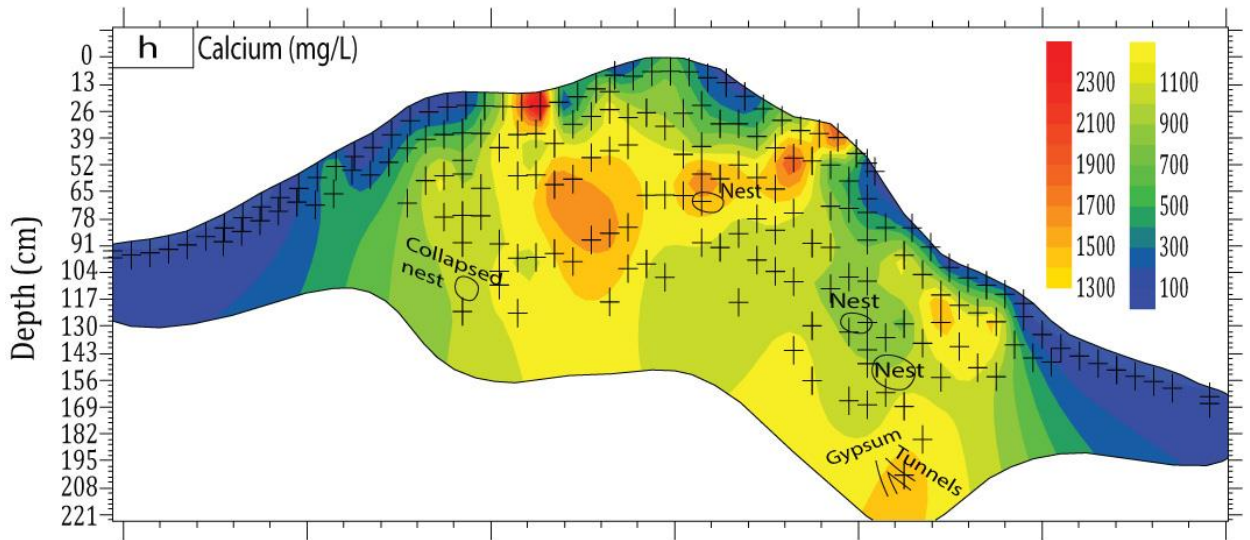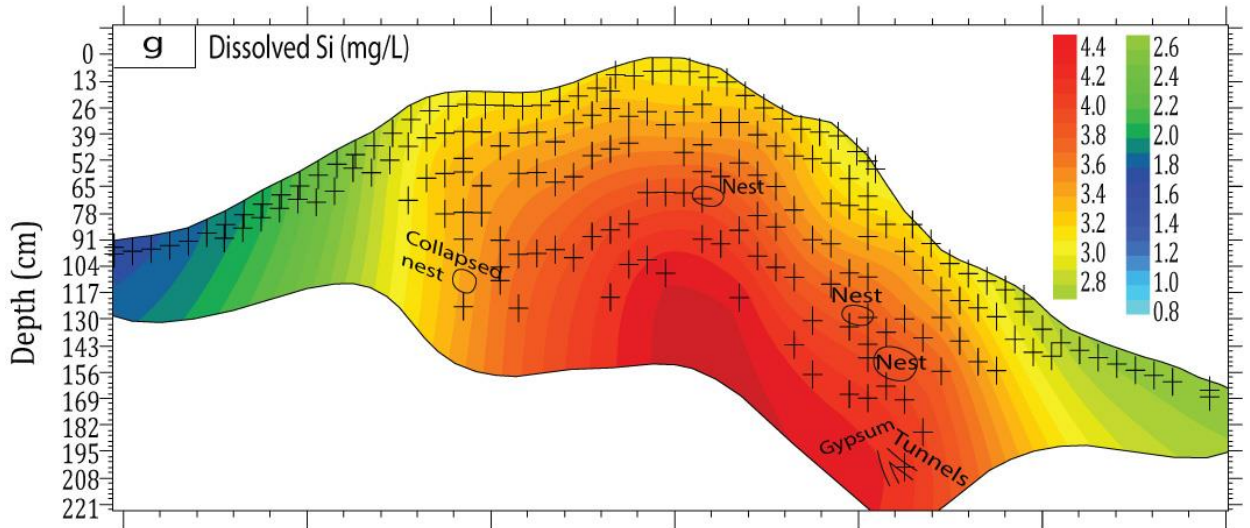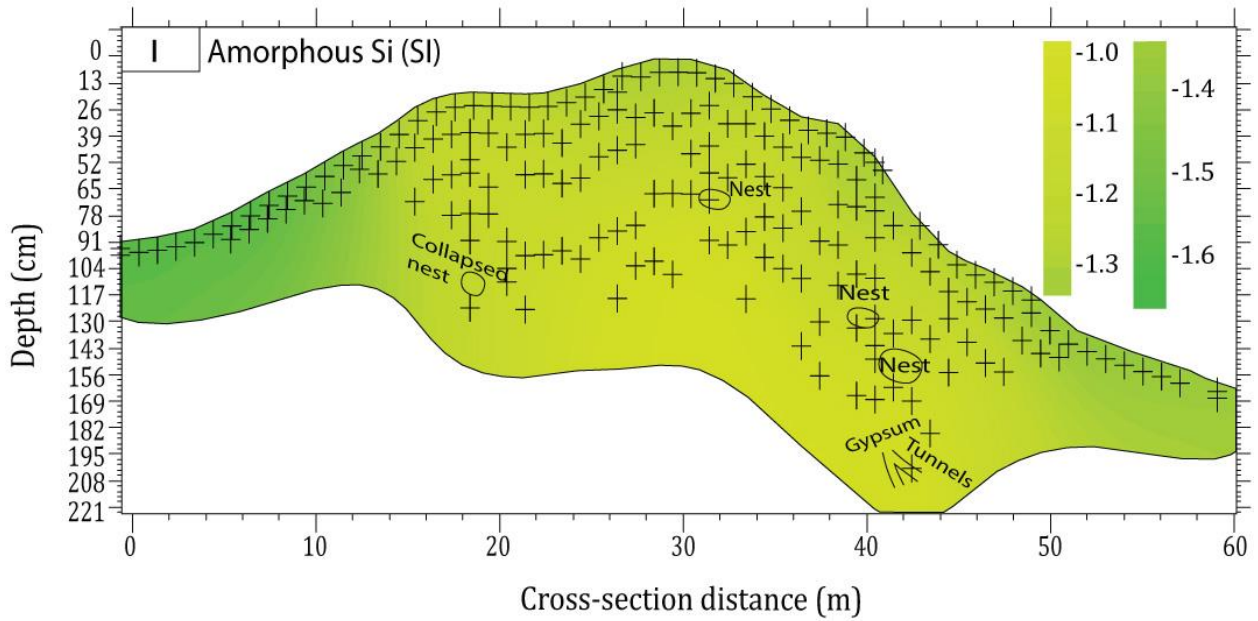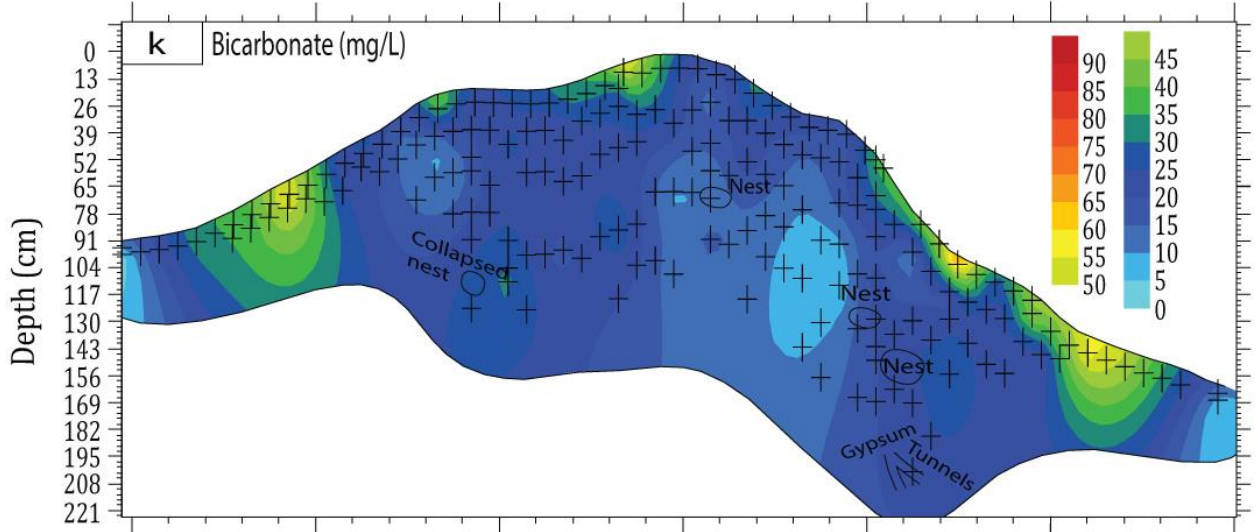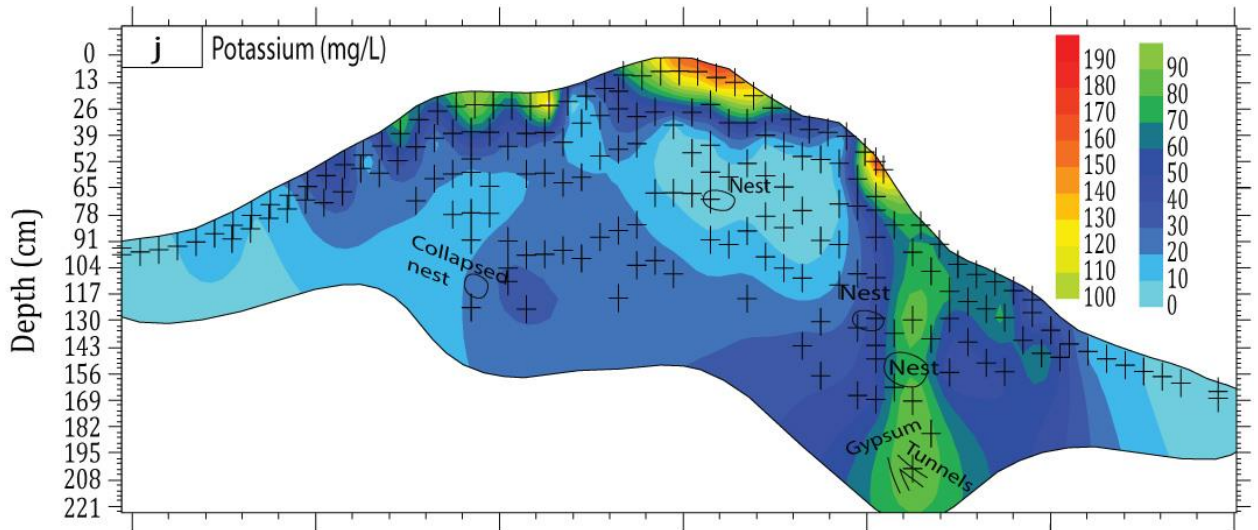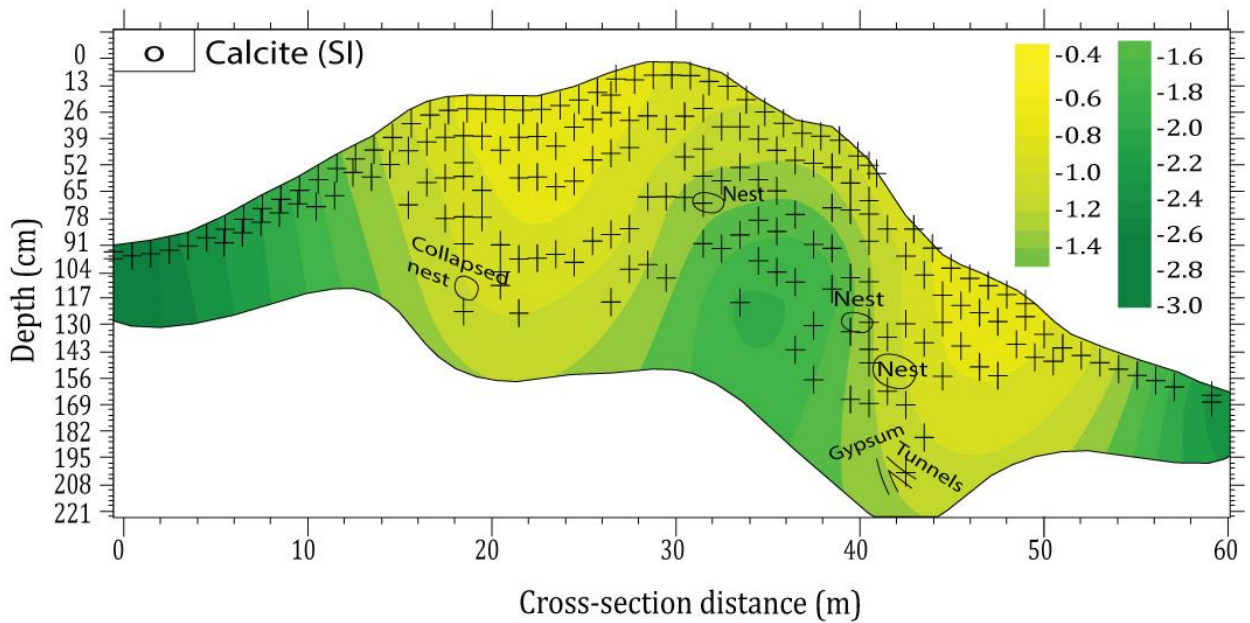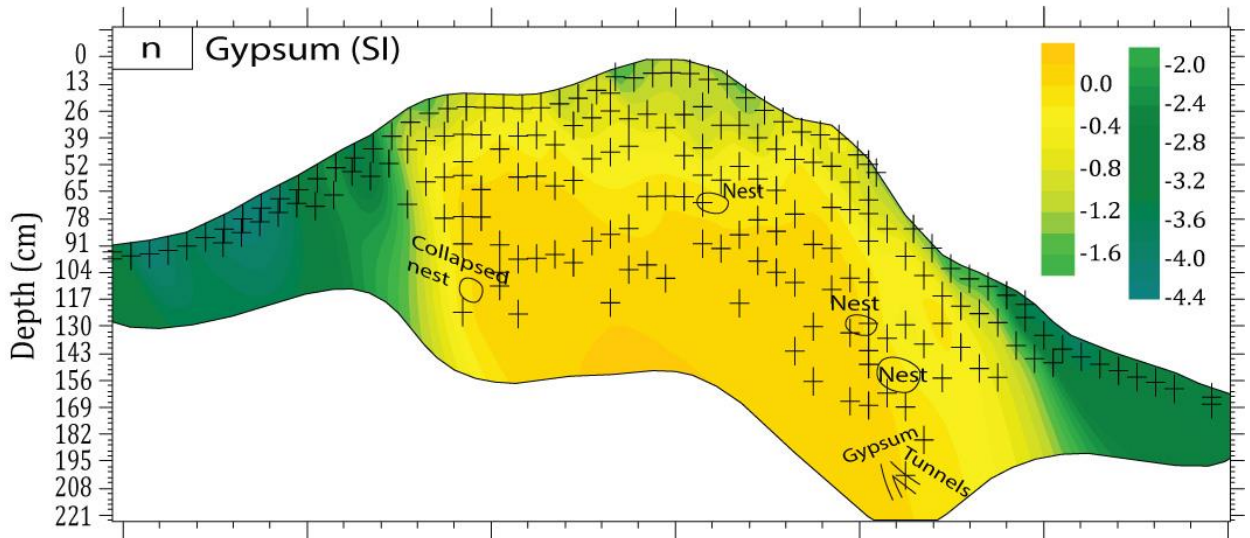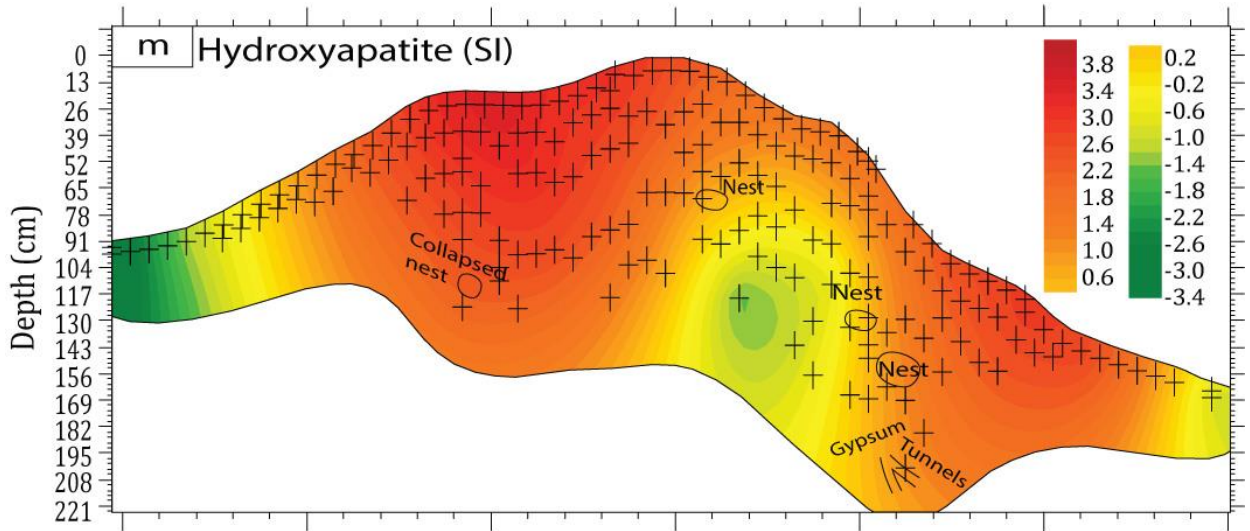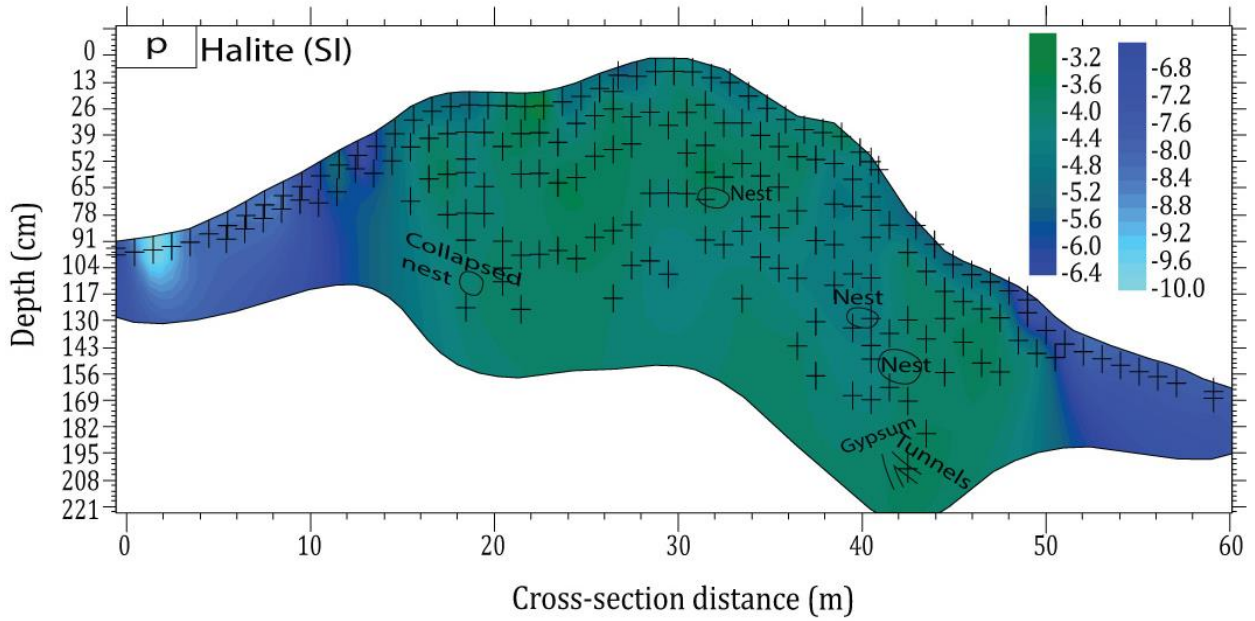
Figure 3.34: + denotes all sampling points within heuweltjie structure. a denotes H4's different soil profile descriptions at a x5 exaggeration (Bk= carbonate accumulation; By= gypsum accumulation; Bqm= silica cementation; Bqym= silica and gypsum cementation). All other graphs are heat maps of concentration and SI down the heuweltjie profile at a x5 exaggeration.

4 Discussion

In this section, results presented above will be used to examine the concentration and distribution of minerals and salts present within the heuweltjie soils, and their relationship to soil texture and the presence of termite nests. This will be done to better understand the role they play in the movement of the salts. The objective of this analysis is to better understand the potential sources of salts and hence the possible mechanisms of salinization. One of the central goals will be to evaluate whether it is possible to determine the direction of salt movement and hence to answer the question of whether heuweltjie salts are contributing to groundwater salinization, or vice versa. The answer to this question will greatly aid in understanding how groundwater salinization occurs in this region and from this it may be possible to suggest mitigation steps that could be taken by landowners.

4.1 Sediment characterization

In the following section, heuweltjie texture and clay mineralogy will be discussed and compared to that of the interheuweltjie soils. The role termites play on the clay mineralogy will also be discussed.

4.1.1 Soil texture

The classification of H1's texture was as anticipated, with the heuweltjie containing more clay than the interheuweltjie area, as was also noted by Francis *et al.* (2007). Singer *et al.* (1995) noted in their study on Namaqualand soils, that the soils were mostly sandy, with only a few sandy loam soils. Although no interheuweltjie soils were analysed for particle size in H4, it is expected that the heuweltjie soils would also contain more clay than the interheuweltjie soils.

Both heuweltjies' soils were similar, other than that the nest at H4-19 did not contain as much clay as the nest in H1-25. This could be because H1's large nest was covered with a silicified layer, and so it remained undisturbed until it was uncovered. Another reason could be that since the nest in H4-19 had collapsed, some of the sediment obtained from these samples may not be part of the nest material, hence altering the particle size description. As there were no discontinuities in grain size for the two heuweltjies (see

textural data in Figure 3.19 and Figure 3.20 as well as Table 3.1 and Table 3.2) no buried soils were present.

It is important to note that, because not all heuweltjies are paleo structures, it cannot be expected that all heuweltjies would have this same soil texture. However, it could be expected that most paleo heuweltjies within this region would exhibit similar traits.

4.1.2 Clay mineralogy

4.1.2.1 *Mineralogy of heuweltjie and interheuweltjie soils*

Very few neoformed clay minerals were present within the heuweltjie soils (section 3.4). Most of the minerals present were clay-sized quartz, illite, and kaolinite. These minerals were also present within the interheuweltjie soils analysed. Quartz, kaolinite and illite were found in XRD data obtained by Singer *et al.* (1995) and Clarke *et al.* (2016) in their studies on Namaqualand soils, indicating that the clay minerals present are as a result of the surrounding soil compositions. A few studies done in this area, such as by Singer *et al.* (1995) and Francis *et al.* (2012a), found sepiolite and palygorskite present within these soils, which was not present within the XRD results (see section 4.4 for discussion on sepiolite presented via PHREEQC data). Calcite was present within the heuweltjie soils, as was also found by Francis *et al.* (2012a). Potts *et al.* (2009) found calcite present within heuweltjies near Worcester (541 km south of Springbok). This is expected, as heuweltjie soils are known to be enriched in calcite compared to the non-heuweltjie soils (Francis *et al.*, 2012a; Midgley *et al.*, 2002; Potts *et al.*, 2009). The interheuweltjie soils analysed did not contain calcite, again indicating that it is only present within the heuweltjie soils.

In their study on clay mineralogy in certain southern African river muds, Setti *et al.* (2014) found that illite is always abundant in rivers within arid regions. Clay minerals dominate river-suspended solids, reflecting the composition of the soils in their drainage basins (Setti *et al.*, 2014). As the heuweltjies analysed lie within the Buffels river drainage basin, this suggests that the illite present within the heuweltjie and non-heuweltjie soils are likely as a result of flooding of the river in previous years, depositing illite-rich minerals within its floodplain. Setti *et al.* (2014) mentioned that illite is normally inherited from ancient rocks that have been modified by physical or chemical weathering, while kaolinite forms as a result of long-term weathering. Therefore, as mentioned by Bühmann

et al. (2004) kaolinite is more than likely inherited from parent materials which have weathered quite extensively.

4.1.2.2   Termite influence on mineralogy

Four of the samples analysed for mineralogy had calcium oxalate peaks, with another suggestive calcium oxalate peak at H1-24 in the termite faecal pellets (Figure 3.25 and Figure 3.26). This is consistent with the findings of Francis & Poch (2019), who also found oxalate present in termite faecal pellets. With calcium oxalate present within the heuweltjie, this enhances the idea that the calcite accumulation could be as a result of the oxalate-carbonate cycle (Francis & Poch, 2019; McAuliffe *et al.*, 2019a). If termites are bringing calcium oxalate rich plant materials into the heuweltjie structure, the decomposition of the plant material and the presence of oxalotrophic bacteria would transform the calcium oxalate to yield $CaCO_3$ (Francis & Poch, 2019; McAuliffe *et al.*, 2019a) The calcium oxalate in H1 occurred right above the nest at H1-24, and 50 cm below the termite frass at H1-32 (Figure 3.1). In H4, it occurred 30 cm above the collapsed nest at H4-19, and 70 cm below the nest at H1-32 (Figure 3.11). Finding calcium oxalate present close to the nests or within the same heuweltjie profiles as some of the nests enhances the idea that it is present as a result of the termite activity. This is discussed in more detail in sections 4.4.1 and 4.4.4.

Gypsum was present throughout both heuweltjies, although more so in H4 (H1-32, Figure 3.24 and H4-19, Figure 3.25). Gypsum was not found within heuweltjies in the study done by Francis *et al.* (2012a), suggesting that gypsum precipitation could be unique to this area of study within the heuweltjies. This may have to do with high SO_4^{2-} concentrations present.

When comparing the termite faecal pellets with the untreated sample in H1 (Figure 3.28), and as mentioned earlier, some differences were noted between the two, suggesting that the termites play a role in formation of the clay minerals discussed for this specific heuweltjie. For the termite faecal pellets in H1-24 (Figure 3.28), the suggestive calcium oxalate peak again indicates that the termites play a role in the oxalate-carbonate pathway. For the comparison within H4 (Figure 3.29), gypsum was present in the termite frass, but not in the untreated soil in the same horizon. This could indicate that the termites may consume some of the minerals present in the heuweltjie soils, although they are not soil feeding termites, and redistribute it elsewhere within the heuweltjie soils via

their excrement (Francis *et al.*, 2012a). Another possibility is that termites may play a role in the formation of gypsum within the heuweltjies by bringing more calcium and sulphates into the heuweltjie soils.

4.2 Mineral saturation relating to evaporation

Na^+ and Cl^- ion activities (Figure 3.30), were consistent with the seawater dilution line. The same was noted by Francis (2008) in her research done for soils of Namaqualand, and by Smith & Compton (2004) in their research done on salt pans close to Darling, Western Cape, South Africa (83.5 km north of Cape Town). K^+ remained stable initially, and then decreased as Cl^- activity increased (Figure 3.30). This differs from the results shown by Francis (2008), where K^+ increased as evaporation increased, although at a slope less than the conservative line. Similar results were also found by Smith & Compton (2004), whose K^+ also increased. This decrease in K^+ could be attributed to uptake onto active soil surfaces (Eugster & Jones, 1979).

SO_4^{2-} increased as evaporation rates increase; however, it decreased slightly after a $\log[Cl^-]$ value of -1 was reached. This follows the reasoning by Eugster & Jones (1979) which indicates that sulphates in many closed basins are removed from solution by precipitation of gypsum and mirabilite ($Na_2SO_4 \cdot 10H_2O$). This can be confirmed in Figure 3.31 (d), where gypsum is seen to start precipitating at a $\log[Cl^-]$ value of -1. This is also confirmed by the presence of gypsum within both heuweltjies (as discussed in section 0).

HCO_3^- followed a decreasing trend as evaporation increased (Figure 3.30), and is also thought to be removed from solution as a result of the precipitation of calcite (Figure 3.31). This is in agreement with the findings of Francis (2008), stating that all soils of Namaqualand are close to saturation with respect to calcite. Mg^{2+} and Ca^{2+} continued increasing with increasing evaporation, although at a slope less than the conservative solutes. This is typical for removal mechanisms, including precipitation of the minerals, degassing, or sorption, operating across the entire evaporative concentration range, resulting in a linear relationship, although at a slope less than the conservative solutes (Eugster & Jones, 1979). When referring to HCO_3^- and Ca^{2+} (Figure 3.30c and f), along with the SI of calcite (Figure 3.31b), it can be seen that, in Namaqualand's soil solutions, calcite precipitates when Ca^{2+} increases in solution, while HCO_3^- decreases in solution, as stated

in the findings by Francis (2008). pH also plays a part in this precipitation, as calcite becomes more saturated as pH increases (Figure 3.32).

$H_4SiO_4^0$ remained constant throughout as evaporation increased, suggesting that silica acts as a conservative element, as noted by Eugster & Jones (1979). Similar results were found by Francis (2008).

Hydroxyapatite was present within one soil horizon in H4-19-60 (fine) in the XRD graphs (see Figure 3.25), the detailed profile closest to the western end of the excavated heuweltjie. HPO_4^{2-} and $H_2PO_4^-$ both decrease consistently as evaporation increases (Figure 3.30), indicating that it is precipitating and forming hydroxyapatite (Figure 3.31). pH plays a major role in this precipitation as well, as most of the oversaturated hydroxyapatite has a pH of 6 or greater (Figure 3.32).

Sepiolite was not identified in XRD graphs (see graphs in section 0), which is consistent with its undersaturation in both heuweltjies (Figure 3.31). This is unlike the results found by Francis *et al.* (2012a), which showed a positive sepiolite identification for a calcareous heuweltjie near Papendorp (267 km south of Springbok).

4.3 Salt movement throughout heuweltjie structures

The ion activity and SI graphs (section 3.5) show that halite remains undersaturated throughout the heuweltjie profile. Amorphous silica and sepiolite are also undersaturated. This suggests that there is a possibility for an expected increase in Na^+, Cl^-, Mg^{2+}, and $H_4SiO_4^0$ ions moving towards the groundwater system. This can be confirmed with the heat maps (Figure 3.33 and Figure 3.34), showing ion concentration movement throughout the heuweltjie structure. Dissolved silica was also present in the deeper soil horizons for both heuweltjies, and Mg^{2+}, although concentrations were mostly higher within the top horizons, also moved deeper down into the soil horizons, especially in H4. It is therefore expected that these ions are moving towards the groundwater system.

$CaCO_3$ content is higher within the heuweltjie structure than the interheuweltjie, agreeing with the findings of McAuliffe *et al.* (2019a) and Schmiedel *et al.* (2016). Silica concentration was also higher within the heuweltjie than interheuweltjie, agreeing with the findings of Francis *et al.* (2007). EC results agree with that found by van Gend (2018), with EC being much higher within the heuweltjie than the interheuweltjie structure.

4.3.1 Validity of heat map distributions

Before discussing the heat map data, it is important to address the validity of the heat map distributions. The interpolation techniques for the heat maps are inherently poor at isolating rapid changes that take place across the heuweltjie structure, and so may depict some areas as having higher concentrations than what it would be within the specific area. As a result, the distributions shown within the heat maps are only potential distributions and are unlikely to represent the exact layering system within the heuweltjie structures. One strength of the interpolated surface, however, is that it aids in visualizing the potential distribution of the salts throughout the heuweltjie structure.

4.3.2 Salt movement with respect to heuweltjie structure

4.3.2.1 Heuweltjie 1

Preferential flow pathways seem to be present throughout both heuweltjies when looking at the heat maps (Figure 3.33 and Figure 3.34). This can especially be seen for EC, Na^+, Cl^-, and K^+ concentrations throughout both heuweltjies, which all have 'strips' of high concentration moving down into the deeper heuweltjie soils. For H1 (Figure 3.33b), the preferential flow pathways have to do with the granular texture of the heuweltjie sediments in this specific region, flowing down to the nest areas at a cross section distance of 24 and 25 m. As granules have more porous space between them, movement of ions would be easier. K^+ (Figure 3.33j) appears to have a very clear preferential flow path through the carbonate cemented (Bkm) nodules and the more platy carbonate and silica cemented (Bkqm) layers. As these soils also have more porous space between the nodules and plates, the K^+ ions can flow freely through these horizons. High concentrations of most ions close to the termite frass samples collected indicates that termites play a role in the saline soils of the heuweltjies by bringing Na^+, Cl^-, Mg^{2+}, Ca^{2+}, and SO_4^{2-} into the soil. The dissolved silica movement throughout the soil profiles shows the movement of water throughout the heuweltjie, as it is mostly transferred through water (Sommer *et al.*, 2006). The water flows in from the edge of H1, as the heuweltjie was situated on a slanted area and appears to percolate downwards into the heuweltjie structure. This is also where the carbonate and silica cemented (Bkqm) horizons reside, indicating that the high concentration of water carrying dissolved silica becomes saturated, which can be seen by the SI of amorphous silica (see Figure 3.33l). SO_4^{2-}

concentration is also higher where more dissolved silica is present, indicating that it moves with the water (Tabatabai, 1987). SO_4^{2-}, Ca^{2+} and Mg^{2+} ions (Figure 3.33f, h and i) are more abundant within the same region of the heuweltjie as each other, hence having the advantage of forming gypsum and magnesium sulphate salts. Ca^{2+} is favoured above Mg^{2+} when binding to SO_4^{2-}; however, as can be seen with where gypsum is most saturated in the heuweltjie (see Figure 3.33n). Since HCO_3^- is only found within the top soils of the heuweltjie structure (Figure 3.33k), this is the only place where calcite favours formation, as seen with the SI for calcite (see Figure 3.33o). Calcite is usually located within the top soil horizons (WRB, 2014), and this can be confirmed within this study. HCO_3^- concentration follows the trend of high pH, as it is highest at high pH values. High concentrations of soluble halite move freely throughout the heuweltjie structure into the deeper soil horizons, and possibly into the groundwater reserves. The high halite SI is present where gypsum is also closest to saturation. As stated by Papadopoulos (1984), precipitation of gypsum increases the amount of harmful salts within the soil, especially of halite. This research proves that to be true, as halite is mostly concentrated where gypsum is present.

Casby-Horton *et al.* (2015) stated that if gypsum precipitates at a greater depth than calcite, the dominant water movement is downwards. As gypsum is a more soluble mineral than calcite, it is expected to move further down the profile. Calcite is found mostly within the top soil horizons, with gypsum precipitating deeper down in the heuweltjie. This follows the trend of soil formation present when water movement is downwards and was concluded since gypsum is more soluble than calcite, moving further down the heuweltjie profile. Therefore, it must be the heuweltjie salts leaching into the groundwater, and not vice versa.

4.3.2.2   Heuweltjie 4

For H4, preferential flow paths are also evident for EC, Cl^-, Na^+, and K^+. For EC and K^+, a preferential flow pathway is evident at a cross section distance of 42 m (Figure 3.34b and j), where the active termite nest and its tunnels are located. High K^+ concentrations are most evident moving from the top to the bottom of the heuweltjie profile, more than likely flowing through the termite tunnels that are present. This can also be seen for EC; however, movement does not seem to be directly from the top heuweltjie soils. EC, Na^+ and Cl^- have evident flow pathways at a cross section distance of around 22 m (Figure

3.34b, d and e). The preferential flow pathway seems to start at the top by flowing through calcite nodules on through the cemented layers. However, Na^+ and Cl^- concentrations do decrease going down the heuweltjie profile, indicating that there is not much flow through space through the cemented layers. For H4, as compared to H1, dissolved silica, and hence water movement, does not come from the one side, as H4 was not situated on a slope. It appears as if the water percolates through from the top heuweltjie soils deeper down into the heuweltjie structure; however, there is also the possibility that the water movement is upwards into the heuweltjie from the groundwater. This area within the heuweltjie is also where the silica and carbonate cemented (Bkqm) horizons are located, indicating that the high concentrations of dissolved silica start to precipitate out. This can be confirmed with the amorphous silica SI values being closest to saturation in this area (Figure 3.34l). SO_4^{2-} concentrations are again higher where dissolved silica is more abundant. Gypsum formation from Ca^{2+} and SO_4^{2-} ions follows the same reasoning as for H1. Calcite, like in H1, is again more present in the top layers (as seen in Figure 3.34a with all the calcite nodules present at the top) due to HCO_3^- and Ca^{2+} concentrations being highest in the top horizons. Termite tunnels aid in the movement of Ca^{2+} and Mg^{2+}, more than likely derived from plant materials, into the groundwater at a cross section distance of 42 m, again showing the presence of preferential flow pathways.

The same trend was noted for H4 with respect to calcite and gypsum presence. Calcite was closest to saturation within the top soil horizons, with gypsum being closest to saturation in the deeper horizons. This therefore again shows that water movement must be down towards the groundwater (Casby-Horton *et al.*, 2015).

4.3.3 Heuweltjie pH

For both heuweltjies, pH is opposite as expected, as most research on heuweltjies found pH to be higher within the heuweltjies than the interheuweltjie soils (McAuliffe *et al.*, 2019a; Schmiedel *et al.*, 2016). Lowest pH values were found by the termite nests and termite frass in H1, indicating that the termites may influence the soil pH in this manner. One reason for this decrease in pH could be due to the fact that pH decreases as evaporation increases (see Figure 3.30) As stated by Tabatabai (1987), sulphates favour adsorption when soils have lower pH. Since gypsum is present throughout the heuweltjie

structure but not so much the interheuweltjie, the lower pH could be the cause of the high presence of gypsum within the heuweltjies (Liu *et al., 2015).*

4.3.4 Validity of Kriging of heat maps

Seeing the preferential flow paths and how they line up with the soil, nest and tunnel distributions throughout the heuweltjie structures shows that the Kriging of the heat maps are fairly accurate and are hence a good depiction of the relative movement of salts throughout the heuweltjie structures.

4.3.5 Insights from PHREEQC analyses

PHREEQC played a crucial role in visualizing the possible distribution of the mineral salts throughout the heuweltjie structures. As not that many samples were analysed for mineralogy via XRD, it could not give such a good representation of how the minerals were spread out within the two heuweltjies. PHREEQC could give this visual representation by analysing the ion data obtained when plotted as heat maps.

4.4 Mechanism of salinization

In this section, possible sources of salts and whether they are moving into the groundwater system (i.e. whether they are undersaturated, saturated or supersaturated) will be discussed. There are three possible sources of the transfer of salts to the heuweltjies: (1) wind-blown salts, (2) evaporative concentration, and (3) rock salts. The first two will be discussed. Another salt source could also be as a result of the termites.

4.4.1 Summary of minerals and salts present within heuweltjies

The dominant minerals, and hence salts, present within the heuweltjies are calcite and gypsum. Other minerals present were calcium oxalate (discussed alongside calcite), hydroxyapatite, amorphous silica, and quartz. These are all outlined below.

Calcite

Calcite is present within the heuweltjies, being close to saturation mostly within the top soils, while also remaining undersaturated at the interheuweltjie and deeper down into the heuweltjie structures. It is dependent upon changes in pH, as its SI increases as pH

increases. In the presence of calcium oxalate and oxalotrophic bacteria and fungi, soils become more alkaline and calcite precipitates (Francis *et al.*, 2012a; Francis & Poch, 2019; Martin *et al.*, 2012; McAuliffe *et al.*, 2019a). This could be the case for the precipitation of calcite within the top soil horizons of both heuweltjies, and the reason why soil pH is much higher in the top horizons compared to the deeper horizons. Some of the calcite ions are still mobile throughout the heuweltjie, however, and these undersaturated minerals aid in the movement of salts within the heuweltjie structure, increasing the amount of salts deeper within the heuweltjie structure.

Gypsum

Gypsum approaches saturation as evaporation increases. It is somewhat pH dependent by becoming less saturated as pH increases as well. This pH dependence is the opposite of what is seen for calcite, as calcite's saturation increases with pH (refer to Figure 3.32b and c). Calcite was mostly saturated in the top horizons of both heuweltjies, where pH was higher, and gypsum was more saturated lower in the heuweltjie, where pH was lower, again suggesting this (refer to Figure 3.33 and Figure 3.34 c, n and o.) As calcite has a lower solubility than gypsum (see Table 2.1), it controls Ca^{2+} activity at the regions within the heuweltjie that have higher pH values. Since gypsum is mostly close to saturation throughout the heuweltjie structure, it is assumed that some of its ions do move freely to the groundwater system.

Hydroxyapatite

Most of the soil solutions were supersaturated with respect to hydroxyapatite. An increase in Cl^- concentration, and hence evaporation, does not influence its saturation. pH, however, influences its saturation. As hydroxyapatite requires OH's in order to form, it makes sense why an increase in pH, and hence OH's, causes it to precipitate out (refer to Table 2.1). Figure 4.1 shows the solubility curves of various calcium orthophosphoric compounds (Kuroda & Okido, 2012). Hydroxyapatite is the most stable of these compounds at pH values greater than 5 and can therefore easily be obtained in solution when the pH is greater than 5. This is in agreement with the findings of this study, as hydroxyapatite was present and mostly saturated when pH values were above 5. Recillas *et al.* (2012) also found in their research that, for hydroxyapatite to precipitate out, a pH greater than 6 is required. As hydroxyapatite is mainly supersaturated, movement of its ions throughout the heuweltjies is highly unlikely, and so it is assumed that it does not

account for the movement of salts present within H1. H4, however, has undersaturated hydroxyapatite deeper within the heuweltjie structure, causing the possibility of the movement of these ions into the groundwater system.
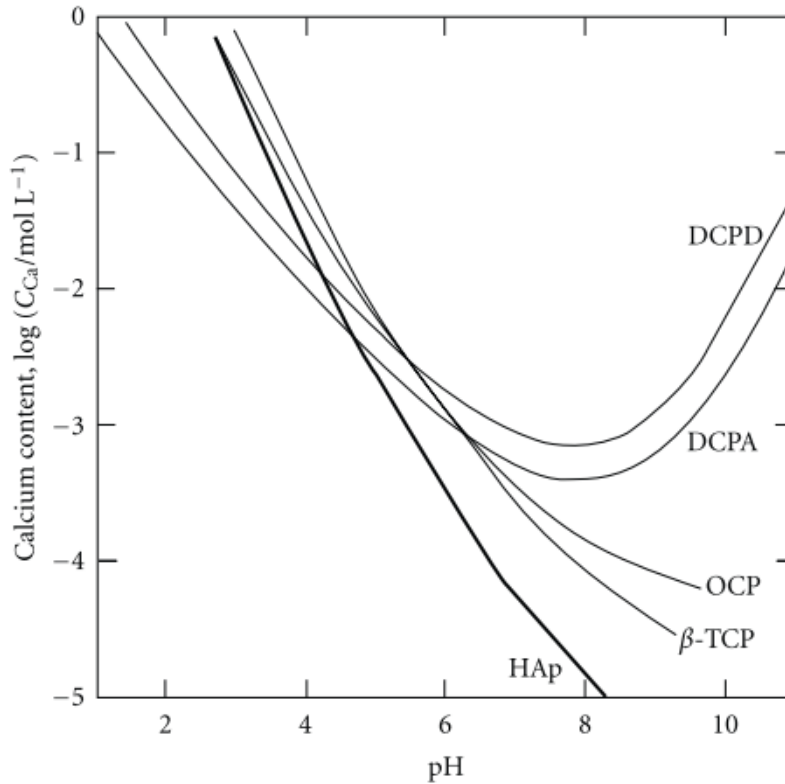
Figure 4.1: Solubility curve diagram showing calcium orthophosphoric compounds at 37℃ with respect to the pH of solution. (by Kuroda & Okido, 2012)*. HAp=hydroxyapatite; TCP= calcium phosphate; OCP= octacalcium phosphate; DCPA= dicalcium phosphate anhydrous; DCPD= dicalcium phosphate dihydrate.*

Quartz and amorphous silica

Both quartz and amorphous silica were not dependent on pH or evaporation, as its saturation remained the same throughout pH and Cl$^-$ concentration changes. Amorphous silica remained undersaturated throughout both heuweltjie structures, however, indicating that it moves freely throughout the heuweltjie.

4.4.2 Marine and evaporative sources of salts

Mineral phase precipitation has a massive influence on the successive evolution of solution compositions (Eugster & Jones, 1979), and is common within arid and semi-arid regions (Francis, 2019; Francis *et al.*, 2007; Schoups *et al.*, 2005; Singer *et al.*, 1995; Wu

131

et al, 2014). Soil and water salinity in such regions is common, resulting due to long-term accumulation of salts through evaporation, and because these salts do not get flushed out of the UZ (Vengosh, 2014). As a result, there have been documentations of salt crusts forming within the upper unsaturated zone and fracture surfaces of soils (Eugster & Jones, 1979; Vengosh, 2014). Most salts that have accumulated in the UZ originate from atmospheric deposition of SO_4^{2-} and Cl^- salts (Vengosh, 2014), most likely through wind-blown marine salts or rain. This dryland salinization cycle is initiated with the accumulation of salts on surface soils, followed by the dissolution and precipitation of non-soluble and soluble minerals (Eugster & Jones, 1979; Vengosh, 2014). The rate of these salts being flushed into the UZ then depends on the solubility of the minerals, along with physical soil properties (such as permeability) – the higher the mineral solubility, the longer the travel of its ions derived from dissolution within the UZ (Vengosh, 2014). This wetting and drying involves precipitation of dissolved salts in dry periods, and dissolution during wet periods, resulting in an uneven distribution of ions throughout the unsaturated zone (Vengosh, 2014). Ca^{2+}, Mg^{2+}, and HCO_3^- are known to accumulate at shallow depths, SO_4^{2-} accumulates at intermediate depths, and Na^+ and Cl^- move freely to greater depths (Vengosh, 2014). This is the case with the heuweltjies (see Figure 3.33 and Figure 3.34) – Na^+ and Cl^- move freely throughout the heuweltjie structures, while Ca^{2+}, Mg^{2+} and HCO_3^- have higher concentrations in the shallower depths, and SO_4^{2-} at intermediate depths. This therefore enhances the possibility of the heuweltjie salts being of marine origin from evaporative and wind-blown salts.

In a study done by Olivier (2002) they found that fog moving inland in Namaqualand had the highest concentration of Na^+ and Cl^- ions while still relatively close to the coast. They suspect that advection sea fog predominates this area, hence accounting for the highest ion concentrations being Na^+ and Cl^-. As the sea fog moves further inland, it could be a source of the salts within the heuweltjie soils. This is possible, as the highest ion concentrations within both heuweltjies were Na^+ and Cl^-.

The ratio of Na^+ and Mg^{2+} with Cl^- for both heuweltjies (Figure 3.30) is in line with the seawater dilution line, suggesting that the predominant source for these ions is from seawater, and hence more than likely from wind-blown salts or fog (marine influence). Smith & Compton (2004) found the same results within their study. Anion dominance within the heuweltjie soils was $Cl>SO_4>>HCO_3$, following the same trend as the saturated

paste extracts on salt pan soils by Smith & Compton (2004). Cation dominance within the heuweltjie soils was Na>Ca>Mg>K. Na^+ and Cl^- are therefore the dominant ions until precipitation of halite, where Ca^{2+} would then become the dominant cation.

It can be concluded that evaporation and wind-blown salts onto the heuweltjies may influence its salt concentration. However, if this is the case, then the question remains as to why only the heuweltjie soils are saline and the interheuweltjie soils are not. In their study, Barica (1972) found that when evaporation rates are high, the highest salt concentrations are found within the top 1 cm of soil. This was not the case for this study, and so brings into question whether wind-blown marine salts or evaporation could cause the salinization of the heuweltjie soils.

4.4.3 Groundwater infiltration

An alternative way in which heuweltjies could become saline would be through saline groundwater infiltration. This could especially be the case if there is rise and fall within the groundwater table. Ibrahimi *et al.* (2014) found that an increase in the fluctuation of the groundwater table brings about an increase in salinization of the soil surface. The saline water moves into the soil through capillary action, so transporting the salts into the root zones of plants (Ibrahimi *et al.* 2014). As the heuweltjies have various preferential flow pathways due to burrowing of termites and various organisms, these may aid in the capillary movement of saline groundwater into the soil. These salts are then also prone to evaporation due to high temperatures and low rainfall (Ibrahimi *et al.* 2014). It was suggested earlier that dissolved silica movement within the heuweltjie soils could be upwards from the groundwater table for H4. This then again could have carried SO_4^{2-} with it, as it also has its highest concentrations deeper in the heuweltjie profile. However, in order to determine whether saline groundwater is the cause of saline heuweltjie soils, heuweltjie data should be related to the groundwater data within this area.

As stated in section 4.3.2, gypsum was closest to saturation within the deeper soil horizons, with calcite closest to saturation at the top, indicating that water movement is downwards (Casby-Horton *et al.*, 2015). Hence, the likelihood of groundwater being the source for heuweltjie salts is low.

4.4.4 Termite influence on salinity

4.4.4.1 Increase in ion concentrations

Another manner of increasing heuweltjie salinity could be through termites bringing saline plant material into the heuweltjies, causing an accumulation of salts over time. Various papers discuss the accumulation of Ca^{2+} within the heuweltjie structure compared to the interheuweltjie (Francis *et al.*, 2012a; Francis & Poch, 2019; McAuliffe, *et al.*, 2019a; McAuliffe *et al.*, 2014), usually in areas where the parent materials do not contain any Ca^{2+} (Francis & Poch, 2019; McAuliffe *et al.*, 2019a). They indicate that this is as a result of termites bringing Ca-rich plant materials, and hence organic matter, into the heuweltjies (Francis *et al.*, 2012a; Francis & Poch, 2019; McAuliffe *et al.*, 2019a). Both heuweltjies in this study had enriched Ca^{2+} concentrations compared to the interheuweltjie soils (Figure 3.33 and Figure 3.34). In their paper, Francis *et al.* (2012a) proposed that the silica, calcite, and sepiolite enriched horizons within heuweltjies are as a result of the high Ca^{2+} and Mg^{2+} in the organic matter introduced by termites into the heuweltjie. High concentrations of Mg^{2+} and silica were also present within both H1 and H4 compared to the interheuweltjie soils, especially in areas where calcite was present. High concentrations of Ca^{2+} and Mg^{2+} were seen especially where the termite frass in H1 and the nests in H4 were located, agreeing with the theory that the enhanced Ca^{2+} and Mg^{2+} concentrations are as a result of the termites. Martin *et al.* (2012) stated that the three factors required for the operation of the oxalate-carbonate pathway are calcium oxalate, oxalate-degrading organisms, and Ca^{2+}. By bringing plant materials into the heuweltjies, the termites are increasing the amount of calcium oxalate present within the heuweltjie structure (Francis & Poch, 2019; McAuliffe *et al.*, 2019a). Once the plant matter decomposes, the calcium oxalate present within these plants can rapidly be consumed by fungi and soil bacteria (Braissant *et al.*, 2002; Francis & Poch, 2019; McAuliffe *et al.*, 2019a). As the top horizons within the heuweltjie have high concentrations of Ca^{2+}, this aids the formation of calcite, especially since the oxalotropic fungi and bacteria also increase the pH of the soil, further enhancing calcite precipitation (Francis & Poch, 2019; Martin *et al.*, 2012; McAuliffe *et al.*, 2019a).

Even though clear evidence is shown for the Ca^{2+} and Mg^{2+} concentrations being as a result of termites, it is still uncertain as to whether or not the other salts present within the heuweltjie soils are as a result of termites. McAuliffe *et al.* (2019a) did, however, find

that *M. viator* termites have an influence on the accumulation of soluble salts within their nests, which is the same as what they found in heuweltjies. Other studies have found similar results (Kunz *et al.*, 2012; McAuliffe *et al.*, 2014). As a result, the plant materials brought into the heuweltjies by termites could have an accumulation of salts within them. If large amounts of saline plants are brought into the heuweltjies over time by termites, an accumulation of these salts is expected. High Na^+ and Cl^- concentrations were recorded for H1 close to the frass chamber as well as the other nests. For H4, on the other hand, Na^+ and Cl^- concentrations were not as high as expected within the termite nest and tunnels (at a cross section of 42 m); however, EC was quite high at this area, suggesting high salt concentrations.

High salt concentrations within plants is common in arid and semi-arid regions of the world. One of these salt-tolerant plants is *Mesembryanthemum crystallinum* (Bartels & Sunkar, 2005), which was also seen on the heuweltjies during preliminary sampling excursions (see Figure 4.2). As these plants are salt tolerant, they also contain salts, and have been found to have up to 8% Na (Milton *et al.*, 1994). If termites harvest these or other salt tolerant plants, as was also noted by Francis *et al.* (2012a), this would increase the amount of salts found within the heuweltjie, therefore increasing the soil salinity over time. However, in order to determine whether or not this is true, more research would have to be done, especially focusing on the salt content of the plants on and surrounding the heuweltjies.
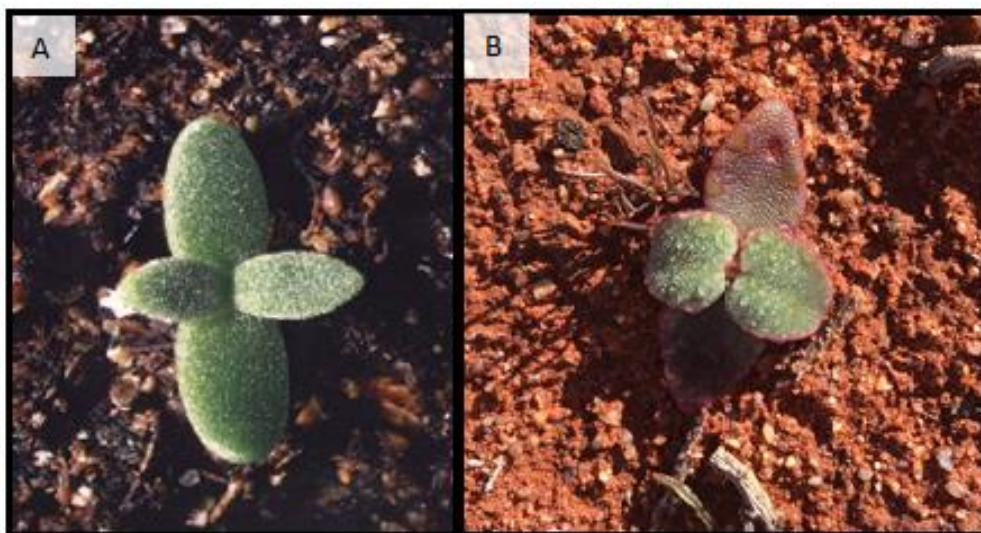
Figure 4.2: Mesembryanthemum crystallinum seedlings. A denotes seedling as depicted by *Bonhert Laboratories (2002)*; *B shows the seedling found on heuweltjies during field trips.*

4.4.4.2   Preferential flow pathways

Termites could also aid in groundwater salinization by creating preferential flow pathways througout the heuweltjie structures. Termites have tunnels leading towards their nests, which aid as preferential flow pathways (Jouquet *et al.*, 2016; McAuliffe *et al.*, 2019a). This was seen throughout the heuweltjie structures, especially for H4. The tunnels are connected to the surface of the soil, aiding in water movement throughout the soil structures (Jouquet *et al.*, 2016), and, as was seen for H4, carry higher concentrations of salts in them possibly towards the groundwater system.

4.4.5   Paleo or modern process?

It is evident that the salt movement is downwards within the heuweltjies. However, the question remains as to whether the movement of the salts is a paleo process or modern process. What is also not known is if the movement of the salts mostly occurred in the past, or if it is occurring more in the present. The ion flow throughout the heuweltjie structures may not always be showing just the current soil chemistry of the heuweltjies – it could be showing past ion movements as well.

In their study, Chase & Meadows (2007) showed that climate was wetter in the Namaqualand region of South Africa from 24 – 18 ka years before present (see Figure 4.3). Along with higher precipitation rates, they also found that evaporation rates were lower during the last glacial maximum. As older heuweltjies can be up to 20,000 – 35,000 years old (Midgley *et al.*, 2002; Potts *et al.*, 2009), this therefore suggests that if there were a lot of salts present in the heuweltjies during those times, the movement of these salts towards the groundwater would have been a much faster process.

There have been accounts of lateral and vertical water movement in soils of Namaqualand on the regional scale (Francis & Poch 2019). However, as little rainfall takes place within the Buffelsrivier area presently (see Figure 1.6a), the salts currently present may remain dormant within the heuweltjie profiles for a long time. Most of Namaqualand receives less than 150 mm rain per annum (Cowling *et al.*, 1999), and so groundwater recharge is slow (Abiye & Leshomo, 2013). This implies that the salt movement through the heuweltjie structures with infiltrated rainwater would be slow. Evaporation rates of around 2000 mm per year are expected to occur (Francis, 2019) due to high temperatures, and so the rainwater evaporates very soon after it has fallen,

limiting the transfer of salts through the heuweltjie structure towards the groundwater even more. If the salts are being transferred to the groundwater system in this manner, it would take very long. On the other hand, freak rainfall events are known to take place in Namaqualand every so many years, where very large amounts of water fall on the ground, sometimes even causing there to be water flowing in the Buffels River itself. When these large rainfall events do take place, it would cause the salts present in the heuweltjies to be flushed into the groundwater system quite rapidly via the preferential flow paths present.

Due to the reasons stated above, the process of the movement of the heuweltjie salts towards the groundwater could either be through high volume rainfall events, or it could have mostly occurred during a wetter past climate.
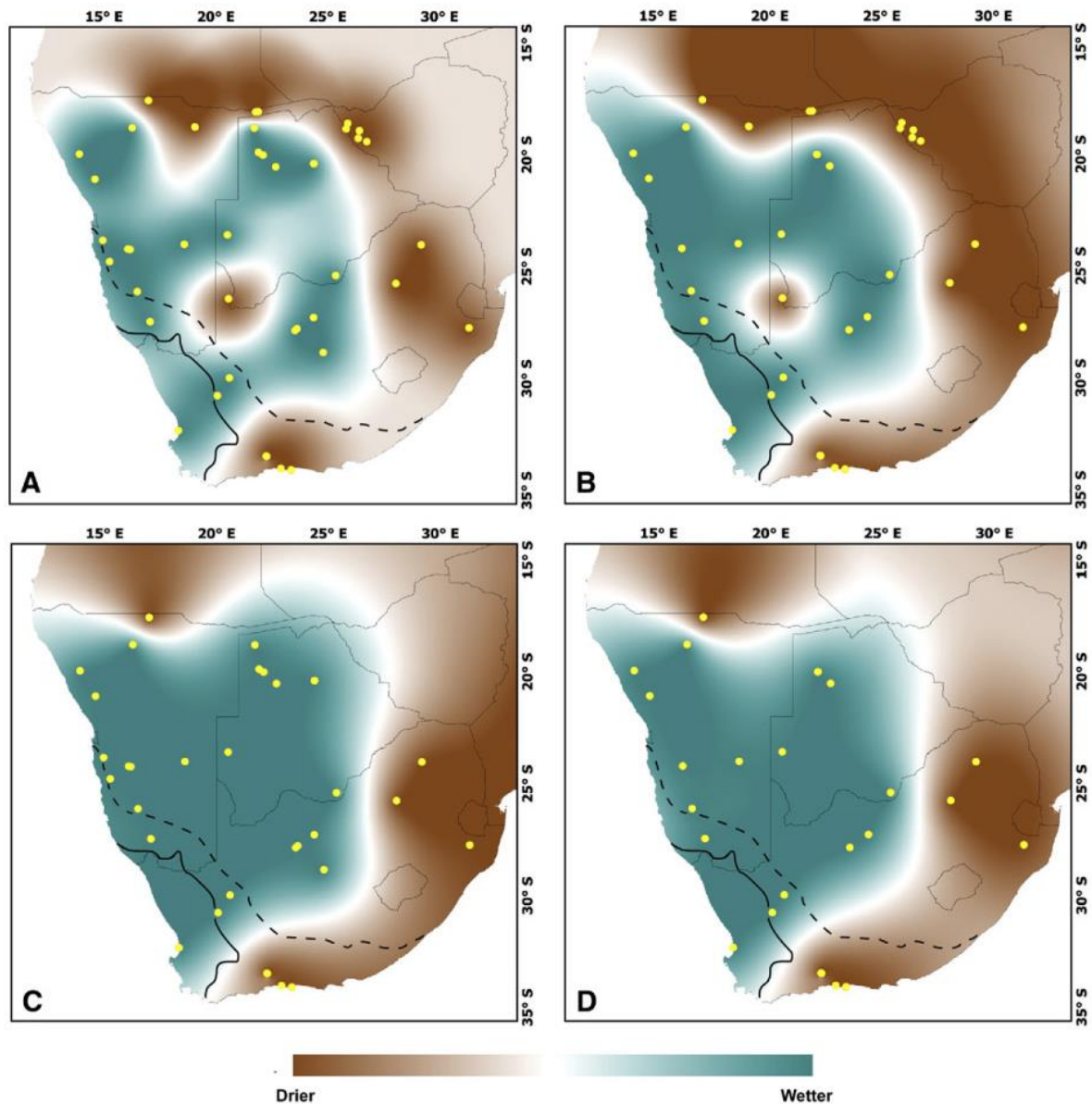
Figure 4.3: Paleooenvironmental evidence (yellow dots) of southern Africa from 24 – 18 ka, showing wetter conditions than present. A shows data when using all available records; B excludes ^{14}C dates and data from silts; C excludes aeolian proxies which show aridity records, as well as silts; D excludes aeolian records, silts, and open-system carbonates.

4.5 Implications of heuweltjie salts on agriculture

After discussing the physical and chemical heuweltjie soil properties, it is important to consider what this means for agriculture and saline groundwater in Buffelsrivier.

4.5.1 Agriculture in Buffelsrivier

As Buffelsrivier is a poor community, it is important to provide more work opportunities for the people living there. One of the best solutions for such an economic problem would be agriculture. However, for agriculture to be possible within this region, the heuweltjie soils would have to be dug up. If the heuweltjie soils are not transported away from the site and are used as agricultural soils, highly salt tolerant crops would have to be used for farming. One advantage of the heuweltjie soils would be its high clay and organic matter content. However, the better solution would be to move all the soil away from the region, since watering the plants grown on heuweltjie soils would increase the groundwater salinity, which is already a threat to the community. By removing all the heuweltjie soils, the salts within the heuweltjie would not be present to be washed into the groundwater system, and hence the groundwater would not become more saline (if the heuweltjie salts were the cause of the saline groundwater, and not vice versa). This is not very feasible, however, as the saline heuweltjie soils extend quite deep down, as was shown with the heat maps, and so a lot of soil would have to be removed and replaced with other soil.

The best method would most likely be planting around the heuweltjies and not on top of them, and so cost would be minimised. Most of the soils within the region, as stated in section 1.3.4 have quite shallow dorbank layers, and as a result, planting crops would not be the most suitable farming. Livestock would be a better option, as grasses would be grown more successfully on the shallow soils.

4.5.2 Groundwater desalinisation

As the groundwater resources are already saline, using this water to water the plants grown would again increase the soil salinity, and therefore, this should also be taken into consideration before implementing agriculture within this region. Groundwater desalinisation is a possible solution if the groundwater is to be used for agriculture. Barica (1972) proposed the idea of desalinisation of saline groundwater within arid and semi-

arid regions, bringing light to the problem of saline groundwater. Water with a moderate salinity (~700 ppm) requires less than twice the amount of energy needed for desalinisation than that of seawater (Kang & Jackson, 2016). Desalinisation of shallow groundwater aquifers within coastal areas is economically feasible, such as at the Richard Reynolds Groundwater Desalinisation Facility in Chula Vista, California (Kang & Jackson, 2016). One downfall of desalinisation, however, is that it produces a concentrated 'brine,' which is of environmental concern (Gude, 2018). Although this is the case, the idea of desalinisation remains a good one for the area of Buffelsrivier. If the brine can be discarded in an environmentally friendly manner, and the town can receive fresh water, this would enhance their quality of life, also increasing work opportunities with the development and upkeep of the desalinisation plant, as well as agriculture.

5 Conclusions

Heuweltjie soils have different texture and soluble ion composition when compared to the interheuweltjie soils. Soil texture was more clayey within the heuweltjie structure than the surrounding soils, as was also found within other studies. Clay mineralogy did not show much variation between heuweltjie and interheuweltjie soils, although calcite, gypsum, calcium oxalate and hydroxyapatite were found within heuweltjie soils and not the interheuweltjie.

Ion activity results indicated that the heuweltjie salts could be of marine origin through wind-blown salts or evaporative transport. SI values for halite, calcite, and gypsum, mostly remained undersaturated, and so the ions present were mobile within the heuweltjie structure. Hydroxyapatite was mostly supersaturated throughout both heuweltjie structures, and so its ions did not move freely towards the groundwater.

Preferential flow pathways were noted for EC, Na^+, Cl^-, and especially K^+ throughout H1 and H4. For Na^+ and Cl^- in H1, it was mostly throughout the granular textured soils produced by termite activity, while K^+ moved from the calcite nodules through to the carbonate cemented (Bkm) and silica and carbonate cemented (Bkqm) horizons. For K^+ in H4, on the other hand, preferential flow seemed to mostly be through the nest and tunnels found within H4. Ca^{2+} and Mg^{2+} concentrations were high near the termite frass within H1, while it was high within the tunnels for H4. SO_4^{2-} for both heuweltjies followed the movement of dissolved silica, indicating that it moves with water throughout the heuweltjies. Gypsum was closest to saturation within the middle of the heuweltjie structure for both heuweltjies, while calcite was mostly present in the top horizons. Halite moved freely throughout both heuweltjie structures, increasing in saturation deeper within the heuweltjie structures. This vertical variation with respect to calcite and gypsum indicates that the water movement within the heuweltjies was downwards, and so the salts are being transferred towards the groundwater. This could be concluded since gypsum is a more soluble mineral than calcite, and so it moves further down the heuweltjie profile.

Salts were present everywhere throughout the heuweltjie structures, while it was found less within the interheuweltjie soils, indicating that something within the heuweltjies must be the cause of this high salinity. If only marine blown salts and evaporative

concentration were the cause, then the interheuweltjie soils should also be more saline. It was concluded that termites may aid in heuweltjie salinity by bringing saline plant materials into it, accumulating the salts over time. The preferential flow pathways found within these heuweltjies, also as a result of termite activity, would then aid in movement of these salts towards the groundwater, causing an increase in groundwater salinity. For this to be concluded with certainty, the heuweltjie data should be correlated with groundwater data for this area. Plants growing on the heuweltjies should also be analysed for salinity, and it should be determined whether these saline plants growing on and around the heuweltjies are being transferred into the heuweltjies through termite activity.

6 References

Abiye, T.A. & Leshomo, J.T. 2013. Groundwater flow and radioactivity in Namaqualand, South Africa. *Environmental Earth Sciences*. 70:281–293.

Aboukila, E.F. & Norton, J.B. 2017. Estimation of saturated soil paste salinity from soil-water extracts. *Soil Science*. 182(3):107–113.

Appelo, C.A.J. & Postma, D. 2005. *Geochemistry, groundwater and pollution*. 2nd ed. Netherlands: A.A. Balkema Publishers.

Atkins, P. & De Paula, J. 2010. *Atkins' Physical Chemistry*. 9th ed. United States: Oxford University Press.

Bailie, R., Armstrong, R. & Reid, D. 2007. The Bushmanland Group supracrustal succession, Aggeneys, Bushmanland, South Africa: Provenance, age of deposition and metamorphism. *South African Journal of Geology*. 110(1):59–86.

Barica, J. 1972. Salinization of groundwater in arid zones. *Water Research Pergamon Press*. 6:925–933.

Bartels, D. & Sunkar, R. 2005. Drought and salt tolerance in plants. *Critical Reviews in Plant Sciences*. 24(1):23–58.

Benito, G., Rohde, R., Seely, M., Külls, C., Dahan, O., Enzel, Y., Todd, S., Botero, B., et al. 2010. Management of alluvial aquifers in two southern African ephemeral rivers: Implications for IWRM. *Water Resources Management*. 24:641–667.

Bial, J., Büttner, S.H. & Frei, D. 2015. Formation and emplacement of two contrasting late-Mesoproterozoic magma types in the central Namaqua Metamorphic Complex (South Africa, Namibia): Evidence from geochemistry and geochronology. *Lithos*. 224–225:272–294.

Bonhert Laboratories. 2002. *Stages of development in mesembryanthemum crystallinum*. [Online], Available: http://www.life.illinois.edu/bohnert/mesem/ [2019, August 22].

Braissant, O., Verrecchia, E. & Aragno, M. 2002. Is the contribution of bacteria to terrestrial carbon budget greatly underestimated? *Naturwissenschaften*. 89:366–370.

Bühmann, C., Nell, J.P. & Samadi, M. 2004. Clay mineral associations in soils formed under Mediterranean-type climate in South Africa. *South African Journal of Plant and Soil*. 21(3):166–170.

Bui, E.N. 2013. Soil salinity : A neglected factor in plant ecology and biogeography. *Journal of Arid Environments*. 92:14–25.

Casby-Horton, S., Herrero, J. & Rolong, N.A. 2015. Gypsum soils—Their morphology, classification, function, and landscapes. *Advances in Agronomy*. 130:231–290.

Chase, B.M. & Meadows, M.E. 2007. Late Quaternary dynamics of southern Africa's winter rainfall zone. *Earth-Science Reviews*. 84:103–138.

Clarke, J. 2003. The occurrence and significance of biogenic opal in the regolith. *Earth-Science Reviews*. 60:175–194.

Clarke, C.E., Majodina, T.O., du Plessis, A. & Andreoli, M.A.G. 2016. The use of X-ray tomography in defining the spatial distribution of barite in the fluvially derived palaeosols of Vaalputs, Northern Cape Province, South Africa. *Geoderma*. 267:48–57.

Clifford, T.N., Barton, E.S., Retief, E.A., Rex, D.C. & Fanning, C.M. 1995. A crustal progenitor for the intrusive anorthosite--Charnockite kindred of the Cupriferous Koperberg Suite, O'okiep District, Namaqualand, South Africa; New isotope data for the country rocks and the intrusives. *Journal of Petrology*. 36(1):231–258.

Clifford, T.N., Barton, E.S., Stern, R.A. & Duchesne, J.-C. 2004. U-Pb Zircon calendar for Namaquan (Grenville) crustal events in the granulite-facies terrane of the O'okiep Copper District of South Africa. *Journal of Petrology*. 45(4):669–691.

Colliston, W.P., Schoch, A.E. & Praekelt, H.E. 2012. Stratigraphy of the Mesoproterozoic Aggeneys terrane, western Namaqua mobile belt, South Africa. *South African Journal of Geology*. 115(4):33-39449–464.

Corwin, D.L. & Lesch, S.M. 2005. Apparent soil electrical conductivity measurements in agriculture. *Computers and Electronics in Agriculture*. 46:11–43.

Cowling, R.M., Esler, K.J. & Rundel, P.W. 1999. Namaqualand, South Africa – an overview of a unique winter-rainfall desert ecosystem. *Plant Ecology*. 142:3–21.

Cramer, M.D. & Midgley, J.J. 2015. The distribution and spatial patterning of mima-like mounds in South Africa suggests genesis through vegetation induced aeolian

sediment deposition. *Journal of Arid Environments*. 119:16–26.

Cramer, M.D., Innes, S.N. & Midgley, J.J. 2012. Hard evidence that heuweltjie earth mounds are relictual features produced by differential erosion. *Palaeogeography, Palaeoclimatology, Palaeoecology*. 350–352:189–197.

Cramer, M.D., von Holdt, J.R.C., Uys, V.M. & Midgley, J.J. 2017. The present and likely past climatic distribution of the termite Microhodotermes viator in relation to the distribution of heuweltjies. *Journal of Arid Environments*. 146:35–43.

Daliakopoulos, I.N., Tsanis, I.K., Koutroulis, A., Kourgialas, N.N., Varouchakis, A.E., Karatzas, G.P. & Ritsema, C.J. 2016. The threat of soil salinity: A European scale review. *Science of The Total Environment*. 573:727–739.

Davis, C.L., Hoffman, M.T. & Roberts, W. 2016. Recent trends in the climate of Namaqualand, a megadiverse arid region of South Africa. *South African Journal of Science*. 112(3/4):1–9.

Derry, L.A., Kurtz, A.C., Ziegler, K. & Chadwick, O.A. 2005. Biological control of terrestrial silica cycling and export fluxes to watersheds. *Nature*. 433:728–731.

Eby, G.N. 2004. *Principles of Environmental Geochemistry*. United States: Brooks/Cole, Cengage Learning.

Edwards, A.C., Ferrier, R.C. & Miller, J.D. 1992. The contribution of sulphate to total sulphur in a range of natural water samples. *Hydrological Sciences Journal*. 37(3):277–283.

Ellis, F. & Lambrechts, J.J.N. 1994. Dorbank, a reddish brown hardpan of South Africa: a proto-silcrete? In Acaoulco, Mexico *15th World Congress of Soil Science*.

Eugster, H.P. & Jones, B.F. 1979. Behavior of major solutes during closed basin- lakes brine evolution. *American Journal of Science*. 279(6):609–631.

Fauriel, S. & Laloui, L. 2012. A bio-chemo-hydro-mechanical model for microbially induced calciteprecipitation in soils. *Computers and Geotechnics*. 46:104–120.

Fey, M.V., Mills, A.J. & Yaalon, D.H. 2006. The alternative meaning of pedoderm and its use for soil surface characterization. *Geoderma*. 133:474–477.

Francis, M.L. 2008. Soil Formation on the Namaqualand Coastal Plain. Stellenbosch

University.

Francis, M.L. 2019. Effect of sepiolite and palygorskite on plant available water in Arenosols of Namaqualand, South Africa. *Geoderma Regional*. 17:1–15.

Francis, M.L., Ellis, F., Lambrechts, J.J.N. & Poch, R.M. 2012. A micromorphological view through a Namaqualand termitaria (Heuweltjie, a Mima-like mound). *Catena*. 100:57–73.

Francis, M.L., Fey, M. V, Ellis, F. & Poch, R.M. 2012. Petroduric and "petrosepiolitic" horizons in soils of Namaqualand , South Africa. *Spanish Journal of Soil Science*. 2(1):8–25.

Francis, M.L., Fey, M.V., Prinsloo, H.P., Ellis, F., Mills, A.J. & Medinski, T.V. 2007. Soils of Namaqualand: Compensations for aridity. *Journal of Arid Environments*. 70(4):588–603.

Francis, M.L. & Poch, R.M. 2019. Calcite accumulation in a South African heuweltjie: Role of the termite Microhodotermes viator and oribatid mites. *Journal of Arid Environments*. 0–1:1–10.

Georgiadis, A., Sauer, D., Herrmann, L., Breuer, J., Zarei, M. & Stahr, K. 2013. Development of a method for sequential Si extraction from soils. *Geoderma*. 209–210:251–261.

Georgiadis, A.A., Sauer, D.B., Herrmann, L.A., Breuer, J.C., Zarei, M.A. & Stahr, K.A. 2014. Testing a new method for sequential silicon extraction on soils of a temperate–humid climate. *Soil Research*. 52:645–657.

Gorji, T., Sertel, E. & Tanik, A. 2017. Monitoring soil salinity via remote sensing technology under data scarce conditions: A case study from Turkey. *Ecological Indicators*. 74:384–391.

Grisso, R., Alley, M., Holshouser, D. & Thomason, W. 2009. Precision farming tools: soil electrical conductivity. *Virginia Cooperative Extension*. 442(508):1–6.

Gude, V.G. 2018. Desalination of deep groundwater aquifers for freshwater supplies – Challenges and strategies. *Groundwater for Sustainable Development*. 6:87–92.

He, Y., DeSutter, T., Prunty, L., Hopkins, D., Jia, X. & Wysocki, D.A. 2012. Evaluation of 1:5 soil to water extract electrical conductivity methods. *Geoderma*. 185–186:12–17.

Huang, T., Yang, S., Liu, J. & Li, Z. 2016. How much information can soil solute profiles reveal about groundwater recharge? *Geosciences Journal*. 20(4):495–502.

Huang, T., Pang, Z., Liu, J., Ma, J. & Gates, J. 2017. Groundwater recharge mechanism in an integrated tableland of the Loess Plateau, northern China: insights from environmental tracers. *Hydrogeology Journal*. 25:2049–2065.

Huang, T., Pang, Z., Liu, J., Yin, L. & Edmunds, W.M. 2017. Groundwater recharge in an arid grassland as indicated by soil chloride profile and multiple tracers. *Hydrological Processes*. 31:1047–1057.

Huber, S., Prokop, G., Arrouays, D., Banko, G., Bispo, A., Jones, R.J.A., Kibblewhite, M.G., Lexer, W., et al. 2008. *Environmental Assessment of Soil for Monitoring Volume I: Indicators and Criteria. EUR 23490 EN/1*. Luxembourg: Office for Official Publication of the European Communities.

Ibrahimi, M.K., Miyazaki, T., Nishimura, T. & Imoto, H. 2014. Contribution of shallow groundwater rapid fluctuation to soil salinization under arid and semiarid climate. *Arabian Journal of Geosciences*. 7:3901–3911.

Jacobs, J., Pisarevsky, S., Thomas, R.J. & Becker, T. 2008. The Kalahari Craton during the assembly and dispersal of Rodinia. *Precambrian Research*. 160:142–158.

Johnston, C.D. 1987. Distribution of environmental chloride in relation to subsurface hydrology. *Journal of Hydrology*. 94:67–88.

Jones, D.L.H.P. & Handreck, K.A. 1963. Effects of iron and aluminum oxides on silica in solution in soils. *Nature*. 198:852–853.

Jones, L.H. & Dreher, G.B. 1996. Silicon. In 5th ed. D.L. Sparks (ed.). Madison, WI, USA *Methods of Soil Analysis. Part 3. Chemical Methods*. 627–637.

Jouquet, P., Bottinelli, N., Shanbhag, R.R., Bourguignon, T., Traoré, S. & Abbasi, S.A. 2016. Termites: The neglected soil engineers of tropical soils. *Soil Science*. 181(3–4):157–165.

Jungerius, P.D., van den Ancker, J.A.M. & Mücher, H.J. 1999. The contribution of termites to the microgranular structure of soils on the Uasin Gishu Plateau, Kenya. *CATENA*. 34:349–363.

Kang, M. & Jackson, R.B. 2016. Salinity of deep groundwater in California: Water quantity,

quality, and protection. *Environmental Earth Sciences*. 113:7768–7773.

Kelso, C. & Vogel, C. 2007. The climate of Namaqualand in the nineteenth century. *Climatic Change*. 83:357–380.

Kendrick, K.J. & Graham, R.C. 2004. Pedogenic silica accumulation in chronosequence soils, southern California. *Soil Science Society of America Journal*. 68:1295–1303.

Kunz, N.S.S., Hoffman, M.T.T. & Weber, B. 2012. Effects of heuweltjies and utilization on vegetation patterns in the Succulent Karoo, South Africa. *Journal of Arid Environments*. 87:198–205.

Kuroda, K. & Okido, M. 2012. Hydroxyapatite coating of titanium implants using hydroprocessing and evaluation of their osteoconductivity. *Bioinorganic Chemistry and Applications*. 2012:1–7.

Liu, K., Deng, M. & Mo, L. 2015. Influence of pH on the formation of gypsum in cement materials during sulfate attack. *Advances in Cement Research*. 27(8):487–493.

Loeppert, R.H. & Suarez, D.L. 1996. Carbonate and gypsum. In 5th ed. D.L. Sparks (ed.). Madison, WI, USA: Soil Science Society of America and American Society of Agronomy *Methods of Soil Analysis. Part 3. Chemical Methods*. 437–474.

Luther-Mosebach, J., Dengler, J.J., Schmiedel, U., Röwer, I.U., Labitzky, T. & Gröngröft, A. 2012. A first formal classification of the Hardeveld vegetation in Namaqualand, South Africa. *Applied Vegetation Science*. 15(3):401–431.

Ma, R., Mcbratney, A., Whelan, B., Budiman, M. & Short, M. 2011. Comparing temperature correction models for soil electrical conductivity measurement. *Precision Agriculture*. 12:55–66.

Macey, P.H., Thomas, R.J., Minnaar, H.M., Gresse, P.G., Lambert, C.W., Groenewald, C.A., Miller, J.A., Indongo, J., et al. 2017. Origin and evolution of the ~1.9 Ga Richtersveld Magmatic Arc, SW Africa. *Precambrian Research*. 292:417–451.

Macey, P.H., Bailie, R.H., Miller, J.A., Thomas, R.J., de Beer, C., Frei, D. & le Roux, P.J. 2018. Implications of the distribution, age and origins of the granites of the Mesoproterozoic Spektakel Suite for the timing of the Namaqua Orogeny in the Bushmanland Subprovince of the Namaqua-Natal Metamorphic Province, South Africa. *Precambrian Research*. 312:68–98.

MacKellar, N.C., Hewitson, B.C. & Tadross, M.A. 2007. Namaqualand's climate: Recent historical changes and future scenarios. *Journal of Arid Environments*. 70:604–614.

Martin, G., Guggiari, M., Bravo, D., Zopfi, J., Cailleau, G., Aragno, M., Job, D., Verrecchia, E., et al. 2012. Fungi, bacteria and soil pH: The oxalate-carbonate pathway as a model for metabolic interaction. *Environmental Microbiology*. 14(11):2960–2970.

Martinez, C.E., Kleinschmidt, A.W. & Tabatabai, M.A. 1998. Sulfate adsorption by variable charge soils: Effect of low-molecular-weight organic acids. *Biology and Fertility of Soils*. 26:157–163.

McAuliffe, J.R., Hoffman, M.T., McFadden, L.D., Bell, W., Jack, S., King, M.P. & Nixon, V. 2019. Landscape patterning created by the southern harvester termite, Microhodotermes viator: Spatial dispersion of colonies and alteration of soils. *Journal of Arid Environments*. 162:26–34.

McAuliffe, J.R., Hoffman, M.T., McFadden, L.D., Jack, S., Bell, W. & King, M.P. 2019. Whether or not heuweltjies: Context-dependent ecosystem engineering by the southern harvester termite, Microhodotermes viator. *Journal of Arid Environments*. 163:26–33.

McAuliffe, J.R., Hoffman, M.T., McFadden, L.D. & King, M.P. 2014. Role of aeolian sediment accretion in the formation of heuweltjie earth mounds, western South Africa. *Earth Surface Processes and Landforms*. 39:1900–1912.

McAuliffe, J.R., McFadden, L.D. & Hoffman, M.T. 2018. Role of aeolian dust in shaping landscapes and soils of arid and semi-arid South Africa. *Geosciences*. 8(171):1–34.

McKeague, J.A. & Cline, M.G. 1963. Silica in soil solutions: I. The form and concentration of dissolved silica in aqueous extracts of some soils. *Canadian Journal of Soil Science*. 43(1):70–82.

Midgley, J.J., Harris, C., Hesse, H. & Swift, A. 2002. Heuweltjie age and vegetation change based on δ13C and 14C analyses. *South African Journal of Science*. 98:202–204.

Miller, J.A. & Watson, A.P. 2018. *Application of isotope hydrology to understand saline groundwater and surface water systems and the interaction between them in the Western and Northern Cape provinces of South Africa. WRC Report No K5-2442*. Pretoria: Water Research Commision.

Millot, R., Vigier, N. & Gaillardet, J. 2010. Behaviour of lithium and its isotopes during weathering in the Mackenzie Basin, Canada. *Geochimica et Cosmochimica Acta*. 74:3897–3912.

Milnes, A.R. & Twidale, C.R. 1983. An overview of silicification in Cainozoic landscapes of arid central and southern AustraIia. *Australian Journal of Soil Research*. 21:387–410.

Milton, S.J., Richard, W., Dean, J. & Siegfried, W.R. 1994. Food selection by ostrich in southern Africa. *Journal of Wildlife Management*. 58(2):234–247.

Monger, H.C., Daugherty, L.A., Lindemarin, W.C. & Liddell, C.M. 1991. Microbial precipitation of pedogenic calcite. *Geology*. 19:997–1000.

Murphy, J. & Riley, J.P. 1962. A modified single solution method for the determination of phosphate in natural waters. *Analytica Chimica Acta*. 27:31–36.

Naicker, S. & Demlie, M. 2014. Environmental isotopic and hydrochemical characteristics of groundwater from the Sandspruit Catchment, Berg River Basin, South Africa. *Water Science & Technology*. 69(3):601–611.

Nordstrom, D. K. Plummer, L.N., Wigley, T.M.L., Wolery, T.J., Ball, J.W., Jenne, E.A., Bassett, R.L., Crerar, D.A., Florence, T.M., et al. 1979. A comparison of computerized chemical models for equilibrium calculations in aqueous systems. In E.A. Jeanne (ed.) *Chemical modeling in aqueous systems, speciation, sorption, solubility, and kinetics*. American Chemical Society: Washington D.C. 857-892.

Olivier, J. 2002. Fog-water harvesting along the West Coast of South Africa: A feasability study. *Water SA*. 28(4):349–360.

Papadopoulos, I. 1984. Effect of sulphate waters on soil salinity, growth and yield of tomatoes. *Plant and Soil*. 81(3):353–361.

Parkhurst, D.L. & Appelo, C.A.J. 2013. Description of input and examples for PHREEQC version 3 - A computer program for speciation, batch-reaction, one-dimensional transport, and inverse geochemical calculations. In 6th ed. *U.S. Geological Survey Techniques and Methods*. 497. [Online], Available: http://pubs.usgs.gov/tm/06/a43/.

Picker, M.D., Hoffman, M.T. & Leverton, B. 2007. Density of Microhodotermes viator (Hodotermitidae) mounds in southern Africa in relation to rainfall and vegetative

productivity gradients. *Journal of Zoology*. 271:37–44.

Potts, A.J., Midgley, J.J. & Harris, C. 2009. Stable isotope and 14C study of biogenic calcrete in a termite mound, Western Cape, South Africa, and its palaeoenvironmental significance. *Quaternary Research*. 72(02):258–264.

Raith, J.G. 1995. Petrogenesis of the Concordia Granite Gneiss and its relation to W-Mo mineralization in western Namaqualand, South Africa. *Precambrian Research*. 70:303–335.

Recillas, S., Rodríguez-Lugo, V., Montero, M.L., Viquez-Cano, S., Hernandez, L. & Castaño, V. 2012. Studies on the precipitation behaviours of calcium phosphate solutions. *Journal of Ceramic Processing Research*. 13(1):5–10.

Rhoades, J.D. 1996. Salinity: Electrical conductivity and total dissolved solids. In 5th ed. D. Sparks (ed.). Madison, WI, USA *Methods of Soil Analysis. Part 3. Chemical Methods*. 417–437.

Saccone, L., Conley, D.J., Sauer, D., Saccone L., Conley D.J. & Sauer, D. 2006. Methodologies for amorphous silica analysis. *Journal of Geochemical Exploration*. 88:235–238.

Scanlon, B.R., Keese, K.E., Flint, A.L., Flint, L.E., Gaye, C.B., Edmunds, W.M. & Simmers, I. 2006. Global synthesis of groundwater recharge in semiarid and arid regions. *Hydrological Processes*. 20:3335–3370.

Schmiedel, U., Kühne, N., Twerski, A. & Oldeland, J. 2015. Small-scale soil patterns drive sharp boundaries between succulent "dwarf" biomes (or habitats) in the arid Succulent Karoo, South Africa. *South African Journal of Botany*. 101:129–138.

Schmiedel, U., Röwer, I.U., Luther-Mosebach, J., Dengler, J., Oldeland, J. & Gröngröft, A. 2016. Effect of grazing on vegetation and soil of the heuweltjieveld in the Succulent Karoo, South Africa. *Acta Oecologica*. 77:27–36.

Schoups, G., Hopmans, J.W., Young, C.A., Vrugt, J.A., Wallender, W.W., Tanji, K.K. & Panday, S. 2005. Sustainability of irrigated agriculture in the San Joaquin Valley, California. *Proceedings of the National Academy of Sciences*. 102(43):15352–15356.

Seilsepour, M. & Rashidi, M. 2008. Modeling of soil sodium adsorption ratio based on soil electrical conductivity. *Journal of Agricultural and Biological Science*. 3(5/6):27–31.

Setti, M., Lopez-Galindo, A., Padoan, M. & Garzantii, E. 2014. Clay mineralogy in southern

Africa river muds. *Clay Minerals*. 49:717–733.

Singer, A., Kirsten, W. & Buhmann, C. 1995. Fibrous clay minerals in the soils of Namaqualand, South Africa: characteristics and formation. *Geoderma*. 66:43–70.

Skoog, D.A., West, D.M., Holler, F.J. & Crouch, S.R. 2004. *Fundamentals of Analytical Chemistry*. 8th ed. United States: Brooks/Cole, Cengage Learning.

Smith, M. & Compton, J.S. 2004. Origin and evolution of major salts in the Darling pans, Western Cape, South Africa. *Applied Geochemistry*. 19(5):645–664.

Soil Classification Working Group. 1991. Methods of analysis. In 2nd ed. South Africa *Soil classification: A taxonomic system for South Africa*. 194–197.

Soil Survey Staff. 2015. *Illustrated Guide to Soil Taxonomy, version 2.0.* Lincoln, Nebraska: U.S. Department of Agriculture, Natural Resources Conservation Service, National Soil Survey Center.

Sommer, M., Kaczorek, D., Kuzyakov, Y. & Breuer, J. 2006. Silicon pools and fluxes in soils and landscapes - a review. *Journal of Plant Nutrition and Soil Science*. 169:310–329.

Sonmez, S., Buyuktas, D., Okturen, F. & Citak, S. 2008. Assessment of different soil to water ratios (1:1, 1:2.5, 1:5) in soil salinity studies. *Geoderma*. 144:361–369.

Sudduth, K.A., Kitchen, N.R. & Drummond, S.T. 2017. Inversion of soil electrical conductivity data to estimate layered soil properties. *Advances in Animal Biosciences: Precision Agriculture*. 8(2):433–438.

Summerfield, M.A. 1983. Geochemistry of weathering profile silcretes, southern Cape Province, South Africa. *Geological Society Special Publication*. 11:167–178.

Tabatabai, M.A. 1987. Physicochemical fate of sulfate in soils. *JAPCA*. 37(1):34–38.

Uren, N.C. 2018. Calcium oxalate in soils, its origins and fate - a review. *CSIRO Publishing*. 56:443–450.

van Gend, J. 2018. 36 Chlorine isotope systematics in saline groundwater in the Buffels River Valley. Stellenbosch University.

Vengosh, A. 2014. *Salinization and Saline Environments*. 2nd ed. Vol. 11. Durnham, North Carolina: Elsevier Ltd.

World Reference Base for Soil Resources (WRB). 2014. *World Soil Resources Reports no*

84. Rome: Food and Agricultural Organization of the United Nations (FAO).

Wu, J., Li, P., Qian, H. & Fang, Y. 2014. Assessment of soil salinization based on a low-cost method and its influencing factors in a semi-arid agricultural area, northwest China. *Environmental Earth Sciences.* 71:3465–3475.

Yang, H., Li, C., Wei, C., Li, M., Li, X., Deng, Z. & Fan, G. 2015. Molybdenum blue photometry method for the determination of colloidal silica and soluble silica in leaching solution. *Analytical Methods.* 7(13):5462–5467.

Zhang, H., Schroder, J.L., Pittman, J.J., Wang, J.J. & Payton, M.E. 2005. Soil salinity using saturated paste and 1:1 soil to water extracts. *Soil Science Society of America Journal.* 69:1146–1151.

Zhang, Z., Wang, Q., Wang, H., Nie, S. & Liang, Z. 2017. Effects of soil salinity on the content, composition, and ion binding capacity of glomalin-related soil protein (GRSP). *Science of the Total Environment.* 581–582:657–665.

7 Appendix A

Detailed soil profile descriptions

The following tables are those of all detailed soil profile descriptions done in the field.

See FAO (2006) Guidelines for Soil Description (available for download). Bw: development of colour and structure ; Bk: carbonate accumulation; Bkm: carbonate cementation; Bq: silica accumulation; Bqm silica cementation; By: gypsym accumulation; Bym: gypsum cementation; Bkqm: carbonate and silica cementation; Bqym: silica and gypsum cementation.

Table 7.1: Detailed profile description for each horizon within H1-0.

Profile H1-0	14 Sept 2018	Diagnostic horizon *
Depth (cm)	**2 active 1 cm long maggots at base**	
0-5	Dry, 2 mm thick surface crust, dry, loose, apedal, few fine roots, yellowish red (5YR 5/6), coarse sandy loam (2% clay), non-sticky, non-plastic, -ve HCl reaction, abrupt transition to	Orthic A
5-22	Dry, slightly hard, apedal to weakly platy, coarse sandy loam (5% clay), slightly sticky, non-plastic, few fine roots, increasing at base of horizon, few fine calcite-filled (+ve HCl) root channels, platy to coarse blocky, -ve HCl reaction, strong brown (5YR5/6) abrupt wavy transition to	Bw Neocutanic B
22-30+	Dry, massive to platy, very hard, locally very slightly calcareous, pink (5YR7/4), base not reached	Bqm Dorbank

Table 7.2: Detailed profile description for each horizon within H1-2.

Profile H1-2	14 Sept 2018	Diagnostic horizon
Depth (cm)	**Active termites at base**	
0-5	3 mm thick surface crust, dry, loose, apedal, few fine roots, yellowish red (5YR 5/8), coarse sandy loam (3-5% clay), non-sticky, non-plastic -ve HCl reaction, gradual transition to	Orthic A
5-30	Fine sandy loam (8% clay), slightly sticky, non-plastic, fine root hairs, platy to coarse blocky, few 8 mm diameter tunnels, -ve HCl reaction, light reddish brown (5YR6/4) abrupt wavy transition to	Bw Neocutanic B
30+	Very firm, locally very slightly. calcareous, pink (5YR7/4) local disseminated Mn, base not reached	Bqm Dorbank

Table 7.3: Detailed profile description for each horizon within H1-4.

Profile H1-4	14 & 15 Sept 2018	Diagnostic horizon
Depth (cm)	1st calcareous profile from outer edge. Lateral intergrade between Bw (0-4 m) and Bk (>4 m);	
0-10	Dry, loose, apedal, few fine roots, yellowish red (5YR 5/8), coarse sandy loam (3-5% clay), non-sticky, non-plastic +ve HCl reaction, gradual transition to	Orthic A
10-38	Dry, friable, platy (1-3 cm thick) structure, non-plastic non-sticky, coarse sandy loam (10% clay), +ve HCl reaction, gradual transition to	Bk1 Neocarbonate B
38-50+	Dry, firm to very firm, +ve HCl reaction, light reddish brown (5YR6/4) Transition not reached	Bkm Hard carbonate

Table 7.4: Detailed profile description for each horizon within H1-13.

Profile H1-13	14 & 15 Sept 2018	Diagnostic horizon
Depth (cm)		
0-3	Like others; dry, loose, apedal,+ve HCl	Orthic A
3-40	Dry, apedal, loose, 5YR6/6 reddish yellow, sandy silt loam (7% clay), sand grains 1 mm diameter, slightly sticky slightly plastic, many fine roots, weak coarse platy structure, strong +ve HCl reaction, wavy gradual transition through a zone of many pinkish white (5. YR 8/2) calcite nodules (1-2 cm diameter) to	Bk1 Neocarbonate B
40-50	Dry, wavy gradual transition zone of many pinkish white (5. YR 8/2) calcite nodules (1-2 cm diameter), wavy gradual transition to nodular carbonate from hardpan	Bk(m)
50-110	Dry, white (5 YR8/1) strongly calcareous 5 cm thick laminar capping with massive to coarse platy structure, highly indurated at top, less indurated at base, grading to	Bkm Hardpan carbonate
110-140	Indurated alluvium? Yellowish-red 5YR 4/6), slightly calcareous, very firm, highly cemented, few well rounded cobbles and many angular fragments 4 cm dam. Interstitial material coarse loamy sand (10% clay), transition not reached. Very difficult to sample.	Bkqm

157

Table 7.5: Detailed profile description for each horizon within H1-16.

Profile H1-16	14 & 15 Sept 2018	Diagnostic horizon
Depth (cm)	***Active termites at base***	
0-5	Dry, reddish-yellow (5YR6/6), fine silty loam (12% clay), apedal structure, loose consistency; +ve HCl; slightly sticky, few fine roots; few fine weakly impregnated calcite nodules with strong HCl reaction; many 1 mm – 1 cm pores, gradual transition to	Orthic A
5-35	Dry, pink (5YR7/4), fine silty loam (17% clay), +ve HCl; moderately large platy structure; loose consistency; slightly sticky; many fine roots; many 1 mm pores; few slightly impregnated medium calcite nodules (4 cm); gradual wavy transition to	Bk1 Neocarbonate B
35-80	Slightly moist; medium sandy loam, apedal, friable, slightly sticky, many moderately impregnated calcite nodules, more nodules with greater degree of impregnation at base; few fine roots; many pores (1 mm diameter); many macropores (1 cm); abrupt wavy transition to	Bk2 Neocarbonate B grading to Soft carbonate
80-90	Laminar calcrete; platy at upper horizon grading to nodular structure, pinkish white (5YR8/2), grading to	Bkm Hard carbonate
90-190	Pinkish white (5YR 8/2) coarse loamy sand (10% clay); slightly hard; non sticky; massive to weakly coarse platy; strongly indurated with calcite; calcareous nodules with silica impregnation (yellowish-red 5YR 4/6) crosscut with calcite veins; transition not reached.	Bkqm Calcareous dorbank (?)

Table 7.6: Detailed profile description for each horizon within H1-20.

Profile H1-20	15 Sept 2018	Diagnostic horizon
Depth (cm)	***Active termites at base***	
0-5	Dry, gradual transition to	Orthic A
5-70	Dry, apedal to granular structure (granules 1 mm diameter) (granular structure makes gradual appearance and is present from H1-22 to H1-28). Gradual wavy transition to	Bk1 Neocarbonate B
70-200	Nodular calcrete; transition not reached.	Bkm Hard carbonate (nodular)

Table 7.7: Detailed profile description for each horizon within H1-24.

Profile H1-24	14, 15, 16 Sept 2018	Diagnostic horizon
Depth (cm)	***Active termites at base***	
0-5	**Sample possibly contaminated by overlying soil** Dry, light reddish brown (5YR6/4), silty loam/fine silty loam (10% clay), slightly sticky, apedal structure, loose consistency, few fine roots, very strong HCl reaction, gradual transition to	Orthic A

159

5-80	Dry, granular structure (granules 1 mm diameter; granular structure makes gradual appearance and is present from H1-22 to H1-28), loose to slightly firm; yellowish red (5YR5/6); slightly sticky non plastic fine sandy loam (12% clay); very strong HCl reaction; many 1 mm diameter micro tunnels/pores filled with white precipitate; elongated chamber 2 cm x 1 cm diameter, filled with micro excrement pellets (0.5-1 mm diameter), gradual transition to	Bk1 Neocarbonate B
80-140	Slightly moist, reddish brown (5YR5/4) friable, coarse sandy loam (17% clay); granular structure (typical of termite activity; granules are 1-2 mm diameter microaggregates), non-plastic slightly sticky, many 1 mm diameter micro tunnels and pores filled with white precipitate; strong HCl reaction; many tunnels 3-8 mm diameter lined internally with orientated clay; many micro tunnels (1 mm diameter); few white weakly impregnated calcite nodules with accessory Mn (3-4 cm diameter, irregular boundary with matrix) and strongly impregnated Mn concretions (1 cm) gradual transition to	Bk2 Neocarbonate B
140-220	Slightly moist; friable to hard; reddish brown (5YR 5/4); slightly angular blocky structure; non-sticky; non-plastic; coarse to very coarse loamy sand (sand size 1-2 mm); positive HCl reaction; less pellets/more cemented pellets than overlying horizon; dark; very indurated calcareous (+ve HCl) nodules (<1 cm diam.) possibly with some Si and Mn in cement; nodules colour yellowish red (5 YR 5/6); pendants under clast; light reddish brown (5 YR 6/4) nodules 3 cm diameter strongly impregnated with calcite (very strong effervescence), with 0.5 mm white calcite laminae.	Bk3
220-240cm	Nest, 1) 30 cm wide, 18 cm high, possibly silicified, very slight localised reaction with HCl, possibly calcite finely layered with silica.	Nest*

240-	Same as 140-220 cm but darker concretions (yellowish red, 5YR5/6), no calcite nodules; matrix has strong +ve HCl reaction), some Mn precipitates	Bk4

Table 7.8: Detailed profile description for each horizon within H1-25.

Profile H1-25	14, 15, 16 Sept 2018	Diagnostic horizon
Depth (cm)	***Active termites at base***	
0-5	Dry, light reddish brown (5YR6/4), silty loam/fine silty loam (10% clay), slightly sticky, apedal structure, loose consistency, few fine roots, very strong HCl reaction, gradual transition to	Orthic A
5-80	Dry, granular structure (granules 1 mm diameter, granular structure makes gradual appearance and is present from H1-22 to H1-28), loose to slightly firm; yellowish red (5YR5/6); slightly sticky non plastic fine sandy loam (12% clay); very strong HCl reaction; many 1 mm diameter micro tunnels/pores filled with white precipitate; elongated chamber 2 cm x 1 cm diameter, filled with micro excrement pellets (0.5-1 mm diameter), gradual transition to	Bk1 Neocarbonate B
80-120	Slightly moist, reddish brown (5YR5/4) friable, coarse sandy loam (17% clay); granular structure (typical of termite activity; granules are 1-2 mm diameter microaggregates), non-plastic slightly sticky, many 1 mm diameter micro tunnels and pores filled with white precipitate; strong HCl reaction; many tunnels 3-8 mm diam. lined internally with orientated clay; many micro tunnels (1 mm diameter); few white weakly impregnated calcite nodules with accessory Mn (3-4 cm diameter, irregular boundary with matrix) and strongly impregnated Mn concretions (1 cm) gradual transition to	Bk2 Neocarbonate B

161

120-230	Nest 2: Larger nest, 1m away from H1-24. 1.1 m x0.8 m diameter nest, oval in shape, tapering downwards and grading to a highly bioturbated, very indurated layer (200-230 cm depth) that may be part of the nest. Nest 2 coated with 1 mm to 3-5 cm thick very hard coating (silica?). Speculation: predator proof. Material inside nest is moist, loose, slightly sticky to sticky, slightly plastic (can bend a 1 cm diameter 10 cm long roll into a donut), clayey loam 30% clay (hands very clayey afterwards), granular (1 mm) structure, reddish brown (5YR 5/4) with many fine white precipitates. Many tunnels 1 cm in diameter, many mottles 1 cm in diameter (possibly more calcite impregnated), very strong HCl reaction.	Nest set in Bk3 described in H-24 (140-220 cm)
230-270	Lightly moist; friable to hard; reddish brown (5YR 5/4); slightly angular blocky structure; non-sticky; non-plastic; coarse to very coarse loamy sand (sand size 1-2 mm); darker (yellowish red, 5YR5/6) concretions, no calcite nodules; matrix has strong +ve HCl reaction), some Mn precipitates.	Bk4

Table 7.9: Detailed profile description for each horizon within H1-32.

Profile H1-32	15 Sept 2018	Diagnostic horizon
Depth (cm)	***Active termites in profile**	
0-10	Dry, loose, apedal, light reddish brown (5YR 6/4), fine silty loam, slightly sticky, +ve HCl reaction, gradual transition to	Orthic A
10-76	Dry, apedal with local areas of granular structure, loose to slightly firm; light reddish brown (5YR6/4); slightly sticky non plastic fine sandy to silty loam (12% clay) many 1 mm diameter root hairs filled with white precipitate; tunnels 1 cm diam.; at 20 cm depth active termites repairing 2 cm diameter chamber wall with freshly prepared clearly moist microaggregates (1-2 mm diameter) (saliva aggregated microaggregates of immediately adjacent soil material dried very quickly); that are wet when placed, and dry to the same soil colour; at 40 cm depth is 12 cm diam. chamber filled with 1-2 mm granules of aggregated matrix (termite frass); at 60 cm depth is an organic matter filled chamber; gradual transition to	Bk1 Neocarbonate B
76-90	Slightly moist, many yellowish red (5YR5/8), rounded Si impregnated nodules 0.8-1.5cm diameter (durinodes?), in pink (5YR8/1) powdery matrix, induration decreases with depth, -ve to very sl local HCl reaction, gradual transition to	Bq
90-123	Dry; white (7.5YR8/1) hard platy structure more indurated at top grading to less induration at base with increasingly developed platy structure with depth; very slight localised HCl reaction; lenses of 3-5 cm diameter yellowish red (5YR5/8), hard, silica-rich nodules -ve to very slightly local HCl reaction on whites coatings on some (0.1 mm thick, very thin); set in matrix of white powdery material that is slightly moist and showed no HCl reaction, gradual transition to	Bqm
123-200	Very hard, reddish brown (5YR5/4), coarse (up to 10 cm thick) platy structure, many fine 0.5 mm diameter micropores, localised	B(k)qm

+ve HCl reaction, many Mn coatings on plates, infilling channels and micropores throughout matrix.	164

Table 7.10: Detailed profile description for each horizon within H1-35.

Profile H1-35	15 Sept 2018	Diagnostic horizon
Depth (cm)		
0-10	Dry, loose, apedal, light reddish brown (5YR 6/4), fine silty loam, slightly sticky, +ve HCl reaction, gradual transition to	Orthic A
5-70	Slightly moist, apedal structure, loose to friable; light reddish brown (5YR6/4); slightly sticky non plastic sandy clay loam (17% clay), many fine roots; many 1 mm diameter root hairs and channels filled and coated with white precipitate; many 3-15 cm diameter pinkish white (5YR8/2)weak to moderately impregnated calcite nodules (strong +ve HCl) with irregular outlines, (30% of horizon), many fine pores (0.5 mm diameter) and occ. fine channels, micro excrement (0.5 mm diameter) occurs in this layer and 3 dead black beetles 5 mm diameter present just above it; clear transition to	Bk Neocarbonate B
70-85	Dry, pink (5YR 7/3) very hard (Si?) nodules 0.5-1.5 cm diameter coated with 0.1 mm thick white coatings (5YR8/1), no HCl reaction; many fine white precipitates; few fine roots; gradual transition to	Bq
85-185+	Dry, pinkish white (5YR8/2), very hard (silica induration), coarse platy structure (plates 10 cm thick), very slight +ve HCl reaction, Mn disseminated throughout matrix; many Mn lenses up to 5 mm thick; few fine roots in upper part.	B(k)qm

Table 7.11: Detailed profile description for each horizon within H4-19.

Profile H4-19	13 Sept 2018	Diagnostic horizon
Depth (cm)		
0-10	Dry, pink (5YR7/4), fine sandy loam (15% clay), apedal structure, loose consistency, few weakly to moderately impregnated fine (0.2-0.5 cm diameter) calcite nodules, few fine roots, very strong HCl reaction, gradual transition to	Orthic A
10-30	Dry, pink (5YR7/4), fine sandy loam (17% clay), apedal structure, loose consistency, many weakly to moderately impregnated medium to coarse (1-10 cm diameter) calcite nodules, few fine roots, strong HCl reaction, abrupt transition to	Bk Neocarbonate B
30-60	Fine fraction (55%): dry, pinkish white (5YR8/2), fine silty clay (18% clay), appears to be gypsum precipitate, loose, sticky. Indurated material (45%): large platy structure, hard consistency, highly indurated, white precipitate coatings, no HCl reaction on precipitate	Bqym1 Dorbank with powdery gypsum
60-90	Dry, pinkish white (5YR8/2), large platy structure, with white precipitates on ped surfaces, hard consistency, very few fine roots and white precipitate root clasts, negative HCl reaction	Bqym2 Dorbank with gypsum
90-110	Slightly moist, colour dry 5YR7/4, few paler mottles, medium sandy loam (12%), granular, friable consistency, many elongated filled indurated burrows (0.8 cm diameter)	Nest within Bqym2
110-160	Silica indurated unconsolidated material; very hard, very firm, abundant disseminated Mn.	Bqym3 Dorbank with accessory gypsum

Table 7.12: Detailed profile description for each horizon within H4-22.

Profile H4-22	13 Sept 2018	Diagnostic horizon
Depth (cm)		
0-10	Dry, pink (5YR7/4), fine sandy loam (15% clay), apedal structure, loose consistency, few medium calcretized nodules, few fine roots, few white fine micro-channels, very strong HCl reaction, gradual transition to	Orthic A
10-30	Dry, pink (5YR7/4), fine sandy loam (17% clay), apedal structure, loose consistency, many medium and large weakly impregnated calcite nodules, few fine roots, few white fine filament-type precipitates, strong HCl reaction, abrupt wavy transition to	Bk Neocarbonate B
30-60	Dry, pinkish white (5YR8/2), large platy structure, hard consistency, highly indurated (silica), white precipitate (gypsum) coating indurated platy structures, no HCl reaction on white precipitate; gradual transition to	Bqym1 Dorbank with gypsum
60-90	As above but white coatings less prominent and more white and pinkish-white powdery interstitial material present; diffuse transition to	Bqym2 Dorbank with gypsum
90-120	Unconsolidated to platy dorbank, gypsum coatings not as prominent; more reddish brown, hard, angular, irregular silica-cemented nodules (durinodes) and lenses that form a matrix area to the white powdery interstitial precipitate; diffuse transition to	Bqym3 Dorbank with gypsum
120-160	Similar as above, diffuse transition to	Bqym4
160-180	As above but coatings not present; platy structure and induration increases towards base (140 cm+).	Bqm Dorbank

Table 7.13: Detailed profile description for each horizon within H4-32.

Profile H4-32	13 Sept 2018	Diagnostic horizon
Depth (cm)		
0-10	Dry, pink (5YR7/4), fine sandy loam (15% clay), apedal structure, loose consistency, few medium calcretized nodules, few fine roots, few white filament-type precipitates, very strong HCl reaction, gradual transition to	Orthic A
10-30	Dry, pink (5YR7/4), fine sandy loam (17% clay), apedal structure, loose consistency, many medium and large weakly to moderately impregnated calcite nodules, few white filament-type precipitates, strong HCl reaction, gradual transition to	Bk1 Neocarbonate B
30-60	Dry, reddish yellow (5YR7/6), medium sandy loam, granular structure (1-2 mm granules), loose, very many medium, moderately to strongly impregnated calcite nodules, few white filament-type precipitates, few fine roots, strong HCl reaction in the matrix, abrupt transition to	Bk2 Neocarbonate B
60-90	Dry, reddish yellow (5YR7/6), medium sandy loam, granular, slightly firm, very many indurated nodules (0.5 mm-1.2 mm diameter), few white filament-type precipitates, few fine roots, no HCl reaction, abrupt clear transition to	Nest
90-160	Pinkish white, 5YR8/2, fine silty loam, apedal, loose, sticky (wet), coarse platy structure; no HCl reaction, many indurated silica nodules, finely disseminated Mn; many lenses (10-30 cm) of fine pinkish white powdery gypsum; gradual transition to	Bqym
160+	Indurated, platy, silica cemented colluvium/alluvium	Bqm

Table 7.14: Detailed profile description for each horizon within H4-38.

Profile H4-38	13 Sept 2018	Diagnostic horizon
Depth (cm)		
0-10	Dry, pink (5YR7/4), fine sandy loam (15% clay), apedal structure, loose consistency, few medium calcretized nodules, few fine roots, few white filament-type precipitates, very strong HCl reaction, gradual transition to	Orthic A
10-40	Dry, pink (5YR7/4), fine sandy loam (17% clay), apedal structure, loose consistency, many medium and large calcretized nodules especially from 25-40 cm deep, few fine roots, few white filament-type precipitates, strong HCl reaction, abrupt wavy transition to	Bk Neocarbonate B
40-70	Dry, pinkish white 5YR8/2, fine silty loam (18%), apedal, loose (dry), sticky (wet)	By1 Gypsum
70-100	Dry, white (2.5Y8/1), fine silty loam (18%), apedal, loose (dry), sticky (wet)	By2 Gypsum
100-130	Dry, reddish yellow 5YR7/6, coarse loamy sand, apedal, moderately loose, few indurated infilled termite burrows, very many white filament-type precipitates, no HCl reaction, gradual wavy transition to	Bqy
130-160+	Dry, hard, reddish yellow 5YR7/6, silica-indurated alluvium/colluvium with a coarse platy structure, with many angular and a few very well-rounded cobbles (3-10 cm), few white lense-like precipitates around the redder silica indurated material.	Bqm Dorbank

169

Table 7.15: Detailed profile description for each horizon within H4-42N.

Profile H4-42	13 Sept 2018	Diagnostic horizon
Depth (cm)	**Nest with active termites**	
0-4	Dry, pink (5YR7/4), fine sandy loam (15% clay), apedal structure, loose consistency, few medium calcretized nodules, few fine roots, very strong HCl reaction, gradual transition to	Orthic A
4-46	Dry, pink (5YR7/4), fine sandy loam (17% clay), granular structure, loose consistency, many medium and large calcite nodules, few fine roots, few white filament-type precipitates, strong HCl reaction, 5 mm long black beetles in horizon (dead); voids filled with amorphous black organic matter; abrupt, wavy transition to	Neocarbonate B Bk1
46-96	Dry, pinkish white 5YR8/1, medium/weak platy structure, slightly hard consistency, weakly indurated with calcite, many weakly calcite-impregnated nodules 1-10 cm diameter (mostly 3-4 cm diameter) strong HCl reaction, no roots, many white filament-type precipitates, abrupt change to	Soft carbonate B to neocarbonate B Bk2-Bk(m)
96-125	Moist in nest; sidewalls dry; 5YR7/6, fine sandy loam, granular, loose, few white filament-type precipitates; many dark reddish, clay and organic matter lined, indurated tunnels up to 2 cm diameter; inner side lined with orientated clay 1 mm thick; amorphous organic matter on inner side of clay lining; active *M. Viator* present; few medium silica nodules	Nest; active M. Viator
125-150	135-160 cm is a large tunnel; some apparent gypsum present on the upper side of the tunnel (tunnel clay-lined, represents impermeable barrier, gypsum in coarser soil matrix above that barrier); tunnel more moist that surrounding soil; tunnels actively repaired over 3 days.	Lower part of nest; tunnels
150-196+	Weakly indurated (silica), transported material (some rounded, some angular cobbles up to 15 cm diameter (colluvium/alluvium).	Bqm

Table 7.16: Detailed profile description for each horizon within H4-42S.

Profile H4-42 South	13 Sept 2018	Diagnostic horizon
Depth (cm)	**Active termites at base**	
0-10	Dry, pink (5YR7/4), fine sandy loam (15% clay), apedal structure, loose consistency, few fine roots, very strong HCl reaction, gradual transition to	Orthic A
10-30	Dry, pink (5YR7/4), fine sandy loam (17% clay), granular structure, loose consistency, few fine roots, strong HCl reaction; abrupt wavy transition to	Bk Neocarbonate B
30-110	Dry, very firm, pink (5YR7/4), silica-induration, no HCl reaction; coarse platy structure; abrupt transition to	Bqm1
110-150	Oval shaped nest with 3-5 cm thick chert/silica coating/impregnation on outer edge of nest; M. Viator termites active along inner edge of silica-lining; many 12 mm diameter tunnels inside nest, some tunnels partially filled with 1-2 mm micro aggregates (granules) of soil (frass); moist inside nest; dry outside;	Nest
150+	Indurated (silica), transported material (colluvium/alluvium).	Bqm2

8 Appendix B

The following tables contain all the raw data for this thesis.

Table 8.1: All pH and EC data for both H1(left) and H4 (right; note that the A in H1A and H4A refers to the smaller samples obtained in each soil profile).

Sample ID	pH	EC (μS/cm)	Sample ID	pH	EC (μS/cm)
H1A-0-10	8,18	119	H4A-1-10	9,01	47
H1A-1-10	8,27	101	H4A-2-10	8,96	50
H1A-1-30	8,83	1536	H4A-3-10	8,94	38
H1A-2-10	9,23	114	H4A-4-10	8,88	82
H1A-2-30	9,29	198	H4A-5-10	8,82	343
H1A-3-10	8,98	29	H4A-6-10	9,10	48
H1A-3-30	8,99	107	H4A-6-20	9,26	112
H1A-4-10	9,06	85	H4A-7-10	9,21	43
H1A-4-30	8,89	235	H4A-7-20	8,28	796
H1A-5-10	9,32	114	H4A-8-10	9,33	106
H1A-5-40	9,38	203	H4A-8-20	9,05	495
H1A-6-10	9,70	259	H4A-9-10	9,10	50
H1A-6-40	8,98	188	H4A-9-20	8,54	314
H1A-7-10	9,62	399	H4A-10-10	9,02	48
H1A-7-40	9,58	310	H4A-10-20	7,84	390
H1A-7-70	8,88	403	H4A-11-10	9,51	70
H1A-8-10	9,32	129	H4A-11-30	7,68	1104
H1A-8-40	9,48	204	H4A-12-10	7,80	1953
H1A-8-70	9,06	478	H4A-12-30	8,11	1454
H1A-9-10	8,90	82	H4A-13-10	9,87	254
H1A-9-40	9,39	210	H4A-13-20	8,47	847
H1A-9-70	9,48	642	H4A-14-10	9,42	142
H1A-10-10	9,16	145	H4A-14-30	8,89	468
H1A-10-40	9,82	1685	H4A-15-10	8,71	989
H1A-10-60	8,53	2452	H4A-15-30	8,23	1088
H1A-11-10	8,90	1838	H4A-16-10	8,99	844
H1A-11-40	9,54	1256	H4A-16-30	8,20	3771
H1A-11-70	8,68	3261	H4A-16-70	8,15	4065
H1A-12-10	8,82	606	H4A-17-10	9,16	1439
H1A-12-70	9,05	3218	H4A-17-30	8,11	5098
H1A-12-110	8,77	2720	H4A-17-60	7,77	6446
H1A-13-10	9,30	386	H4A-18-10	8,79	1996
H1A-13-50	9,65	1086	H4A-18-30	8,28	4579
H1A-13-60	8,90	2357	H4A-18-60	7,86	5596
H1A-13-140	8,73	2674	H4A-18-90	7,74	6066
H1A-14-10	9,78	324	H4A-19-10	8,65	1540

H1A-14-40	9,17	3626	H4A-19-30	7,28	6335
H1A-14-80	7,78	5200	H4A-19-50	7,14	7944
H1A-14-110	8,12	3689	H4A-19-90	7,27	6387
H1A-15-10	9,50	301	H4A-19-110	7,54	5826
H1A-15-50	8,39	7645	H4A-20-10	9,11	1423
H1A-15-80	8,69	4856	H4A-20-30	8,10	7889
H1A-15-150	8,13	8089	H4A-20-70	7,92	6017
H1A-15-180	8,24	6644	H4A-20-90	7,91	5832
H1A-16-10	9,39	974	H4A-20-130	8,26	3855
H1A-16-60	8,72	6295	H4A-21-10	8,27	8135
H1A-16-100	8,59	6942	H4A-21-40	8,02	7204
H1A-16-140	8,27	5582	H4A-21-110	8,05	7732
H1A-16-200	8,68	3365	H4A-21-140	8,08	6335
H1A-17-10	9,41	724	H4A-22-10	8,21	9430
H1A-17-40	8,79	7167	H4A-22-30	8,12	8736
H1A-17-100	8,21	11000	H4A-22-60	8,12	6137
H1A-17-150	8,19	9844	H4A-22-120	8,10	5091
H1A-17-180	8,27	9515	H4A-22-160	8,02	5231
H1A-18-10	8,21	4473	H4A-23-10	8,15	12457
H1A-18-70	8,19	9337	H4A-23-30	8,10	9050
H1A-18-110	7,98	12234	H4A-23-60	8,08	6179
H1A-18-160	7,67	9805	H4A-23-120	8,02	5170
H1A-18-190	7,62	13794	H4A-24-10	8,29	7297
H1A-19-10	9,32	351	H4A-24-40	8,13	8211
H1A-19-70	7,88	4986	H4A-24-70	7,98	9066
H1A-19-150	7,36	7853	H4A-24-120	8,00	6160
H1A-19-200	7,65	9499	H4A-25-10	8,24	6527
H1A-20-10	9,23	477	H4A-25-30	8,25	4802
H1A-20-70	8,75	4676	H4A-25-70	7,84	8427
H1A-20-110	7,73	9480	H4A-25-130	7,75	8011
H1A-20-160	7,50	9133	H4A-26-10	8,84	1762
H1A-20-200	7,49	11887	H4A-26-30	8,35	3978
H1A-21-10	8,54	7535	H4A-26-60	8,22	4376
H1A-21-70	8,45	5887	H4A-26-120	7,83	8331
H1A-21-130	8,12	10350	H4A-27-05	9,06	85
H1A-21-170	8,05	9593	H4A-27-30	8,41	4430
H1A-21-200	6,09	9994	H4A-27-60	8,05	7207
H1A-22-10	7,58	4777	H4A-27-120	7,99	8110
H1A-22-90	7,68	10715	H4A-27-170	7,95	7215
H1A-22-160	7,32	10910	H4A-28-10	8,96	666
H1A-22-200	8,08	9427	H4A-28-40	8,29	4177
H1A-22-240	8,07	9949	H4A-28-60	6,81	8713
H1A-23-10	8,37	6312	H4A-28-120	6,86	11507
H1A-23-70	8,29	7085	H4A-28-150	7,03	8704

H1A-23-140	8,04	8958	H4A-29-10	8,08	1952
H1A-23-210	8,20	5634	H4A-29-40	7,87	6454
H1A-23-250	8,14	5647	H4A-29-100	7,84	6992
H1A-24-10	8,11	6788	H4A-29-150	7,70	6648
H1A-24-60	8,37	4868	H4A-30-10	8,00	4501
H1A-24-120	8,12	7448	H4A-30-50	8,08	7799
H1A-24-150	8,17	6588	H4A-30-100	7,81	7541
H1A-24-180	8,18	8563	H4A-30-160	7,87	7014
H1A-24-210	8,48	4451	H4A-31-10	8,02	6958
H1A-24-240	8,28	3718	H4A-31-40	8,02	9098
H1A-25-10	8,30	5453	H4A-31-70	7,79	8807
H1A-25-60	8,41	5114	H4A-31-100	7,78	7182
H1A-25-90	8,09	6324	H4A-32-10	8,29	3777
H1A-25-160	8,20	8089	H4A-32-30	8,26	3451
H1A-25-190	8,10	6913	H4A-32-60	8,34	4352
H1A-25-230	8,41	5385	H4A-32-80	7,97	5923
H1A-26-10	9,17	1599	H4A-32-100	7,71	5851
H1A-26-70	8,12	7944	H4A-32-130	7,74	5481
H1A-26-110	8,04	7698	H4A-33-10	8,05	6150
H1A-26-160	7,98	8045	H4A-33-40	8,11	8256
H1A-26-190	7,93	8538	H4A-33-80	7,84	8581
H1A-26-230	8,22	5815	H4A-33-130	7,85	7084
H1A-27-10	8,16	5087	H4A-34-10	8,68	1640
H1A-27-70	8,09	7092	H4A-34-30	8,08	6273
H1A-27-100	8,06	7382	H4A-34-60	7,87	9654
H1A-27-160	6,36	7127	H4A-34-110	6,27	5326
H1A-27-190	6,94	8253	H4A-34-160	6,75	5702
H1A-27-240	7,48	6901	H4A-35-10	9,05	1181
H1A-28-10	8,09	3364	H4A-35-30	8,20	5403
H1A-28-40	7,98	7836	H4A-35-60	7,90	8376
H1A-28-110	7,95	7628	H4A-35-90	7,79	5945
H1A-28-170	7,91	6027	H4A-35-120	7,66	5514
H1A-28-230	7,94	6127	H4A-36-10	8,26	1983
H1A-28-290	8,10	4243	H4A-36-30	8,08	5680
H1A-29-10	9,21	1748	H4A-36-60	8,02	4773
H1A-29-40	8,22	5609	H4A-36-90	7,72	5293
H1A-29-100	7,61	6512	H4A-36-120	7,64	4773
H1A-29-130	7,47	10330	H4A-37-10	8,11	3801
H1A-29-180	7,78	4187	H4A-37-30	7,80	8833
H1A-29-210	7,91	6626	H4A-37-70	7,75	8299
H1A-30-10	6,17	2992	H4A-37-120	7,65	5208
H1A-30-40	6,89	8843	H4A-37-170	7,51	5983
H1A-30-100	6,95	6454	H4A-38-10	8,78	1253
H1A-30-130	7,23	5076	H4A-38-30	8,28	4288

H1A-30-160	7,61	3899	H4A-38-90	6,05	4829
H1A-30-190	7,88	4314	H4A-38-150	6,46	6124
H1A-31-10	7,89	5625	H4A-38-190	6,64	6225
H1A-31-40	8,11	6476	H4A-39-10	7,18	3382
H1A-31-110	7,61	5345	H4A-39-30	7,05	8482
H1A-31-140	7,70	7473	H4A-39-60	7,13	4596
H1A-31-190	8,05	3384	H4A-39-90	6,95	5434
H1A-32-10	9,14	752	H4A-39-120	6,78	4706
H1A-32-40	8,10	5213	H4A-40-10	7,65	4393
H1A-32-80	7,54	5389	H4A-40-30	7,85	6337
H1A-32-120	7,40	4704	H4A-40-50	7,71	10192
H1A-32-180	8,40	1327	H4A-40-100	7,57	4787
H1A-33-10	8,37	1821	H4A-40-140	7,37	5494
H1A-33-40	8,25	2511	H4A-40-190	7,52	5746
H1A-33-70	7,53	4431	H4A-41-10	8,04	2629
H1A-33-100	7,51	4597	H4A-41-30	8,15	4809
H1A-33-150	8,03	3591	H4A-41-60	7,80	9034
H1A-34-10	9,17	159	H4A-41-90	7,53	7258
H1A-34-30	8,33	4848	H4A-41-120	6,42	7050
H1A-34-60	7,44	6784	H4A-41-150	7,05	6745
H1A-34-90	8,08	4110	H4A-42		
H1A-35-10	8,51	833	H4A-43-10	8,31	1673
H1A-35-30	8,31	4586	H4A-43-30	8,22	4885
H1A-35-60	7,66	5768	H4A-43-80	7,92	8672
H1A-35-90	7,89	4707	H4A-43-140	7,81	8849
H1A-36-10	9,25	356	H4A-43-190	7,63	8134
H1A-36-30	8,12	7391	H4A-44-10	8,35	4157
H1A-36-60	7,87	5697	H4A-44-30	8,14	8713
H1A-36-90	7,89	4762	H4A-44-80	7,96	9419
H1A-37-10	8,42	1169	H4A-44-150	8,14	4829
H1A-37-30	8,02	6619	H4A-45-10	9,32	1051
H1A-37-60	8,14	4931	H4A-45-30	7,97	9255
H1A-37-90	7,82	6407	H4A-45-50	7,96	7922
H1A-37-120	6,75	5572	H4A-45-90	8,15	4983
H1A-38-10	8,66	556	H4A-46-10	8,95	927
H1A-38-20	8,07	3516	H4A-46-30	8,04	8168
H1A-38-30	8,03	5785	H4A-46-60	7,79	10827
H1A-38-60	7,80	8075	H4A-47-10	8,28	2711
H1A-38-90	7,78	7385	H4A-47-30	7,99	7249
H1A-38-120	8,19	3308	H4A-47-70	8,10	5120
H1A-39-10	8,22	1113	H4A-48-10	8,68	1486
H1A-39-40	8,61	1111	H4A-48-30	7,85	9618
H1A-39-80	8,19	3837	H4A-48-70	7,25	4818
H1A-39-110	7,94	6205	H4A-49-10	9,59	245

H1A-40-10	8,73	626	H4A-49-40	8,27	2849
H1A-40-40	8,15	3859	H4A-50-10	9,69	264
H1A-40-70	8,11	3751	H4A-50-40	9,06	807
H1A-40-100	8,12	2927	H4A-51-10	9,59	260
H1A-41-10	9,24	334	H4A-51-30	8,84	1495
H1A-41-40	8,08	4404	H4A-52-10	9,26	159
H1A-41-80	7,63	6856	H4A-53-10	9,79	304
H1A-42-10	9,79	601	H4A-54-10	9,23	170
H1A-42-40	8,17	4044	H4A-55-10	9,00	103
H1A-42-80	7,93	3978	H4A-56-10	8,91	90
H1A-43-10	8,10	660	H4A-57-10	8,83	105
H1A-43-40	8,68	3187	H4A-58-10	8,95	67
H1A-43-80	6,75	2260			
H1A-44-10	8,16	1475			
H1A-44-30	7,68	4267			
H1A-45-10	8,36	1180			
H1A-45-30	7,97	1882			
H1A-46-10	8,07	2023			
H1A-46-40	8,34	1039			
H1A-47-10	8,24	1339			
H1A-47-40	8,78	317			
H1A-48-10	8,48	749			
H1A-48-40	9,59	142			
H1A-49-10	8,73	343			
H1A-49-40	9,45	70			
H1A-50-10	8,59	544			
H1A-50-40	9,46	72			
H1A-51-10	9,00	258			
H1A-51-30	9,11	52			
H1A-52-30	9,16	58			
H1A-53-30	9,02	78			
H1A-54-30	9,03	53			
H1A-55-10	9,14	56			
H1A-56-20	9,16	49			
H1A-57-20	9,18	88			
H1A-58-20	9,26	53			

Table 8.2: Anion, cation and dissolved Si data for H1 (Note H1A refers to smaller samples obtained in each profile, while H1 refers to detailed soil profile samples).

Sample ID	Concentration (mg/L)								
	Cl^-	SO_4^{2-}	HCO_3^-	PO_4^{3-}	Ca^{2+}	K^+	Mg^{2+}	Na^+	Dissolved Si
H1-0-5	5,0	18,1	13,6	0,47	16,2	18,8	4,0	11,0	0,96
H1-0-22	76,2	2,0	13,0	0,17	13,9	75,9	3,8	25,5	1,33
H1-0-30	236,0	27,2	15,8	0,12	23,3	16,2	7,6	172,2	2,68
H1-2-5	5,0	2,0	14,8	0,60	17,2	29,5	4,2	7,2	1,14
H1-2-30	5,0	2,3	14,8	0,34	11,9	13,6	3,7	25,3	2,15
H1-2-50	292,0	52,6	11,6	0,22	32,5	4,0	14,3	197,2	3,49
H1-4-10	7,9	2,7	12,4	0,51	18,5	18,4	4,0	12,1	1,29
H1-4-38	8,8	91,6	14,8	0,32	26,1	7,1	5,1	43,6	1,66
H1-4-50	150,2	39,2	14,6	0,06	15,5	3,8	7,8	157,6	2,47
H1A-6-10	102,4	82,4	26,4	1,34	11,1	27,5	3,0	198,1	1,14
H1A-6-40	42,8	6,1	18,2	0,23	15,6	17,3	4,7	57,3	1,17
H1A-8-10	5,0	2,0	24,2	0,83	8,5	21,8	1,7	23,0	1,10
H1A-8-40	31,6	14,2	128,8	0,34	7,5	23,0	2,9	82,9	1,59
H1A-8-70	84,6	2,0	63,2	0,55	3,4	5,5	1,5	112,2	4,13
H1A-10-10	5,0	2,0	67,6	0,31	12,3	22,1	4,3	23,3	1,25
H1A-10-40	504,0	102,8	58,8	0,50	7,8	45,2	2,9	439,2	0,80
H1A-10-60	1422,0	268,0	6,8	0,09	51,1	32,5	35,2	966,6	4,41
H1A-12-10	116,6	426,0	23,4	0,09	73,1	63,8	21,2	175,0	1,02
H1A-12-70	1590,0	268,0	28,6	0,03	66,6	81,8	24,1	1125,2	3,58
H1A-12-110	1910,0	334,0	32,0	0,02	169,6	72,9	83,6	1111,6	3,54
H1-13-40	10,3	7,4	83,8	0,09	4,0	18,1	0,9	55,4	1,14
H1-13-50	458,0	41,8	49,8	0,18	16,4	52,0	5,2	339,4	1,74
H1-13-110	2584,0	954,0	29,2	0,04	356,4	126,7	117,8	1740,5	3,96
H1-16-5	60,2	8,1	46,4	0,40	7,2	24,1	2,0	72,2	1,33
H1-16-35	1104,0	88,8	49,2	0,03	51,5	90,4	17,5	753,5	1,43
H1-16-80	2232,0	272,0	28,6	0,04	150,0	94,4	77,8	1405,6	0,88
H1-16-90	5354,0	924,0	24,4	0,02	586,8	148,4	240,6	2963,9	3,11
H1-16-190	3574,0	2566,0	19,6	0,03	944,6	120,5	236,8	2251,3	3,45
H1A-18-10	1362,0	1138,0	24,2	0,07	392,0	164,9	78,9	963,9	1,23
H1A-18-70	2038,0	1630,0	18,0	0,03	647,8	67,3	155,0	1416,3	1,31
H1A-18-110	1884,0	2146,0	16,2	0,02	809,0	64,6	145,4	1160,3	1,94
H1A-18-160	3250,0	2602,0	7,6	0,06	839,0	93,4	216,6	2102,8	3,03
H1A-18-190	5508,0	2532,0	13,8	0,02	1117,0	119,1	385,6	3011,0	3,19
H1A-20-10	248,0	112,4	54,2	0,10	34,9	58,4	7,2	150,9	1,31
H1A-20-70	1696,0	166,4	44,0	0,03	99,4	30,1	47,1	1162,9	1,80
H1A-20-110	1986,0	2274,0	20,0	0,08	814,8	46,2	149,6	1309,0	2,31
H1A-20-160	2594,0	2434,0	10,8	0,05	868,2	61,5	197,4	1713,5	3,17
H1A-20-200	4998,0	2360,0	21,0	0,08	1119,0	83,2	355,4	2525,2	3,37
H1A-22-10	2170,0	133,6	33,8	0,03	299,0	77,5	92,8	1115,6	1,21

H1A-22-90	3056,0	1894,0	16,2	0,03	1088,4	42,7	269,4	1567,3	1,10
H1A-22-160	3662,0	1970,0	11,0	0,01	1056,2	44,7	274,2	1791,0	1,80
H1A-22-200	4704,0	2144,0	12,8	0,03	1116,2	53,8	373,4	2197,8	1,96
H1A-22-240	5658,0	2168,0	13,2	0,03	1318,4	57,7	481,0	2583,0	2,31
H1-24-5	4768,0	638,0	22,6	0,02	855,8	61,1	291,2	1981,6	0,67
H1-24-30	5452,0	1480,0	22,0	0,02	1326,8	36,9	465,4	2321,9	0,78
H1-24-140	4856,0	1836,0	26,0	0,02	1330,0	39,4	392,8	2128,9	1,41
H1-24-220	5,0	1798,0	20,6	0,05	1511,0	44,6	489,0	2638,6	1,92
H1-24-270	4502,0	1706,0	19,2	0,07	1150,6	39,1	414,6	2180,7	2,17
H1A-25-10	6180,0	262,0	26,4	0,03	1070,0	70,2	373,2	2604,4	0,94
H1A-25-60	5388,0	402,0	25,8	0,02	862,6	28,4	377,4	2189,2	0,84
H1A-25-90	4536,0	1816,0	21,2	0,03	1335,6	30,8	394,2	2011,6	1,14
H1-25-160	5522,0	1756,0	23,6	0,04	1491,0	34,7	504,0	2416,1	0,86
H1A-25-190	4576,0	1958,0	19,2	0,04	1300,2	30,3	411,6	2029,4	1,78
H1A-25-230	3726,0	838,0	21,8	0,03	664,8	24,6	299,0	1792,7	2,15
H1A-28-10	2778,0	758,0	27,8	0,03	541,2	87,0	139,8	1427,0	1,53
H1A-28-40	5518,0	1292,0	21,8	0,02	1326,0	13,9	403,4	2651,5	1,57
H1A-28-110	4752,0	1794,0	19,6	0,05	1388,4	13,2	408,0	2077,5	2,00
H1A-28-170	2546,0	2326,0	22,0	0,05	920,4	9,4	248,8	1501,6	3,17
H1A-28-230	3006,0	2230,0	23,0	0,03	1009,4	15,4	309,6	1515,5	2,43
H1A-28-290	3224,0	1222,0	21,8	0,03	822,4	15,2	308,4	1470,4	2,80
H1A-30-10	2210,0	264,0	33,0	0,03	367,2	19,0	99,4	932,0	1,12
H1A-30-40	7304,0	1338,0	20,8	0,03	1885,8	9,0	504,4	2983,2	1,96
H1A-30-100	3404,0	1874,0	15,8	0,03	1151,6	5,4	277,6	1663,0	2,53
H1A-30-130	3828,0	1948,0	26,4	0,03	1193,6	7,4	337,0	1770,9	3,13
H1A-30-160	2590,0	1910,0	18,2	0,02	933,4	11,1	281,6	1364,9	3,23
H1A-30-190	3044,0	810,0	20,6	0,03	626,8	12,0	267,0	1380,7	2,53
H1A-32-10	870,0	83,4	59,0	0,05	52,3	16,6	11,6	558,8	1,61
H1A-32-40	5678,0	1386,0	21,0	0,03	1630,2	2,3	334,8	2223,5	2,23
H1A-32-80	3884,0	1668,0	10,4	0,06	1418,2	4,8	299,4	1535,2	2,43
H1A-32-120	4888,0	1806,0	11,8	0,05	1365,8	10,1	451,8	1983,8	2,98
H1A-32-180	1952,0	218,0	25,8	0,02	234,0	9,7	117,9	1000,5	4,56
H1-35-70	5550,0	1392,0	28,6	0,04	1582,6	4,6	490,6	2144,3	2,35
H1-35-85	6092,0	1728,0	12,6	0,06	1701,8	7,7	585,8	2424,6	4,33
H135-180	4792,0	1836,0	11,0	0,03	1304,4	17,3	506,8	1861,6	4,43
H1A-38-10	352,0	109,4	33,0	0,05	55,7	35,4	13,8	184,5	2,27
H1A-38-30	4722,0	1596,0	13,2	0,03	1562,0	11,5	589,6	1503,8	1,33
H1A-38-60	9584,0	1626,0	13,4	0,03	2380,0	24,6	1128,6	2760,6	3,94
H1A-38-90	8636,0	1672,0	21,6	0,05	2146,0	27,7	999,6	2709,2	4,95
H1A-39-10	1240,0	92,8	40,6	0,06	188,2	21,3	76,2	593,9	1,19
H1A-39-40	4072,0	488,0	30,4	0,04	944,0	9,9	464,0	1323,4	0,98
H1A-39-80	5418,0	1578,0	25,2	0,03	1615,6	17,1	652,6	1799,1	2,64
H1A-39-110	2336,0	248,0	24,6	0,06	535,8	7,4	244,6	778,3	1,33
H1A-41-10	191,0	64,6	76,8	0,04	24,8	26,7	5,1	127,0	1,37

H1A-41-40	1806,0	300,0	22,6	0,04	392,4	7,2	163,0	683,5	1,33
H1A-41-80	5904,0	1680,0	12,8	0,06	1689,0	16,5	663,2	2094,2	4,64
H1A-43-10	344,0	190,6	43,4	0,06	91,5	31,3	23,1	169,5	1,98
H1A-43-40	2642,0	160,4	24,2	0,04	700,2	3,7	238,2	830,7	2,76
H1A-43-80	2734,0	158,6	20,8	0,04	638,0	4,6	215,4	1014,1	0,67
H1A-45-10	772,0	648,0	21,2	0,05	259,6	36,9	58,9	456,2	2,10
H1A-45-30	2358,0	376,0	8,2	0,03	783,8	3,9	250,2	610,5	2,64
H1A-48-10	490,0	117,2	15,2	0,06	124,9	20,7	30,7	218,3	1,41
H1A-48-40	45,2	11,1	54,6	0,05	10,1	2,3	2,3	77,6	1,68
H1A-50-10	332,0	106,8	35,8	0,05	81,5	16,9	19,2	148,3	1,55
H1A-50-40	28,0	13,6	75,8	0,26	3,9	6,1	0,8	57,7	1,78
H1A-52-30	8,3	3,4	44,0	0,19	8,8	8,0	1,5	21,7	1,90
H1A-54-30	5,0	2,0	31,0	0,17	11,4	12,7	2,1	12,2	1,23
H1A-56-20	5,6	2,0	35,6	0,26	8,8	14,8	1,7	11,9	1,06
H1A-58-20	17,2	2,0	34,2	0,32	12,0	11,8	3,4	29,1	1,12

Table 8.3: Anion, cation and dissolved Si data for H4 (Note H4A refers to smaller samples obtained in each profile, while H4 refers to detailed soil profile samples).

Sample ID	Concentration (mg/L)								
	Cl⁻	SO₄²⁻	PO₄³⁻	HCO₃⁻	Ca²⁺	K⁺	Mg²⁺	Na⁺	Dissolved Si
H4-0-10	46,2	5,9	0,86	13,4	6,4	4,0	1,9	44,5	1,31
H4-0-10+	206,0	81,4	0,02	2,0	27,0	2,2	22,0	115,2	1,43
H4A-2-10	5,0	5,8	0,34	21,2	0,6	1,0	0,1	0,2	1,23
H4A-4-10	14,0	3,4	0,58	32,4	19,7	19,9	5,5	18,2	1,55
H4A-7-10	8,1	2,0	0,72	38,4	3,1	9,7	0,7	25,0	0,98
H4A-9-10	5,0	2,0	0,64	56,4	6,3	16,3	2,1	19,9	1,02
H4A-12-10	2052,0	64,8	0,05	18,4	548,8	59,3	130,2	685,9	1,04
H4A-13-10	25,6	2,0	0,47	27,6	1,2	4,4	0,4	70,1	2,78
H4A-15-10	1126,0	175,2	0,05	14,4	173,1	81,6	39,8	587,0	3,84
H4A-17-10	922,0	96,4	0,04	40,8	62,2	48,5	13,0	642,0	3,23
H4A-17-30	3492,0	692,0	0,03	11,8	696,4	16,2	190,1	1736,2	3,84
H4A-17-60	5518,0	1822,0	0,02	9,6	1321,4	22,5	374,6	2788,4	4,99
H4-19-10	604,0	404,0	0,04	20,2	130,0	102,1	20,8	402,1	2,96
H4-19-30	2280,0	708,0	0,02	20,6	590,6	62,2	109,6	1189,4	3,07
H4-19-60 (fine)	1808,0	1820,0	0,06	17,6	876,6	13,6	123,0	1136,3	4,74
H4-19-60 (coarse)	2730,0	1990,0	0,06	81,6	982,2	17,5	181,7	1731,0	4,64
H4-19-110 (nest)	2500,0	1800,0	0,05	23,2	1048,4	17,7	209,4	1380,9	2,27
H4-19-110 (not in nest)	2098,0	1938,0	0,04	28,4	890,8	17,8	164,7	1347,8	2,94
H4-19-160	2762,0	1960,0	0,06	27,0	1019,0	21,5	230,0	1636,5	2,72
H4A-21-10	4116,0	450,0	0,23	24,8	975,2	54,2	284,2	1686,3	2,45
H4A-21-40	4892,0	1724,0	0,04	26,2	1413,0	26,7	342,8	2182,8	3,94
H4A-21-140	4256,0	1826,0	0,02	31,6	1273,0	34,4	348,6	2094,4	4,72
H4A-23-10	15110,0	628,0	0,02	27,2	3362,0	147,0	920,6	5370,0	2,00
H4A-23-30	4868,0	298,0	0,03	20,8	910,8	33,7	282,6	2000,7	3,66
H4A-23-60	3130,0	1752,0	0,05	24,8	1221,4	21,2	266,8	1564,1	4,66
H4A-23-120	3080,0	1784,0	0,05	20,4	1126,6	27,6	295,0	1524,5	3,97
H4A-24-10	8082,0	1266,0	0,03	31,6	35,2	1,8	9,1	53,7	1,63
H4A-24-40	3346,0	1694,0	0,02	19,0	1269,4	19,0	264,4	1451,6	4,29
H4A-24-70	6862,0	1590,0	0,02	25,0	1871,4	28,8	496,0	2510,0	2,53
H4A-24-120	4812,0	1778,0	0,15	18,4	1427,4	29,0	430,4	2056,3	3,39
H4A-27-05	302,0	62,6	0,30	58,8	25,9	70,6	5,9	169,2	1,27
H4A-27-30	5830,0	268,0	0,02	26,8	1222,8	46,1	473,6	1880,2	1,25
H4A-27-120	5306,0	1716,0	0,05	29,0	1688,8	27,1	567,4	2098,9	5,87
H4A-27-170	4716,0	1862,0	0,03	22,8	1390,8	32,5	495,4	1860,3	7,23
H4A-30-10	3962,0	195,2	0,02	24,2	829,4	145,3	257,4	1389,1	2,35
H4A-30-50	4142,0	510,0	0,03	24,0	1056,4	5,5	402,6	1359,5	1,94
H4A-30-100	3356,0	1704,0	0,06	8,6	1312,2	8,9	379,0	1212,1	4,68
H4A-30-160	1998,0	1850,0	0,02	12,6	1003,8	25,4	241,4	832,7	6,46
H4-32-10	1276,0	350,0	0,03	18,2	216,0	166,0	70,7	621,0	2,74

H4-32-30	3884,0	106,8	0,01	12,4	605,2	59,7	193,8	1827,1	2,70
H4-32-60	4324,0	177,2	0,02	17,6	844,2	4,2	344,2	1752,9	2,56
H4-32-80 (fine)	5916,0	808,0	0,03	15,0	1317,6	6,7	518,2	2005,8	5,80
H4-32-80 (coarse)	8530,0	920,0	0,03	11,2	1949,8	8,8	842,4	3115,8	4,56
H4-32-100	4890,0	1596,0	0,02	11,6	1526,6	6,6	469,4	1686,7	4,97
H4-32-130	2982,0	1732,0	0,02	16,4	1219,0	10,8	324,8	1186,6	4,48
H4A-34-10	1236,0	83,6	0,02	32,2	135,9	126,5	48,5	609,9	1,88
H4A-34-30	3640,0	174,4	0,01	20,8	665,0	12,7	301,4	1406,6	6,03
H4A-34-60	4932,0	1692,0	0,04	23,2	1458,8	8,5	503,8	1918,3	3,62
H4A-34-110	2220,0	1844,0	0,04	13,2	1023,2	13,5	263,4	959,6	4,35
H4A-34-160	5460,0	1918,0	0,01	11,8	1027,2	26,2	302,0	1075,1	6,95
H4A-37-10	2366,0	330,0	0,03	22,2	995,4	47,1	408,2	1324,7	3,74
H4A-37-30	4276,0	1598,0	0,02	15,0	2226,0	5,1	828,6	2786,3	4,27
H4A-37-70	3484,0	1774,0	0,03	10,0	1187,0	2,7	338,2	1358,7	2,49
H4A-37-120	2224,0	1860,0	0,03	7,6	993,6	12,5	269,8	904,6	2,45
H4A-37-170	3974,0	1980,0	0,03	9,4	1303,8	34,7	522,2	1611,8	4,52
H4-39-10	8444,0	1660,0	0,04	16,6	2310,0	12,2	1079,6	2381,8	2,76
H4-39-30	2112,0	193,8	0,03	17,8	454,0	16,4	215,4	639,9	1,27
H4-39-60	1664,0	1730,0	0,06	16,8	988,2	5,6	259,8	580,6	2,55
H4-39-90	2168,0	1720,0	0,05	8,4	1051,0	15,0	338,8	854,3	2,90
H4-39-120	1776,0	1810,0	0,08	5,0	943,0	20,8	280,2	764,2	3,49
H4-41-4	1598,0	166,6	0,01	36,2	201,4	172,1	123,1	779,0	2,06
H4-41-40	1916,0	306,0	0,02	27,8	381,4	55,5	227,6	757,1	1,80
H4-41-90	1852,0	1722,0	0,01	22,6	977,8	39,9	277,6	745,4	4,62
H4-41-120	1612,0	1764,0	0,02	22,0	806,6	45,2	235,8	723,2	4,27
H4-41-140	1974,0	1874,0	0,06	16,2	960,0	45,6	315,4	896,0	3,99
H4-41-180	2410,0	1854,0	0,02	19,8	1000,6	48,1	378,2	1069,8	4,54
H4A-43-10	460,0	147,2	0,07	42,6	102,5	66,9	41,0	194,1	1,53
H4A-43-30	4376,0	1834,0	0,04	8,0	1334,0	73,6	661,4	1750,7	6,54
H4A-43-80	3814,0	352,0	0,02	23,2	711,0	96,4	459,4	1426,1	1,82
H4A-43-140	4374,0	1888,0	0,02	22,4	1294,4	94,8	582,4	1741,3	4,66
H4A-43-190	5612,0	1814,0	0,07	23,8	1492,8	92,7	757,0	2042,2	6,21
H4A-45-10	504,0	75,4	0,09	69,4	35,6	59,0	12,6	310,1	1,90
H4A-45-30	5230,0	1638,0	0,03	16,2	1582,8	76,9	662,4	1800,0	3,09
H4A-45-50	4642,0	1618,0	0,01	23,2	1498,8	52,1	586,8	1707,7	5,15
H4A-45-90	4198,0	974,0	0,02	31,6	1099,0	39,0	483,0	1431,2	6,03
H4A-47-10	1228,0	76,6	0,02	25,1	302,0	70,0	117,8	395,5	2,70
H4A-47-30	6294,0	242,0	0,02	24,0	1548,6	74,6	679,2	1877,0	2,53
H4A-47-70	4638,0	338,0	0,02	20,2	990,6	47,1	430,8	1567,8	3,68
H4A-49-10	24,2	2,0	0,17	46,4	4,8	25,4	0,9	61,5	1,49
H4A-49-40	2628,0	145,4	0,02	20,0	420,0	75,0	182,2	1207,4	2,53
H4A-52-10	8,6	2,9	0,60	57,2	6,3	17,5	1,3	29,3	1,63
H4A-54-10	20,0	19,6	0,54	48,2	12,3	11,2	2,4	44,8	1,90
H4A-57-10	12,8	14,4	0,20	29,6	15,4	6,4	3,8	17,9	1,90

181

H4A-58-10	6,1	5,5	0,17	25,8	11,3	9,1	2,8	12,6	2,21
H4-end-10	10,5	8,1	0,33	15,8	22,5	3,4	9,7	45,2	1,55
H4-end-10+	51,4	75,4	0,01	4,8	21,0	2,1	8,8	42,7	3,31